ADENO-ASSOCIATED VIRUS MEDIATED RHODOPSIN DELIVERY IN PREVENTING SECONDARY CONE DEGENERATION IN RHODOPSIN KNOCKOUT MICE



Daniyar Dauletbekov

Merton College

A thesis submitted for the degree of Doctor of Philosophy

Trinity 2016

University of Oxford

Abstract

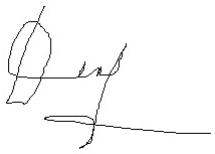
Rhodopsin-linked retinitis pigmentosa (RP) is the most common form of autosomal dominant RP, an inherited retinal degeneration, in which rod degeneration is followed by secondary cone loss leading to loss of vision and blindness. The overall objective of this work was to develop an optimized gene replacement therapy, delivering the rhodopsin gene for rhodopsin-linked RP and establish whether secondary cone loss can be delayed.

A fast-acting single mutant serotype 8 self-complementary adeno-associated virus vector was produced containing the human rhodopsin promoter and the human rhodopsin coding sequence. In vivo studies in rhodopsin knockout mouse showed that the vector administration led to widespread and robust expression of the transgene.

Subretinal injection of the vector into three-week pups of rhodopsin knockout mice with cones expressing green fluorescent protein showed restoration of rod-derived electroretinogram (ERG) responses, and preservation of cone-driven ERG responses three months after injection. Similarly, the longitudinal follow-up with confocal scanning ophthalmoscopy found preservation of fluorescent cones up to three months after injection. Overall, these data provided evidence that the designed vector resulted in significant benefit to rod photoreceptors as well as in delay in secondary cone degeneration and built a basis for future use of this vector on dominant models of RP.

Declaration

I declare that this thesis has been composed solely by myself and that it has not been submitted, in whole or in part, in any previous application for a degree. Except where states otherwise by reference or acknowledgment, the work presented is entirely my own.



Daniyar Dauletbekov

13.02.2017

CONTENTS

Abstract 2

List of abbreviations 5

List of tables 12

List of figures 13

CHAPTER 1 GENERAL INTRODUCTION 16

1.1 The mammalian retina 17

1.1.1 Anatomy of the retina 17

1.1.2 Visual cycle in rod cells 19

1.2 Rhodopsin protein 21

1.2.1 Rhodopsin structure 22

1.2.2 Rhodopsin trafficking 23

1.2.3 Structural role of rhodopsin 24

1.3 Retinitis pigmentosa 25

1.3.1 Clinical course 25

1.3.2 RP classifications 26

1.3.3 Rhodopsin-linked RP 28

1.3.3.1 Classification by clinical phenotype 28

1.3.3.2 Classification on cellular and biochemical features 29

1.3.4 Types of mutation in rhodopsin-linked RP 34

1.3.4.1 Loss-of-function mutations 34

1.3.4.2 Gain-of-function mutations 35

1.3.4.2.1 ER stress 36

1.3.4.2.2 Cell death in retinal degenerations 37

1.3.4.3 Dominant negative mutations 38

1.3.5 Secondary cone degeneration in RP 39

1.3.5.1 Endotoxins release and the Muller cells activation 40

1.3.5.2 Oxidative stress 41

1.3.5.3 Loss of structural support 43

1.3.5.4 Nutrients deprivation 43

1.3.5.5 Rod-derived trophic factors 44

1.4 Gene therapy for retinal degenerations 46

1.4.1 General AAV biology 47

1.4.2 AAV vector design 48

1.4.2.1 Capsid pseudotyping 48

1.4.3 Limiting steps for AAV transduction 51

1.4.3.1 Cell binding and capsid serotypes 51

1.4.3.2 Intracellular degradation of viral vectors 51

1.4.3.3 Conversion to double-stranded DNA 52

1.4.4 Self-complementary AAV 54

1.4.4.1 Mechanism of scAAV production 55

1.4.4.2 Packaging capacity of scAAV 55

1.4.4.3 Transduction superiority of scAAV compared to ssAAV 56

1.4.5 Tissue tropism of AAV gene therapy 59

1.4.5.1 Mode of delivery 59

1.4.5.2 Promoter choice 60

1.4.5.3 AAV capsid modification in directing tropism 61

1.4.6 AAV gene therapy in clinical trials 61

1.4.7 Gene therapy of the rhodopsin-linked RP 63

1.4.7.1 Rhodopsin supplementation 63

1.4.7.1.1 Rhodopsin overexpression 65
1.4.7.2 Suppression methods 66
1.4.7.2.1 Allele-specific suppression 66
1.4.7.2.2 Allele-independent suppression 67
1.4.8 Mouse models of rhodopsin-linked RP 71
1.4.8.1 Rhodopsin knock-out mice 72
1.5 Aim and outline of the thesis 73
CHAPTER 2 METHODS AND MATERIALS 75
2.1 Molecular biology 76
2.1.1 Polymerase Chain Reaction (PCR) 76
2.1.2 DNA ligation 77
2.1.3 Gene cloning using *E.Coli* 77
2.1.4 Agarose gel electrophoresis 78
2.1.5 DNA extraction from agarose gel 79
2.1.6 Restriction enzyme digestion 80
2.1.7 DNA sequencing 80
2.2 Cell cultures 81
2.2.1 HEK cell cultures 81
2.2.2 HEK cells transfection 82
2.2.3 Macaque retinal explants 82
2.3 AAV production 84
2.3.1 Seeding of HEK293T cells with three plasmids 84
2.3.2 Transfection of HEK293T cells 86
2.3.3 Harvesting HEK293T cells 87
2.3.4 Isolation of AAV particles using the Iodixanol gradient 88
2.3.5 Purification and concentration of the isolated AAV vectors 90
2.3.6 SDS-PAGE 91
2.3.7 qPCR 92
2.3.7.1 qPCR primers design 92
2.3.7.2 qPCR protocol 92
2.4 *In vivo* procedures 94
2.4.1 Animals 94
2.4.1.1 Genotyping 94
2.4.2 Subretinal injection 96
2.4.2.1 Anaesthesia 97
2.4.2.2 Pupil dilation 97
2.4.2.3 Paracentesis of the anterior chamber 98
2.4.2.4 Subretinal injection 98
2.4.3 Confocal Scanning Laser Ophthalmoscopy 99
2.4.4 Electroretinography (ERG) 101
2.4.4.1 General ERG set-up 102
2.4.4.2 ERG electrodes 102
2.4.4.3 Dark-adapted ERG 103
2.4.4.4 Light adapted ERG 104
2.4.4.5 ERG data analysis 104
2.4.4.6 ERG protocol 105
2.4.5 Optomotor response 107
2.5 Tissue processing 108
2.5.1 Sections 108
2.5.2 Confocal microscopy 108
2.5.3 Immunohistochemistry 109
2.5.3.1 Quantification of the Hoechst-labelled photoreceptors 111
2.5.3.2 Measurement of EGFP cones 111

2.5.4 Western blot 111
2.5.4.1 Western blot quantification 113
2.6 Statistical analysis 114
CHAPTER 3 AAV DESIGN AND PRODUCTION 115
3.1 Introduction 116
3.1.1 AAV production 116
3.1.2 AAV purification methods 117
3.1.3 Mutant ITR in scAAV production 118
3.1.4 AAV quantification methods 121
3.2 Aims 122
3.3 Methods 123
3.3.1 Vector design 123
3.3.2 Self-complementary plasmid 127
3.3.3 ITR integrity verification 128
3.3.4 The rep/cap and helper plasmids 128
3.3.5 Production of AAV vector 128
3.3.6 AAV assessment 131
3.4 Results 132
3.4.1 Production of the vector plasmids 132
3.4.2 ITR integrity verification 136
3.4.3 AAV production 137
3.4.4 Assessment of AAV purity 137
3.4.5 Quantification of AAV genome copies 139
3.4.6 qPCR with the primers targeting different regions 140
3.5 Discussion 142
3.5.1 scAAV quantification 143
CHAPTER 4 AAV VECTOR EVALUATION 146
4.1 Introduction 147
4.2 Aims 148
4.3 Methods 148
4.3.1 *In vitro* assessment of the human rhodopsin promoter 148
4.1.1 *In vivo* assessment of rhodopsin expression 149
4.1.2 Macaque retinal explants 149
4.1.3 Extent of retinal transduction 150
4.1.4 Western blot 151
4.2 Results 151
4.2.1 Limited transfection of HEK293T cells 151
4.2.2 Regrowing of outer segments upon the rhodopsin gene delivery 153
4.2.3 Rod specificity 157
4.2.4 DsRed expression of in the primate retina *ex vivo* 159
4.2.5 Widespread retinal transduction from the vector assessed by SLO 161
4.2.6 Quantification of rhodopsin by Western blot 164
4.3 Discussion 167
4.3.1 Transgene expression in cell cultures 167
4.3.2 Transgene expression in rhodopsin knockout mice 168
4.3.3 Rod-specificity of the rhodopsin human promoter 168
4.3.4 Primate retinal explants 170
4.3.5 Extent of transduction 171
4.3.6 Rhodopsin expression level 172
CHAPTER 5 AAV VECTOR EFFECTS ON RODS 174
5.1 Introduction 175
5.1.1 ERG 175
5.1.2 ERG amplitude measurements and variability 176

5.1.3 Isolating rod ERG responses 177
5.1.4 ERG in rhodopsin knockout mice 178
5.2 Aims 179
5.3 Methods 179
5.4 Results 181
5.4.1 Dark-adapted flash ERG in unilaterally injected eyes 181
5.4.2 Dark-adapted ERG in bilaterally injected eyes 188
5.4.3 Preservation of the ONL thickness in the unilaterally treated group 193
5.4.4 Preservation of the ONL thickness in the bilaterally injected group 193
5.5 Discussion 197
CHAPTER 6 CONE SURVIVAL 201
6.1 Introduction 202
6.1.1 Cone degeneration in rhodopsin knockout mice 202
6.1.2 Isolating cone-derived ERG responses 203
6.2 Aims 204
6.3 Methods 204
6.3.1 Isolating cone ERG responses 204
6.3.2 SLO imaging 205
6.3.3 Histology analysis of cones 206
6.4 Results 207
6.4.1 Light-adapted ERG in unilaterally treated eyes 207
6.4.2 Light-adapted ERG in bilaterally injected eyes 212
6.4.3 Flicker ERG in unilaterally treated mice 215
6.4.4 Flicker ERG in bilaterally injected mice 215
6.4.5 Rhodopsin vector delays cone degeneration in unilaterally treated group 218
6.4.6 Rhodopsin vector delays cone degeneration in bilaterally injected group 221
6.4.7 Optomotor response 224
6.4.8 Preservation of EGFP-cones six month postinjection on histology 226
6.5 Discussion 229
CHAPTER 7 GENERAL DISCUSSION 233
7.1 Key features of the proposed gene therapy 236
7.1.1 Choice of AAV serotype 236
7.1.2 Self-complementary AAV 236
7.1.3 The human rhodopsin promoter 237
7.1.4 Timing of AAV administration 238
7.1.5 AAV rhodopsin delivery and timing of intervention 243
7.2 Variables affecting treatment efficiency 246
7.2.1 Vector dosing 246
7.2.2 AAV quantification 247
7.2.3 AAV contamination 247
7.2.4 Empty capsids 248
7.2.5 Immunogenicity 249
7.3 Future work 253
7.3.1 Challenges for clinical trials on rhodopsin-linked RP 253
7.3.2 CRISPR-Cas9 approach 254
Appendix 256
Acknowledgements 258
Bibliography 259

List of abbreviations

AAV: adeno-associated virus

ABCA4: Adenosine triphosphate Binding Cassette Subfamily A Member 4

AF: autofluorescence

AmpR: ampicillin resistance sequence

ANOVA: analysis of variance

ART: automatic real-time

BCA: bicinchoninic acid

bp: basepairs

BSA: bovine serum albumin

CAG: a hybrid of CMV enhancer, chicken beta-Actin promoter and rabbit beta-Globin

CBA: chicken beta-actin

cDNA: complementary DNA

cGMP: cyclic guanosine monophosphate

CMV: cytomegalovirus

CNGs: cyclic nucleotide-gated ion channels

CNTF: ciliary neuroprotective factor

CRISPR: clustered regularly interspaced short palindromic repeats

CsCl: caesium chloride

cSLO: confocal scanning laser ophthalmoscopy

DEPC: diethyl pyrocarbonate

dGTP: deoxyguanosine triphosphate

DIC: differential interference contrast

DMEM: Dulbecco's Modified Eagle's Medium

DNA: deoxyribonucleic acid

dsDNA: double-stranded DNA

DsRed: red fluorescent protein

ECL: electrogenerated chemiluminescence

EDTA: ethylenediaminetetraacetic acid

EGFP: enhanced green fluorescent protein

EM: electron microscopy

ER: endoplasmic reticulum

ERG: electroretinogram

FBS: fetal bovine serum

gc: genome copies (vector genomes)

GDP: guanosine-5'-diphosphate

GFP: green fluorescent protein

GPCR: G-protein coupled receptor

GTP: guanosine-5'-triphosphate

HEK: human embryonic kidney

hRHO: coding sequence of the human rhodopsin gene

hRHOp: human rhodopsin promoter

IHC: immunohistochemistry

INL: inner nuclear layer

IPL: inner plexiform layer

IRD: inherited retinal degenerations

IRES: internal ribosome entry site

ITR: inverted terminal repeat

LCA: Leber's congenital Amaurosis

MCS: multiple cloning site

Met II: metarhodopsin II

mRNA: messenger RNA

mTOR: mammalian target of rapamycin

Nab: neutralising antibodies

NC: normalizing control

NF-κB: nuclear factor kappa-light-chain-enhancer of activated B cells

NIR: near infrared reflectance

NMDA: N-methyl-D-aspartate receptor

NRF2: nuclear factor erythroid-derived 2

ns: non significant

OCT: optimal cutting temperature

ONL: outer nuclear layer

OPL: outer plexiform layer

OMR: optomotor reflex

Opn1.EGFP: transgenic mice line B6.Cg-Tg(OPN1LW-EGFP)85933Hue/Mmmh with *EGFP* transgenic insertion

P:I: particle-to-infectious unit

P21: postnatatal day 21

P23H: substitution of proline at residue 23 for histidine in rhodopsin

pA: polyadenylation sequence

PBS: phosphate buffered saline

PBS-T: phosphate buffered saline tween

PDEβ: retinal rod photoreceptor cGMP phosphodiesterase, beta subunit

PEI: polyethylenimine

PFA: paraformaldehyde

PGC1a: peroxisome proliferator–activated receptor γ coactivator 1-α

PM: postnatal month

PNA: peanut agglutinin

polyA: polyadenylation sequence

PVDF: polyvinylidene difluoride

PW: postnatal week

qPCR: quantitative polymerase chain reaction

rd1: retinal degeneration 1

RdCVF: rod-derived cone viability factor

RdCVFL: long isoform of rod-derived cone viability factor

rds: retinal degeneration slow

Rho-/-: rhodopsin knockout

RHO: rhodopsin gene

RIPA: radioimmunoprecipitation assay

RNA: ribonucleic acid

RNAi: RNA interference

ROS: rod outer segment

RP: retinitis pigmentosa

RPE: retinal pigment epithelium

RPE: retinal pigment epithelium

RPE65: retinal pigment epithelium-specific protein 65kDa

rpm: rotations per minute

RPMI: Roswell Park Memorial Institute

RT: room temperature

scAAV.DsRed: scAAV2/8^{Y733F}hRHOp-DsRed

scAAV.RHO: scAAV2/8^{Y733F}hRHOp-RHO

scAAV: self-complementary AAV

scCAG: short CAG

SDS-PAGE: sodium dodecyl sulphate - polyacrylamide gel electrophoresis

SEM: standard error of the mean

shRNA: small hairpin RNA

ssAAV: single-stranded AAV

ssDNA: single-stranded DNA

TAE: tris base, acetic acid and EDTA buffer

TLR: toll-like receptors

TNF: tumour necrosis factor

TRS: terminal resolution site

UPR: unfolded protein response

VP: capsid protein

WPRE: woodchuck hepatitis virus posttranscriptional regulatory element

wt: wild-type

Y733F: substitution of tyrosine residue to phenylalanine residue in the position 733 of the AAV capsid

YEFP: yellow fluorescent protein

ZFP: zinc-finger proteins

List of tables

1.1 Classification of rhodopsin mutations 32
2.1 Components of a typical PCR reaction 76
2.2 Plasmid size and amount per transfection in AAV production 86
2.3 Preparations for two iodixanol gradients 89
2.4 ERG protocol 105
2.5 Primary antibodies used for IHC, Western 110
2.6 Secondary antibodies for IHC, Western 110
3.1 The primers used for qPCR quantification of AAV preparations 132
3.2 Titers obtained with primers targeting different regions within the expression cassette and the plasmid backbone 140

List of figures

1.1 Schematic organisation of the retina 18
1.2 Signal transduction via rhodopsin in rod cells 20
1.3 Schematic structure of a rod photoreceptor and trafficking of rhodopsin 24
1.4 The number of mapped and identified retinal disease genes from 1980 to 2016 27
1.5 Secondary structure of rhodopsin with the sites of known point mutations 33
1.6 Schematic of AAV vector design 50
1.7 scAAV circumvents the double DNA conversion step 58
2.1 Genotyping for rhodopsin and *EGFP* 96
2.2 Schematic of subretinal delivery of AAV vector in mice 99
2.3 Confocal Scanning Laser Ophthalmoscopy (cSLO) 101
2.4 ERG platform 103
3.1 Inverted terminal repeat (ITR) 119
3.2 The difference in genome of single-stranded and self-complementary AAV 120
3.3 Maps of the self-complementary plasmids 126
3.4 Schematic of AAV production 130
3.5 Iodixanol gradient 131
3.6 Isolation of construct fragments of the *hRHOp-RHO-pA* and *hRHOp-DsRed-pA* 133
3.7 Verification of plasmids size by restriction digest 134
3.8 The absence of the terminal resolution site confirmed by dGTP sequencing 136
3.9 SDS-PAGE of AAV samples 138
3.10 qPCR to determine AAV titer 139
3.11 Schematic of qPCR primer placement 141
4.1 Limited expression of DsRed upon the transfection HEK293T cells with the plasmid *pl.hRHOp-DsRed* 152

4.2 Rhodopsin expression in the ROS upon the AAV delivery of the rhodopsin gene one month after injection 154
4.3 ABCA4 expression in outer segments upon the AAV delivery of the rhodopsin gene one month after injection 156
4.4 The human rhodopsin promoter drives the rod-specific expression of DsRed in rhodopsin knockout mice 158
4.5 *scAAV2/8^{Y733F}hRHOp-DsRed* transduces primate retinal explants 160
4.6 Subretinal delivery of *scAAV2/8^{Y733F}hRHOp-DsRed* leads to widespread retinal fluorescence 162
4.7 Subretinal delivery of *scAAV2/8^{Y733F}hRHOp-DsRed* drives widespread retinal expression of DsRed 163
4.8 Rhodopsin protein expression in treated eyes versus fellow untreated eyes 165
4.9 Comparison of rhodopsin protein expression in wild-type mice versus treated rhodopsin knockout mice 166
5.1 Measurements of a- and b-wave amplitudes 177
5.2 Restoration of rod-isolated ERG responses in unilaterally treated eyes at dim light flash intensity 184
5.3 Dark-adapted ERG responses in unilaterally treated rhodopsin knock-out mice 185
5.4 Dark-adapted b-wave amplitudes at different flash intensities and time points in unilaterally treated rhodopsin knockout mice 186
5.5 Dark-adapted a-wave amplitudes at increasing flash intensities in unilaterally treated rhodopsin knockout mice 187
5.6 Dark-adapted ERG responses in the bilaterally injected rhodopsin knockout mice 190
5.7 Dark-adapted b-wave amplitudes at increasing flash intensities in rhodopsin knockout mice injected bilaterally 191
5.8 Dark-adapted a-wave amplitudes at different flash intensities and time points in bilaterally treated rhodopsin knockout mice 192

5.9 Preservation of the ONL and expression of rhodopsin six months after the AAV-mediated rhodopsin delivery in rhodopsin knockout mice 195
5.10 Preservation of Hoechst-labelled photoreceptors in the ONL five months after the delivery of scAAV2/8^{Y733F}hRHOp-RHO..... 196
6.1 Longitudinal quantification of ERGP-cones by SLO..... 206
6.2 Representative light-adapted ERG traces at different time points 209
6.3 B-wave amplitudes in light-adapted ERG in unilaterally and bilaterally treated rhodopsin knockout mice 210
6.4 Light-adapted b-wave amplitudes at increasing flash intensities in unilaterally treated rhodopsin knockout mice 211
6.5 Light-adapted b-wave amplitudes at different flash intensities and time points in bilaterally treated rhodopsin knockout mice..... 214
6.6 Light-adapted b-wave amplitudes flicker ERG after the *scAAV2/8Y733FhRHOp-RHO* delivery 217
6.7 Autofluorescence imaging in *Opn1.Rho-/-* mice treated unilaterally with *scAAV2/8^{Y733F}hRHOp-RHO* 219
6.8 SLO quantification of EGFP-fluorescent cones in mice unilaterally treated with *scAAV2/8^{Y733F}hRHOp-RHO* shows preservation of cones in treated eyes 220
6.9 Fundus imaging in bilaterally injected mouse shows cone preservation in treated eyes 222
6.10 SLO quantification of EGFP-fluorescent cones in bilaterally injected mice shows preservation of cones at PM4 in treated eyes 224
6.11 Optomotor response of Opn1.EGFP Rho-/- mice injected with scAAV2/8^{Y733F}hRHOp-RHO 225
6.12 Histology analysis showed preservation of EGFP-cones in treated eyes 227
6.13 Histology quantification of EGFP-cones in *Opn1.EGFP Rho-/-* mice treated at PW3 with *scAAV2/8^{Y733F}hRHOp-RHO*, six months after injection shows preservation of cones in treated eyes 228
7.1 Effects of treatment on degeneration rate..... 239

Chapter 1 General introduction

1.1 The mammalian retina

1.1.1 Anatomy of the retina

The mammalian retina is a multi-layered structure which is responsible for light capture and stimulus transduction within the eye. Light is primarily absorbed by photoreceptors which are situated in the outer retina adjacent to the retinal pigment epithelium (RPE). To accommodate for the vast array of light intensities encountered within the environment, most mammals have developed two classes of photoreceptor: rods functioning in dim light and providing non-colour vision, and cones operating in high-intensity daylight and supporting colour and high-resolution vision. The photoreceptor bodies form the outer nuclear layer. The processes from the bodies of photoreceptors form synaptic projections (the outer plexiform layer) to bipolar cells (the inner nuclear layer). These second order neurons, in turn, extend their axons (the inner plexiform layer) to the ganglion cells (the ganglion cell layer). These third-order neurons then form axons (the nerve fibre layer) which together constitute the optic nerve which projects primarily to the lateral geniculate body of the thalamus **(Figure 1.1**).

Rodents provide an easily accessible retinal model, however, certain differences exist between the human and mouse eye. Rodents are nocturnal animals relying on the highly sensitive rod system, with cones distributed across the whole retina, whereas in old-world primates, trichromatic colour

vision and high visual acuity are achieved by the concentration of cones within the fovea.

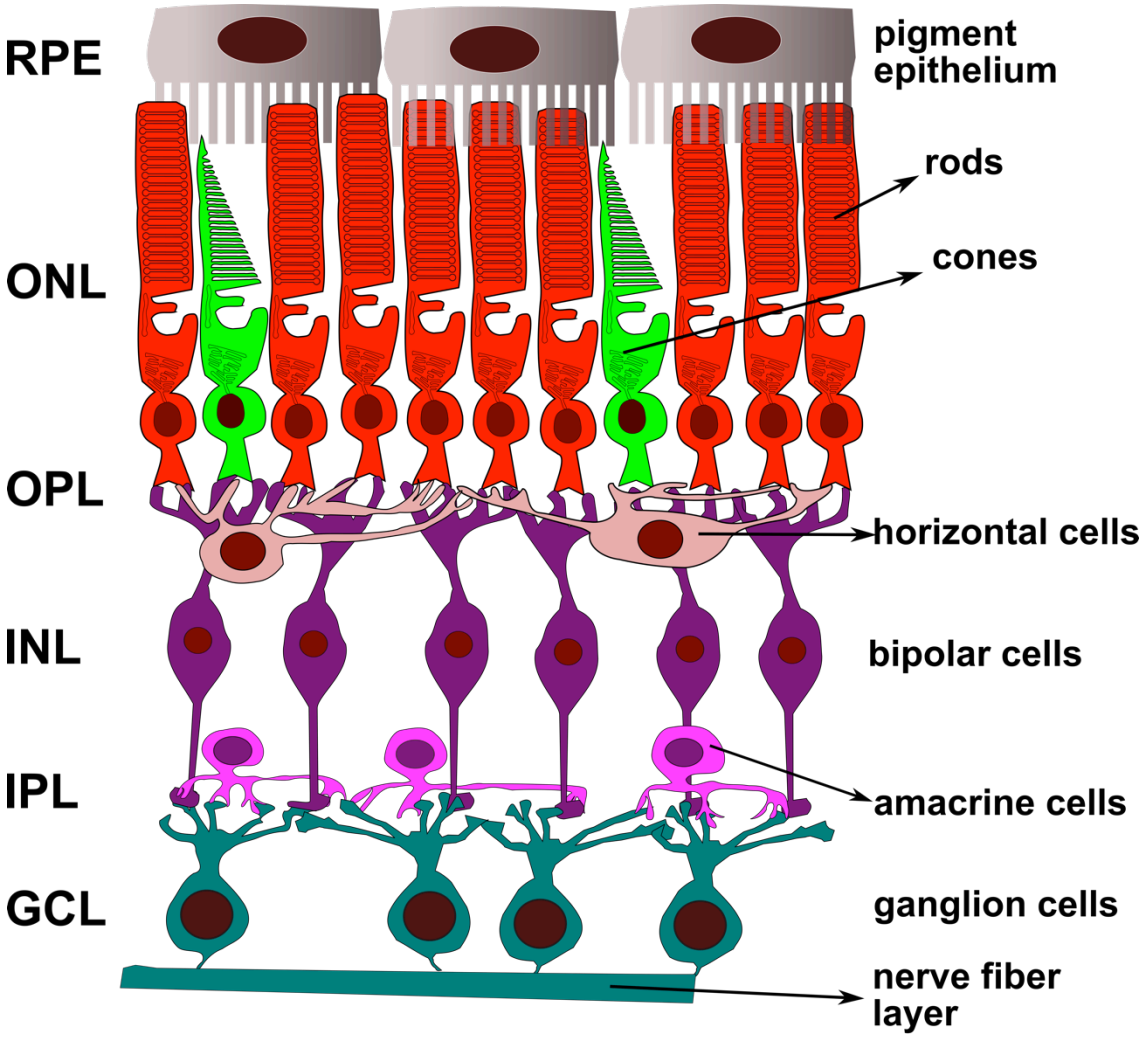


Figure 1.1 Schematic organisation of the retina
Layers of the retina: RPE: retinal pigment epithelium, ONL: outer nuclear layer, OPL: outer plexiform layer, INL: inner nuclear layer, IPL: inner plexiform layer, GCL: ganglion cell layer, and nerve fiber layer.

1.1.2 Visual cycle in rod cells

Light processing within the retina in dim-light conditions starts in the rod outer segment (ROS). A single photon of light can be captured by the chromophore 11-*cis*-retinal, which is covalently linked to rhodopsin, a G-protein coupled receptor (**Figure 1.2**). The photoisomerisation of 11-*cis*-retinal to the all-*trans*-retinol configuration induces a conformational change in rhodopsin to metarhodopsin II. This, in turn, activates transducin (the G-protein) by dissociating the α-subunit from the β- and γ-subunits. The α-subunit binds GTP and prompts phosphodiesterase to hydrolyse cyclic GMP (cGMP) into 5'-GMP. The drop in intracellular concentration of cGMP leads to the closure of cyclic nucleotide-gated cation channels (CNGs). This closing of sodium-conducting channels induces cellular hyperpolarization (lowering of the cell membrane potential from approximately -40 mV to -60 mV) due to the ongoing efflux of potassium ions. Hyperpolarization of the outer segment causes the closure of voltage-gated calcium channels. The resulting drop in intracellular calcium concentration leads to the inhibition of release of the neurotransmitter glutamate at the synaptic junction between the photoreceptor and the bipolar cell. The reduction of glutamate at the synaptic connection leads to the depolarization of On-centre bipolar cells and the hyperpolarization of the cone off-centre bipolar cells.

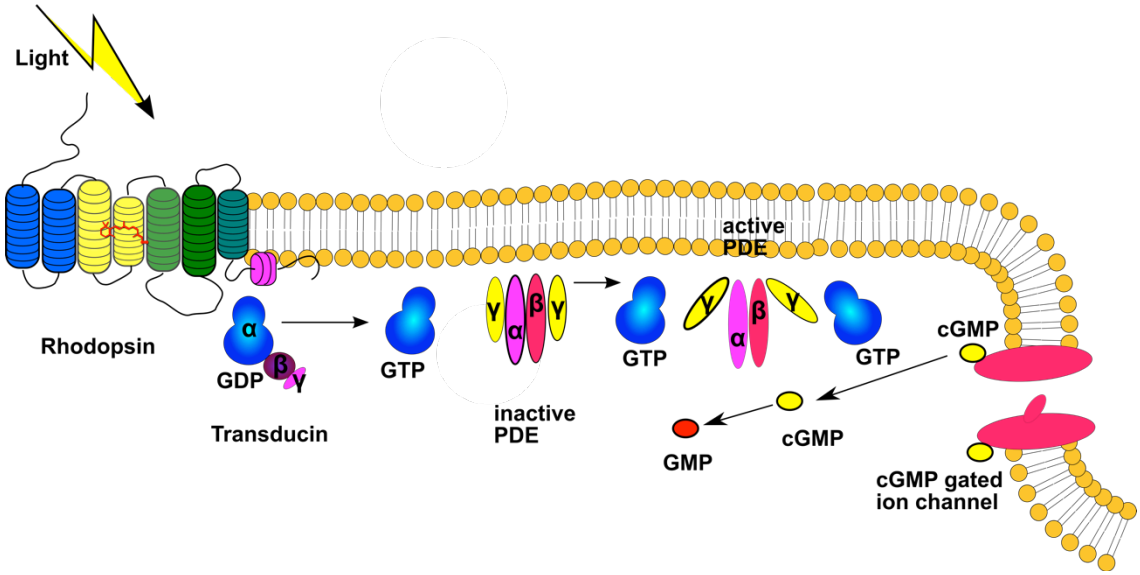


Figure 1.2 Signal transduction via rhodopsin in rod cells
Rhodopsin is the first signalling protein in the visual cascade in rod cells. Its chromophore - 11-*cis*-retinal, absorbs a photon of light and activates rhodopsin. The activated rhodopsin catalyses the exchange of GDP for GTP in the G-protein transducin, leading to the formation of an activated α-subunit bound to GTP. The activated α-subunit of transducin in turn triggers phosphodiesterase (PDE6), which starts to hydrolyse cGMP into 5'-GMP. The drop of the cytoplasmic concentration of cGMP leads to the closure of cGMP-gated cation channels, blocking the influx of the sodium and calcium ions into the cytoplasm. This results in the hyperpolarization of the cell membrane potential which terminates the release of the neurotransmitter glutamate at the synaptic connection between the rod and bipolar cell

1.2 Rhodopsin protein

Rhodopsin, whose central role in vision was identified over a century ago, has received more research attention than any other protein of the visual cascade. Rhodopsin belongs to the superfamily of G-protein-coupled receptors (GPCRs), cell surface signalling proteins coupled to a G-protein and transmitting extracellular signals across the plasma membrane.

The first molecular studies on rhodopsin were performed by the German physiologist F. Kühne, who using bile salts extracted rhodopsin from the bovine retina in 1877. As he found that rhodopsin's colour faded after exposure to light, he named the pigmented material "visual purple" (rhodopsin) (Kühne 1877). Subsequently, Wald provided evidence that rhodopsin consists of two components: a 40 kDa apoprotein opsin and the 11-*cis*-retinal chromophore bound through a protonated Schiff-base linkage to the Lys side chain in the middle of helix VII (Rakshit and Park, 2015; Wald, 1935; Wald and Brown, 1953). Exposure to light of wavelength 498 nm causes the isomerisation of the chromophore to the all-*trans*-isomer and an accompanying shift in the wavelength of the rhodopsin absorption to 380 nm (Palczewski K, 2006). The chromophore is eventually released from the binding pocket of rhodopsin and recycled through transport to the RPE where it enters the retinoid cycle. The release of the chromophore induces a change in the opsin from its inactive to active conformation, producing the highly unstable intermediaries metarhodopsin I and metarhodopsin II (Met II) (Hubard and Wald, 1952). Met II is the heterogeneous form of several photo-activated conformations of

rhodopsin, which consequently activate transducin (G-protein). Rhodopsin protein is so extremely sensitive that it can capture just a single photon of light (Sampath and Rieke, 2004). In its turn, one rhodopsin molecule triggers hundreds of transducin molecules, the first step to amplify the single-photon response.

1.2.1 Rhodopsin structure

Following post-translational modification, the rhodopsin molecule has an elliptical shape due to the arrangement of its seven α-helical transmembrane domains, which vary in length from 20 to 33 residues. The N-terminus is located intradiscally (within the extracellular) whilst the C-terminal region is situated within the cytoplasm, with an almost equal distribution of mass between the extracellular and intracellular domains. An internal hydrophobic binding site within the three-dimensional rhodopsin molecule about 2/3 of the way from the cytoplasmic surface binds to the chromophore, 11-*cis*-retinal, a derivative of vitamin A (Hofmann and Palczewski, 2015).

The visualisation of rhodopsin in native disc membranes by atomic force microscopy and transmission electron microscopy revealed that rhodopsin forms rows of dimers and higher oligomers (Fotiadis et al., 2003).

The rhodopsin gene was identified on the long arm of chromosome 3 in humans and chromosome 6 in mice. It is a highly conserved sequence between species, with >95% similarity between bovine, murine, rabbit and human forms. The murine and human rhodopsin differ by only 18 residues within their amino acid sequences.

1.2.2 Rhodopsin trafficking

Rhodopsin is synthesised within the endoplasmic reticulum (ER) of the inner segment of rod cells, where the nascent protein is modified post-translationally by the formation of disulphide bonds. After having folded, rhodopsin leaves the ER, and upon entering the Golgi apparatus is glycosylated, and then transported to the ROS within the membrane of lipid vesicles (**Figure 1.3**). The glycosylation of rhodopsin occurs at the D2 and D15 residues on the site NXS/T of the N-terminal end (Kaushal et al., 1994; Wheatley and Hawtin; Wheatley et al., 2012). The outer segment is linked to the inner segment by the connecting cilium which contains a stack of microtubules. Given that rhodopsin constitutes around 90% of the total protein content of outer segments and about 10% of the distal tip of the outer segments is recycled daily by the RPE (Liang et al., 2004), the concentration of rhodopsin in the outer segments is extremely high and a prodigious amount of rhodopsin is produced and transported to the outer segments on a daily basis through the connecting cilium. In order to cope with such massive rhodopsin transport, rod cells have developed efficient and complex systems of protein trafficking, many of which still remain to be elucidated (Hollingsworth and Gross, 2012). Mutations in rhodopsin leading to mistrafficking of misfolded protein, and the mutations in genes encoding trafficking proteins are a common cause of retinitis pigmentosa (RP).

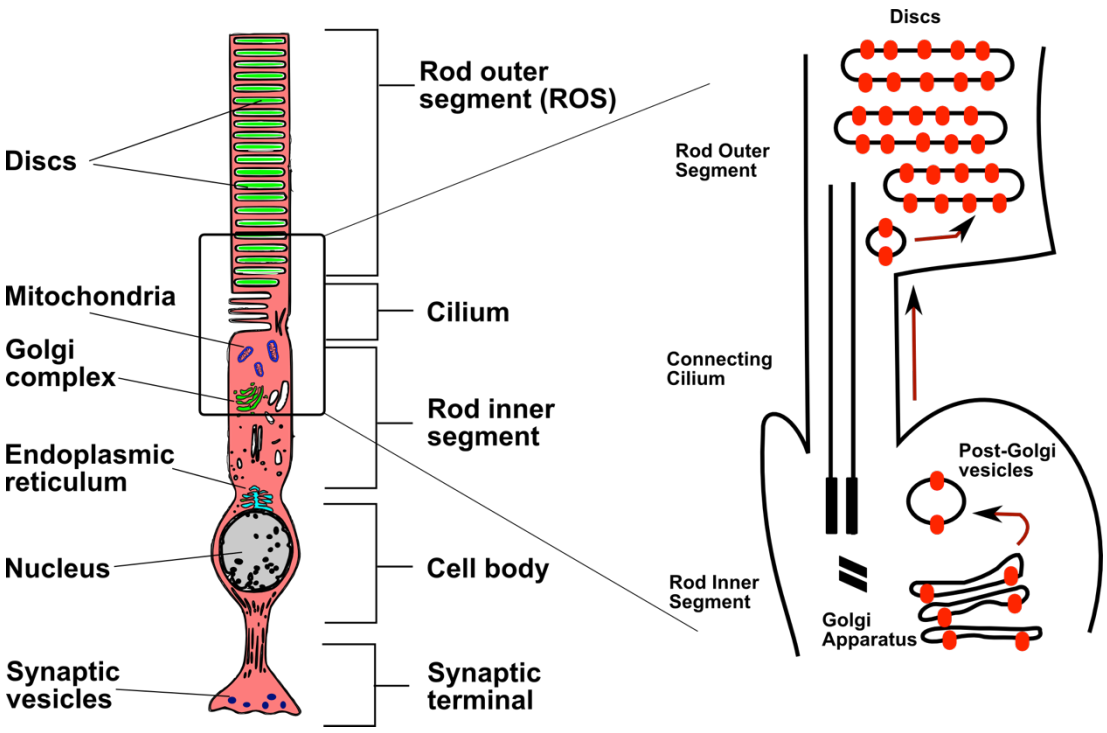


Figure 1.3 Schematic structure of a rod photoreceptor and trafficking of rhodopsin
Rod photoreceptors have a cell body, an inner segment, an outer segment, and a synaptic terminal. The inner and outer segments are connected by the connecting cilium. The synaptic rod spherule terminal connects a rod cell with bipolar and horizontal cells. The inner segment contains organelles, such as the endoplasmic reticulum (ER), Golgi complex, and mitochondria. The connecting cilium contains microtubules providing the transport of proteins to the outer segment. The outer segment contains the membrane discs consisting primarily of rhodopsin.
The schematic on the left shows a zoomed view of a rhodopsin cell. Rhodopsin (indicated by a red ellipse) is synthesised in the rod inner segment and transported to the connecting cilium via post-Golgi vesicles, and then integrated into discs at the base of rod outer segment.

1.2.3 Structural role of rhodopsin

The outer segment of rods is filled with about 900–2000 membranous discs, dependent on the species, containing millions of rhodopsin molecules and surrounded by the plasma membrane (Liang et al., 2004). This rhodopsin-packed outer segment enables the capture of a single photon at the optimal wavelength of around 498 nm, making rod cells extremely sensitive in dim-light conditions. Discs, forming double lamellar membranes restrained by a rim region, continuously move towards the distant end of ROS where they are

phagocytosed by the RPE (Rakshit and Park, 2015). Rhodopsin is the major protein component of rod outer segments (>90%) (Nickell et al., 2007). Given that one bovine retina yields about 0.5-1 mg of protein (Filipek et al., 2003), rhodopsin became popular for the studies on the GPCR family. Rhodopsin also plays a key structural role in the formation of the ROS, since its lack results in the absence of outer segments and leads to rod degeneration (Humphries et al., 1997). Mice heterozygous for the rhodopsin allele (*Rho*+/-), were found to have a smaller volume ROS, with the length being shorter by 30-40% and the average diameter reduced by 20% (Liang et al., 2004). These findings suggest that two functional alleles are necessary to produce the large amounts of rhodopsin protein observed within the mammalian ROS.

1.3 Retinitis pigmentosa

1.3.1 Clinical course

Retinitis pigmentosa is a heterogeneous group of inherited retinal disorders characterised by a progressive degeneration of photoreceptors; with a prevalence of 1 in 4,000 (Daiger et al., 2007; Haim, 2002) it is the most common cause of inherited retinal degeneration worldwide.

The clinical features of RP are night blindness, often starting in adolescence, followed by a progressive loss of peripheral vision and culminating in the loss of central vision and legal blindness in adulthood. The characteristic findings on retinal examination include bone spicule pigmentary formations, attenuated retinal vessels and a waxy pallor of the optic disc. Investigation typically yields

constricted visual fields and reduced or abnormal electroretinograms (ERG). The first symptoms may be experienced in early adolescence, and severe visual loss is common by the age of 40 to 50 years. However, all clinical symptoms and findings are highly variable among different patients with the underlying genetic mutation being sometimes a helpful predictor of the severity of a clinical course.

1.3.2 RP classifications

RP is profoundly heterogeneous on a number of different levels: genetic, alleic, phenotypic and clinical.

On a cellular level, the majority of RP cases are caused by a single gene defect within rod photoreceptors or the RPE which leads to progressive degeneration of rod photoreceptors. This manifests clinically as nyctalopia from adolescence with progressive constriction of peripheral vision. Eventually, secondary cone loss follows due to the preceding rod degeneration. This results in the loss of central cone-mediated vision. Due to the rapid progress in molecular diagnostics, around 300 retinal disease loci, and over 250 diseases-causing genes have been identified to date (**Figure 1.4**).

RP may be classified as non-syndromic (more than 66 genes are known to cause non-syndromic RP (Daiger et al., 2014)), or syndromic (systemic), where organ systems other than the retina are affected. Over thirty RP syndromes have been described to date, the most common being Usher syndrome (12 genes) which is associated with congenital deafness, and Bardet-Biedl

syndrome (17 genes) associated with renal impairment, obesity, and polydactyly.

According to the mode of inheritance, RP may be classified as autosomal dominant (15–20% of cases), autosomal recessive (20–25% of cases), or X-linked (10–15%). Mitochondrial and digenic inheritance are the rarest modalities of inheritance in RP (Nemet et al., 2015). Mitochondrial inheritance may also be associated with muscular dystrophy, defective metabolism, and nerve fibre damage (Mansergh et al., 1999; Da Pozzo et al., 2009). Digenic RP describes the simultaneous presence of pathogenic variants of genes *PRPH2* and *ROM1* which are believed to act synergistically (Dryja et al., 1997; Loewen et al., 2001).

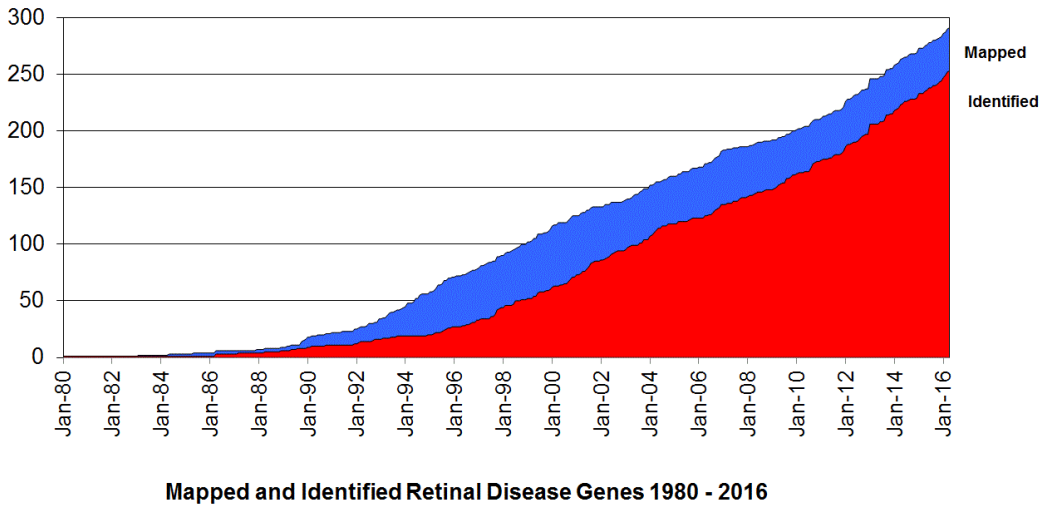


Figure 1.4 The number of mapped and identified retinal disease genes from 1980 to 2016
The graph from the Retinal Information Network provided by the University of Texas-Houston Health Science Centre (www.sph.uth.tmc.edu/RetNet). The slight increase in the steepness of the slope from 2010-12 may reflect the impact of increased use of next generation sequencing in identifying new mutations.

1.3.3 Rhodopsin-linked RP

Rhodopsin was one of first RP genes identified; its mutations account for approximately 15% of all inherited autosomal dominant retinal degenerations (Dalke and Graw, 2005) (**Figure 1.1**). More than 200 mutations have been described so far in the rhodopsin gene and most of them cause autosomal dominant RP (https://sph.uth.edu/retnet/home.htm), but very rarely may cause autosomal recessive RP (Rosenfeld et al., 1992). Four mutations in rhodopsin have been identified as a cause of autosomal dominant congenital stationary night blindness (CSNB), which affects scotopic vision, without affecting cone photoreceptors (Lem and Fain, 2004; McAlear et al., 2010): G90D (Sieving et al., 1995), *T94I* (al-Jandal et al., 1999), *A292E* (Dryja et al., 1993), and *A295V* (Zeitz et al., 2008). Although localising to different transmembrane helices, all four mutations are found near the chromophore-binding pocket and cause the constitutive activity of the mutant receptor (Park, 2014).

Rhodopsin mutations may be classified based upon clinical findings, biochemical features, localisation within the receptor molecule and how they affect the intracellular transport of rhodopsin.

1.3.3.1 Classification by clinical phenotype

Based on the severity of the clinical phenotype in families of patients, Cideciyan and co-workers (1998) distinguished two classes of rhodopsin-linked RP. Families of Class A (*R135G, R135L, R135W, V345L*, and *P347L*) showed early and severe loss of rod function demonstrated through rod b-wave amplitudes and perimetry, with early onset of night blindness. The milder phenotype of

Class B families (*T17M, P23H, T58R, V87D, G106R, and D190G*) was characterised by a patchy retinal fundus appearance with areas of advanced retinal degeneration neighbouring areas which were normal or far less affected, the preservation of rod-isolated ERG (33-93% of mean normal), a normal ROS length, normal rod activation kinetics and sensitivity with an inferior-superior gradient of disease expression (Cideciyan et al., 1998). The authors suggested that the severe phenotype of Class A originated from the cytotoxic heterozygous alleles or homozygous loss-of-function mutations, whereas the milder phenotype of Class B was explained by heterozygous loss-of-function mutations.

1.3.3.2 Classification on cellular and biochemical features

Mutations have been described throughout the rhodopsin gene localising along the three domains of the rhodopsin protein: the intradiscal, transmembrane and cytoplasmic domains (**Figure 1.5**). The large number of pathogenic mutations found in rhodopsin is indicative of how finely tuned its molecular structure is to allow the intricate interactions necessary for chromophore binding and second messenger signalling. It would seem that any minute alteration of this complex system leads to the breakdown of rhodopsin function.

Sung and colleagues suggested two distinct biochemical defects in rhodopsin-linked RP. Class I mutants (*F45L,* deletion *G344,* and *P347L*), localising in the C-terminus, resembled the wild-type rhodopsin in yields, regenerated with 11-*cis*-retinal, and were translocated to the plasma membrane, whereas class II mutations (*T17M, P23H, T58R, V87N, G89N, G106W, R135L, R135W, Y178C,*

and N190G), localised in the intradiscal, transmembrane and cytosolic domains, accumulated to lower levels, variably regenerating with 11-*cis*-retinal and were not transported to the plasma membrane, remaining primarily in the ER (Sung et al., 1991).

Expanding the previous classification and basing theirs on cellular and biochemical characteristics, Mendes and coworkers distinguished six classes of rhodopsin mutation, consisting of two major classes and four minor ones (**Table 1.1**) (Mendes et al., 2005). Class I mutations, clustered around the C-terminus, preserve normal rhodopsin folding, however, trafficking of the protein to outer segments is impaired. This class includes mutants such as *G344W* and *P347S* (Illing et al., 2002). Class II mutations, the most common autosomal dominant RP mutations (85%), localise within the intradiscal, transmembrane and cytoplasmic domains. They bind poorly with 11-*cis*-retinal and result in the improper folding of the opsin with subsequent retention of the protein within the endoplasmic reticulum (Hollingsworth and Gross, 2012). The resultant aggregation of mutant rhodopsin leads to congestion of the ER and the apoptosis through the proteasome pathway (Illing et al., 2002). Mutations such as *P23H* and *C187Y* fall into this class. Class III mutations, such as *R135*, hinder endocytosis and have a high affinity with arrestin, forming stable rhodopsin-arrestin complexes affecting the endosomal compartments and severely altering receptor-mediated endocytic functions (Chuang et al., 2004). Class IV, affecting the protein stability and post-translational modification, includes *T17M*. This mutation alters the glycosylation of the N-terminus of the mature rhodopsin by disrupting the NXS/T consensus sequence, making the

protein less stable and leading to sectoral RP with preferential degeneration of the inferior retina, which may result from increased sunlight exposure to this area (Tam and Moritz, 2009). Terminal signalling is affected in Class V mutations which includes those that alter the highly conserved glutamate/arginine sequence in the cytoplasmic domain of rhodopsin responsible for GDP release from the G-protein transducin. These mutations, such as *R135L*, result in a highly varied ability to activate transducin (Acharya and Karnik, 1996). The final class, Class VI, comprises the mutations of the lysine residue at position 296, which is responsible for the binding of 11-*cis*-retinal via the Schiff's base linkage. Such substitutions prevent the association of the apoprotein to 11-*cis*-retinal to form rhodopsin. *L296Q* is such a mutation leading to an intense level of transducin activation independently of light (Brill et al., 2007).

Table 1.1 Classification of rhodopsin mutations

The six classes of rhodopsin mutations, the affected cellular process, localisation of mutation in the rhodopsin molecule and known point mutations. (Adapted from Mendes et al. 2005.)

Class	Intracellular process affected	Localisation within the rhodopsin molecule	Mutations	Mis-folding
Class I	Transport to the ROS	C-terminus	*L328, T342, Q344, V345, A346, P347*	No
Class II	Proper folding and traffic from the ER	Intradiscal, transmembrane, cytosol domains	*T17, P23, G51, T58, V87, G89, G106, C110, L125, A164, C167, P171, Y178, E181, G182, C187, G188, D190, H211, C222, P267, S270, K296*	Yes
Class III	Endocytosis	Cytoplasmic domain	*R135*	No
Class IV	Protein stability and posttranslational modification	N-terminus	*T4*	No
Class V	Stimulation of the GDP releases from the G-protein transducin	Glutamate/ arginine sequence in the cytoplasmic d	*M44, V137*	No
Class VI	Binding of 11-*cis*-retinal	Lysine residue at position 296	*G90, T94, A292,*	No
Unclassified			*N15, Q28, L40, F45, L46, P53, G109, G114, S127, L131, Y136, C140, E150, P170, G174, P180, Q184, S186, T193, M207, V209, P215, M216, F220, E249, G284, T289, S297, E341*	

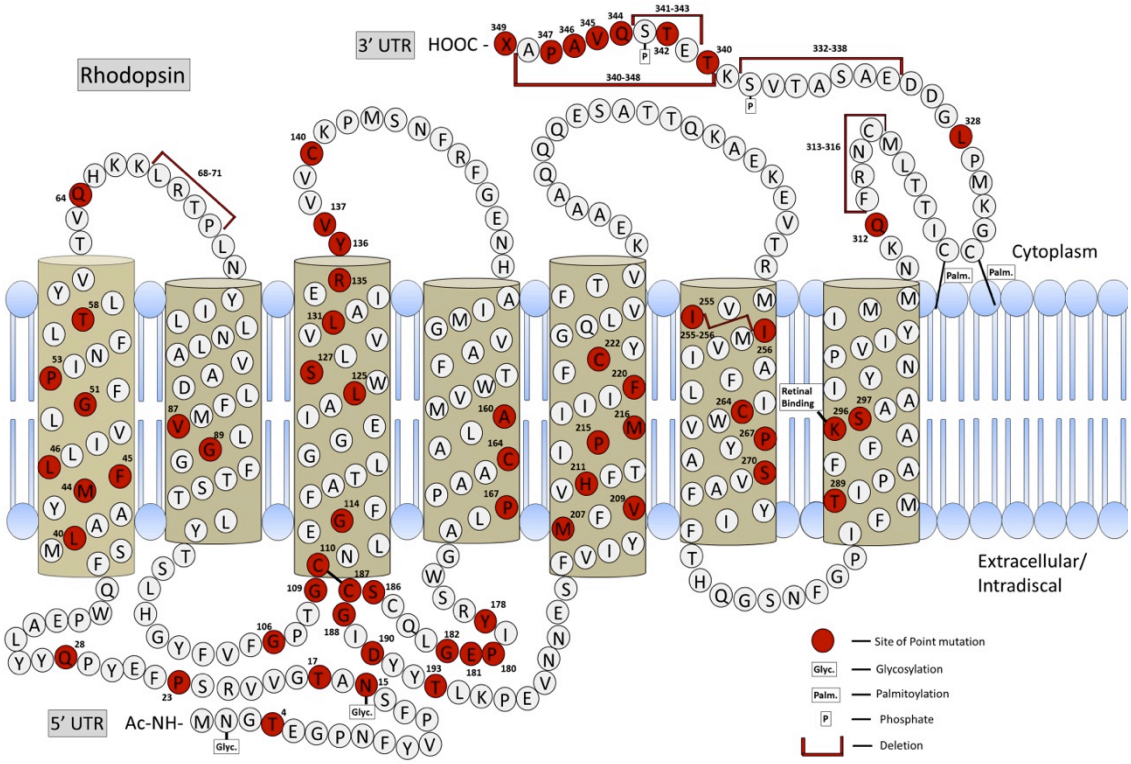


Figure 1.5 Secondary structure of rhodopsin with the sites of known point mutations Seven transmembrane helices are shown as boxed sections. Mutated residues are indicated by red circles. (Adapted from Mendes et al. 2005).

1.3.4 Types of mutation in rhodopsin-linked RP

The potential mechanisms of the retinal degeneration characteristic of rhodopsin-linked RP can be explained by the type of the causative mutation: loss-of-function, gain-of-function, dominant negative or combination of all the three (Wilson and Wensel, 2003).

1.3.4.1 Loss-of-function mutations

Loss-of-function mutations are usually recessive, but they can have dominant inheritance if the production of a protein from a single functional copy of a gene is not sufficient to maintain normal function, the gene is then called haploinsufficient. Haploinsufficiency occurs when both alleles are needed to produce wild-type levels of a protein, and haploinsufficient genes are sensitive to a loss of one allele (Huang et al., 2010). Rhodopsin knockout mice lack rod outer segments and develop progressive photoreceptor degeneration indicating that rhodopsin plays an important structural role by stabilising outer segments (Humphries et al., 1997). Data from the heterozygous rhodopsin knockout mice (having one single functional copy of the rhodopsin gene) indicate an abnormal phenotype, with the levels of rhodopsin assessed by Western blot decreased to 57% compared to the wild-type (Lem et al., 1999). Additionally, microspectrophotometry evaluating the specific density of individual rods estimated the concentration of rhodopsin within a single rod in the rhodopsin heterozygous (*Rho +/-)* mice to be reduced to 50% (Lem et al., 1999). A slow degeneration in the heterozygous mouse was confirmed by the observation of shortened of outer segments and the thinning of the ONL by one or two rows by

90 post-natal days. Furthermore, *Rho +/-* rods demonstrated an alteration in function with a reduced light sensitivity and increased levels of the protein phosducin by ~50% relative to wild-type levels (Lem et al., 1999; Liang et al., 2004). In another heterozygous rhodopsin model, Humphries and co-workers found that the ONL was thinner and the rod outer segments shorter in the 4-month old-retina compared with wild-type controls, and a closer examination of 8-week old animals revealed a clear disorganisation of rod outer segments (Humphries et al., 1997). The morphology and photoresponse kinetics of the *Rho +/-* rod outer segments, examined by transmission electron microscopy, demonstrated the following alterations: an elliptical disk shape (circular in wild-type), reduction of the disk surface area, and the presence of longer single incisures dividing the disk into two sectors. Single cell recording studies further showed that the overall light sensitivity of rod photoreceptors in the mutant mice was reduced (Makino et al., 2012). In the ROS, rhodopsin not only plays a signalling role, but also has an important structural function: because of its high concentration, it is absolutely essential for the development of ROS and disc membranes. Taken together, these data showing an altered phenotype, reduced levels of rhodopsin, and modified photoresponse kinetics in the rhodopsin heterozygous mice are indicative that the presence of both alleles is necessary for a healthy retina.

1.3.4.2 Gain-of-function mutations

Gain-of-function mutations arise when an altered protein has a novel activity which affects cell metabolism. One of most studied rhodopsin mutations is a substitution of proline at residue 23 for histidine (*P23H*) located in the N-

terminus of rhodopsin, within the intradiscal space. The *P23H* rhodopsin mutation is the most prevalent cause of rhodopsin-linked RP in the United States, suggesting a founder effect (Malanson and Lem, 2009). *In vitro* expression of the *P23H* mutant rhodopsin in cultured HEK293 and COS7 cells showed the mislocalisation of the misfolded protein, the formation of aggregates close to the centrosome and leading to the dispersal of the Golgi apparatus (Saliba et al., 2002). Given that protein folding is an elaborate process, changes in the primary amino acid sequence of rhodopsin can disequilibrate the folding efficiency leading to the retention of misfolded products within cell compartments, such as ER.

1.3.4.2.1 ER stress

Since the ER carries out essential cellular functions such as lipid synthesis and calcium ion storage, the accumulation of misfolded rhodopsin stimulates the formation of complexes with the ER-resident chaperones GRP78 (BiP) and GRP94 which is turn activates a cellular stress reaction, the unfolded protein response (UPR). The UPR is directed to restore normal function of the cell by blocking protein translation and triggering the signaling pathways that raise the production of molecular chaperones involved in protein folding (Tzekov et al., 2011). The increased levels of molecular chaperones enable cell survival by reducing misfolded protein levels (Bernales et al., 2006). However, when ER-stress is not alleviated by the UPR, the final common pathway leading to the retinal degeneration, apoptosis or cell death, is initiated (Schröder and Kaufman, 2005; Szegezdi et al., 2006).

1.3.4.2.2 Cell death in retinal degenerations

Classical apoptosis involves the caspase-mediated pathway through caspase-3 as the prototypic mediator and executioner (Jellinger, 2006), which was found to be activated in transgenic rats carrying the S334T rhodopsin mutation (Liu et al., 1999). However, in *P23H* rats caspase-3 was not significantly higher than in age-matched wild-types, indicating that caspase-3 was not implicated in the apoptosis observed in this model (Kaur et al., 2011). The non-classical apoptosis pathway involves the calpains — the cysteine proteases synthesized as inactive pro-enzymes and activated by an increase in intracellular calcium levels. Activated calpains induce apoptotic factors such as caspase-12 and AIF (apoptosis-inducing factor). The active form of caspase-12 translocates to the nucleus and activates apoptosis through other caspases. The inactive form of AIF is localised to the mitochondrial intermembrane space. After its activation, AIF translocates to the nucleus where it participates in chromosome fragmentation and eventual cell death (Marigo, 2007).

In *P23H* rats, calpastatin down-regulation corresponded to the up-regulation of calpain activity strengthening the view of calpain activation as an important step in rhodopsin-linked retinal degeneration (Kaur et al., 2011). Furthermore, the ablation of caspase-12 in caspase knock-out mice with the rhodopsin mutation T17M prevented the decline in ERG amplitudes for up to three months confirming the role of caspase-12 in the pathway leading to rhodopsin-linked retinal degeneration (Bhootada et al., 2015).

1.3.4.3 Dominant negative mutations

Dominant negative mutations usually involve genes which encode proteins forming multimeric complexes with themselves, or with other products. In dominant negative mutations, the altered protein acts antagonistically to the wild-type product (Herskowitz, 1987). Similar to almost all other GPCRs, rhodopsin forms dimers and oligomers in the disc membranes of rod outer segments (Fotiadis et al., 2003; Liang et al., 2004; Park et al., 2004). If a mutant rhodopsin can dimerize, it may interfere with the normal protein altering its function. Co-expression of *P23H* rhodopsin with wild-type rhodopsin in COS-7 cells disrupted the processing of the normal protein and led to the formation of intracellular proteinaceous aggregates containing both the wild-type and mutant protein (Saliba et al., 2002). Furthermore, the *P23H* mutant protein impaired the delivery of wild-type protein to the plasma membrane and enhanced proteasome-mediated degradation and the steady-state ubiquitination of normal protein in HEK293 cells (Rajan and Kopito, 2005), suggesting a dominant negative mechanism.

Frederick and coworkers showed that the presence of the wild-type rhodopsin slowed down the retinal degeneration in the *P23H* mouse (Frederick et al., 2001). In the transgenic mouse with no wild-type rhodopsin, only 20% of the ONL remained at postnatal day 30; in mice with one copy of wild-type rhodopsin, 50% of the ONL remained; in the mice with two copies of wild-type rhodopsin there was no reduction of the ONL by postnatal day 30; however, by postnatal day 90 the ONL was completely degenerate in all groups of mice. These data showed that an increase in the ratio of wild-type/mutant rhodopsin

can diminish the damage to photoreceptors.

Price also demonstrated that the dominant-negative effects of the *P23H* rhodopsin mutation can be largely overcome by increasing the levels of the wild-type protein: the transgenic *P23H* mouse with three copies of wild-type rhodopsin showed an initial loss of the ONL from one to three postnatal months and then the degeneration markedly slowed down, such that no loss was detected from month 3 to month 6 (Price et al., 2012).

Taken together, these data suggest that certain rhodopsin mutations, which initially were thought to be gain-of-function type, have some features of dominant negative and loss-of-function types of mutation and may benefit from the delivery of wild-type rhodopsin

1.3.5 Secondary cone degeneration in RP

Although the genes leading to RP are expressed exclusively in rods, and the early stages of the disease are characterised only by rod degeneration, it is the secondary cone degeneration which follows rod loss at later stages of RP which eventually leads to functional vision loss and blindness (Carter-Dawson et al., 1978; Jiménez et al., 1996; Ogilvie et al., 1997). Even if rods largely outnumber cones, humans rely predominantly on cone photoreceptors for their daily tasks as cones mediate high-resolution daylight colour vision, and most of us spend time in lighted conditions. With this regard, the secondary cone loss and associated blindness is most debilitating for RP patients and significant research effort has been spent in understanding its mechanisms. Today, there is no known rod degeneration which is not followed by cone loss, except in

stationary rod diseases (such as congenital stationary night blindness) (Punzo et al., 2009). In contrast, rods do not degenerate in cone diseases (for example, in CNGA3 cone degeneration), suggesting that this particular dependence of cones on rods for survival is unique and not interchangeable (Koenekoop, 2009).

Although the mouse and human retina are disparate anatomically as the human retina has a fovea, a central zone in the retina rich in cones and devoid of rods; the studies on mice provided some insight into the molecular pathways of secondary cone loss. An accurate understanding of these mechanisms, which represent the major cause of vision loss in RP patients, may allow for the development of novel therapies which may at least delay photoreceptor degeneration providing patients with additional years of useful vision.

1.3.5.1 Endotoxins release and the Muller cells activation

It has been suggested that dying rods excrete toxic agents into the extracellular milieu, which in turn induces apoptosis of neighbouring cones. Two putative substances have been proposed as key factors – glutamate, and the products of apoptosis (Ripps, 2002). Glutamate, an excitatory amino acid and excitotoxin which had been implicated in a number of neurodegenerative diseases, has been found in higher concentrations in the degenerate retina (Ulshafer et al., 1990). However, retinal Muller cells possess a highly efficient glutamate uptake system which maintains extracellular glutamate levels below the neurotoxic threshold (Sarantis and Attwell, 1990), making glutamate release an unlikely candidate (Bush et al., 1995). The mechanism involving the release of toxic

products of apoptosis by degenerating rods was studied by Kedzierski and colleagues on the hemizygous-transgenic *rds* mouse which demonstrates mosaic expression of the *rds* transgene due to its integration into the X-chromosome. It was expected that the expression of the transgene would lead to the rescue in the areas expressing it, however, a significant photoreceptor cell loss was observed in both transgene-expressing and non-expressing patches. This phenomenon of propagation was explained by the toxic products released by genetically damaged cells being propagated to genetically healthy cells (Kedzierski et al., 1998). However, release of apoptotic factors by dying rods does not explain the observed delayed loss of cones (Ma et al., 2015).

A proposed mechanism involving Muller glial cells suggested that the quiescent retinal microglia once activated, move to the impaired area and phagocytose cellular fragments, killing adjacent otherwise healthy cone photoreceptors around the area of primary damage due to the release of toxic factors such as nitric oxide, reactive oxygen species and others, thus producing a 'bystander' effect (Gupta et al., 2003). Again, as some cones survive longer than rods in rod degenerations, this theory can only partly explain secondary cone loss.

1.3.5.2 Oxidative stress

Photoreceptors, which consume large amounts of oxygen, are supported by the choroid vasculature which lacks autoregulation in response to fluctuations in tissue oxygen concentration. Rod photoreceptors being, by far, more numerous than cones, consume a greater share of oxygen, and therefore, after rod loss, the unadjusted choroidal circulation provides the same oxygen delivery and

leads to hyperoxia and oxygen overload in the ONL. It has been proposed that subsequent cone damage may result from oxidative stress (Yu et al., 2000). Immunostaining for specific biomarkers of lipid peroxidation, such as acrolein and 4-hydroxynonenal-adducts revealed their presence in cone axons and bodies in a transgenic pig model of RP supporting the hypothesis of hyperoxia leading to cone loss (Shen et al., 2005). An increase in the levels of antioxidants, such as the coexpression of superoxide dismutase 2 and catalase significantly promoted cone survival and maintenance of cone function in the *rd*10 mice, without slowing down rod cell death, confirming the role of oxidative stress in secondary cone degeneration (Usui et al., 2009). However, this protective role of antioxidants was shown only in the *rd10* and not in the *rd1* mouse assessed in the study, which may be suggestive of a model-dependent effect.

To assess the potential of antioxidative treatment, Xiong and colleagues used AAV vectors to deliver nuclear factor erythroid-derived 2 (*NRF2*) gene to cone cells in three different mouse models of RP. NRF2 is a master antioxidant transcription factor which globally regulates antioxidant defence responses (Xiong et al., 2015). NRF2 promoted cone survival by boosting cone numbers and cone function as detected by the optomotor assay. Furthermore, photopic ERG measurements which reflect mass cone responses were higher in the treated eye at P40. Taken together, these data provide compelling evidence for the role of an oxidative component in the secondary cone loss observed in RP and open potential avenues for treatment.

1.3.5.3 Loss of structural support

Given that the outer nuclear layer (ONL) of the entire murine retina and the periphery of the human retina is composed mostly of rod cells (Jeon et al., 1998; Masland, 2001), the lack of architectural support from degenerated rod cells was suggested to compromise the survival of cones leading to their subsequent loss. However, applying this theory to the human fovea, where most of the photoreceptors are cones, would require recruitment of additional pathways of cone damage.

1.3.5.4 Nutrients deprivation

Another theory explaining the cone demise in rod degenerations suggested that a shortage of nutrients induced by the reduction of nutrient flow from the adjacent cell layer and the RPE leads to cone starvation, which can be identified on a molecular basis. The implication of the metabolic insulin/mTOR pathway in secondary cone loss was interpreted as a sign of cone starvation and nutrient shortage by Punzo and co-workers (Punzo et al., 2009). The insulin/mTOR (mammalian target of rapamycin) pathway is a signalling pathway regulating the cell's growth and proliferation depending on nutrient availability: in an environment rich with energetic nutrients, this pathway enables energy-consuming processes such as protein synthesis, whereas in energy deficient conditions, the mTOR pathway represses such processes and autophagy may be initiated (Reiling and Sabatini, 2006). The assessment of the RNA expression array of 195 genes in 4 different models of secondary cone loss showed that the highest number of hits (12 genes) involved genes of the

insulin/mTOR signalling pathway. To further assess whether the activation of the insulin/mTOR pathway through the glucose-dependent mechanism can prolong cone survival, a fast-progressing mouse model of RP, *rd1,* was administered daily injections of insulin. As a result, treated animals demonstrated increased survival rates compared to the untreated group, however the rescue effect was short-lived, not exceeding 4 weeks (Punzo et al., 2009).

To evaluate the potential long-term effect of the insulin/mTOR pathway on delaying cone degeneration, the group of Claudio Punzo studied the effects of constitutive activation of mTOR complex 1 (mTORC1), which resulted in enhanced uptake, retention and utilization of glucose as well as increased levels of the key metabolite NADPH. The demonstrated cone survival rate from the activation of mTORC1 opens new potential avenues for therapeutic intervention aiming to prolong vision in humans affected by RP (Venkatesh et al., 2015).

However, the theory implicating the insulin/mTOR pathway in secondary cone degeneration does not explain how a state of nutrient deficiency arises in the rod-depleted retina in the first place. Furthermore, it remains unclear whether the involvement of the insulin/mTOR pathway could be a biomarker reflecting poor cell health and being triggered by another upstream pathway.

1.3.5.5 Rod-derived trophic factors

An additional mechanism of rod-cone interaction suggests the release of neurotrophic agents by healthy rod photoreceptors: once dying rods stop

producing them, cone demise follows. The presence of such factors was suggested when it was shown that transplantation of healthy photoreceptors into the degenerating retina before cone loss delays cone degeneration. (Mohand-Said et al., 1998). Later, Leveillard and colleagues, by analysing the cDNA expression cloning library secreted from rods, identified a trophic factor promoting cone survival, named the Rod-derived Cone Viability Factor (RdCVFs) (Léveillard et al., 2004). Subsequently, the RdCVF receptor, Basigin-1, was found to interact with the glucose transporter GLUT1, both being expressed within inner segments of photoreceptors and increasing glucose transport and concomitant aerobic glycolysis (Aït-Ali et al., 2015). The intravitreal delivery of *AAV9-RdCVFL* (containing the full-length isoform of RdCVF) slowed down cone loss as demonstrated by the counting of immunofluorescence-labelled cone outer segments. However, cone ERG responses after an initial increase were found to be no different than those recorded in sham-treated eyes 6 weeks post injection. Interestingly, rhodopsin mRNA levels detected by qRT-PCR in animals injected systemically with AAV9-scCAG-RdCVFL were increased compared to sham-injected animals, suggesting that RdCVF also promotes rod survival (Byrne et al., 2015). Although these results suggest that RdCVF and its long isoform function as neurotrophic factors delaying the loss of photoreceptors, as rod survival was not fully addressed in this study, more research is required to exclude the possibility that the effect of these molecules on cone longevity is simply through an enhancement of rod survival.

Given that such a multitude of potential causes for secondary cone loss has been suggested, it is possible that a combination of various molecular pathways contribute to different degrees to the observed cone demise, making the development of a treatment highly challenging. One of the aims of this research project was to evaluate the effects of treating a primary genetic defect in rod photoreceptors on secondary cone degeneration.

1.4 Gene therapy for retinal degenerations

Gene therapy implies the delivery of nucleic acids into target cells with a therapeutic goal. The success of gene transfer is dependent on the efficiency and safety of delivery vectors. Delivery modality may be broadly classified as viral or non-viral.

Over last decades, the adeno-associated virus (AAV) has emerged as a highly attractive gene transfer vector, its main advantages including the ability to mediate long-term gene expression in non-dividing cells and a high safety profile (Gaj et al., 2015; Kotterman and Schaffer, 2014). Over 20 clinical trials using AAV for gene therapy have been conducted world-wide to date, including those for hemophilia B (Nathwani et al., 2011, 2014), Leber's congenital amaurosis type II (Bainbridge et al., 2015; Bennett et al., 2012), choroideremia (MacLaren et al., 2014), lipoprotein lipase deficiency (Stroes et al., 2008) and many other monogenic diseases.

Inherited retinal degenerations represent an ideal target for gene therapy as they are exclusively caused by a single mutation in one of more than 200 genes expressed in photoreceptor or RPE cells. Furthermore, the eye is an immune-privileged site minimising the risk of immune reactions directed against a gene vector and any effects of the therapy can be safely and non-invasively assessed through the transparent ocular media by a variety of readily available ocular examinations methods. The advantage of the eye as a target of gene therapy was evidenced by the success of the first clinical trials to deliver gene therapy via AAV vectors into RPE cells (Bainbridge et al., 2015; Bennett et al., 2012).

1.4.1 General AAV biology

AAV is a small (25nm), non-enveloped, icosahedral single-stranded DNA parvovirus which requires coinfection with a helper virus, such as an adenovirus or herpes simplex virus, for its replication. The wild-type AAV viral genome is 4,679 bp (Srivastava et al., 1983) in length and contains the following open reading frames: *rep*, required for DNA replication, and *cap*, encoding the three structural proteins of the viral capsid and a protein needed for capsid assembly in the nucleolus (**Figure 1.6**) (Sonntag et al., 2010). Inverted terminal repeats (ITRs) flank either side of the viral genome and contain palindromic sequences that form internal T-shaped base-paired hairpin structures. These motifs form specific binding sites for Rep proteins and serve as the *cis*-priming sites required for DNA replication.

1.4.2 AAV vector design

Therapeutic AAV vectors are designed by modifying a wild-type virus genome by replacing the *rep* and *cap* genes with a transgene cassette, which usually includes a promoter, therapeutic transgene (usually a cDNA sequence) and poly-adenylation (poly-a) signal (**Figure 1.6**). The ITRs are left intact to flank the transgene cassette as they are the *cis*-sequences necessary for packaging during AAV production and they are responsible for the episomal persistence of AAV-delivered DNA. The total packaging capacity of AAV, excluding the ITRs, is ~4.4 kb, which makes possible the use of AAV vectors for the delivery of small-sized genes.

1.4.2.1 Capsid pseudotyping

The viral capsid is assembled with three structural proteins at a ratio VP1:VP2:VP3 of 1:1:10 into 60 subunits arranged in T = 1 icosahedral symmetry. The monomeric motif of AAV is an eight-stranded antiparallel β-barrel motif (jelly-roll β-barrel) (Chapman and Rossmann, 1993). The AAV capsid has long interstrand loops comprising the β-ribbons and elements of secondary structure that form the surface features of the capsid (Van Vliet et al., 2008). The externally exposed loops, associated with antigenicity, have high sequence variability, whereas the inner surface residues of the capsid are more highly conserved (Chapman and Rossmann, 1993).

A significant advance in AAV design was attained with the production of recombinant AAV vectors. These are produced by cross-packaging the prototypic AAV2 genome into the capsids of multiple different variants of AAV

isolated from various species; conventionally, they are usually designated as AAV2/8 or AAV2/5, with the first number reflecting the serotype of ITRs and the second number, the capsid serotype.

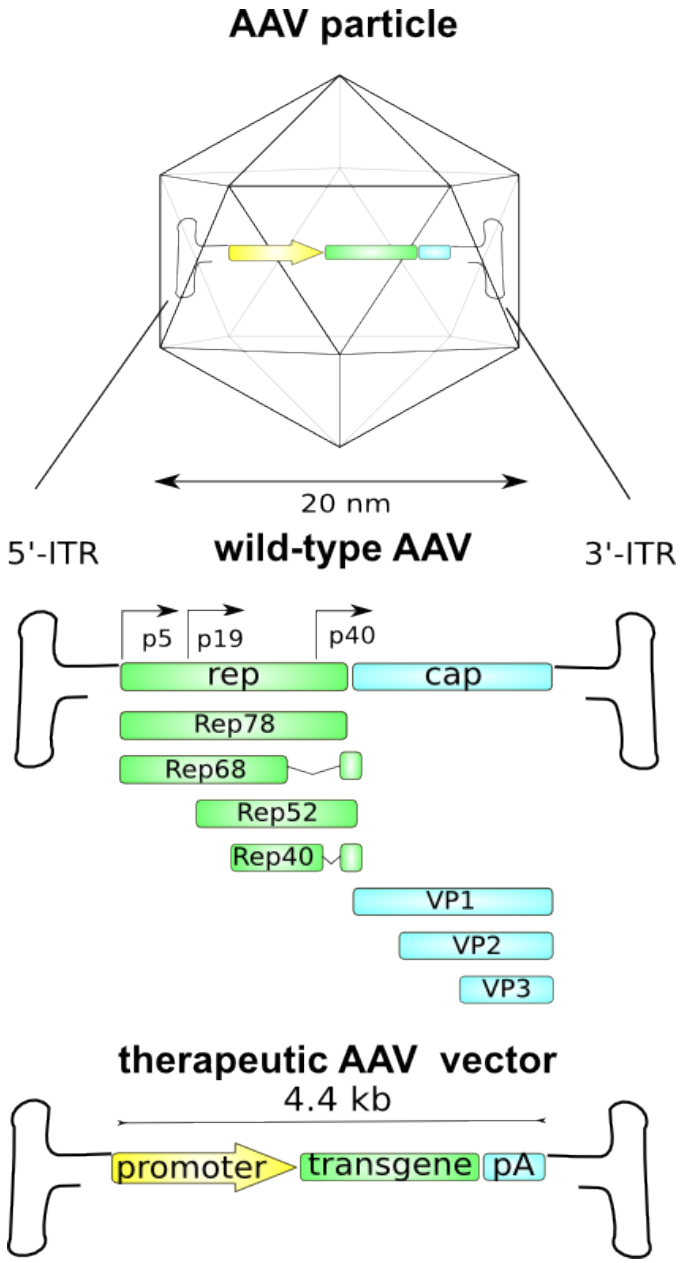


Figure 1.6 Schematic of AAV vector design

The AAV particle consists of a 20 nm icosahedral capsid containing the single-stranded AAV genome. The wild-type AAV genome, containing the *rep* and *cap* opening reading frames, is flanked by hairpin-like structures – the Inverted Terminal Repeats (ITRs). The *rep* gene encodes for four non-structural proteins: Rep78, Rep68, Rep52 and Rep40 and contains promoters p5, p19, p40 (depicted by arrows), the *cap* gene encodes for capsid viral proteins (VP): VP1, VP2, VP3.

A therapeutic AAV vector is made by inserting a transgene cassette between two wild-type ITRs. A transgene cassette typically comprises a promoter, transgene and polyadenylation sequence (pA). The carrying capacity of AAV vector is approximately 4.4 kb (excluding ITRs).

1.4.3 Limiting steps for AAV transduction

The desired outcome of AAV-based gene therapy is to attain high expression from the vector. During their passage through the cell to the nucleus, AAV virions encounter several hurdles, which may severely limit the subsequent expression from their genomes. These include cell binding, intracellular trafficking and conversion to double-stranded DNA.

1.4.3.1 Cell binding and capsid serotypes

The first step in AAV infection is the binding of viral particles to the cell's surface via one or more receptors. As AAV2 was the first identified serotype, initial studies focused on AAV2 cellular receptors. AAV2 primarily attaches to heparin sulphate proteoglycan (HSPG) receptors, with the following co-receptors for optimal binding: fibroblast growth factor receptor 1, integrin aVb5, integrin a5b1, laminin receptor and hepatocyte growth factor receptor. Other AAV serotypes use other distinct receptors for binding: AAV8 attaches to the 37/67 kD laminin receptor (LamR) whilst AAV9 binds to N-linked galactose (Nonnenmacher and Weber, 2012). Studies comparing the transduction efficiency after the subretinal delivery in mice showed AAV8 vectors were more efficient in transducing photoreceptors than AAV2 and AAV5 (Natkunarajah et al., 2008).

1.4.3.2 Intracellular degradation of viral vectors

Another step limiting transduction potency involves intracellular degradation of viral particles. During AAV intracellular trafficking, the exposed surface tyrosine

residues in the capsid undergo phosphorylation which marks them for subsequent ubiquitination and proteasomal degradation. This process may significantly reduce transduction efficiency (Zhong et al., 2008a). An improvement in the expression of the transgene protein was observed when the capsid tyrosine residues were substituted for phenylalanine, resulting in inhibition of the ubiquitination and subsequent proteasomal degradation of the viral capsids This allowed a ten-fold reduction in the dose of mutated capsid AAV to achieve the same level of transduction as with non-mutated AAV. (Zhong et al., 2008b). Furthermore, Petrs-Silva et al. established that the capsid mutant AAV8, named AAV2/8^{Y733F} achieved not only higher, but also more widespread transduction compared to non-mutated AAV2, AAV2/8 and AAV2/9 in subretinal injections in mice (Petrs-Silva et al., 2009). The current project made use of these advancements in the AAV vectorology by using the AAV2/8^{Y733F} serotype to package the therapeutic vector.

1.4.3.3 Conversion to double-stranded DNA

Upon reaching the nucleus, the AAV genome is released from its capsid, however, as the viral DNA is single-stranded (ssDNA), it needs to be converted into double-stranded DNA (dsDNA) in order to be transcriptionally active (Ferrari et al., 1996). This conversion to dsDNA is regarded as a significant rate-limiting step in the AAV viral transduction and it is thought to contribute to the partial loss of gene expression (Ferrari et al., 1996; Fisher et al., 1996). Two potential mechanisms of this conversion were suggested: the first - the synthesis of the complementary second DNA strand (McCarty, 2008; Zhong et al., 2008c; Zhou et al., 2008); and the second - the annealing of the plus and

minus DNA viral strands from two infecting viruses, which does not require DNA synthesis (Nakai et al., 2005).

The first mechanism, the synthesis of complementary DNA strand, is enhanced by either the presence of adenovirus, which provides the adenoviral DNA polymerase required for the conversion, or the treatment with genotoxic agents (such as ionizing radiation, hydroxyurea, UV, topoisomerase inhibitors), which induce the host-cell's DNA polymerase. However, the use of these enhancers in the clinical setting is severely limited as adenovirus is highly immunogenic and the use of genotoxic agents can compromise even further already degenerate cells.

An alternative mechanism for conversion to double-stranded DNA involves base-pairing (annealing) of plus and minus strands from two infecting particles. This strand annealing mechanism is possible due to the equal packaging of either plus or minus strand into the AAV capsid during virus production (Berns and Adler, 1972). To demonstrate that strand annealing is the primary mechanism of conversion to dsDNA, Nakai and his colleagues, in an experiment on mouse liver *in vivo,* used adenine-methylated DNA in AAV vectors as a molecular marker to recognize the input molecules for newly synthesized DNA. Given that eukaryotic cells lack methylases, all methylated DNA was supposed to be originated from the administered AAV genomes. As 99% of the AAV genomes were found to be methylated, the authors concluded that strand annealing and not the second strand DNA synthesis was the primary conversion mechanism (Nakai et al., 2000). However, this annealing of the plus and minus strands requires a high multiplicity of infection to assure that

each transduced cell has a sufficient number of copies of both positive and negative strands, placing additional limitations on transduction efficiency (McCarty, 2008).

The process of converting single-stranded viral DNA to double-stranded DNA results in a lag in the transduction peak. Indeed significant transgene expression using ssAAV2 is not observed until 1–2 weeks, reaching a plateau at week 4–6 (Miao et al. 2000; J. Wang et al. 2007). This delay in the expression of a therapeutic protein can result in additional damage in rapid degenerations that could be avoided if this conversion step can be overcome.

1.4.4 Self-complementary AAV

A way to circumvent the double-stranded DNA conversion step and thus enhance transduction was found with the discovery of dimer AAV molecules, the self-complementary hairpin-like genomes produced as a byproduct of conventional AAV vectors. They were subsequently called self-complementary AAVs (scAAV). These dimers, representing only a small fraction in a conventional AAV preparation, were generated for AAVs with a genome half the size of a wild-type AAV (Hirata and Russell, 2000; McCarty et al., 2001). An additional improvement in scAAV production was achieved when Wand and colleagues showed that the deletion of the D-sequence in the terminal resolution site in one of the ITRs prevented monomer formation and dramatically increased (>90%) the yield of dimeric genomes (Wang et al., 2003).

1.4.4.1 Mechanism of scAAV production

scAAVs are produced by altering the replication process during AAV production. During a normal replication, DNA polymerase (either from helper virus or the host cell) makes a complementary strand thus forming a duplex DNA molecule cross-linked at one end by the terminal hairpin. Subsequently, the Rep protein (78/68) binds to the ITR, and, acting as an endonuclease, nicks the original parental strand at the terminal resolution site (TRS), thus creating two separate DNA molecules. The process is completed by the synthesis of a terminal ITR on each molecule (Snyder et al., 2011).

In scAAV production, during the replication process, the host replication machinery begins DNA synthesis at the end containing the wild-type ITR; once it reaches the mutant ITR lacking the terminal resolution site, the resolution of strands is impossible, so the DNA machinery continues to the other end of the genome containing the wild-type ITR, where upon meeting of the terminal resolution site, DNA synthesis terminates (**Figure 3.1**). The final product is the DNA molecule containing two self-complementary halves and linked by the mutant ITR in the middle and the wild type ITRs at the each end of the genome. Inside a viral capsid the scAAV genome is packaged as ssDNA. Upon entry into the nucleus, the self-complementary genome anneals on itself and forms a dsDNA hairpin molecule (McCarty, 2008).

1.4.4.2 Packaging capacity of scAAV

The packaging capacity of a canonical AAV vector (4.4 kb without ITRs) restricts the choice of RP mutations which can be targeted using AAV gene

therapy, as the size of the cDNA of causative genes cannot exceed about 4 kb. Given that the scAAV genome contains two self-annealing halves, the gene cargo of scAAV is reduced even further to 2.2 kb. Wu and his co-workers suggested that the maximum packaging capacity of scAAV2 could be stretched to 3.3 kb (Wu et al., 2007), however, his group later demonstrated that the use of oversized AAV2 DNA sequences led to the encapsidation of subgenomic or defective viral genomes (Wang et al., 2012). The limited packaging capacity of scAAV demands careful design of the transgene cassette using the minimal possible size of each constitutive element, such as the promoter and transgene.

1.4.4.3 Transduction superiority of scAAV compared to ssAAV

Although the design of scAAV reduces the carrying capacity by two-fold, by circumventing the conversion to dsDNA step and generating an immediate release of transcriptionally active dsDNA (**Figure 1.7**), scAAVs possess a dramatically increased transduction efficiency (reportedly 10-100 fold) and speed of expression onset compared to ssAAVs which have been confirmed in numerous studies (for review see McCarty, 2008). Long-term transduction superiority was illustrated by the intramuscular injection of equal doses of sc- and ssAAV vectors in mice, showing robust gene expression from scAAV throughout the entire 6-month time course at a level a minimum of 15 times that of ssAAV (Nathwani et al., 2006). In trabecular meshwork cells, a challenging target for the conventional AAV, scAAV2-GFP injection in rats resulted in the appearance of fluorescence as soon as 4 to 9 days after injection, maintained for >3.5 months, whereas the AAV2-GFP injection did not show any GFP transduction from 1 week to 27 days after injection (Buie et al., 2010). In non-

human primates, liver transduction levels of the transgene product achieved with scAAV2/8 were 20- to 35-fold higher, and with scAAV2/7 vectors, 80- to 120-fold higher, compared to the ssAAV counterparts by 6 weeks (Gao et al., 2006). ScAAV5.smCBA.GFP injected subretinally achieved fluorescence at day 3, whereas ssAAV5.smCBA.GFP required 14 days to achieve similar expression levels in the RPE cells. Additionally, scAAV resulted in pronounced expression in photoreceptors and other retinal neurons (Yokoi et al., 2007).

To summarize, data comparing scAAV to ssAAV, are highly indicative that scAAV possess higher transduction qualities as well as a faster onset of transduction compared to equivalent ssAAV irrespectively of the capsid type and transgene. In this research project, the scAAV vector design was used in engineering the therapeutic vector.

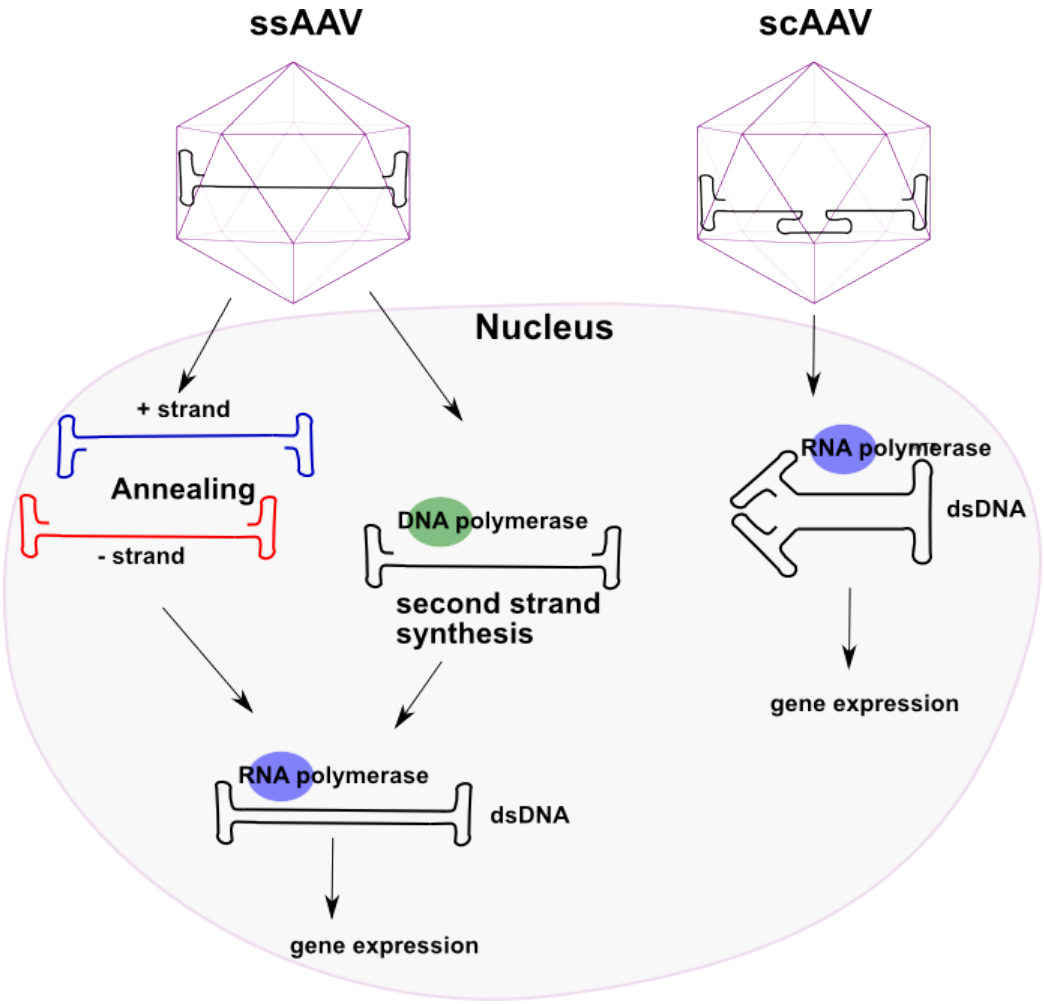


Figure 1.7 scAAV circumvents the double DNA conversion step
The genome of a single-stranded AAV (ssAAV, on the left) is transcriptionally inactive and needs to be converted to double-stranded DNA (dsDNA). This conversion is achieved by two mechanisms: either through annealing of '+' and '-' strands or the synthesis of the second DNA strand by the host-cell DNA polymerase. Following the conversion, the double-stranded viral genome can be transcribed and translated into a protein.
The scAAV genome (on the left) is packaged as a single-stranded DNA molecule inside the viral capsid. Upon uncoating, it undergoes a rapid self-annealing process facilitated by the base-paired structure of its genome. The produced transcriptionally active dsDNA is immediately available for transcription and subsequent translation.

1.4.5 Tissue tropism of AAV gene therapy

One of the major determinants of gene therapy's success and safety is targeting it to correct cell types and avoiding expression in bystander cells. The tropism of an AAV vector can be modified in several ways: the mode of delivery, choice of promoter and AAV capsid.

1.4.5.1 Mode of delivery

The two classical routes of delivery of gene therapy to transduce retinal cells are intravitreal and subretinal (Liang et al., 2001). Intravitreal injection is considered less traumatic as it does not require the production of a retinal detachment. Further, it is easier to perform as it does not necessitate the penetration of the choroid (in animals) or the retina (in humans). Moreover, the intravitreal approach is particularly desirable in targeting photoreceptors as it permits a more widespread and evenly distributed transduction. Modifying the viral capsid proteins has permitted the use of photoreceptor-targeted AAV vectors via the intravitreal injection, however, the transduction efficiency in primate photoreceptors is still too low for use in gene therapy targeting the outer retina (Dalkara et al., 2013; Kay et al., 2013). Furthermore, diffusion of the therapeutic vector is limited by several anatomical barriers, such as the vitreous, inner limiting membrane, and inner retina. In another route of delivery - the subretinal injection, the therapeutic agent is released into the subretinal space between the photoreceptors and the RPE. Because of the high efficiency of transduction in the gene therapy delivered by a subretinal injection, demonstrated in numerous studies (Bainbridge et al., 2008; Hauswirth et al.,

2008; Maguire et al., 2009), this route of administration became the route of choice to target the RPE and photoreceptors (Colella and Auricchio, 2012) and it was used in this study.

1.4.5.2 Promoter choice

Promoters generally used in gene therapy can be categorised into two groups: ubiquitous and tissue-specific. The ubiquitous promoters are usually potent promoters often including viral enhancers to boost transduction rates, however, they lack tissue-specificity and will transduce most cells within the area of injection. Initially, potent and powerful ubiquitous promoters such as the immediate-early cytomegalovirus (CMV) enhancer-promoter (Du et al., 1996) and the CAG promoter (a hybrid of CMV enhancer, chicken beta-Actin promoter and rabbit beta-Globin intron) (Sawicki et al., 1998) were widely used to induce transduction. These promoters however transduce many types of cell within the retina. Ideally, the expression of a transgene protein in off-target cells should be be avoided to increase the safety of treatment.

To target photoreceptors, the constitutively expressed cell-specific promoters such as the rhodopsin kinase and rhodopsin promoter gained in acceptance. Given its small size (292 bp), the human rhodopsin kinase is an ideal promoter for scAAV. However, it targets both types of photoreceptors: rods and cones (Boye et al., 2012). Whereas similarly the murine rhodopsin promoter has been shown to target both rods and cones in the murine retina (Glushakova et al., 2006), it appeared to be rod-specific in the canine retina (Beltran et al., 2010). The rhodopsin promoter was found to be more potent than the ubiquitous promoters CMV, CAG (10-13 fold) and rhodopsin kinase promoter (24-fold) in

transducing murine photoreceptors (Allocca et al., 2007). Another study found the rhodopsin promoter to be 5-fold more efficient than the CMV promoter in mice (Palfi et al., 2010).

1.4.5.3 AAV capsid modification in directing tropism

Another way to manipulate viral vector targeting is the use of different AAV variants - pseudotyping. Over 100 serotypes have been identified so far, with the most variability found in the surface exposed regions of the capsid. Given that the capsid proteins use different molecular receptors to bind to host cells, various serotypes show different tissue tropism. AAV2/8 was identified as one of most efficient serotypes for photoreceptor transduction in mice (Allocca et al., 2007), pigs (Mussolino et al., 2011) and non-human primates (Vandenberghe et al., 2011). Furthermore, AAV8 capsid protein proved to be less immunogenic than AAV2 (Vandenberghe et al., 2006) and uncoated earlier resulting in a more rapid onset of expression (Thomas et al., 2004).

1.4.6 AAV gene therapy in clinical trials

AAV was discovered accidentally over 50 years ago (Atchinson et al., 1965) and over past decades, a wealth of research has propelled AAV into becoming the most attractive gene therapy vector, already assessed in a number of prominent clinical trials.

The first three clinical trials on gene therapy in inherited retinal degeneration investigated the effects of the AAV-delivered *RPE65* gene in Leber's congenital amaurosis (LCA) (Bainbridge et al., 2008; Hauswirth et al., 2008; Maguire et al.,

2008). LCA is a severe, early onset form of RP and RPE65 is a protein responsible for recycling the all-*trans*-retinol chromophore. The trials demonstrated the excellent safety of AAV delivery, as well as improvements in some measures of vision (such as best-corrected visual acuity, kinetic visual field, nystagmus testing, pupillary light reflex, microperimetry, dark-adapted perimetry, and dark-adapted full-field sensitivity testing). Long-term follow-up confirmed safety and efficiency of the gene therapy (Bainbridge et al., 2015). In addition, functional magnetic resonance imaging (fMRI) evaluation demonstrated a correlation between preserved light sensitivity and the cortical projection zone of the pseudo-foveas developed in treated retinal regions (Cideciyan et al., 2015). Along with these positive results, however, Jacobson and colleagues reported that in three treated patients sustained improvement in visual sensitivity over three years was followed by subsequent reduction of the areas of improved vision (Jacobson et al., 2015). Similarly, Bainbridge and coworkers reported a peak in visual sensitivity 6-12 months after treatment with a subsequent variable decline of the initial improvement, excepting one of 12 patients (Bainbridge et al., 2015). This decline in function was explained by various mechanisms including ongoing degeneration of photoreceptors and the treatment not fully meeting the demand of RPE65 protein. Another clinical trial, using *AAV2.REP1* in choroideremia patients, casts a more optimistic outlook, as the latest results showed that the early improvements in visual acuity in two of the six patients were sustained at 3.5 years after the treatment. The other four patients, possessing good visual acuity at the baseline, did not have scope for improvement (Edwards et al., 2016; MacLaren et al., 2014). The successes of AAV gene therapy in recessive forms of RP highlight the potential of bringing

the treatment to dominant forms of RP with their larger share of patients. Other ongoing clinical trials include those targeting the following diseases: Stargardt disease (the *ABCA4* gene), X-linked retinoschisis (*RS1*), Usher syndrome 1b (*MYO7A*) and *MERTK*-linked RP (Dalkara et al., 2016).

1.4.7 Gene therapy of the rhodopsin-linked RP

Given significant heterogeneity and the dominant nature of rhodopsin mutations, the gene therapy of rhodopsin-linked RP is particularly challenging. Two major questions in choosing an appropriate therapeutic strategy for the rhodopsin-linked RP are: firstly, the pace of degeneration — whether rods die quickly, necessitating a treatment which gives a fast onset of expression, or, in the case of advanced rod degeneration, directing gene delivery at surviving cones. Secondly, how the mutant rhodopsin interacts with cellular biochemistry: if the mutant protein interacts with the wild-type rhodopsin in a dominant-negative fashion, interfering with normal functioning of rhodopsin, then the supplementation approach by increasing the levels of wild-type rhodopsin may offset the negative effects of the mutant protein. In cases where the mutant rhodopsin exerts toxic gain-of-function effects, then the therapeutic approach should aim to suppress the expression from the mutant allele (Lewin et al., 2014).

1.4.7.1 Rhodopsin supplementation

The success of the single supplementation approach on the *P23H* mouse, a model of rhodopsin-linked dominant RP containing a copy of the human rhodopsin transgene *P23H* and two copies of the endogenous mouse

rhodopsin gene (*P23H Rho+/+*), was demonstrated by Mao and coworkers through delivery of an AAV vector expressing the murine rhodopsin gene driven by the murine opsin promoter. Treated eyes showed preserved retinal function at six months as evidenced by higher a-wave amplitudes by 100% and b-wave amplitudes by 79% compared to untreated controls. These ERG data correlated with an observed improvement of retinal structure: the ONL was thicker by 80% in treated eyes compared to controls. Taken together, this provides proof-of-concept that the supplementation of wild-type rhodopsin without concurrent suppression of the mutant gene is sufficient to slow down rod degeneration in a dominant form of rhodopsin-linked RP (Mao et al., 2011).

To recapitulate endogenous rhodopsin levels with exogenous AAV gene transfer, Palfi and coauthors delivered an AAV2/5 vector containing the cDNA sequence of the human rhodopsin gene driven by an optimized murine rhodopsin promoter to rhodopsin knockout mice, which do not produce rod-derived ERG responses due to lack of rod outer segments (Humphries et al., 1997). The rhodopsin promoter was extensively optimized to assure high levels of rhodopsin expression with the final promoter containing the long version of the mouse opsin promoter (1.7 kb) with two additional conserved elements to promote greater expression. In their study, Palfi et al. were able to demonstrate restoration of scotopic ERG responses measured 6 and 12 weeks after injection of their optimised rhodopsin vector. The amplitudes of the recorded b-waves, however, diminished three-fold at 12 weeks compared to the 6-week measurements, suggesting ongoing rod degeneration in spite of successful delivery of rhodopsin delivered even at that early age. The functional benefit of

rhodopsin delivery was demonstrated by transmission electron microscopy which confirmed the presence of rod outer segments in transduced areas and absence in non-transduced and non-injected areas 6 weeks post-injection (Palfi et al., 2010). Given that the data showed progressive degeneration and apparent loss of therapeutic effect despite significant efforts to increase expression of rhodopsin. This study by Palfi and coworkers highlights the implicit challenge of achieving wild-type levels of rhodopsin through AAV-mediated gene delivery, a protein which is very highly expressed to support the 10% daily turnover of rod outer segments that occurs *in vivo*.

1.4.7.1.1 Rhodopsin overexpression

The rhodopsin supplementation approach attempts to restore physiologic levels of rhodopsin. Control over the expression from an AAV supplemented gene is however limited, given that the replaced gene is not integrated into the genome but persists extra-chromosomally as an 'episome'. Since negative feedback loops are lacking for AAV-delivered genes, it is possible that gene therapy could also result in overexpression of rhodopsin, which may have deleterious effects on rod health. Price and co-workers explored the impact of additional copies of the human rhodopsin gene on the geneticallz engineered mice with a range of copy numbers of endogenous rhodopsin (Price et al., 2012). Three copies of rhodopsin (two mouse and one human) led to a 30% decline in ONL thickness over 6 months, whilst four copies (two mouse and two human) led to a 60% decrease over 5 months. The authors suggested that the mechanism of cell death maybe cellular crowding secondary to the increases in outer segment size observed as a result of rhodopsin overexpression. The toxicity of rhodopsin

overexpression was further confirmed by Mao and colleagues, who delivered an AAV vector containing rhodopsin cDNA into wild-type mice. This led to a 70% reduction in ERG responses measured 6 months after injection (Mao et al., 2011). Although rhodopsin is a highly expressed protein and recapitulating endogenous levels is a challenge, these studies suggest that overexpression may also be deleterious to rod health. As such, dosing for rhodopsin gene therapy must be finely tuned to fall within a certain therapeutic window.

1.4.7.2 Suppression methods

In gain-of-function mutations, the production of the toxic mutant protein can be knocked down at different levels, either at the DNA level using transcription blockade with zinc-fingers, or at mRNA level with ribozymes or RNA interference. These methods can be further categorised into allele-specific and allele-independent methods. Allele-specific agents target a specific site within the mutated gene preserving expression from the second wild-type allele. Allele-independent constructs, by contrast, knock down both alleles necessitating the provision of a replacement gene, which is resistant to the suppression agent and responsible for expression of the normal protein.

1.4.7.2.1 Allele-specific suppression

Ribozymes site-specifically cleave mRNA molecules (Hauswirth and Lewin, 2000) and when delivered by AAV vectors, were able to slow down rod degeneration by showing functional and anatomical rescue up to four months in transgenic *P23H* rats (LaVail et al., 2000). However, given the use of allele-specific therapeutic agents is hampered by the sheer number of mutations in

the rhodopsin gene, this approach would necessitate an almost customised approach for each mutation.

1.4.7.2.2 Allele-independent suppression

The allele-independent approach potentially makes treatment more universal and applicable to a variety of rhodopsin mutations. Such an approach has been applied using zinc-finger artificial transcription factors. These knock down expression at the DNA level and are based on the ability of zinc-fingers' binding domains to recognise specific DNA sequences coupled to DNA repressing domains, such as the Kruppel-associated box repressor domain. Mussolino and colleagues injected an AAV containing a zinc-finger artificial transcription repressor targeting the human rhodopsin promoter into mice with one copy of the human *P347S* mutant rhodopsin transgene and two copies of endogenous murine rhodopsin (Mussolino et al., 2011). The treatment reduced the expression of the human transgene by 26% and preserved ERG responses: two months after treatment b-wave amplitudes were higher by nearly 30% in treated eyes compared to untreated controls. However, if this therapeutic agent is to be used in humans, then a replacement gene must be provided as the zinc-finger repressor by binding to the human rhodopsin promoter will suppress the expression from both mutant and wild-type alleles.

Using this independent-allele approach necessitates the provision of a replacement gene that is resistant to the suppression agent. This resistance is made possible through the introduction of "silent mutations" in the rhodopsin gene.

This dual approach was assessed by Millington-Ward and colleagues by delivering two AAV5 viruses — one containing a shRNA (small hairpin RNA) driven by the H1 promoter and a separate virus encoding a codon-modified and thus shRNA-resistant human rhodopsin gene driven by the murine opsin promoter — into 5-day-old *P347S* mice, a model with slow photoreceptor degeneration. Rod-isolated ERG responses in treated eyes showed a moderate protective effect lasting up to 20 weeks, being threefold higher than in control eyes. However, b-wave amplitudes at 20 weeks diminished threefold compared to 6 week measurements, suggesting that the effect of treatment was fading with time. The histological findings correlated with ERG preservation: with a 3-4 layered ONL being present in treated eyes at 20 weeks compared with complete loss of the ONL in control eyes (Millington-Ward et al., 2011).

Greenwald and co-workers also used dual component therapy with a scAAV2/9 vector expressing a microRNA targeting the human rhodopsin gene and another scAAV2/9 containing a codon-modified replacement in the *P347S* transgenic mouse model (Greenwald et al., 2013). As this model was raised on a rhodopsin knockout background and lacks any murine rhodopsin, expressing only the mutant human rhodopsin *P347S*, it undergoes fast degeneration within one month of birth. The vectors were administered at postnatal day 19. The level of rescue using both vectors, however, was not significantly greater than that seen with the delivery of the AAV vector delivering rhodopsin alone, highlighting the lack of efficiency of the suppression mechanism on this model which lacks any wild-type rhodopsin.

Although the use of two viruses - one for suppression and one for replacement - appears attractive, as it allows optimisation of the ratio of viruses depending on the kind of rhodopsin mutation and the patient, the two virus approach might pose technical and regulatory barriers. It is likely on a probabilistic basis that individual photoreceptors would be infected with different ratios of viruses, which may produce a variety of responses in transduced cells. Furthermore, each ratio would need to be validated and approved in separate safety studies. Considering that RNA interference does not require large space in an AAV vector, the use of a single vector combining the suppression and replacement agents seems desirable (Lewin et al., 2014).

To deliver this dual component treatment in a single AAV, O'Reilly and co-workers used an AAV2/5 vector containing both a shRNA driven by the pol III promoter to knock down endogenous rhodopsin expression and the murine rhodopsin promoter driving expression of rhodopsin cDNA harbouring several altered nucleotides to make it resistant to shRNA-mediated suppression (O'Reilly et al., 2007). The mouse model used in the study (*P23H +/- Rho-/-)* presented an extremely rapid degeneration as it had one copy of the human transgene *P23H* on the rhodopsin knockout background. This resulted in complete loss of photoreceptors by the age of two weeks. The mice were treated just after birth and the ONL thickness was measured at postnatal day 10. Since only a part of the retina was transduced by injection, the ONL measurements were divided depending on their value into low and high groups. This analysis allowed the authors to demonstrate partial preservation (33%) of ONL thickness in treated eyes compared to the eyes injected with a virus

expressing GFP protein. The study highlights the challenges of gene therapy in extremely rapid degenerations.

Mao and co-workers used a slower model of RP containing a single copy of the human transgene *P23H* on a heterozygous rhodopsin knockout background (*P23H Rho+/-)* (Mao et al., 2011). Injection of the AAV2/5 vector which expressed shRNA under the human H1 promoter (which cleaves both mouse and human mRNA) and a shRNA-resistant cDNA sequence for murine rhodopsin (containing five silent mutations) at postnatal day 15 led to the long-term preservation of rod function. This was evidenced by ERG a-wave amplitudes six-fold greater in treated eyes at 9 months compared to controls and 50% improvement in the ONL thickness 9 months after injection compared to control-injected eyes (Mao et al., 2012). The model used in this experiment (the human transgene *P23H* was expressed on a heterozygous rhodopsin background, *P23H* Rho+/-) differed from that used in the study where a single replacement AAV vector containing only the rhodopsin gene was used in the number of copies of murine rhodopsin (*P23H Rho+/+)*. Given that both models have the human transgene *P23H* inducing the degeneration, it remains unclear whether a single replacement vector expressing the rhodopsin gene would have achieved similar effects.

Approaches using RNA interference-mediated suppression possess certain safety disadvantages: overexpressed shRNAs have been reported to cause both central nervous system and liver toxicity (Grimm et al., 2006; Martin et al., 2011), whilst retinal degeneration has been demonstrated in animal models triggered through Toll-like receptor-3 (TLR3) (Kleinman et al., 2012; Sioud,

2007). Furthermore, a number of other toxic effects from shRNAs and miRNAs stemming from “off-target” effects have been reported (Beer et al., 2010; Boudreau et al., 2008; McBride et al., 2008).

A further substantial challenge to putative dual therapy treatments is the attainment of the exceptionally high levels of rhodopsin expressed in native rod photoreceptors. Indeed, rhodopsin comprises 90% of the protein of rod outer segment and 30% of the rod proteome. If all endogenous rhodopsin production is suppressed, then an AAV rhodopsin supplement vector would need to reinstate these high levels of expression.

The cited papers (Frederick et al., 2001; Mao et al., 2011; Price et al., 2012) suggest a dominant-negative mechanism of certain rhodopsin mutations opening the possibility that a replacement AAV vector promoting high levels of rhodopsin expression may be sufficient to delay rod and cone degeneration in these models.

1.4.8 Mouse models of rhodopsin-linked RP

As rhodopsin mutations present exceptional heterogeneity and different mechanisms of degeneration may be involved depending on the location of the mutation within the rhodopsin molecule, several kinds of models have been proposed. In general, they can be categorised by the nature of the generated mutation: knockout, transgene, and knock-in models. The nomenclature of transgenic or knock-in mouse models of rhodopsin-linked RP reflects the amino acid substitution in the rhodopsin gene and they also differ in the background on which they were raised. The most common model is *P23H*, with other

common models including *T17M, P347S, and S2334X*. The rate of degeneration in these models is dependent on the number of copies of endogenous mouse rhodopsin and the ratio of copies of endogenous rhodopsin to mutant rhodopsin. On the rhodopsin knockout background, lacking any wild-type rhodopsin, the degeneration is fast, whereas in the mice with one or more copies of the murine rhodopsin gene the rate of degeneration is slower. Other animal models include canine (Cideciyan et al., 2005; Komáromy et al., 2008; Zeiss et al., 2006; Zhu et al., 2004), and porcine models (Ghosh et al., 2007; Hauck et al., 2006), which have the advantage of possessing larger eyes. In the present study, the rhodopsin knockout murine model was used to study the effects of delivering the rhodopsin gene via an AAV vector.

1.4.8.1 Rhodopsin knock-out mice

Rhodopsin knockout mice were generated by disrupting the rhodopsin gene at codon 135 in exon 2 with the neomycin cassette. These mice lack rod outer segments, and as such, they produce no ERG responses in scotopic conditions and lose photoreceptors over a 6 month period. Consequent to rod degeneration, the mice show signs of secondary cone loss: initially cone ERG responses are similar to wild-type but then progressively decline to a flat line by postnatal day 80 (Humphries et al., 1997). The two features of rhodopsin knockout mice: a null background for rhodopsin and secondary cone degeneration, make it a valuable model to assess the effects of delivery of wild-type rhodopsin on both rod and cone photoreceptors.

1.5 Aim and outline of the thesis

The overall aim of this thesis was to develop a highly efficient AAV vector for rhodopsin delivery in rhodopsin-linked RP. The rhodopsin gene is the most common gene implicated in RP, accounting for approximately 15% of autosomal dominant forms of RP (Dalke and Graw, 2005). Consequently, a large number of affected patients may benefit from the development of treatment for this disease. Given that rhodopsin mutations are autosomal dominant, it had been suggested that these mutations require therapy combining both the inhibition of production of mutant protein and supplementation of inhibition-resistant wild-type rhodopsin. However, evidence from the above-cited papers suggested that rhodopsin mutations involve the dominant negative and loss-of-function mechanisms and that by increasing the ratio of wild-type to mutant rhodopsin might be sufficient to slow down rod degeneration. The success of this supplementation approach was confirmed by Mao et al. through the delivery of murine rhodopsin gene driven by the cytomegalovirus promoter in the *P23H* mouse model (Mao et al., 2011). The goal of this project was therefore to build a highly efficient vector delivering wild-type human rhodopsin, which may subsequently be used in clinical trials aiming to delay rod and secondary cone degeneration in rhodopsin-linked RP and thus stabilise or slow visual loss in these patients. As the vector was intended for use in subsequent clinical trials, it was planned to include human sequences for the rhodopsin promoter and the rhodopsin gene. This is in contrast to previous studies, which generally employed the mouse rhodopsin gene and ubiquitous or

murine promoters. Given that the pathway to clinical trial can be long and may be comprised of various consecutive steps, this project targeted the production and assessment of the rhodopsin vector on rhodopsin knockout mice given that these mice, lacking rhodopsin, present an ideal model to assess the potency of the vector. The novelty of our study is the observation of preserved rod and cone function through the provision of wild-type rhodopsin gene to the rhodopsin knockout model at a later stage of the disease. This more closely mimics the situation for human patients who usually present to the clinic with progressive rod degeneration.

To achieve this aim, a stepwise approach is presented in the following chapters. Firstly, the design and production of the vector are described in Chapter 3. Building on that, the assessment of this vector through *in vivo* and *ex vivo* experiments and quantitative evaluation of the administered vector are presented in Chapter 4. Following these studies, the effects of the AAV-mediated gene therapy on rod photoreceptors are assessed in Chapter 5. Consequently, the treatment effects on the cone system are evaluated in Chapter 6. Finally, the general discussion with potential future work is presented in Chapter 7.

Chapter 2 Methods and Materials

2.1 Molecular biology

2.1.1 Polymerase Chain Reaction (PCR)

The primers and plasmid maps were designed using the Geneious software (version 6.1.6; Biomatters Ltd, Auckland, New Zealand).

The PCR primers were manufactured to order by Sigma-Aldrich (Dorset, UK) and used in a PCR mix prepared as shown in Table 2.1**.** The Thermococcus kodakaraensis (KOD) polymerase enzyme was used because of its accurate reading properties and low PCR error rate.

Table 2.1 Components of a typical PCR reaction

Component	Amount, µl
10x Reaction Buffer	2.5
dNTPs	2.5
MgSO4	1.5
Primers (10 mM)	1 of each forward and reverse
DNA	1 (in amount of ~ 500 ng)
H_20	33
KOD polymerase	1

A PCR cycle usually included: an initial hot-start at 95^0C for 2 minutes and 35 cycles of PCR. The annealing and extension temperatures and their duration were adjusted to each reaction accordingly to the size of amplicon and melting temperatures of primers.

2.1.2 DNA ligation

DNA ligation was performed by adding a vector and an insert in a corresponding ratio 1:3. The ligation mixture containing the vector (25 ng), insert (75 ng), 1 µl of T4 DNA ligase (New England Biolabs, UK), 1 µl of ligase buffer, and water to 10 µl, was left overnight for full ligation.

2.1.3 Gene cloning using *E.Coli*

The MAX Efficiency® Stbl2™ Cells were used for cloning since they are high-efficient chemically competent cells specifically designed for cloning of unstable inserts such as direct repeat and tandem array genes. The MAX Efficiency® Stbl2™ Competent Cells (Invitrogen) were transformed using a heat shock at 42^0C for 30 seconds, then, placed into enriched medium SOC (Invitrogen). Afterwards, the bacteria were plated on LB-agar plates with ampicillin (50 µg/ml) overnight at 37^0C. Bacterial colonies were inoculated into 7 ml of the LB medium with 50 µg/ml of ampicillin and incubated at 37^0C in a shaker overnight.

For mini preparation of plasmid DNA (mini preps), DNA was extracted using the GenElute™ Plasmid miniprep kit (Sigma-Aldrich) according to the standard protocol. Inoculated LB medium was centrifuged, bacterial pellet resuspended, lysed and neutralised using respective buffers. After the cell debris were removed by centrifugation, the supernatant was passed through a DNA-binding column, washed with the ethanol-containing solution and finally, the DNA eluted with the preheated elution buffer. Obtained mini-preps were assessed spectrophotometrically by Nanodrop® for quality and quantity of DNA, the ratio

of absorbance at 260 nm and 280 nm between 1.7 to 1.9 was considered as an acceptable DNA purity. The DNA size was determined by restriction enzyme digest and subsequent agarose gel electrophoresis. Furthermore, the mini-preps were analysed for ITR integrity using a restriction digest with *XmaI*, which cuts the CCCGGG sequence present in each ITR. One of the mini-preps with the correct digestion pattern was sent for standard Sanger sequencing. From mini-preps with correct sequencing results, mega preparations of plasmid DNA (mega-preps) were made.

For mega preparation of plasmid DNA, bigger volumes of the LB with 50 ug/ml of ampicillin (up to 3 liters) were inoculated with 1 ml of LB culture, shaken at 37^0C overnight. For these big scale DNA preparations, the Endofree Megaprep Kit (Qiagen, UK) was used. The bacterial pellet was separated from the medium, resuspended, lysed; the plasmid DNA was separated from the cell debris by the QIAfilter Mega Cartridge. Supernatant was passed through a resin column QIAGEN-tip to bind the DNA. DNA was washed with wash buffer, eluted with elution buffer, precipitated with isopropanol, and centrifuged to obtain DNA pellet. DNA pellet was washed with 70% ethanol solution and DNA then dissolved in TE buffer.

2.1.4 Agarose gel electrophoresis

DNA products were separated on an agarose gel, in order to visualise nucleic acids under UV light, ethidium bromide was added (to final concentration 0.5 µg/ml). DNA bands were assessed by comparison with commercial DNA ladders (Norgen,UK), DNA samples were loaded with 6x loading dye

(Geneflow, UK). In the majority of cases 2% agarose was used, in the case of a smaller or of a bigger DNA fragment the agarose percentage was changed accordingly.

Agarose gels were made by adding 2.0 g of agarose (AGTC Bioproducts, UK) to 200 ml of 1% buffer solution containing a mixture of Tris base, acetic acid and EDTA (TAE), heating the mixture in a microwave for two minutes until complete dissolution of agarose particles. After cooling and adding the ethidium bromide, the gel was poured into a plastic mould. Gel electrophoresis was carried out at 130 V until DNA ladder bands were clearly resolved (generally 60-90 minutes).

2.1.5 DNA extraction from agarose gel

The DNA fragment was cut from the agarose gel with a scalpel. The gel slice was weighed and 3 volumes Buffer QG (Qiagen, UK) were added to 1 volume gel (100 mg gel ~ 100 µl). The mixture was incubated at 50°C for 10 minutes. Afterwards, one gel volume of isopropanol was added to the sample and mixed, the mixture was placed into a QIAquick spin column (Qiagen, UK) in a provided 2 ml collection tube. The QIAquick column was centrifuged for 1 min until the sample has passed through the column. The flow-through was discarded and the QIAquick column was placed back into the same tube. Then the QIAquick column was centrifuged in the provided 2 ml collection tube for 1 min to remove residual wash buffer. Afterwards. the QIAquick column was placed into a clean 1.5 ml microcentrifuge tube, and to elute DNA 50 µl Buffer EB (Qiagen, UK) was added to the center of the QIAquick membrane and centrifuged for 1 min.

2.1.6 Restriction enzyme digestion

Digestions using restriction enzymes (New England Biolabs, UK) were performed using 1 µg of DNA, 1 µl of enzyme and 5 µl of appropriate buffer, Bovine Serum Albumin (BSA) was added at a final concentration of 100 µg/m, if recommended by the manufacturer; the digests were incubated for 1 hour at 37^0C. The analysis of digestion was performed by agarose gel electrophoresis.

2.1.7 DNA sequencing

To confirm the precise order of nucleotides in plasmids sequencing was outsourced to Source Bioscience UK Ltd at the Biochemistry Department, University of Oxford, that used the standard Sanger DNA and dGTP (`deoxyguanosine triphosphate) sequencing protocols. The primers used for sequencing were apart each by approximately 600 bp and included the PCR primers used previously for PCR splicing reactions or were designed specifically for sequencing. In the case of the ITRs with high GC content, the dGTP sequence protocol was applied. The concentration for primers sent was 3.2 pmol/µl and for plasmid at least 100 ng/µl. The chromatogram files (*.abi) were opened in Geneious software (version 6.1.7; Biomatters Ltd, Auckland, New Zealand) and regions with numerous ambiguous calls at both 5’ and 3’ ends were trimmed to a rough size of 600-1000 bp. Remaining sequences were aligned with a reference sequence in a pairwise fashion using Geneious software.

2.2 Cell cultures

2.2.1 HEK cell cultures

Human embryonic kidney 293T (HEK293T) cells were used to study the expression from the human rhodopsin promoter, and for production of AAV vectors. All cell culture work was carried out in cell culture hoods, and plates and flasks containing HEK293T cells were kept at 37^0C and 5% CO_2 conditions in an incubator.

HEK293T cells are highly transfectable cells derived from HEK293 cells which were originally generated from the normal human embryonic kidney cells by transformation with sheared adenovirus 5 DNA (Graham et al., 1977). HEK293T cells contain the simian virus 40 T-antigen to facilitate viral DNA replication (Patel and Tikoo, 2006).

The HEK293T cells were procured from the European Collection of Cell Cultures and stored at -196^0C in liquid nitrogen. Resuscitated HEK293T cells were cultured in Dulbecco's Modified Eagle's Medium (DMEM) completed with L-glutamine (2 mM), penicillin (100 units/ml), streptomycin (100 µg/ml) and 10% Fetal bovine serum (all Sigma-Aldrich). Cells were cultured every 3-4 days, prior to reaching confluence. To refresh media, old media was removed, cells were washed with 5 ml of PBS, PBS was removed and again 5 ml of PBS added and flask incubated for 5 min at 37^0C. Cells were mobilised with a quick tap on a side of flask, 5 ml of DMEM were added to the cell solution. The cell solution was transferred to a 15 ml Falcon tube and centrifuged for 5 min at

room temperature at 1,200 *g*. The obtained cell pellet was resuspended in 12 ml of complete DMEM and transferred to a T75 flask to be placed into standard incubation settings.

2.2.2 HEK cells transfection

HEK293T cells, in 2 x 10^5, were seeded in 6-well tissue culture plates (Sarstedt Inc., Newton NC, USA) with complete growth medium DMEM. Next day, when they achieved 60-80% confluence, they were transfected with plasmid DNA using the GeneJuice Transfection Reagent (Norgen, UK) according to the manufacturer's instruction. Briefly, 3 µl of Genejuice reagent was added to 100 µl of serum-free Roswell Park Memorial Institute (RPMI) 1640 Medium (Sigma-Aldrich, UK). The solution was briefly vortexed and allowed to equilibrate to room temperature (RT) for 10 min. Approximately 1 µg of plasmid DNA was mixed into a solution and left for 20 min at room temperature to allow for the complex formation of liposomes. Next, the Genejuice-DNA mixture was added to HEK293T cells in a dropwise fashion followed by incubation at 37°C for 72 h. The expression of DsRed protein was assessed by fluorescent microscopy 72 hours after transfection. The expression was assessed in three separate experiments, each experiment including two wells per transfection.

2.2.3 Macaque retinal explants

Macaque eyes were collected post-mortem from sacrificed healthy male and female macaques at the age between 5 and 19 years old at the MRC Centre for Macaques (Porton Down, UK). The macaques were scheduled by administering

ketamine 10 mg/kg intramuscularly and pentobarbitone 200-300 mg/kg intravenously, eyes were immediately enucleated and placed in a dish with complete Neurobasal A. Complete neurobasal A comprised Neurobasal A (Gibco) with the following ingredients added: penicillin (final concentration: 100 units/ml), streptomycin (100 µg/ml; Sigma-Aldrich), L-glutamine (800 µM; Sigma-Aldrich), B-27 supplement (2%; Gibco) and N-2 supplement (1%; Gibco). After the removal of the cornea and lens, radial cuts were performed to make the retina flat. Using a 3 mm diameter biopsy tool, disks of neuroretina were produced from the retina area to the periphery of major vascular arcades. After disks were liberated from the underlying RPE, they were placed in a tube with cold complete Neurobasal A. A cooled polystyrene box was used to transport samples to the laboratory.

Upon the delivery to the laboratory, under a tissue culture hood, 500 µl of complete Neurobasal A were placed into wells of a 24-well plate, then a culture insert (0.4 µm pore size, VWR International) was placed in a well and each retinal disc was put into culture insert. 200 µl of complete neurobasal A were placed on top of insert and the explants were cultured at 34°C, 5% CO_2.

AAV transduction was performed 24 hours after culturing the explants. The media below the insert were refreshed and above the insert 200 µl of Neurobasal A with *scAAV2/8^{Y733F}hRHOp-DsRed* in either higher dose (10^{10} genome copies) (gc) or lower dose (10^{9} gc) were added. The explants continued to be kept at 34°C, 5% CO_2, with media replaced every two days. Eight days after transduction the explants were fixed in PFA 4%, placed in sucrose gradients (10%, 20%, and 30%), cryopreserved in OCT (optimal cutting

temperature) and cryosectioned. The sections were immunolabeled with the polyclonal rabbit anti-rhodopsin antibody.

2.3 AAV production

AAV vector production traditionally involves the following steps:

1. Seeding HyperFlasks with HEK293T;

2. Transfection of HEK293T cells with plasmids;

3. Harvesting cells;

4. Isolating AAV fraction through iodixanol gradient;

5. AAV purification through centrifugation with PBS.

2.3.1 Seeding of HEK293T cells with three plasmids

A Corning HYPER*Flask* vessel was used for the AAV production protocol as it allows for greater cell surface area than in a traditional T-flask by using a multilayer design and a gas permeable film for gas exchange between the interior of the flask and atmospheric air.

T75 flasks were seeded with 1.7 x 10^7 HEK293T cells in culture media and incubated at 37^{o}C, 5% CO_2 for 48 hours. The culture media were prepared as follows: 500 ml of high glucose Dulbecco's Modified Eagle's Medium (DMEM), (Sigma-Aldrich); 10% Fetal Bovine Serum (FBS), non-USA origin, sterile filtered, suitable for cell culture (Sigma-Aldrich); 5 ml of L-glutamine, 200 μM

solution, sterile-filtered, BioXtra, suitable for cell culture, (Sigma-Aldrich); 5 ml Penicillin-Streptomycin, 10,000 units penicillin, 10mg streptomycin/ml, sterile-filtered, BioReagent, suitable for cell culture, (Sigma-Aldrich).

After HEK293T cells reached 80% confluency, the media were removed and the cells washed with 5 ml of PBS. After removing the wash, 2 ml of PBS were added and the cells incubated at 37^{o}C, 5% CO_2 for 10 minutes. 8 ml of culture media were added to flask and the cells were loosened and re-suspended by gently pipetting up and down, further 190 ml of media were added.

One Corning HYPER*Flask* cell culture vessel (Corning Incorporated) was seeded with two T75 flasks, and two HYPER*Flask*s were used to produce one AAV batch. Cell suspension from T75 flasks was poured slowly into HYPER*Flask*. When 200 ml of cell suspension were transferred to HYPER*Flask*, it was placed on its long, thin side to allow even distribution of the cell suspension between the layers of the HYPER*Flask*. The HYPER*Flask* was then filled with culture media to the rim so that it held in total 560 ml of culture media. The HYPER*Flask* was placed upright, leant to one side and tapped, to dislodge all bubbles, which were trapped in the flask layers. Excessive bubble formation was aspirated using a pipette and additional culture media were added so that no headspace with air would be left. After capping the flask tightly, flask was placed horizontally, so that the angled neck was facing down. Ensuring that all air bubbles remained in the neck, the flask was placed in an incubator at 37^{o}C, 5% CO_2 for 72 hours.

2.3.2 Transfection of HEK293T cells

For each HyperFlask a mixture of three plasmids containing in total 500 µg DNA was prepared, with the ratio of plasmids dependent on the size of the plasmids being used (**Table 2.2**).

Table 2.2 Plasmid size and amount per transfection in AAV production

Plasmid	Size (kb)	Amount per transfection (µg)
pΔΔF6	15.4	15.4 x R
pRepCap	7.3	7.3 x R
pTransgene	T	T x R
Total	K	500 µg
Ratio (R) mass/kb	500/K	

The plasmids were added to a 50 ml Falcon tube and up to 10 ml of 150 mM NaCl were added. In a separate 50 ml Falcon tube 1.125 ml of 10 mM Polyethylenimine (PEI) were added and volume filled to up to 10 ml with 150 mM NaCl. To complex the DNA and PEI, 10 ml of PEI were added drop by drop into the tube containing the 10 ml DNA. The DNA/PEI/NaCl mixture was left to incubate at room temperature for 20 minutes.

The transfection media were prepared as follows: 500 ml of high glucose Dulbecco's Modified Eagle's Medium (DMEM), (Sigma-Aldrich); 2% Fetal Bovine Serum (FBS), non-USA origin, sterile filtered, suitable for cell culture (Sigma-Aldrich); 5 ml of L-glutamine, 200 mM solution, sterile-filtered, BioXtra, suitable for cell culture, (Sigma-Aldrich); 5 ml Penicillin-Streptomycin, 10,000 units penicillin, 10 mg streptomycin/ml, sterile-filtered, BioReagent, suitable for cell culture, (Sigma-Aldrich).

Fifty ml of transfection media were set aside in a Falcon tube. Then the DNA/PEI/NaCl complexes were poured into the remaining volume of transfection media (~500ml). Afterwards, 20 ml of the 50 ml of transfection media aliquot was added into the now empty DNA/PEI/NaCl tube to collect any remaining solution and then poured into the ~500 ml of transfection media containing the DNA/PEI/NaCl. The HYPER*Flask* was gently drained and transfection media with DNA/PEI/NaCl complexes were added. The HYPER*Flask* was filled from the remaining 30 ml aliquot of transfection media. All air bubbles were removed by pipetting and the HYPER*Flask* incubated at 37^{o}C, 5% CO_2 for 72 hours.

2.3.3 Harvesting HEK293T cells

Two hundred ml of the HYPER*Flask* media were removed and discarded, the lid of the HYPER*Flask* secured, and the HYPER*Flask* shaken vigorously to loosen the cells. A microscope was used to assess that all cells were dislodged and floating free. The cell suspension was poured into a 500 ml flask and centrifuged for 10 minutes at 1,000 rpm, 20^{o}C. During this step 1 ml of Lysis Buffer (1M Tris(hydroxymethyl)aminomethane (AnalaR NORMAPUR, VWR), 150 mM NaCl, Molecular biology grade water, DEPC-treated and sterile filtered (Sigma-Aldrich) with one protease inhibitor tablet (cOmplete mini EDTA-free protease inhibitor cocktail tablets (Roche)) was prepared. The media were removed from the pelleted HEK293T cells, leaving about 30 ml of media in flask, the cells were resuspended in this volume. The suspension was then placed in a 50 ml Falcon tube and centrifuged as above with the removal of the

media at the end of the run. 15 ml of Lysis Buffer were added to the cell pellet and carefully pipetted up and down to mix. Five hundred µl of the prepared protease inhibitor were added to this and mixed again, afterwards, the tube was labeled and placed in -80 freezer for one hour. Then, the lysis sample was placed in a 37^{o}C water bath for 15 minutes to thaw, shaking well half way through the incubation time. The sample was then placed back in the -80 freezer and the freeze/thaw cycle was repeated two more times. After the final thawing, the samples were placed in -80 freezer again and stored there until the purification step.

2.3.4 Isolation of AAV particles using the Iodixanol gradient

The lysate was thawed at 37^{o}C for 15 minutes, then Benzonase (EMPROVE bio Benzonase, Merck Millipore) added to the lysate making a final concentration 50U/ml. The mixture was incubated at 37^{o}C for a further 45 minutes, the tubes were shaken vigorously every 15 minutes during this incubation. The lysate was centrifuged at 3,700 *xg* for 20 minutes at room temperature. The iodixanol gradients were prepared by layering the different preparations detailed in **Table 2.3.**

Table 2.3 Preparations for two iodixanol gradients

Fraction	Iodixanol	5 M NaCl	5X PBS-MK	H_2O	Phenol Red
15%	4 ml	3.2 ml	3.2 ml	5.6 ml	-
25%	5 ml	-	2.4 ml	4.6 ml	20 µl
40%	6.7 ml	-	2 ml	1.3 ml	-
60%	10 ml	-	-	-	20 µl

Components of iodixanol gradients comprised the following: Iodixanol 60% (OptiPrep density gradient medium, Sigma-Aldrich), Phenol Red (Phenol red solution, 0.5% liquid, sterile-filtered, BioReagent, suitable for cell culture, Sigma-Aldrich), 5x PBS-MK (Gibco phosphate buffered saline tablets, Life Technologies, 5 mM magnesium chloride ($MgCl_2$), Sigma-Aldrich; 12.5 mM potassium chloride (KCl), Sigma-Aldrich; Molecular biology grade water, DEPC-treated and sterile filtered, Sigma-Aldrich. 5X PBS was autoclaved before adding 0.22 µm filtered solutions of $MgCl_2$ and KCl.

Three gradients were used to make one AAV preparation. 7.2 ml of the 15% preparation were added directly into an OptiSeal 32.4 ml ultracentrifuge tube. 4.8 ml of the 25% preparation were placed into a separate 15 ml Falcon tube. Half of the 4.8 ml aliquot was drawn using a long neck Pasteur pipette. Carefully moving the Pasteur pipette through the 15% iodixanol fraction until the tip touched the bottom of the ultracentrifuge tube, the 25% fraction was slowly layered below the 15% fraction without allowing air to pass out of the pipette and disturb the iodixanol layers. Once the Pasteur was empty, it was carefully withdrawn from the gradient without drawing up or disturbing the fractions in

place. The remaining volume of the 25% fraction was transferred into the Pasteur pipette and the process of placing it beneath the 15% fraction was repeated. Once the 25% fraction was in place, the same process was repeated to add 4 ml of the 40% preparation beneath the 25% fraction and the gradient was completed by adding 4 ml of the 60% preparation beneath the 40% fraction.

The lysate was then added drop by drop on the top of the iodixanol gradient, filling the ultracentrifuge tube to the top, using the Lysis Buffer to top up if necessary. The tubes were cupped and placed into the Optima XE-90 ultracentrifuge (Beckman Coulter). The gradients were spun at 59,000 rpm for 1 hour and 30 minutes at 20^{o}C. After the spin, the centrifuge tube caps were removed and the OptiSeal tubes were pierced with an 18G needle attached to a 5 ml syringe at the interface between the 60% and 40% phases, keeping the bevel facing up. The whole 40% phase was collected avoiding the debris from the 25% phase. Approximately 2-3 ml were recovered from each gradient. The collected fraction was stored overnight at 4^{o}C.

2.3.5 Purification and concentration of the isolated AAV vectors

5 ml of PBS were added to an Amicon Ultra 100 K filter and spun at 3,000 *g* for 15 minutes, 20^{o}C. The flow through was discarded. 5 ml of PBS were added to the collected iodixanol fraction and carefully pipetted up and down to mix. The total volume was added to the filter and then spun at 3,000 *g* at 20^{o}C until the volume was reduced to 500 µl. The flow through was discarded. 15 ml of PBS were added to the filter and spun at 3,000 *g*, 20^{o}C until the volume was again

reduced to 500 µl. The flow through was discarded. This was repeated twice. On the third and final PBS wash, the volume was reduced to between 250 µl and 400 µl, obtaining purified AAV. To rinse AAV particles, the AAV preparation was drawn and dispensed back over the filter 20 times on each side of the Amicon filter using a 200 µl pipette, 12 µl aliquots were made and stored at -80^{o}C.

2.3.6 SDS-PAGE

To qualitatively assess vector purity Sodium Dodecyl Sulphate - Polyacrylamide Gel Electrophoresis (SDS-PAGE) and a colloidal protein stain were used to visualise capsid proteins, which should be the only visible proteins in the gel. To 10 µl of concentrated virus preparation 10 µl of molecular biology grade water were added, then incubated with 20 µl of Laemmli buffer (BioRad, UK) and heated to 95^{o}C for 15 minutes, then loaded into 10% w/v reducing SDS-polyacrylamide electrophoresis gel (Criterion TGX precast gel, BioRad, UK), a prestained protein ladder (Geneflow, UK) to identify protein size was run alongside. To separate proteins, the gel was run at 100 volts until the loading dye reached the bottom of the gel, approximately two hours. The gel was washed in distilled water for 3 x 5 minutes, incubated in the Coomassie Brilliant Blue protein stain (EZBlue^{TM} Gel Staining reagent, Sigma-Aldrich, UK) for 45 minutes, followed by a brief destaining step in water for 5 minutes. The gel was then scanned with the Odyssey imaging system (LI-COR Biosciences, Lincoln, NE, USA) using the 700 nm channel at 2 minutes exposure and acquired into the Image Studio Lite software, version 5.0.

2.3.7 qPCR

Quantitative PCR (qPCR) based on SYBR Green was used to assess the titer of AAV vectors.

2.3.7.1 qPCR primers design

Quantitative PCR (qPCR) (Biorad CFX Connect Real-Time System) was used to quantify AAV titre and assess reverse packaging. The design of primers was performed using the Geneious software applying the following rules:

- The primers targeting the rhodopsin gene were separated by exon 1-exon 2 boundaries to reduce genomic background contamination;
- The amplified region was usually not bigger than 220 base pairs (bp);
- The GC content of the primers was roughly 50-60%;
- The minimal length of primer was 18 nucleotides, maximal length 24 bp, aiming to have at 20 bp;
- The minimal melting temperature was 60^0C, maximal 63^0C, aiming for 60^0C;
- The maximum difference in melting temperature did not exceed 10^0C.

2.3.7.2 qPCR protocol

To assess viral titer, 1 µl of AAV preparation or AAV wash were diluted in 7 µl of molecular biology grade water (Sigma-Aldrich, Stenheim, Germany); 1 µl of DNAse I (New England Biolabs, Herts, UK) and 1 µl of the DNAse I buffer were added; and the mixture was incubated for 30 minutes at 37^0C, this allowed removal of all DNA residues outside of viral capsids. In order to deactivate

DNAses and denature viral shells, samples were heated at 95°C for 10 minutes. After dilution by 10 times with molecular biology water, samples in a volume of 1 µl were placed on a Hard-shell 96 Well qPCR plate (Biorad) and 9 µl of qPCR mix were added. The qPCR mix was made as follows: 1 µl of forward primer (2 µM), 1 µl of reverse primer (2 µM), 2 µl of molecular biology water and 5 µl iTaq (iTaq™ Universal SYBR® Green Supermix, Biorad). In order to quantify viral vectors, purified, quantified, and sequence-verified plasmids with the identical expression cassette to viral vector were used as standards in the following concentrations: 10 ng, 1 ng, 100 pg, 10 pg. Each plasmid standard, sample, and a negative control were run in triplicates of 10 µl reaction on a 96 well plate. The plate was briefly spun in the Miniplate Spinner (Labnet) and placed into the CFX Connect Real-Time System (Biorad). The qPCR protocol included an initial activation step at 95°C for 3 minutes followed by 40 cycles of denaturation at 95°C for 10 seconds and the annealing/extension at 60°C for 30 seconds, followed by a melt curve stage. The data obtained were analysed in the Applied Biosystems StepOne software v2.1 before exporting to the Microsoft Excel. In order to determine the number of molecules of plasmid (copy number), the amount of DNA in nanograms and the length of the template in base pairs were entered in the online calculator (Andrew Staroscik, URI Genomics & Sequencing Center, available at http://cels.uri.edu/gsc/cndna.html).

2.4 *In vivo* procedures

2.4.1 Animals

All animal experiments were performed in compliance with the ARVO Statement for the Use of Animals in Ophthalmic and Vision Research and UK Home Office guidelines. Animals were kept in individually ventilated cages and followed a 12-hour light (<100 lux)/12-hour dark cycle, with food and water available *ad libitum*.

To assess *in vivo* cone survival a mouse model expressing Enhanced Green Fluorescent Protetin (EGFP) in M-cones and having a rod degeneration due to the targeted rhodopsin gene disruption had been created previously in the lab (Lipinski et al., 2015) by crossing the *B6.Cg-Tg(OPN1LW-EGFP) 85933Hue/Mmmh* mice (with *EGFP* transgenic insertion) with the *Rho-/-* (homozygous for rhodopsin knockout), only heterozygous mice for *Opn1.EGFP* were used, referred to herein as *Opn1.EGFP* rhodopsin knockout *or Opn1.EGFP Rho-/-.*

2.4.1.1 Genotyping

To determine genotype, ear notches were collected at the age of 2 weeks. DNA was extracted by adding 100 µl 0.05 M NaOH to ear notches, heating for 1 hour at 95°C, vortexing (900 rpm), spinning (10,000 rpm) for 2 minutes, and adding 10 µl of neutralisation buffer (1 M tris, 10 mM EDTA, pH 8.0). After vortexing and spinning at the same conditions, 20 µl of supernatant were transferred to a new tube, diluted with 100 µl molecular biology water. 2 µl of diluted DNA was

used in a PCR reaction using 6.25 µl Immomix Red (Bioline Reagents, London, UK), 0.63 µl of one forward (5'-AGGTTAGAGCTGGAGGACTG-3') and reverse (5'- AAGACTGATTGGACCATTC-3') primers binding to the wild-type exon II allele and 0.3 µl of reverse primer to the pol2:neo insertion designed to disrupt the exon II (5'-TTCAAGCCCAAGCTTTCGCG-3') (Humphries et al., 1997). The PCR was performed as follows: 1 cycle of 10 minutes at 95^0C (initial denaturation step), 30 cycles of 10 seconds at 95^0C (denaturing phase); 30 cycles of 30 seconds at 58^0C (annealing phase), 30 seconds of 72^0C (elongation phase), 1 cycle of 10 minutes at 72^0C (final elongation). DNA products were resolved on 2% agarose gel containing ethidium bromide (Sigma-Aldrich, UK, 10 µl of 10 mg/ml concentration per 200 ml of gel). The band size was determined by comparison to 100 bp DNA ladder (New England Biolabs, Hichin, UK), a band of 139 bp and 394 bp were characteristic of knockout and wild-type alleles correspondingly (**Figure 2.1,** panel A). The genotype of *Opn1-EGFP* positive animals was determined by a PCR using forward 5'-CAATTAAGAGATCAGGTAGTGT-3' and reverse 5'-AGTTCACCTTGATGCCGTTCTT-3' primers (the same PCR reagents were used as described for rhodopsin mutant allele genotyping) with a final product size of 641 bp resolved on 2% agarose gel (**Figure 2.1,** panel B). The following PCR conditions were applied: 1 cycle of 10 minutes at 95^0C (initial denaturation step), 30 cycles of 10 seconds at 95^0C (denaturing phase); 30 cycles of 30 seconds at 55^0C (annealing phase), 30 seconds of 72^0C (elongation phase), 1 cycle of 10 minutes at 72^0C (final elongation).

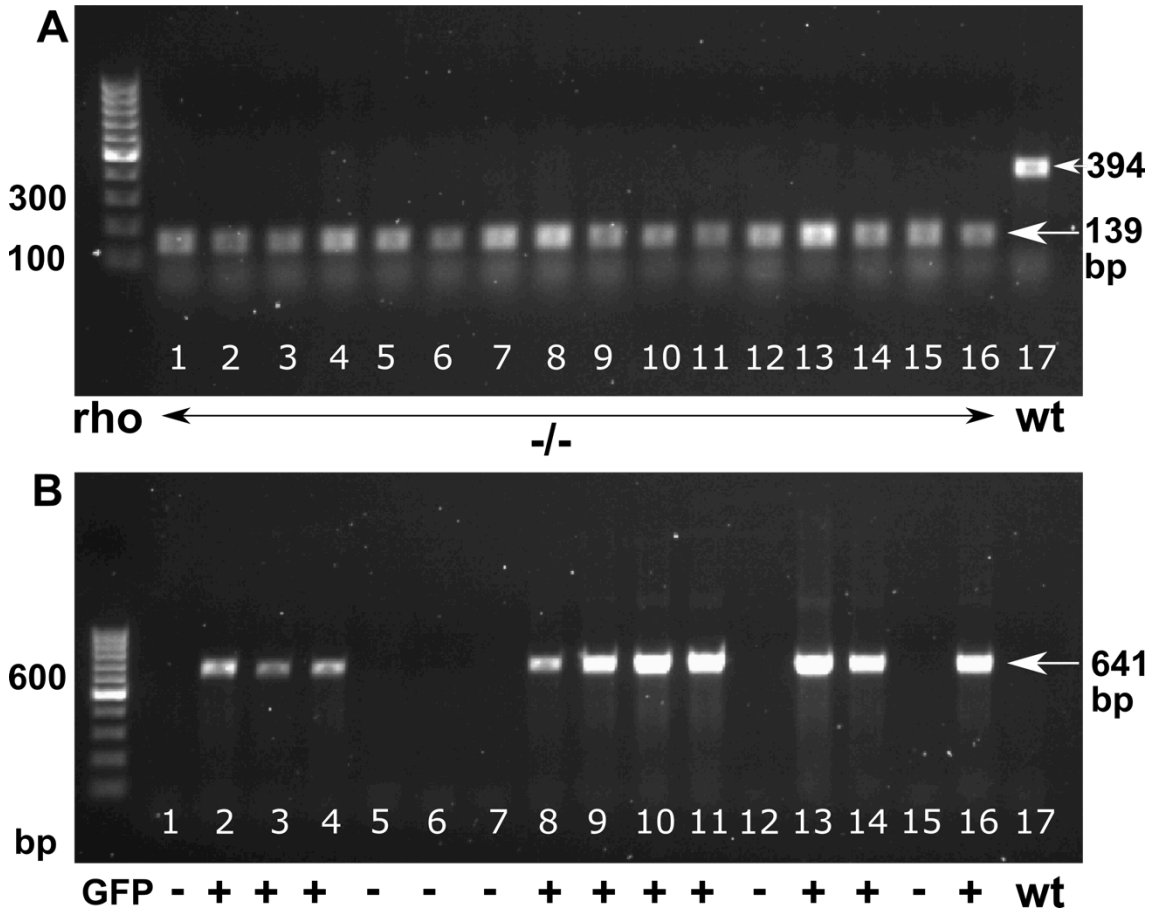


Figure 2.1 Genotyping for rhodopsin and *EGFP*

A) Genotyping for rhodopsin: the first sixteen lanes show a band corresponding to 139 bp, corresponding to rhodopsin knockout genotype (*rho*). The last lane (17), wild-type (wt, the DNA was obtained from a *C57Bl/6* mouse) served as a control and shows a band of 394 bp corresponding to wild-type rhodopsin. The additional bands below 100 bp correspond to unspecific primer-dimer formation.

B) *EGFP* genotyping shows that some mice (2,3,4, 8, 9, 10, 11, 13, 14, and 16) have bands of 641 bp corresponding to *EGFP*-positive genotype (+), and other mice (1, 5, 6, 7, 12, 15, and 17) are negative for *EGFP* (-).

2.4.2 Subretinal injection

The optimal route of application of AAV vectors to transduce photoreceptor cells efficiently is a subretinal injection. Due to the particular anatomy of the mouse eye with a disproportionally large lens and very narrow pars plana, an *ab externo* approach was chosen as described in more detail below.

2.4.2.1 Anaesthesia

After being weighed, mice received an intraperitoneal injection of the induction mix by 29G 1 ml insulin syringe (Myjector, Terumo N.V., Leuven, Belgium). The volume of the induction mix was 0.1 ml per 10 grams of body weight. The induction mix included: the NMDA receptor antagonist ketamine and the α_2 adrenergic receptor agonist xylazine mixed at the following proportion: 0.8 ml Vetalar™ V (100mg/ml ketamine; Zoetis UK Ltd, London, UK) and 0.5 ml Rompun® (20 mg/ml xylazine; KVP Pharma + Veterinärprodukte GmbH, Kiel, Germany) in 8.7 ml sterile H_2O.

At the end of the procedure, to reverse the effects of xylazine and shorten recovery period, the α_2 adrenergic receptor atipamezole was injected using the same technique as described for the injection of anaesthesia. This 'reversal-solution' was prepared by mixing 0.4 ml Antisedan® (5 mg/ml atipamezole; Elanco Animal Health, Basingstoke, UK) with 9.6 ml sterile H_2O. The reversal solution was given in the same volume as the induction mix administered before. After the administration of reversal, mice were placed in a heated chamber and kept there till a full recovery.

2.4.2.2 Pupil dilation

In order to dilate pupils a mixture of mydriatics was prepared by mixing 1% tropicamide (Mydriaticum 1%; Bausch & Lomb, Kingston-on-Thames, UK) and 2.5% phenylephrine (phenylephrine hydrochloride 2.5%; Bausch & Lomb).

2.4.2.3 Paracentesis of the anterior chamber

Mice were further anesthetised by applying anaesthetic eye drops Proxymetacaine hydrochloride 0.5%® (Bausch & Lomb, Kingston-on-Thames, UK), then the animal was placed on a custom-made foam mat to keep the mouse warm and facilitate surgical access.

A toothed titanium forceps (WPI, Hitchin, UK) were used to ensure the eye stability; and using a 33 G needle (TSK Laboratory, The Hague, Netherlands) a shallow, self-sealing paracentesis was made just anterior to the limbus in the inferior-nasal quadrant of the cornea. The paracentesis lowered eye pressure thus preparing the eye for subsequent subretinal injection.

2.4.2.4 Subretinal injection

A viscous coupling gel (Viscotears® Liquid Gel,0.2 mg/g polyacrylic acid; Alcon Laboratories (UK) Ltd., Camberley, UK) was placed on the top of the cornea before covering it with a round coverslip of 6 mm diameter (VWR International, East Grinstead, UK) to allow a direct view of the fundus via the Leica operating microscope (Leica Biosystems, Newcastle Upon Tyne, UK). The NanoFil subretinal injection syringe (WPI, Hitchin, UK) possessing a 35 gauge bevelled needle with a 25° tri-surface bevel optimized for microinjection was loaded with 1.5 µl of vector suspension. The toothed titanium forceps (WPI, Hitchin, UK) were used to stabilize the eye by holding the superior rectus muscle, and under direct visual guidance, the needle was slowly advanced to penetrate the sclera, choroid and retinal pigment epithelium (RPE) posterior to the equator. Once the tip of the needle was seen under the retina, the needle was directed more

posterior. After visualizing the full bevel opening, the vector suspension was injected in a slow fashion to create a hemiretinal detachment (Figure 2.2). The needle was retracted slowly, and the antibiotic eye drops (0.5% w/v chloramphenicol; Mercury Pharmaceuticals Ltd, Croydon, UK) placed on the cornea, to be replaced by the Viscotears® Liquid Gel to prevent eye desiccation.

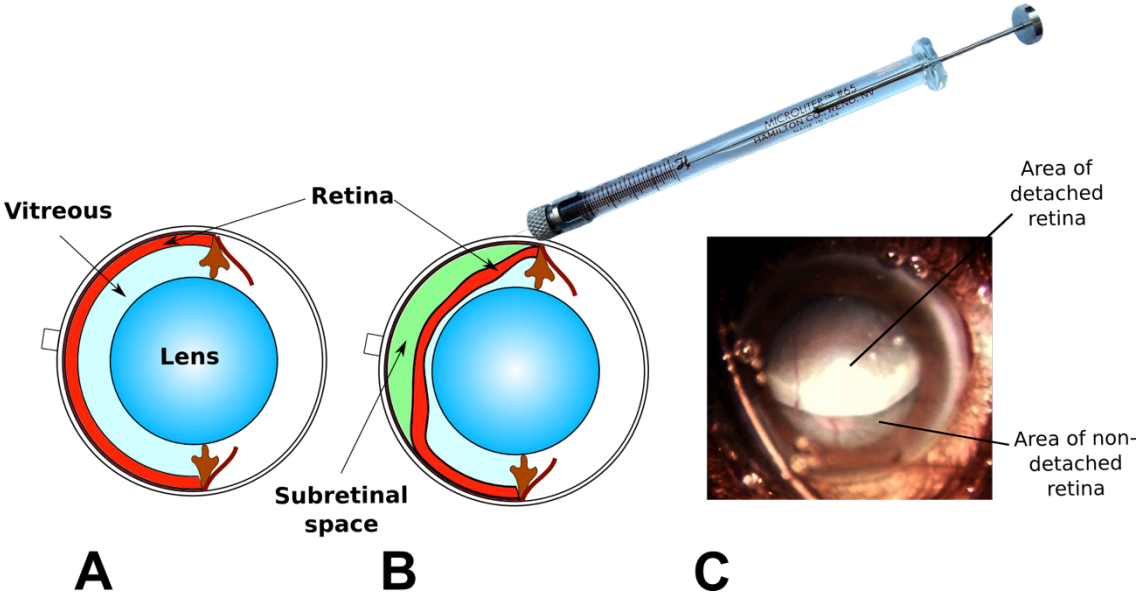


Figure 2.2 Schematic of subretinal delivery of AAV vector in mice
A) Mouse eye B) Formation of subretinal detachment between the neurosensory retina and RPE. C) Photo after a subretinal injection of an AAV vector with the bullous superior retinal detachment.

2.4.3 Confocal Scanning Laser Ophthalmoscopy

Confocal Scanning Laser Ophthalmoscopy (cSLO; Spectralis HRA, Heidelberg Engineering, Heidelberg, Germany) was used to image the ocular fundus in mice. Mice were anesthetised, pupils dilated with mydriatics, and a drop of artificial tears (Hypromellose BPC 0.3% (Matindale Pharmaceuticals, Romford, UK)) was placed on the corneal apex to improve image quality and keep the eye from desiccation and subsequent cataract formation. A contact lens (PMMA

mouse lens, back optic zone radius of 1.7 mm, total diameter of 3.2 mm, centre thickness of 0.4 mm, straight sides Cantor and Nissel, Brackley, UK) (Charbel Issa et al., 2012) was placed on the cornea and the mouse was put on the raised platform (Figure 2.3). The Spectralis™ HRA device from Heidelberg Engineering (Heidelberg Engineering, Heidelberg, Germany) has two diode lasers with the emission spectra centred around λ = 488 nm and 785 nm. The appropriate barrier filters at 500 and 800 nm remove the reflected light with unchanged wavelength while recording the emissions between ca. 500-700 nm in autofluorescence (AF) channel or above 800nm in near infrared (NIR) channel.

EGFP expression was assessed in autofluorescence (AF) imaging mode (excitation: 480 nm), images were taken at different sensitivity levels varying from the maximum level 107 to 70 using the automatic real-time (ART) mode, which is able to track slight movements of the fundus (e.g. caused by respiration). Images were exported from the Heidelberg Eye Explorer as uncompressed TIFF files in high resolution (1536 x 1536 pixels) and processed using ImageJ 1.48v (Wayne Rasband, National Institutes of Health, Bethesda, USA).



Figure 2.3 Confocal Scanning Laser Ophthalmoscopy (cSLO)
The Heidelberg Spectralis Confocal Scanning Laser Ophthalmoscopy for use on mice.

2.4.4 Electroretinography (ERG)

Electroretinogram (ERG) recordings are used to assess the function of rods and cones separately by varying the background light intensity and the intensity of flashes.

2.4.4.1 General ERG set-up

Electroretinograms (ERG) were recorded using the commercially available Multifocal system (Diagnosys LLC, Cambridge, UK) with the ColorDome Ganzfeld Stimulator (Diagnosys LLC, Cambridge, UK). The mice were anesthetised and their pupils were dilated using mydriatics (tropicamide 1% and phenylephrine 2.5%). Mice were kept warm using a heated platform (**Figure 2.4**) kept at a constant temperature at 37°C with a circulating pump-water bath. A drop of Hypromellose BPC 0.3% (Matindale Pharmaceuticals, Romford, UK) eye drops was placed on the corneal apex to maintain moisture and support a good electrical connection for the corneal electrode.

2.4.4.2 ERG electrodes

Subdermal platinum needle electrodes (Grass, West Warwick, USA) were placed subcutaneously: one as a reference electrode in the scruff and another one as a ground electrode at the base of the tail.

A contact lens for the corneal electrode was made by inserting a sheet of transparent Aclar embedding film (Honeywell International, Inc.) between the two jaws of custom made pliers and slowly hole punching the jaws of the pliers to extrude a lens (Sagdullaev et al., 2004). Small slits were cut into the opposite edges of a contact lens so a thin silver coated nylon fiber of a DTL-plus electrode (Diagnosys, Lowell, USA) was inserted through two slits, so when a contact lens was placed on the cornea a thin wire electrode was running horizontally across the cornea surface.

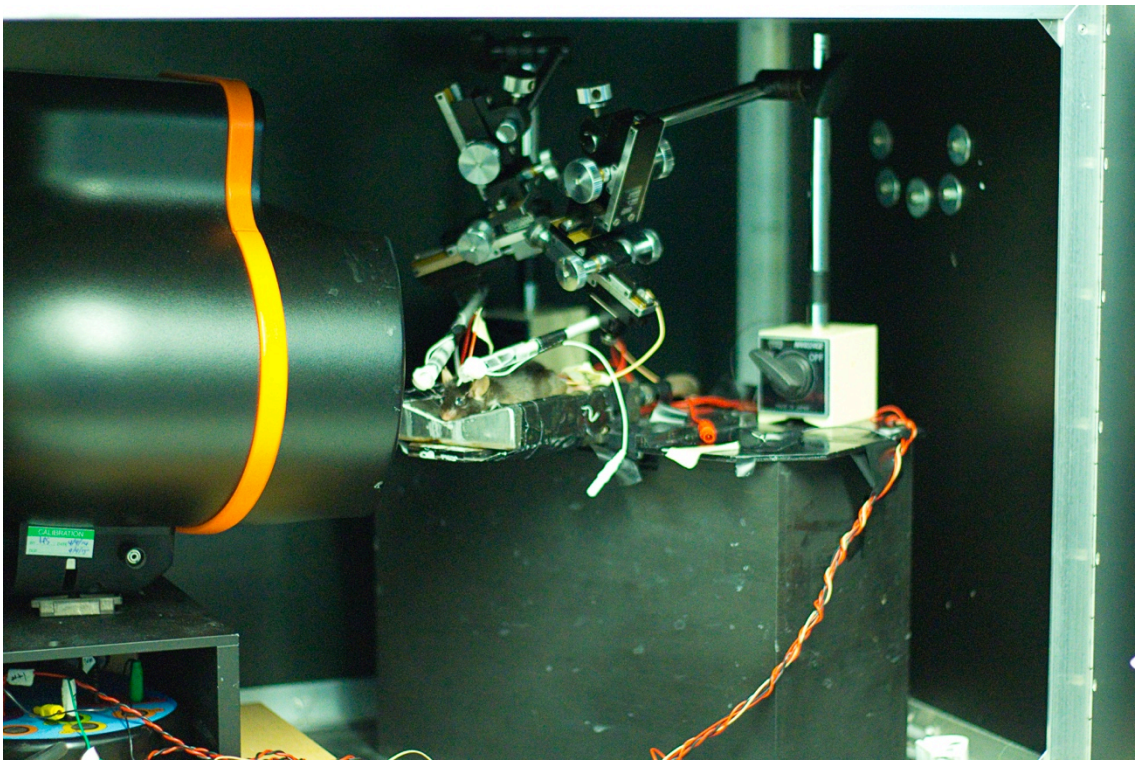


Figure 2.4 ERG platform
The mouse is placed on a heated pad, the mounts of the platform allow positioning of the electrodes. On the left side the Ganzfeld recording bowl, where the mouse will be placed after adjusting the electrodes. The whole set-up is within a metal Faraday box to control for light levels and reduce electric interference.

2.4.4.3 Dark-adapted ERG

Before the ERG all mice were dark-adapted for 12 hours. All further animal handling was performed under dim red light (>650 nm) to keep the retina dark adapted.

After the set-up the animals were placed under the Ganzfeld dome of the Multifocal system and dark adapted for a further 10 minutes. This time allowed the electrodes to stabilise, dark adapt the mice from red light exposure or reset the set-up in a case of excessive baseline deviations from one of the electrodes.

The dimmest light stimuli were presented at the beginning of a session and then the flash intensity was increased by 1 log unit steps. Each step with higher radiance was followed by several seconds of dark adaptation. The frequencies of light stimuli varied between 0.5 Hz to 6 Hz, the source of light was 6500 K, 3-15 trials (repetitions) were collected to produce an average response.

2.4.4.4 Light adapted ERG

To isolate cone-mediated activity, after collection of dark adapted responses mice were adapted for 10 minutes using 30 cd.s/m^2 polychromatic white light stimulus; and bright flashes were administered against rod-saturating background 30 cd.s/m^2 polychromatic white light. 20 repetitions were collected and computer averaged. Flashes were presented with increasing light intensity by 0.5 log unit steps at a rate of 1 Hz.

2.4.4.5 ERG data analysis

A- and b-waves were verified using Multifocal software, then exported as the tab delimited text files into Excel version 14.1.0 (Microsoft, Redmond, USA) to calculate the amplitude of a- and b-waves, the statistical analysis was performed using SPSS (Statistical Package for Social Sciences version 21 by IBM, SPSS Inc., Chicago, USA). The investigator was blinded to which treatment each mouse received.

2.4.4.6 ERG protocol

The ERG protocol for dark and light-adapted ERG is summarised in Table 2.4.

Table 2.4 ERG protocol

Step	Trials	inter-sweep delay	Sweep length	Total step length ms	Step length m	Delay to next step (s)	Description	cd.s/m^2	log
0						**600**	**Dark adaptation (10 min after set-up in dim red light)**		
1	15	0	3000	45000	0.75	15	Single 0.5 Hz 0.0001 (P)cd.s/m1 0 (P)cd/m1 Peak	0.0001	-4
2	10	1000	3000	39000	0.65	15	Single 0.5 Hz 0.001 (P)cd.s/m1 0 (P)cd/m1 Peak	0.001	-3
3	10	5000	3000	75000	1.25	30	Single 0.5 Hz 0.01 (P)cd.s/m1 0 (P)cd/m1 Peak	0.01	-2
4	7	13000	3000	99000	1.65	60	Single 0.5 Hz 0.1 (P)cd.s/m1 0 (P)cd/m1 Peak	0.1	-1
5	4	23000	3000	81000	1.35	120	Single 0.5 Hz 1 (P)cd.s/m1 0 (P)cd/m1 Peak	1	0
6	3	47000	3000	103000	1.7	180	Single 0.5 Hz 10 (P)cd.s/m1 0 (P)cd/m1 Peak	10	1
7	20	0	500	10000	0.17	0	Continuous 6 Hz 0.0001 (P)cd.s/m1 0 (P)cd/m1 Peak	0.001	-3
8	20	0	500	10000	0.17	0	Continuous 6 Hz 0.01 (P)cd.s/m1 0 (P)cd/m1 Peak	0.01	-2
9	20	0	500	10000	0.17	0	Continuous 6 Hz 0.1 (P)cd.s/m1 0 (P)cd/m1 Peak	0.1	-1
10	20	0	500	10000	0.17	0	Continuous 6 Hz 1 (P)cd.s/m1 0 (P)cd/m1 Peak	1	0

Table 2.4 continued

Step	Trials	inter-sweep delay	Sweep length	Total step length ms	Step length m	Delay to next step (s)	Description	cd.s/m^2	log
11	20	0	500	10000	0.17	0	Continuous 6 Hz 10 (P)cd.s/m⁻¹ 0 (P)cd/m⁻¹ Peak	10	1
12	20	0	500	10000	0.17	0	Continuous 20 Hz 10 (P)cd.s/m⁻¹ 0 (P)cd/m⁻¹ Peak	10	1
13	20	0	500	10000	0.17	0	Continuous 30 Hz 10 (P)cd.s/m⁻¹ 0 (P)cd/m⁻¹ Peak	10	1
						600	**Light adaptation (10 min background light 30 cd.s/m-2)**		
14	20	0	1000	20000	0.33	0	Single 1 Hz 1 (P)cd.s/m⁻¹ 30 (P)cd/m⁻¹ White-6500K	1	0
16	20	0	1000	20000	0.33	0	Single 1 Hz 3 (P)cd.s/m⁻¹ 30 (P)cd/m⁻¹ White-6500K	3	0.5
16	20	0	1000	20000	0.33	0	Single 1 Hz 10 (P)cd.s/m⁻¹ 30 (P)cd/m⁻¹ White-6500K	10	1
17	20	0	1000	20000	0.33	0	Single 1 Hz 25 (P)cd.s/m⁻¹ 30 (P)cd/m⁻¹ White-6500K	25	1.4
18	26	0	500	13000	0.22	0	Continuous 20 Hz 10 (P)cd.s/m⁻¹ 30 (P)cd/m⁻¹ White-6500K	10	1

2.4.5 Optomotor response

Optomotor response (OMR) allows evaluation of reflexive vision. To assess OMR a custom-made rotating drum was used, which contained a raised immobile platform in the centre and a rotating cylinder outside the platform. The interior of the cylinder was lined with a paper sheet with 100% contrast black and white vertical stripes and 0.2 cycles/degree spatial frequency. Custom-made software allowed the control of the direction and speed of the cylinder. The drum was illuminated by a fluorescent white light with the brightness of 400 lux, which is considered photopic in mice (Abdeljalil et al., 2005). After the start of rotation, a video was recorded by a digital camera placed on the top of the drum in the centre.

Each mouse was placed on the platform and left for two minutes to habituate. The cylinder was rotated clockwise and anti-clockwise in 30 second intervals for two minutes. Each animal was evaluated three times independently. The cylinder rotated at two revolutions per minute, the optimal velocity established in previous studies (Mangini et al., 1985; Mitchiner et al., 1976).

The OMR was quantified by visualising recorded videos and scoring them blindly with regard to treatment. The experimenter judged whether a mouse made a slow tracking head movement to the direction of the drum's rotation followed by a fast repositioning of the head in the opposite direction. Since it has been shown that slow head tracking movements are driven by each eye independently, each eye was score individually according to the drum's

rotation (Douglas et al., 2005; Harvey et al., 1997; Hobbelen and Collewijn, 1971).

2.5 Tissue processing

2.5.1 Sections

After enucleation, eyes were placed in 4% paraformaldehyde (PFA) on a dish plate, and the cornea and lens excised using forceps and scissors, the excised eyes remained in 4% PFA for 30 minutes, then were transferred into sucrose 10% until the eyecup sunk. Applying the same principle, eyes were then placed into sucrose 20% and then sucrose 30%, washed quickly in PBS. Moulds were made from aluminium foil and filled with OCT compound (VWR, Lutterworth, UK). The eyecups were embedded into moulds filled with OCT, the optic nerve facing upwards. Moulds were frozen in isopentane cooled by dry ice and stored at -80^0.

The blocks of OCT with eyecups were serially sectioned on a cryostat at 18 µm thickness and collected on polylysine coated glass slides (Gerhard Menzel, Braunschweig, Germany), dried overnight and kept at -80^0 until needed.

2.5.2 Confocal microscopy

Confocal microscope (Zeiss LSM710) was used to view stained retinal sections. The 350 nm UV, 488 nm argon, and 543 nm HeNe lasers were used sequentially to excite fluorescence from corresponding dyes. Stack

images were obtained at the resolution of 1024 X 1024 pixels, and processed in ImageJ 1.46r (Wayne Rasband, National Institutes of Health, Bethesda, USA)

2.5.3 Immunohistochemistry

The glass slides from the freezer were dried at room temperature, the area on the slides to stain was circumscribed with an ImmEdge hydrophobic pen (Vector laboratories, Burlingame, US), the slides then were rinsed 3 x 5 minutes with PBS and permeabilised for 20 minutes with 0.4% Triton-X in PBS, rinsed again for 3 X 5 minutes with PBS and blocked for 1 hour with the PBS containing 0.1% Triton-X and 10% serum, the serum used depended on the host species of secondary antibody. Following washing for 3 X 5 minutes with PBS, sections were incubated with a primary antibody at the appropriate concentration diluted in PBS with 0.1% Triton-X, 1% normal donkey or goat serum. After rinsing 3 x 5 minutes with 0.05% Tween in 1 X PBS, slides were incubated in secondary antibody in 0.1% Triton-X, 1% normal donkey or goat serum for 2 hours at room temperature. Following washing for 3 X 5 minutes in 0.05% Tween in 1 X PBS , slides were counter-stained with Hoechst 33342 (Molecular Probes, UK) for 30 minutes (1:1000 in PBS). Sections were washed again (5 minutes) in PBS, a drop of ProLong® (Life Technologies) was applied to preserve fluorescence, slides covered with coverslips and stored at -20^{0}C. The primary and secondary antibodies used are listed in **Table 2.5** and **Table 2.6**.

.

Table 2.5 Primary antibodies used for IHC, Western

Antigen	Raised in	Source	Dilution	Nature
Rhodopsin	Rabbit	Abcam (AB3424)	1:1,000	Polyclonal
Rhodopsin	Mouse	Abcam (AB5417)	1:1,000	Monoclonal
Cone arrestin	Rabbit	Millipore (AB15282)	1:1,000	Polyclonal
GFP	Chicken	Abcam (AB13970)	1:1,000	Polyclonal
ABCA4	Rabbit	Abcam (72955)	1:1,000	Polyclonal

Table 2.6 Secondary antibodies for IHC, Western

Fluorescent dye	Raised in	Source	Antigen	Dilution
Alexa Fluor 568	Donkey	Invitrogen (A10042)	Anti-Rabbit	1:200
Alexa Fluor 635	Donkey	Invitrogen (A31576)	Anti-Rabbit	1:200
Alexa Fluor 647	Donkey	Invitrogen (A31571)	Anti-Mouse	1:200
Alexa Fluor 647	Goat	Invitrogen (A21449)	Anti-Chicken	1:200

2.5.3.1 Quantification of the Hoechst-labelled photoreceptors

To quantify the ONL thickness, 4 non-overlapping high-power images from the opposite sides of the middle retina were taken with a 63X objective on the confocal microscope Zeiss LSM710. The investigator was blinded to the treatment which each mouse received. The number of Hoechst-positive nuclei in the ONL was counted in each image and then averaged per animal.

2.5.3.2 Measurement of EGFP cones

To measure the number of EGFP-expressing cones, 3 non-overlapping high-power images from the middle retina were taken with a 63X objective on the confocal microscope (Zeiss LSM710). The investigator was blinded to treatment, which each mouse received and the number of EGFP cones per image was counted manually using the ImageJ plug-in Cell counter, then averaged per animal.

2.5.4 Western blot

Mouse eyes after enucleation were placed into a dish plate in ice-cold 0.01 M PBS and anterior segment removed (cornea and lens) under a dissection microscope. Eye cups were immediately transferred to 100 µl of RIPA (radioimmunoprecipitation assay) lysis buffer containing protease inhibitors. The RIPA lysis buffer was prepared by mixing of the following: 9 µl of 0.01 M PBS; 1 µl of the RIPA Lysis buffer 10 x (Millipore, UK); 1 tablet of cOmplete, Mini, EDTA-free Protease Inhibitor Cocktail (Roche, UK). The samples were then stored at -80^{0}C until needed. Thawed samples were homogenised with

polypropylene pellet pestles using a hand-held homogenizer (Sigma- Aldrich, UK) and rotated for 30 minutes at 4^0C, vortexed and then spun down at 14,000rpm for 30 min at 4°C. The supernatant was transferred to new tubes and the Pierce™ bicinchoninic acid (BCA) Protein Assay Kit (Thermo Scientific) was used to determine total protein.

Equal amounts of volume of Laemmli protein loading buffer (2X concentrate, Sigma-Aldrich) were added to supernatant, and left at room temperature for 15 minutes before loading into a 10% precast gel Criterion™ TGX™ gel (Biorad). Protein electrophoresis was run at 100 volts until loading dye reached the bottom of gel, approximately two hours. A protein ladder was run alongside the samples to determine protein size. The gel was removed from the tank, the gel cassette was opened using the lid of the gel tank. Two filter pads and a polyvinylidene difluoride (PVDF) membrane with 0.2 µm pore size from Trans-Blot® Turbo™ Midi PVDF (Bio-Rad) were placed on a tray of the Trans-Blot® Turbo™ Transfer Starter System (Bio-Rad), the gel was carefully placed on the top of the membrane, proteins were blotted by using the midi setting (7 min at 25 V) of the TransBlot machine. After the blotting the filter pads and gel were discarded, the membrane was blocked in blocking solution of PBS with 3% BSA and 0.1% Tween 20 for 40 minutes at room temperature on a shaker. The blocking solution was prepared by mixing 0.01 M PBS, with Tween-20 to make 0.1% solution of Tween-20. BSA powder was added to make 3% BSA solution and sterile filtered using 0.22 µm filter.

After the blocking step the membrane was incubated in the primary antibody solution for 1 hour at room temperature on a shaker. The primary antibody mix contained: the polyclonal rabbit anti-rhodopsin antibody (Abcam 3424) in 1:1,000 dilution with 0.01 M PBS with 3% BSA and 0.1% Tween-20.

To wash away antibody, the membrane was washed in the wash buffer (PBS with 0.1% Tween-20) on a shaker, 3 X 7 minutes, then the membrane was incubated with the secondary antibody for 1 hour at room temperature on a shaker and washed. The kit components from Clarity™ western ECL substrate (Biorad) were mixed at a ratio 1:1; added to membrane and incubated for 2 minutes. The membrane was imaged with the Odyssey imaging system (LI-COR Biosciences, Lincoln, NE, USA) using Chemi channel at 2 minutes exposure and analysed with the Image Studio Lite software, version 5.0.

After taking images, the membrane was washed in the wash buffer (PBS with 0.1% Tween-20) on a shaker for 7 minutes, stripped by using the Restore™ Western Blot Stripping Buffer (Thermo Scientific) for 15 minutes on a shaker, the steps were taken as described previously to apply the primary antibody for β-actin (Life Technologies, clone AC-15, Lot 1401025) 1:15,000 (1:10,000) and then the secondary antibody to β-actin (1:10,000), the imaging step was performed as above.

2.5.4.1 Western blot quantification

The background-subtracted densities were determined for rhodopsin and the normalizing control (NC) β-actin bands. The NC with the highest density

value was identified. In order to get a relative NC value, all NC values were divided by the highest NC density value. All densities values for rhodopsin were divided by relative NC values in corresponding lanes.

2.6 Statistical analysis

All data are presented as the mean and standard error of the mean (SEM). To assess the normality of data, Shapiro-Wilk test was used, and to assess homogeneity of variance Levin's test. Means between groups were assessed by factorial ANOVA for repeated measures with Bonferroni-adjusted post hoc test for multiple comparisons. Where appropriate, a paired t-test was used when variables were tested on the same individual. Difference between groups was deemed statistically significant at $\alpha<0.05$. Non-parametric tests such as the Kruskal-Wallis and Mann-Whitney U test were performed when data were non-parametric. Statistical analysis was performed using SPSS version 21 (IBM).

Chapter 3 AAV design and production

3.1 Introduction

3.1.1 AAV production

The development of an AAV gene therapy requires reliable and replicable methods of AAV production. Early methods of AAV production included a transient co-transfection with two plasmids: one with an expression cassette and the other with the viral *rep* and *cap* sequences necessary for viral capsid production and packaging. These early protocols were based on the use of helper viruses, usually adenoviruses, to mediate AAV encapsidation and replication (Samulski et al., 1989). However, the contamination of AAV preparations with highly immunogenic helper virus proteins (adeno- and herpesviruses), was highly undesirable as this could lead to increased immunogenicity of AAV preparations (Yang et al., 1994, 1995). When the genes inside adenoviral genome responsible for mediating AAV production were identified, their incorporation into helper plasmids allowed the implementation of a triple transient transfection method in cultured cells using three plasmids: (1) the plasmid containing a therapeutic gene of interest with regulatory sequences and flanked by two AAV2 ITRs; (2) the *rep/cap* plasmid encoding for the rep and capsid proteins and thus determining a particular serotype of the virus; and (3) the helper plasmid (*pΔΔF6*) providing the required adenoviral helper genes: *EA2*, *E4*, the virus-associated RNA (Matsushita et al., 1998; Xiao et al., 1998). HEK293T cells constitutively express *E1a/b*, another adenoviral gene needed for AAV replication. This

significant advancement allowed for exclusion of adenoviral particles from AAV preparations and elimination of potential immune reactions to adenoviruses.

Further developments in the AAV helper plasmid design enabled the achievement of higher AAV yields by reducing the levels of rep protein expression. The levels of rep protein were decreased by substituting the strong start codon ATG of *Rep78* gene to a non-canonical codon start site ACG, which led to higher level of the *cap* protein production and subsequently to higher AAV titers (Grieger and Samulski, 2012; Li et al., 1997).

Nowadays, this triple plasmid transient transfection of adherent HEK293 cells remains one of the most widely used techniques for AAV production (Clément and Grieger, 2016).

3.1.2 AAV purification methods

Traditionally, the main method of purifying AAV was three rounds of ultrahigh speed density gradient centrifugation by cesium chloride (CsCl). The centrifugation in a buoyant density gradient helps to separate full from empty capsids, however, it has been demonstrated that the CsCl had deleterious effects on AAV infectivity (Auricchio et al., 2001), moreover, the centrifugation by CsCl is a time-consuming process taking about two weeks to complete.

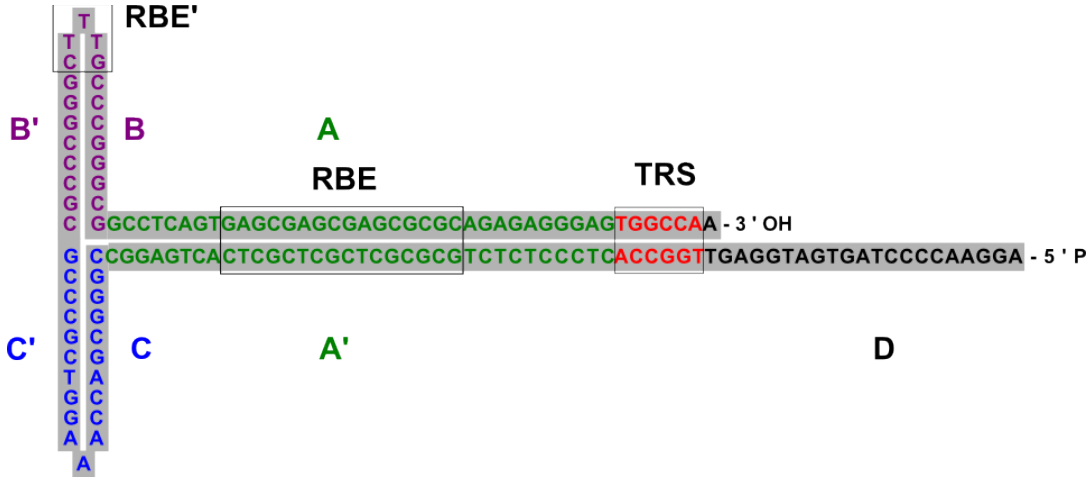
An alternative to the CsCl purification was suggested by Zolotukhin and colleagues who used a non-ionic gradient medium, iodixanol, originally produced as an X-ray contrast compound for clinical use. After one hour of centrifugation, AAV was concentrated in the 40% iodixanol density step and could be recovered with a syringe. Iodixanol offered higher viral recovery and vector purity compared to CsCl (Zolotukhin et al., 1999), although the Iodixanol reagent is more expensive.

In this research project, the transient triple transfection protocol of adherent HEK293T cells with the iodixanol purification method was used for AAV production.

3.1.3 Mutant ITR in scAAV production

One of the ways to improve the transduction efficiency of AAV vectors was the use of self-complementary AAV, which bypass the rate-limiting step of converting single-stranded to double-stranded DNA. The production of self-complementary AAV is achieved by the deletion of the terminal resolution site in the D-sequence in one of the ITRs (Wang et al., 2003). The mutant ITR with the deleted terminal resolution site results in the production of AAV DNA genome containing two self-complementary halves bound by a mutant ITR in the middle and wild-type ITRs at the each end of the genome (**Figure 3.1**).

In this study, the self-complementary plasmid was obtained commercially and the absence of the terminal resolution site in the 3'-ITR was confirmed by dGTP sequencing.



The secondary structure of 3'-ITR in the adeno-associated virus 2 (GenBank accession number NC_001401). ITR plays a key role in the AAV replication and chromosome integration, functioning as the replication origin and priming site for conversion of single-stranded DNA into double-stranded DNA. Its first 125 base pairs are rich in GC content and form a T-shaped thermostable hairpin flanking the AAV genome. The hairpin contains A-palindrome forming the stem; with B and C small internal palindromes forming the cross-arms of the hairpin. The D-sequence comprises the remaining 20 bases of the ITR and the terminal resolution site (TRS). The A and B palindromes contain the Rep-binding elements RBE and RBE' respectively.
The deletion of the terminal resolution site in the 3'-ITR and the use of half wild-type AAV genomes results in the production of scAAV.

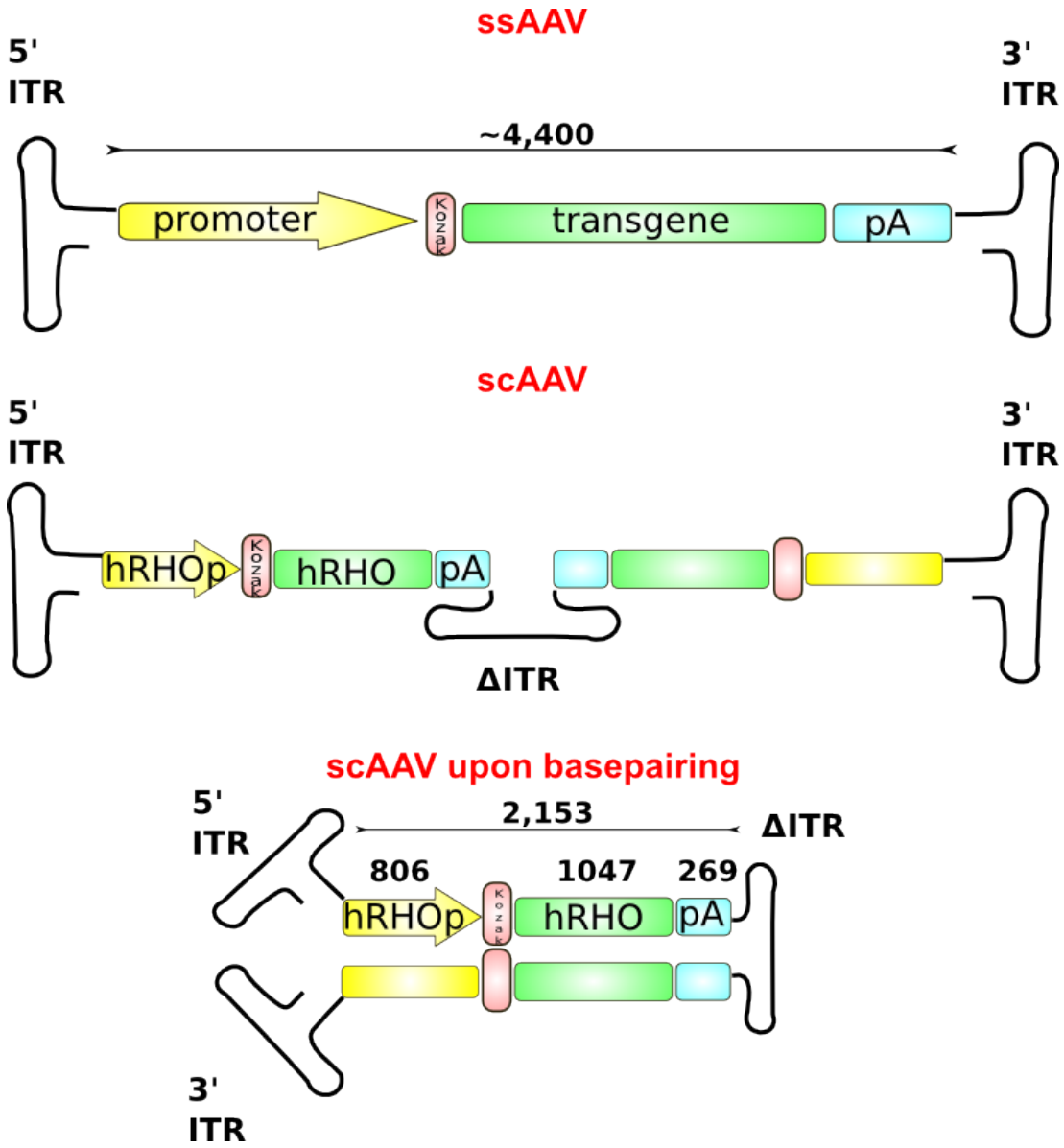


Figure 3.1 The difference in genome of single-stranded and self-complementary AAV

The single-stranded AAV (ssAAV) is flanked by two ITRs and usually contains the promoter, transgene and polyadenylation (pA) signal, the packaging capacity of ssAAV is 4,400 bp.

The designed self-complementary *scAAV2/8-hRHOp-RHO* contains two normal ITRs flanking its genome and a mutant ITR in the middle of the genome (ΔITR). Given that the other half of the scAAV genome contains the base-pairing sequence, the packaging capacity of scAAV is reduced by half.

Upon uncoating in the nucleus, the scAAV rapidly folds on itself by base pairing and forms a double-stranded DNA molecule.

hRHOp: human rhodopsin promoter; Kozak: Kozak sequence; *RHO*: human rhodopsin gene, pA: polyadenylation sequence, ΔITR: mutant ITR. The size of the sequences is indicated above in numbers (bp), the size of the packaging capacity of AAV vectors is indicated above the arrows: approximately 4.4 kb for ssAAV and 2.1 kb for scAAV.

3.1.4 AAV quantification methods

An accurate titer evaluation is a prerequisite for the success of studies comparing different types of AAV vectors. Given that a critical determinant of the therapeutic effect of an AAV vector is its titer, different techniques have been developed to accurately quantify AAV. The dot-blot hybridization assay, a quantitative method based on detecting packaged AAV genomes using DNA probes (Brown, 2001), has been extensively used in the past. Since the dot-blot DNA assay is time-consuming and labour intensive, it has been replaced by absolute quantitative polymerase chain reaction (qPCR), which measures amplification of targeted DNA in real time, and established itself as a reliable, robust, and widely accepted technique to assess AAV titer (Clark et al., 1999). The absolute qPCR quantification is based on a standard curve generated by amplifying a dilution series of standard DNA, usually it can be a plasmid carrying the target DNA (Hou et al., 2010). To assess viral titer, specific qPCR primers are designed to target a small fragment (<200 bp) within a transgene cassette. This research project used the qPCR quantification method to assess AAV titer.

Despite apparent reliability of qPCR, a discrepancy in scAAV titers determined by qPCR to other methods of evaluation was reported: upon the production of a clinical grade scAAV, dot blot hybridization and UV spectrophotometry showed 10-fold higher titer than determined by qPCR (Allay et al., 2011), however it was not reported whether the same discrepancy was observed in ssAAV. Fagone and coworkers hypothesized

that the covalently closed hairpin formed by the mutant ITR in scAAV would enhance reannealing of the viral genome on itself and prevent primer binding during qPCR, thus contributing to the underestimation of scAAV (Fagone et al., 2012). To remove the interference of the terminal hairpin with primers binding, he suggested to use the endonuclease digestion qPCR protocol where the ITR hairpin was removed by endonuclease digestion. In this project we also used the endonuclease digestion qPCR protocol to compare the titers of scAAV and ssAAV.

Additionally, Fagone demonstrated that the distance of qPCR primers to the terminal hairpin affected the titer of scAAV by affecting binding of primers (Fagone et al., 2012). In this research project, to accurately quantify scAAV titers different pairs of primers targeting different regions of the expression cassette were used to eliminate any possible errors in quantification.

3.2 Aims

The aim was to engineer a pseudotyped, recombinant AAV vector with the single mutant capsid (Y733F) from the AAV8 serotype and self-complementary AAV genome for efficient delivery of the rhodopsin gene and assess the produced AAV vectors qualitatively and quantitatively.

3.3 Methods

3.3.1 Vector design

To produce AAV vector, the plasmid map was designed using the Geneious software including the expression cassette with three essential elements: the promoter, transgene and polyadenylation sequence (polyA) flanked by a normal ITR on the 5'-end and the mutant ITR on the 3'-end (**Figure 3.2,** panels B and C).

The following vectors were designed to produce:

the therapeutic vector: *scAAV2/8^{Y733F}hRHOp-RHO-pA*;

the reporter vector: *scAAV2/8^{Y733F}hRHOp-DsRed-pA*.

Subsequent experiments showed that the DsRed reporter protein from the initial control vector: *scAAV2/8^{Y733F}hRHOp-DsRed* conferred fluorescence to rod photoreceptors in *in vivo* cSLO imaging and another control vector was produced: *AAV2/8^{Y733F}-Ia.loxP[EYFP].loxP.WPRE*, hereafter called *AAV-control.*

The human rhodopsin promoter (−800 to +6; GenBank accession number HSU49742) was cloned from human DNA using the following primers:

forward: 5'- CCGGTACCCAGATCTTCCCCACCTAG -3';

reverse: 5'- ATGGTGGCGGATGACTCTGGGTTCTG -3'.

The coding sequence of the rhodopsin gene was cloned from the *RH1-pMT4* plasmid (a kind gift of Dr Wayne Davies) using the following primers, with the Kozak consensus sequence (5'-GCCACC-3'), which facilitates the initiation of the translation process (Kozak, 1999) added to the primer sequence of the rhodopsin forward primer just before the start codon (shown as underlined):

forward: 5'- CATCCGCCACCATGAATGGCACAG-3';

reverse: 5'- CTGATCAGCGGAGTCCTTAGGCCGGGGCCACC-3'.

The bovine growth hormone polyadenylation sequence was amplified from the plasmid *AAV-CAG* with the following primers:

forward: 5'- CCGGCCTAAGGACTCCGCTGATCAGCCTCGAC-3'

reverse: 5'- CCGGCCTAAGGACTCCGCTGATCAGCCTCGAC -3'

The rhodopsin promoter, rhodopsin gene, and polyA sequence were then spliced together to produce full construct *hRHOp-RHO-polyA* using the following primers:

forward: 5'- CCGGTACCCAGATCTTCCCCACCTAG -3';

reverse: 5'- CCGGCCTAAGGACTCCGCTGATCAGCCTCGAC -3'

The reporter vector contained a reporter molecule – the red fluorescent protein DsRed, which was derived from the coral *Discosoma* and has an emission maximum at 583 nm. The DsRed gene was cloned from the plasmid *pI.CAG-Opn4-IRES-DsRed* (a kind gift from Dr Samantha de Silva).

The expression cassettes were spliced together using the SPLICE technique, which allows ligating *in vitro* constructed exons into a single piece of DNA using swift PCR (Davies et al., 2007). After the splicing reaction, the

constructs *hRHOp-RHO-pA* (2.1 kb) and *hRHOp-DsRed-pA* (1.8 kb) were run on 2% agarose gel, the bands corresponding to the size of the constructs were excised from the gel, and purified using the QIAquick gel extraction kit (Qiagen) (section 2.1.5)

The control vector was produced using the plasmid with the stuffer sequence (double-floxed and reversed fluorescent protein EYFP) between two *ITRs:EF-Ia.loxP[EYFP].loxP.WPRE*, which did not encode for any protein expression (not shown).

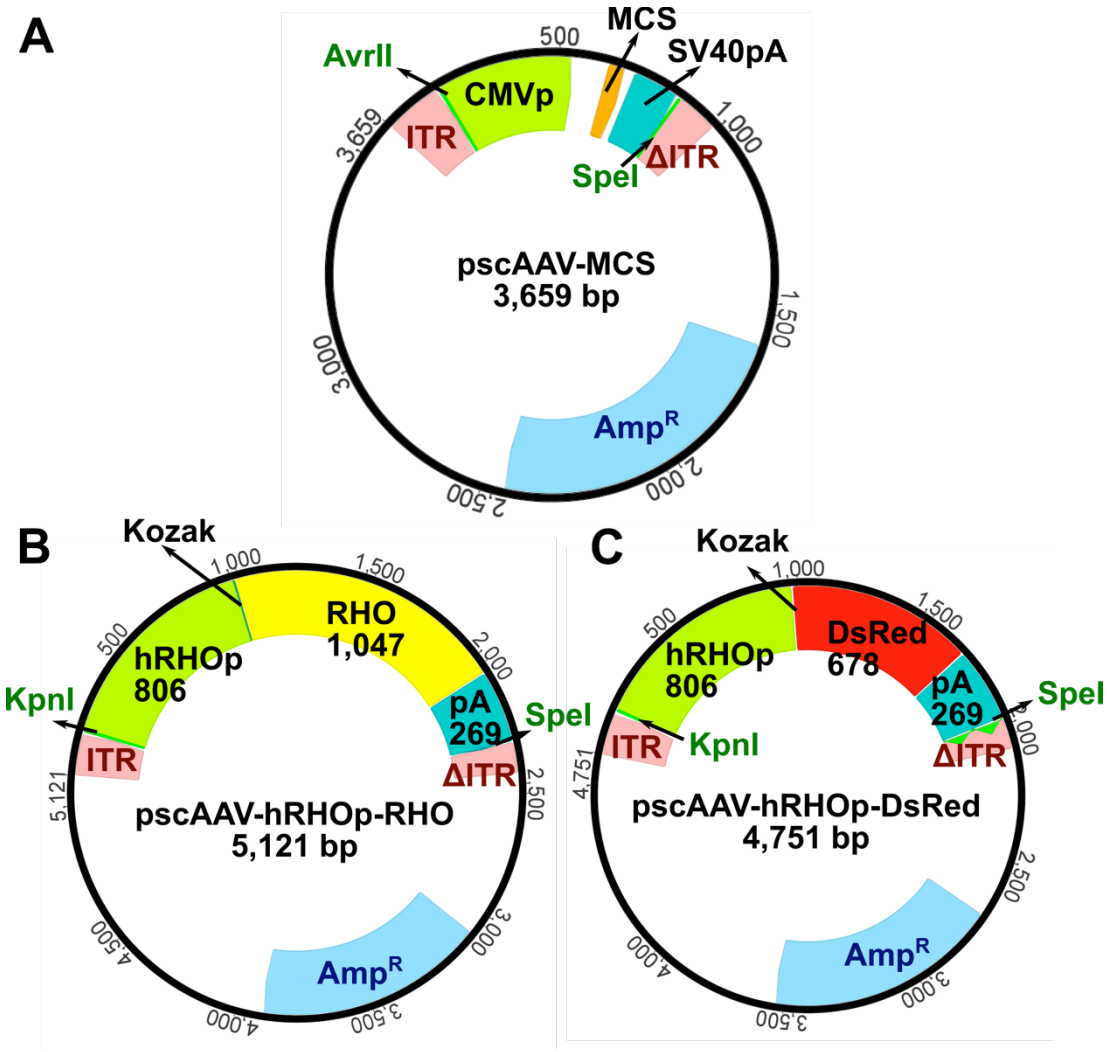


Figure 3.2 Maps of the self-complementary plasmids

A) Schematic of the plasmid *pscAAV-MCS*, which was commercially obtained from Cell Biolabs. The original plasmid contained a normal ITR, a mutant ITR (ΔITR), the cytomegalovirus promoter (*CMV*), Multiple Cloning Site (*MCS*), *SV40pA* polyadenylation signal and the ampicillin resistance gene (Amp^R), restriction sites on the original plasmid were: *AvrII* and *SpeI*. The original plasmid was altered to insert the *KpnI* restriction site and then subsequent cloning allowed inserting the expression cassettes.

B) Schematic of the *scAAV2-hRHOp-RHO-pA* plasmid: *hRHOp*: the human rhodopsin promoter (806 bp), *RHO*: the coding sequence of the human rhodopsin gene (1047 bp), and pA: the bovine growth hormone polyadenylation sequence (269 bp). The restriction sites: *KpnI* and *SpeI*; the Kozak sequence at the start of the rhodopsin gene.

C) Schematic of the *scAAV2-hRHOp-DsRed-pA* plasmid: the rhodopsin gene was replaced with the red reporter gene *DsRed* (678 bp). The Kozak sequence at the start of the *DsRed* gene.

3.3.2 Self-complementary plasmid

In order to produce a self-complementary AAV, the plasmid *pscAAV-MCS* containing a mutant ITR was commercially obtained from Cell Biolabs (San-Diego, USA). The originally obtained plasmid contained the cytomegalovirus (*CMV*) promoter which needed to be replaced by the human rhodopsin promoter. As the multiple cloning site was located after the *CMV* promoter in the plasmid (**Figure 3.2,** panel A), additional alterations of the plasmid were performed to allow the insertion of the desired transgene cassette. To insert the *KpnI* restriction site into the backbone a fragment from the plasmid *pscAAV-MCS* was amplified by PCR with a forward primer containing AvrII and KpnI restriction sites and a reverse primer. Both the self-complementary plasmid and the fragment *AvrII-CMV-MCS* were digested by the restriction enzymes *AvrII* and *ClaI*, then, the fragment *AvrII-CMV-MCS* and the backbone of the plasmid were ligated using the T4 DNA ligase (the details of the ligation protocol in section 2.1.2).

The self-complementary plasmid with the inserted *KpnI* restriction site was digested with the *KpnI* and *SpeI* restriction enzymes, thus removing all elements between the ITRs, and further ligated overnight with the constructs *hRHOp-RHO-pA* (2.1 kb) and *hRHOp-DsRed-pA* (1.8 kb) using T4 DNA ligase (see Appendix for the full sequence of the vector plasmid *hRHOp-RHO-pA)*. After the ligation, mini preparations were further grown up to mega preparations of vector DNA and verified by restriction digest and Sanger sequencing.

3.3.3 ITR integrity verification

The restriction enzyme analysis using the *XmaI* endonuclease was used to verify for ITR integrity in all plasmid preparations in a 10 µl reaction using 1 µg of plasmid left for two hours at 37^0C.

The self-complementary plasmid vectors were sent to Source BioScience for dGTP sequencing to confirm the absence of the terminal resolution site in the mutant ITR using the following primers:

forward polyA.RHO_FW:

5'- CCGGCCTAAGGACTCCGCTGATCAGCCTCGAC -3';

reverse: pscSec2_RC: 5'- GGATGTGCTGCAAGGCGA -3'

3.3.4 The rep/cap and helper plasmids

The *rep/cap* plasmid containing the single amino acid substitution of tyrosine to phenylalanine in the position 733 (Y733F) was previously created in the lab and amplified from the glycerol stock (kind gift of Dr. Michelle McClements). The helper plasmid was also amplified from the glycerol stock to a megaprep DNA. The quantity and purity of all three plasmids used for the HEK293T cells transfection were assessed by Nanodrop.

3.3.5 Production of AAV vector

The virus was produced using the standard AAV production protocol as described in section 2.3 by the method of triple co-transfection using the rep/cap plasmid, helper plasmid, and vector plasmid containing the

transgene cassette (**Figure 3.3**). The AAV preparations were purified by iodixanol gradient (**Figure 3.4**), see section 2.3.4 for details.

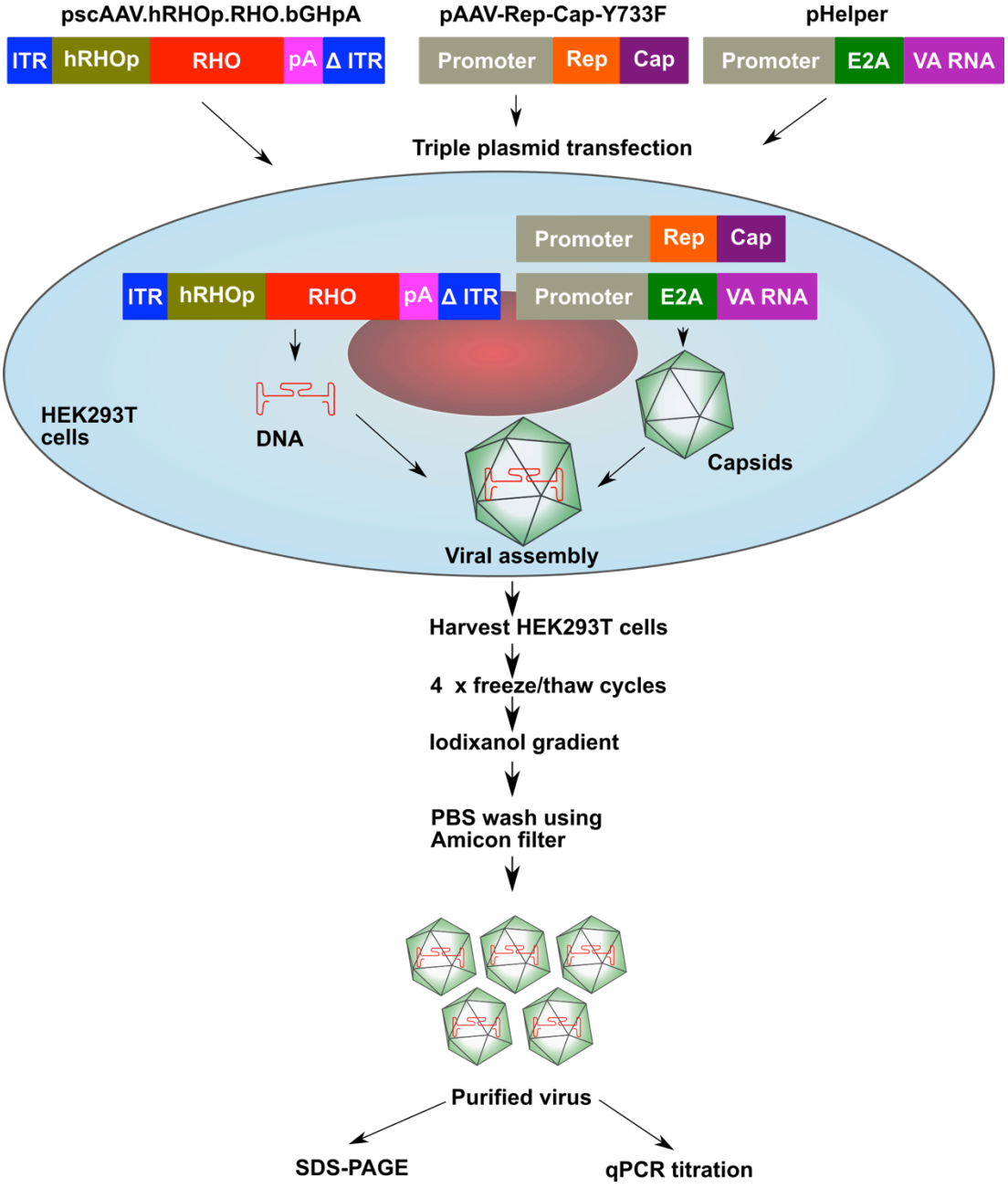


Figure 3.3 Schematic of AAV production
AAV production involved the triple plasmid co-transfection of adherent HEK293T cells, collecting the HEK293T cells' pellet, the freeze-thaw cycles to liberate viral particles from cells, the iodixanol gradient centrifugation, and the final purification with PBS using an Amicon filter. After aliquoting, quantitative (qPCR) and qualitative (SDS-PAGE) evaluation of virus preparations were performed.

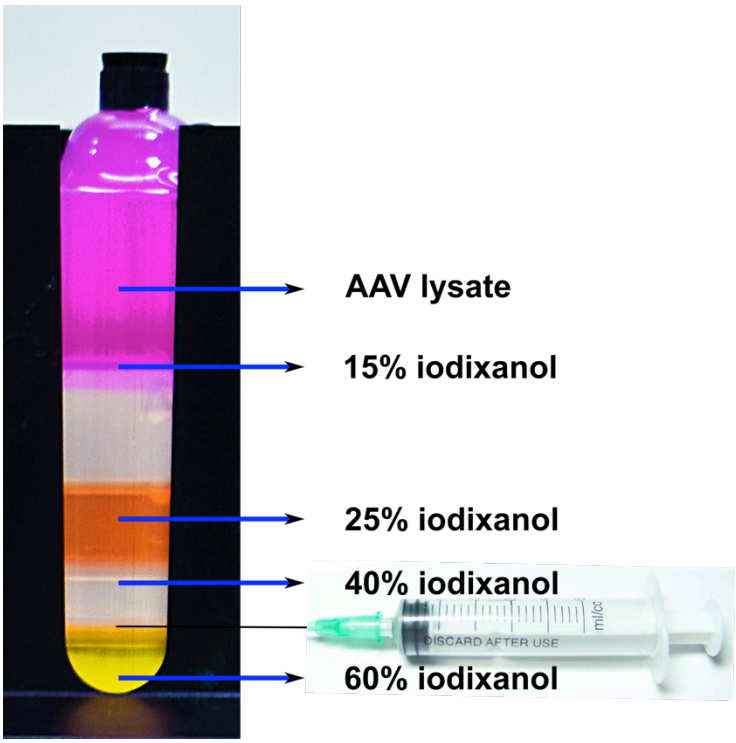


Figure 3.4 Iodixanol gradient
Iodixanol gradient was prepared by layering different gradients of iodixanol (from 15% to 60%), with a final step of placing the AAV lysate obtained from the transfected HEK293T cells on top of the gradient. After centrifugation at 59,000 prm, the AAV fraction was aspirated in the 40% gradient using a syringe placed at the interface of 40% and 60% gradients.

3.3.6 AAV assessment

All AAV preparations were assessed for purity by running SDS-PAGE electrophoresis (described in detail in sectiom 2.3.6).

AAV preparations were quantified by qPCR using different pairs of qPCR primers (section 2.3.7.1). The primers for the ampicillin resistance gene inside the plasmid's backbone were used to assess the reverse packaging. All primer sequences and the length of amplified regions are summarised in Table 3.1. To reflect the presence of two transgene cassettes inside one dimeric genome, the qPCR titers were divided by two (McCarty et al., 2003).

The viral preparations were run in triplicate and were repeated in three separate experiments.

Table 3.1 The primers used for qPCR quantification of AAV preparations

Plasmid sequence	Forward (5' to 3')	Reverse (5' to 3')	Length of the amplified region, bp
Human rhodopsin promoter	CTGACCTCAGGCTTCCTCCT	CCAATCTCCCAGATGCTGAT	118
Rhodopsin	CCTCTCTGCATGGATACTTCGTC	GTGGTGGTGTGTAAGCCCAT	139
Bovine growth hormone polyadenylation	CAGCCATCTGTTGTTTGCCC	GCCACTCCCACTGTCCTTTC	71
Ampicillin resistance	GCGGTATTATCCCGTA	CGAAGGAGCTAACCGCT	216
DsRed	GAAGGGCGAGATCCACAAG	TCCTCGTTGTGGGAGGTGA	150

3.4 Results

3.4.1 Production of the vector plasmids

The human rhodopsin promoter, rhodopsin gene, and polyA sequences were successfully amplified from the corresponding plasmids and their size was verified by agarose gel electrophoresis (**Figure 3.5**). Subsequently, the expression cassettes were spliced together using SPLICE technique and cloned into the self-complementary plasmid. The size of the plasmid and the presence of the insert were verified by agarose gel run and Sanger sequencing **(Figure 3.6**).

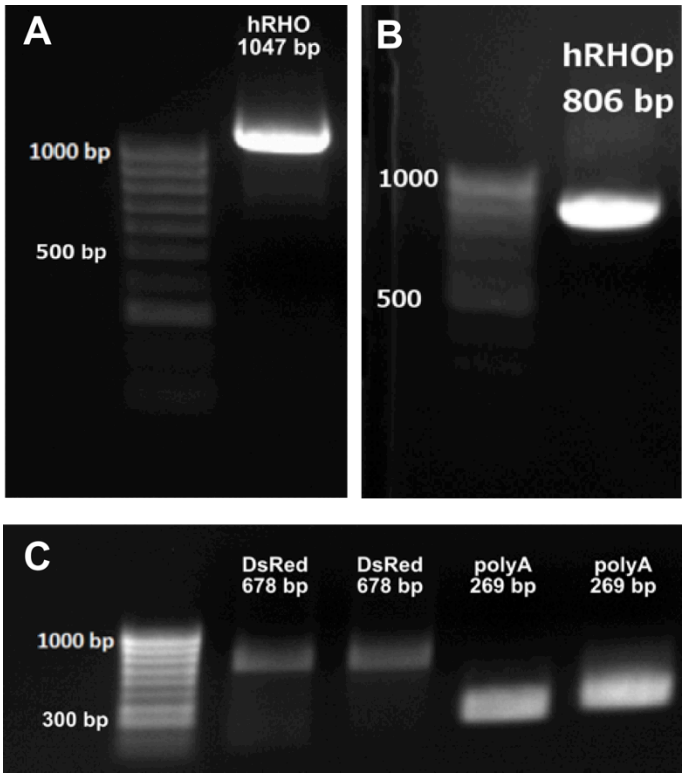


Figure 3.5 Isolation of construct fragments of the *hRHOp-RHO-pA* and *hRHOp-DsRed-pA*

A) The agarose gel with a band of the rhodopsin sequence (*hRHO*) with the correct size of 1047 bp, the DNA ladder shown to the left;
B) The human rhodopsin promoter (*hRHOp*) 806 bp;
C) The *DsRed* and *polyA* bands with the correct corresponding size of 678 bp and 269 bp.

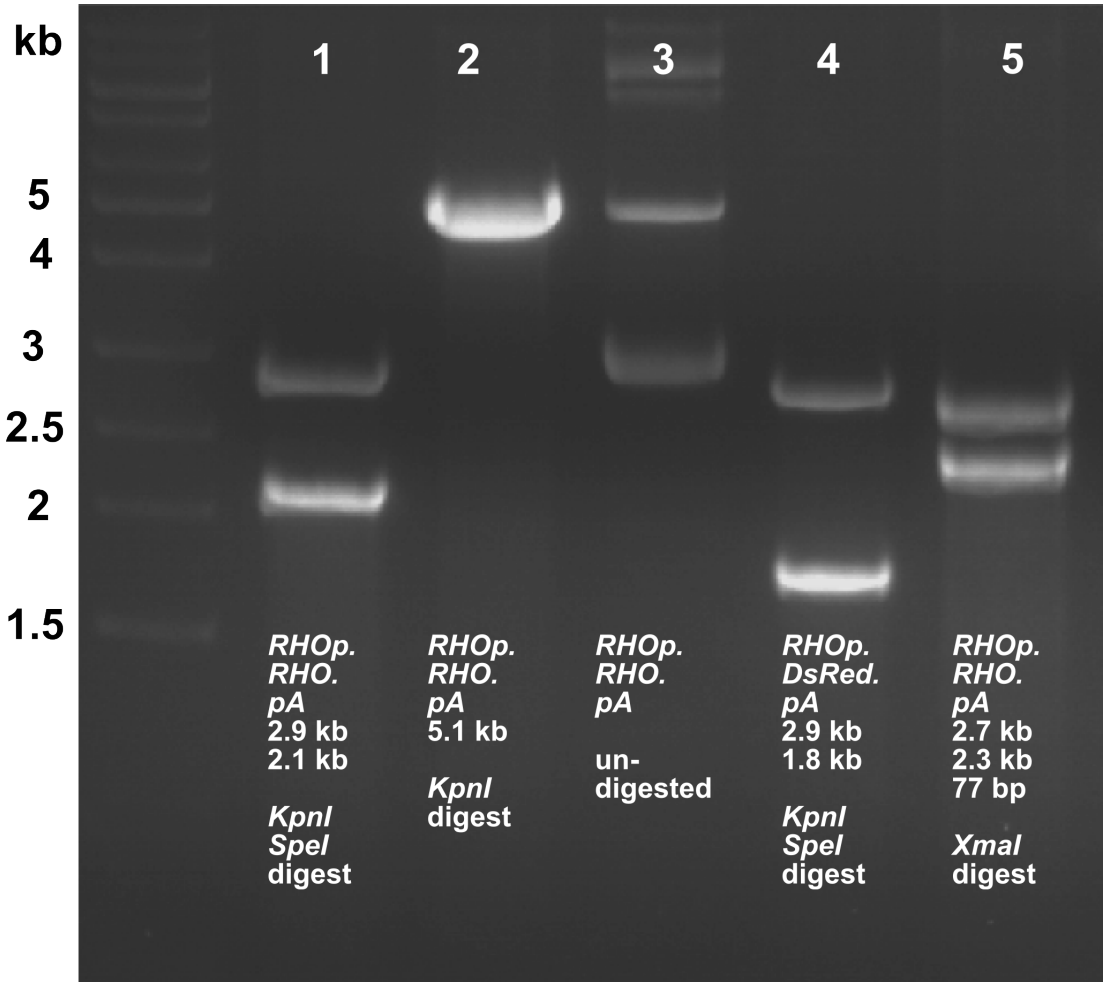


Figure 3.6 Verification of plasmids size by restriction digest

1st lane: *scAAV2-hRHOp-RHO-pA* plasmid after the restriction digestion with *KpnI* and *SpeI* enzymes, the expected size of bands: 2.9 and 2.1 kb.

2nd lane: linearized *scAAV2-hRHOp-RHO-pA* plasmid after the restriction digest with the single enzyme *KpnI* , the expected size - 5.1 kb.

3rd lane: *scAAV2-hRHOp-RHO-pA* plasmid undigested forming two bands corresponding to a fast-migrating coiled fraction and a slow-migrating uncoiled fraction of the plasmid.

4th lane: *scAAV2-hRHOp-DsRed-pA* plasmid, after the restriction digest with the *KpnI* and *SpeI* enzymes, the expected size of bands: 2.9 and 1.8 kb.

5th lane: *scAAV2-hRHOp-RHO-pA* plasmid after the restriction digest with the *XmaI* enzyme to check ITRs' integrity, the expected size of bands: 2.7 kb; 2.3 kb and 77 bp. The presence of the smaller fragment of 77 bp is not visible on this gel due to the scale of the gel and was verified separately (not shown).

The human rhodopsin promoter (806 bp) was selected, as this promoter was shown to efficiently target photoreceptors in mice (Allocca et al., 2007). The therapeutic vector also included the rhodopsin gene coding sequence (1,047 bp) and the polyadenylation sequence to stabilise mRNA. Given the small packaging capacity of scAAV, no additional expression enhancing elements were added.

3.4.2 ITR integrity verification

The ITR integrity was verified by the *XmaI* digest (**Figure 3.6**) and the absence of the terminal resolution site in the mutant ITR was confirmed by dGTP sequencing (**Figure 3.7**).

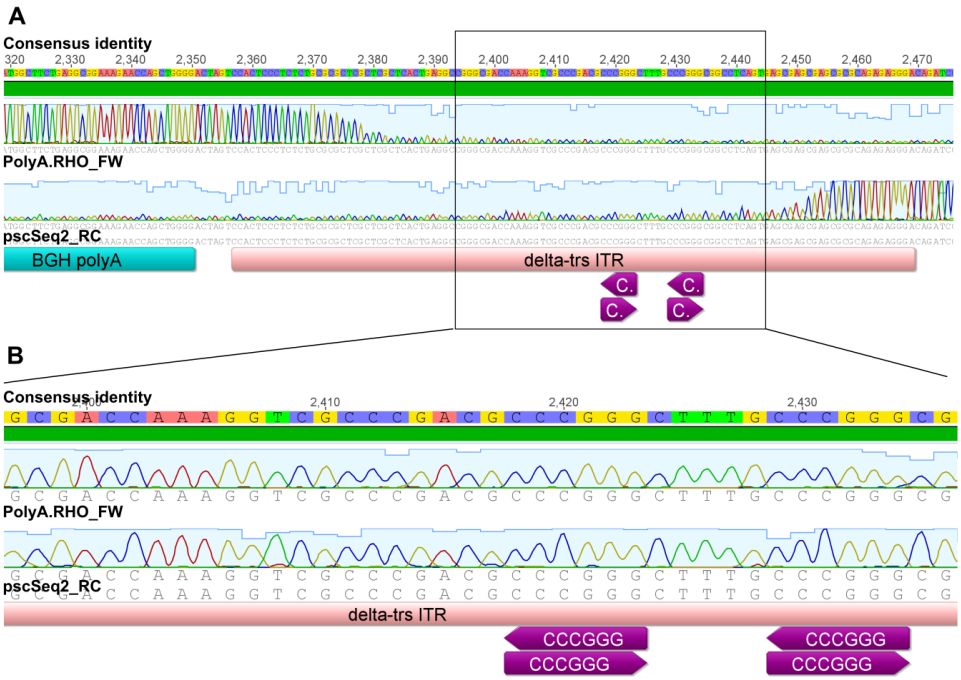


Figure 3.7 The absence of the terminal resolution site confirmed by dGTP sequencing
dGTP sequencing (optimised for GC-rich structures) was used to confirm the mutant ITR integrity and the absence of the terminal resolution site (its absence is crucial for DNA dimers generation in self-complementary AAV production).
A. Consensus identity between the projected mutant ITR (delta-trs ITR) structure and the chromatograms of two sequence reactions readings through the ITR.
B. The magnified view of the chromatograms peaks reading through ITR and confirming its integrity and the absence of the terminal resolution site.
The *XmaI* digest sites are shown in purple.

3.4.3 AAV production

Upon transfection and harvesting of HEK293T cells and purifying viral preparations using an iodixanol gradient and PBS, the following recombinant viruses were produced:

therapeutic vector: *scAAV2/8^{Y733F}hRHOp-RHO;*

reporter vector: *scAAV2/8^{Y733F}hRHOp-DsRed*;

control vector: *AAV2/8^{Y733F}la.loxP[EYFP].loxP.WPRE*.

3.4.4 Assessment of AAV purity

To scrutinize the AAV preparations for purity and the presence of cellular or transgene protein contaminants, the stained SDS-PAGE analysis of rAAV preparations was carried out on all generated vectors (section 2.3.6). **Figure 3.8** shows a typical SDS-PAGE gel of an AAV vector and its diluted preparation (wash) with three bands of viral capsid (VP) proteins of approximate molecular weight of 87, 73, and 62 kDa at a ratio of 1:1:8.

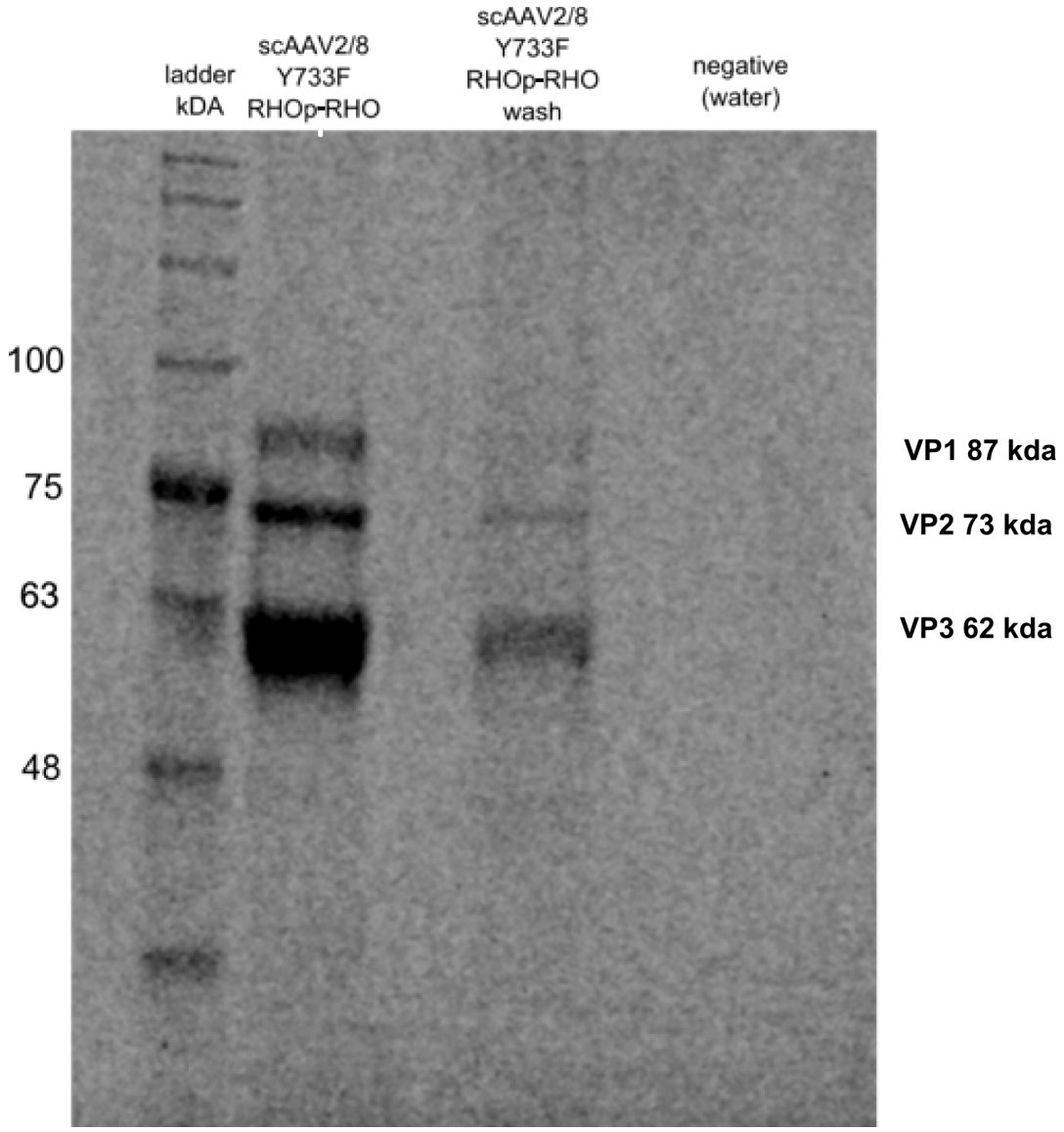


Figure 3.8 SDS-PAGE of AAV samples
The SDS-PAGE gel electrophoresis of the concentrated *scAAV2/8^{Y733F}hRHOp-RHO* vector, its wash, and negative control (water). The concentrated vector shows three bands corresponding to the size of viral capsid (VP) proteins VP1 (87 kDa), VP2 (73 kDa) and VP3 (62 kDa). No other bands are visible indicating the absence of contamination by cellular and other transgene proteins.

3.4.5 Quantification of AAV genome copies

In total two batches of the therapeutic vector *scAAV2/8^{Y733F}hRHOp-RHO* and one batch of the reporter vector *scAAV2/8^{Y733F}hRHOp-DsRed* were made and the following titers based on the qPCR quantification by qPCR primers targeting the polyA sequence compared with a supercoiled reference plasmid standard were obtained:

scAAV2/8^{Y733F}hRHOp-RHO:

1st batch - 5.5 x 10^{11} genome copies/ml (gc/ml);

2nd batch - 1.7 x 10^{12} gc/ml;

scAAV2/8^{Y733F}hRHOp-DsRed – 2.7 x 10^{11} gc/ml;

AAV2/8^{Y733F}Ia.loxP[EYFP].loxP.WPRE – 2.1 x 10^{12} gc/ml.

The typical curves obtained on qPCR measurements are shown in **Figure 3.9**.

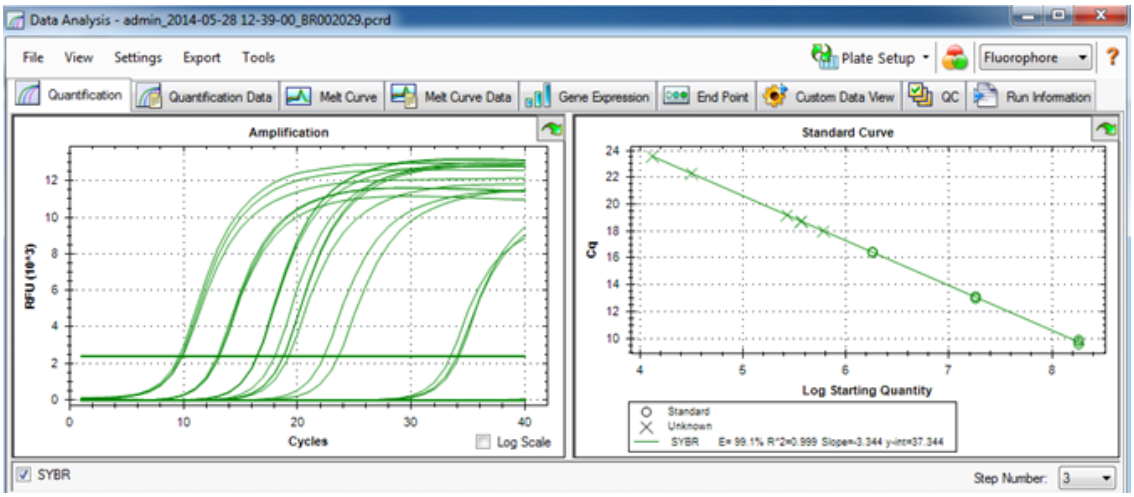


Figure 3.9 qPCR to determine AAV titer
Amplification curves show clear exponential phase. The standard curve indicated the efficiency of 99% confirming high efficiency of primer binding.

3.4.6 qPCR with the primers targeting different regions

The results of qPCR quantification with different qPCR primers targeting different regions of the vector (**Figure 3.10**) did not show a large disparity between the primer pairs within the expression cassette **(**Table 3.2**).**

To analyse the backbone 'reverse' packaging, the quantification with the qPCR primers targeting the ampicillin resistance sequence inside the backbone was performed for *scAAV2/8^{Y733F}hRHOp-RHO*, the results showed, as expected, over a log unit lower compared with titers from within the packaged transgene. (**Table 3.2**)

Table 3.2 Titers obtained with primers targeting different regions within the expression cassette and the plasmid backbone

Primers' target	**Average qPCR titer**	**Efficiency of primers**	**% to the titer determined by *polyA* primers**
RHO promoter	6.1 x 10^{11}	94%	110.9%
RHO gene	7 x 10^{11}	89%	127.2%
polyA	5.5 x 10^{11}	99%	100%
Ampicillin resistance	2.7 x 10^{10}	92%	4.9% *

* The titers obtained with the primers targeting ampicilline resistance should be low, as they represent the backbone of the plasmid packaged into AAV particles.

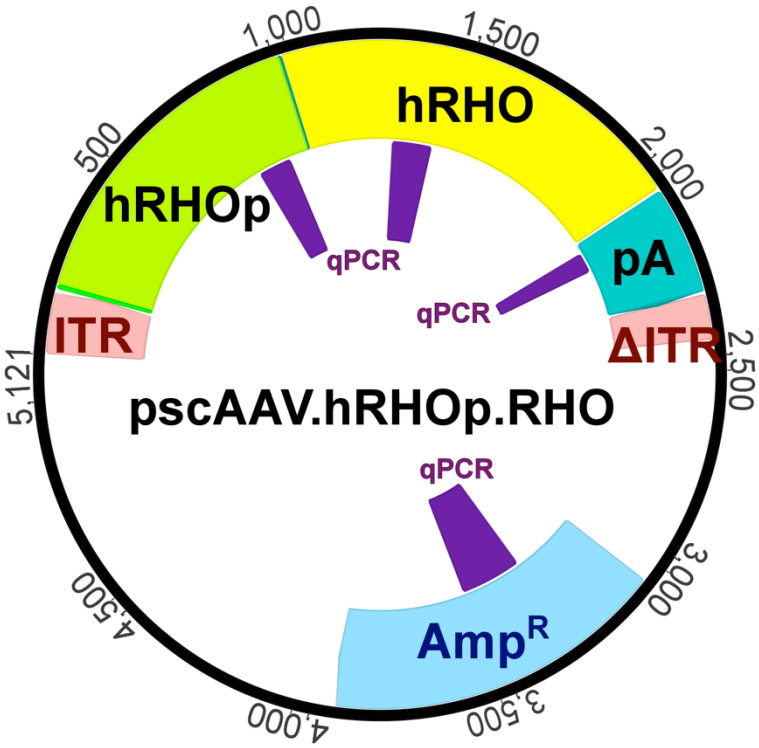


Figure 3.10 Schematic of qPCR primer placement

The map of the plasmid *scAAV2-hRHOp-RHO* showing the placement of qPCR primers (in purple) targeting different regions within the expression cassette and the backbone of the plasmid: The qPCR primers targeted the following regions:
hRHOp: the rhodopsin promoter; *hRHO*: the rhodopsin gene; *pA*: the polyadenylation sequence; *AmpR*: the ampicillin resistance gene.

3.5 Discussion

In this chapter, the therapeutic AAV vector containing the coding sequence of the human rhodopsin gene and a vector with the reporter gene DsRed were developed and produced. The qualitative assessment showed that AAV virions were built from three major capsid proteins: VP1, VP2, and VP3, at a ratio of 1:1:8 and demonstrated the absence of major protein contaminants. The quantitative assessment by qPCR showed the AAV titers were appropriate for further experiments.

The AAV production and subsequent purification aim to make highly potent vectors in large quantities, however, during the production process, various impurities could challenge the potency of the vector *in vitro*. One of the challenges to AAV gene therapy relates to the presence of residual DNA impurities encapsidated into vector particles. These DNA contaminants can not be removed with conventional Benzonase treatment as Benzonase eliminates all DNA outside viral particles and does not have an impact on packaged DNA. The reports in the literature suggested the evidence of packaging of prokaryotic sequences from plasmid backbone (namely, the ampicillin resistance gene) achieved up to 6% of a total viral DNA (Chadeuf et al., 2005). In this research project, the fraction containing the ampicillin resistance sequence achieved 5%, which was comparable to what had been described in the literature.

3.5.1 scAAV quantification

When scAAV were introduced, they were widely reported to have superior transduction efficiency and faster transduction onset compared to conventional AAV (McCarty, 2008). However, Allay and co-workers examining the clinical grade scAAV found a discrepancy between scAAV titers determined by qPCR and other quantitative techniques, such as UV spectophotometry and dot-blot hybridization (Allay et al., 2011). However, the dot-blot DNA assay was found to be highly dependent on the placement of a DNA probe, with the probes hybridizing closer to the ends of viral genomes resulting in fivefold higher signal due to the packaging of terminal genome fragments (Wang et al., 2012) so the discrepancy found by Allay can be explained partly by the dot-blot DNA assay variability. Furthermore, Fagone and colleagues hypothesized that the covalently closed hairpin formed by the mutant ITR in scAAV would enhance reannealing of the viral genome on itself and prevent primer binding during qPCR (Fagone et al., 2012). Fagone and coworkers showed that qPCR primer location proximal to the terminal hairpin compared to the primers targeting central regions of transgene cassette could produce a titer discrepancy in scAAV. However, it was shown that ssAAV titers were affected by the qPCR primer placement in a similar fashion (D'Costa et al., 2016; Wagner et al., 2013; Wang et al., 2013; Werling et al., 2015), so it remains to be elucidated whether qPCR primer placement relative to ITRs affects both scAAV and ssAAV to the same degree. In this project, the use of different qPCR primer pairs targeting various regions within the expression cassette showed variation going up to ~30%,

suggesting some influence of qPCR primers placement on titer evaluation of the produced vectors, however the described variation was smaller than 5-6 fold difference described in literature (Fagone et al., 2012; Wang et al., 2012)

The Inverted Terminal Repeats (ITRs) in AAV are crucial for virus production and subsequent transduction, however, ITRs are notorious for being lost or deleted during *E.coli* propagation (Gray and Zolotukhin, 2011). Therefore, it is critical to verify the integrity of ITRs in produced plasmids before AAV production. Since ITRs have very high GC content (70%) and form strong secondary hairpin structures, Sanger DNA sequencing is unable to read through ITR. Therefore the restriction enzyme analysis with the *XmaI* endonuclease is traditionally used to verify for ITR integrity since *XmaI* cuts within ITRs. To confirm ITR's integrity, the restriction digest using *XmaI* was performed in all plasmid preparations.

However, Mroske et al. (2007) proposed the amplification sequencing method using 7-deaza-dGTP, which allowed reading through the ITR hairpin. As the commercial company Bioscience to which we delegated Sanger sequencing offered a dGTP Cycle Sequencing protocol optimized for sequencing through GC-rich templates, we used this dGTP protocol to sequence through the mutant ITR.

Interpretable results were obtained for the mutant ITR, and its whole sequence was confirmed using dGTP sequencing. Though the amplitude of fluorescent peaks in the hairpin region of ITR was significantly diminished, however, all the peaks were unambiguous and confirmed the absence of the

terminal resolution site in the 3'-ITR which corresponds to the mutant ITR structure allowing for viral dimer formation and thus critical for self-complementary viral production.

Taken together, the data in this chapter suggest that the produced self-complementary AAV presented high-purity preparations in terms of protein contaminants and titer significant enough for further experiments.

In the next chapter, the ability of the produced vectors to transduce cells will be examined on cultured cells *in vitro*, rhodopsin knockout mice *in vivo* and primate retina *ex vivo*.

Chapter 4 AAV vector evaluation

4.1 Introduction

In the previous chapter, two vectors (one with the rhodopsin gene and one with the red fluorescent reporter gene DsRed, both driven by the human rhodopsin promoter) were successfully produced by the triple co-transfection of HEK293T cells. The current chapter presents the data assessing the specificity of the human rhodopsin promoter and evaluating the ability of the vectors to drive expression in photoreceptors.

After the production of a vector, it is imperative to demonstrate that upon delivery the administered gene drives the expression of the protein in the correct cell compartment. In a healthy rod photoreceptor, rhodopsin is produced in the inner segment and then transported through the connecting cilium to the rod outer segment, where it is localised on histology analysis. Given that many rhodopsin mutations lead to the ectopic expression of the rhodopsin protein not only in the outer segment but in the bodies of photoreceptors (on histology analysis rhodopsin is expressed in the whole outer nuclear layer) and the sequence difference between the human and mouse protein (95% of sequence similarity), it was important to establish whether the delivery of the AAV vector with the human rhodopsin gene into rhodopsin knockout mice would lead to rhodopsin expression in rod outer segments.

Moreover, the successful therapeutic effect can be achieved only if a large enough area of the retina is transduced and considerable effort had been

spent in the AAV field to establish the most efficient vectors in terms of transduction. In order to compare rhodopsin levels from the AAV vector to wild-type levels, quantitative Western blot analysis is presented in this chapter.

4.2 Aims

- To assess the ability of the human rhodopsin promoter to drive expression in HEK293T cells;
- To assess the expression of the AAV-delivered rhodopsin gene in rhodopsin knockout mice and to evaluate the rod-specificity of the rhodopsin promoter on the primate and mouse retina;
- To assess the extent of transduction upon the subretinal delivery of the AAV vector using cSLO imaging;
- To compare the level of rhodopsin protein expression from the AAV-delivered rhodopsin gene in rhodopsin knockout mice with wild-type mice using Western blotting.

4.3 Methods

4.3.1 *In vitro* assessment of the human rhodopsin promoter

In order to provide evidence for the biological efficiency of the human rhodopsin promoter, HEK293T cells were transfected with the plasmid containing the reporter gene *DsRed* driven by the human rhodopsin promoter

pl.hRHOp-DsRed. As a control in this experiment, the plasmid *pl.CAG.Opn4.IRES.dsRed.wPRE-pA* (a kind gift of Dr de Silva), in which the DsRed expression was driven by the ubiquitous promoter *CAG* was used (the transfection protocol described in detail in section 2.2.2).

4.1.1 *In vivo* assessment of rhodopsin expression

Rhodopsin knockout mice at the age of three weeks were injected subretinally with *scAAV2/8^{Y733F}hRHOp-RHO* in one eye, and *scAAV2/8^{Y733F}hRHOp-DsRed* in fellow eye in total volume of 1.5 µl containing the dose of 8.4 x 10^8 gc (section 2.4.2).

To evaluate rhodopsin expression, one month after injection, mice were sacrificed and eyes collected for histology analysis. Rhodopsin and Adenosine triphosphate Binding Cassette Subfamily A Member 4 (ABCA4) expression was assessed by staining eye sections with the corresponding antibodies (for more details, see section 2.5.3).

To assess whether the human rhodopsin promoter transduced rods only or both rod and cone photoreceptors, the eye sections of the rhodopsin knockout mice injected with the *scAAV2/8^{Y733F}hRHOp-DsRed* vector were immunolabelled with cone arrestin antibody and analysed for co-localisation of DsRed-expressing photoreceptors and arrestin-stained cones.

4.1.2 Macaque retinal explants

Macaque retinal explants of 3 mm diameter were transduced with *scAAV2/8^{Y733F}hRHOp-DsRed* in either a higher dose (10^{10} gc) or a lower

dose (10^9gc) (section 2.2.3). The explants were kept at 34°C, 5% CO_2 for eight days after transduction, and then they were fixed and cryosectioned. Sections were immunolabelled with the polyclonal rabbit anti-rhodopsin antibody (Abcam ab3424).

4.1.3 Extent of retinal transduction

To control for the surgical intervention and the extent of viral transduction, rhodopsin knockout mice at the age of three weeks were injected subretinally creating a bullous detachment of the superior retina with 1.5 µl containing 8.1 x10^8 gc of *scAAV2/8^{Y733F}hRHOp-DsRed* in one eye, the other eye was left uninjected.

To examine the presence of autofluorescence, one month after surgery the mice were anesthetised again and confocal laser ophthalmoscopy (cSLO) was performed *in vivo* (section 2.4.3). The detected autofluorescence pattern in the eyes injected with *scAAV2/8^{Y733F}hRHOp-DsRed* and the absence of fluorescence in the contralateral uninjected eyes suggested that autofluorescence in injected eyes derived from the DsRed protein delivered by the viral therapy and reflected the efficiency and extent of transduction. Untreated eyes served as a negative control to confirm the absence of autofluorescence. The mice were sacrificed after the procedure and eyes enucleated for consequent histology analysis.

4.1.4 Western blot

To evaluate protein expression by Western blot, six *Opn1.EGFP Rho-/-* at the age of three weeks were injected subretinally with 1.5 µl of the viral vector containing *scAAV2/8^{Y733F}hRHOp-RHO* 2.5 x 10^9 gc/ml, the fellow eye was left untreated. Two months after injection, the mice were sacrificed and eyes collected for Western immunoblotting (see section 2.5.4).

To compare the production of the AAV-delivered rhodopsin in rhodopsin knockout mice to wild-type mice, six age-matched *Opn1.EGFP* Rho+/+ mice which have a normal level of rhodopsin expression were used as wild-type. Western blotting was performed using the polyclonal rabbit anti-rhodopsin antibody (Abcam ab3424).

4.2 Results

4.2.1 Limited transfection of HEK293T cells

Fluorescent microscopy showed markedly lower levels of expression of the DsRed protein in the HEK293T cells transfected with the plasmid pl.*hRHOp-DsRed* compared to the control plasmid pl.*CAG.Opn4.IRES.DsRed.WPRE* three days after transfection. Further optimisation of the transfection protocol including various cell density, amount of the transfection reagent, plasmid, the use of another transfection reagent, Mirus TransIT-LT1 (Geneflow) and longer post-transfection time did not improve transfection results (**Figure 4.1**).

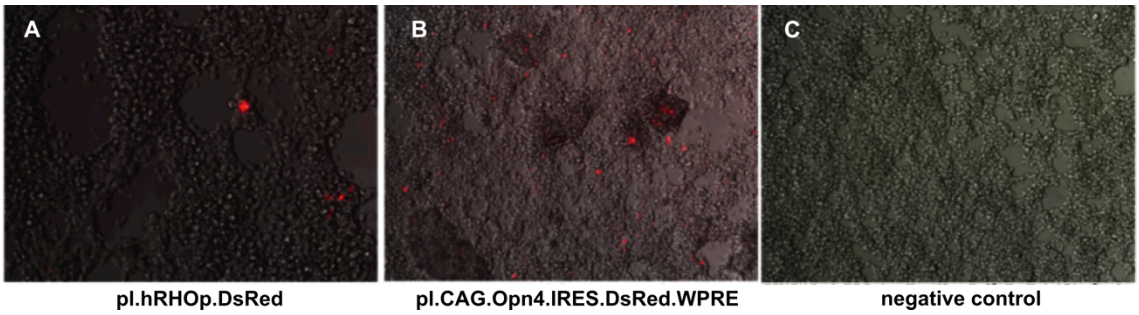


Figure 4.1 Limited expression of DsRed upon the transfection HEK293T cells with the plasmid *pl.hRHOp-DsRed*

The expression level of DsRed from the plasmid *pl.hRHOp-DsRed* was markedly lower compared to the control plasmid *pl.CAG.Opn4.IRES.DsRed.WPRE* assessed by fluorescent microscopy on HEK293T cells.

A) The HEK293T cells 3 days after transfection with the *pl.hRHOp-DsRed*;

B) The HEK293T cells 3 days after transfection with the *pl.CAG.Opn4.IRES.Dsred.WPRE* (positive control);

C) The HEK293T cells 3 days after transfection with only the transfection reagent added without DNA (negative control).

HEK293T cells (2 x 10^5) were seeded in 6-well tissue culture plates with complete growth medium DMEM and transfected next day with plasmid DNA using a mixture of 3 µl GeneJuice Transfection Reagent with approximately 1 µg of a plasmid and assessed 3 days later using fluorescent microscopy.

4.2.2 Regrowing of outer segments after the rhodopsin gene delivery

The rhodopsin staining of the eyes of the rhodopsin knockout mice, which received the subretinal injection of *scAAV2/8^{Y733F}hRHOp-RHO* in one eye and *scAAV2/8^{Y733F}hRHOp-DsRed* in the fellow eye demonstrated the expression of rhodopsin in ROS in the eyes treated with *scAAV2/8^{Y733F}hRHOp-RHO*, whereas the fellow eye, clearly showed the DsRed expression in the outer nuclear layer with the absence of rhodopsin expression (**Figure 4.2**).

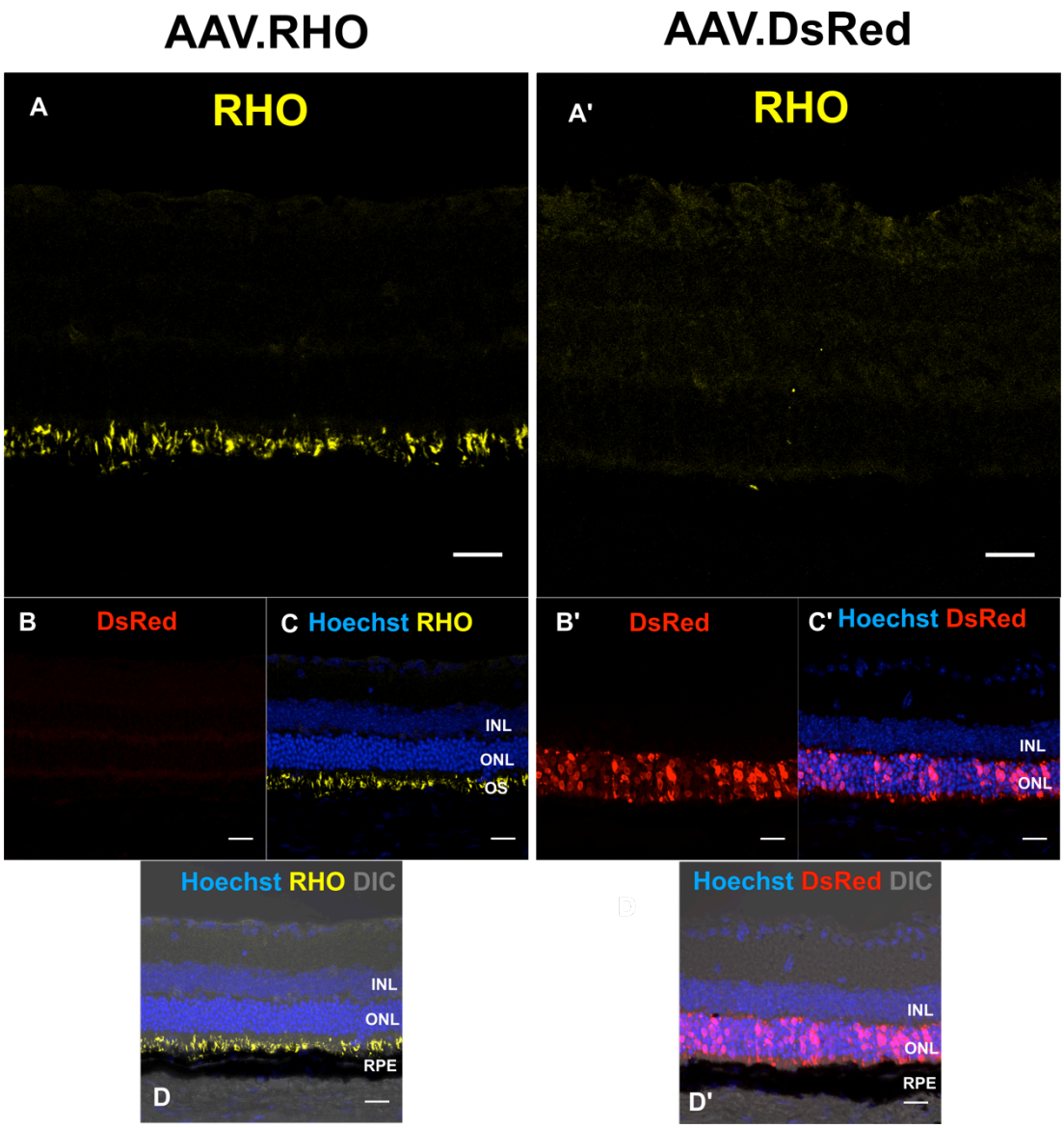


Figure 4.2 Rhodopsin expression in the ROS upon the AAV delivery of the rhodopsin gene one month after injection

Rho-/- mice were injected at age 3 weeks with *scAAV2/8^{Y733F}hRHOp-RHO* (the panel on the left, AAV.RHO) in one eye and *scAAV2/8^{Y733F}hRHOp-DsRed* in the fellow eye (the panel on the right, AAV.DsRed), histology one month post-injection. The eye treated with *scAAV2/8^{Y733F}hRHOp-RHO* shows rhodopsin expressed in rod outer segments (yellow), whereas the contralateral eye treated with *scAAV2/8^{Y733F}hRHOp-DsRed* shows the absence of rhodopsin expression and the DsRed expression limited to the ONL.

Scale bar 20 µm. INL: inner nuclear layer, ONL: outer nuclear layer, OS: outer segments, RPE: retinal pigment epithelium.

Panel A, A': RHO: rhodopsin staining (yellow);

Panel B, B':DsRed fluorescence (red);

Panel C: Hoechst: blue nuclear stain, RHO: rhodopsin staining (yellow);

Panel C': Hoechst: blue nuclear stain, DsRed fluorescence (red);

Panel D: RHO: rhodopsin staining (yellow), Hoechst: blue nuclear stain, DIC: differential interference contrast (grey);

Panel D': Hoechst: blue nuclear stain, DsRed fluorescence (red), DIC (grey).

Similarly, ABCA4 staining was localised to the outer segments one month after injection in the eyes injected with *scAAV2/8^{Y733F}hRHOp-RHO*, whereas no ABCA4 expression was evident in the eyes treated with *scAAV2/8^{Y733F}hRHOp-DsRed* (**Figure 4.3**).

.

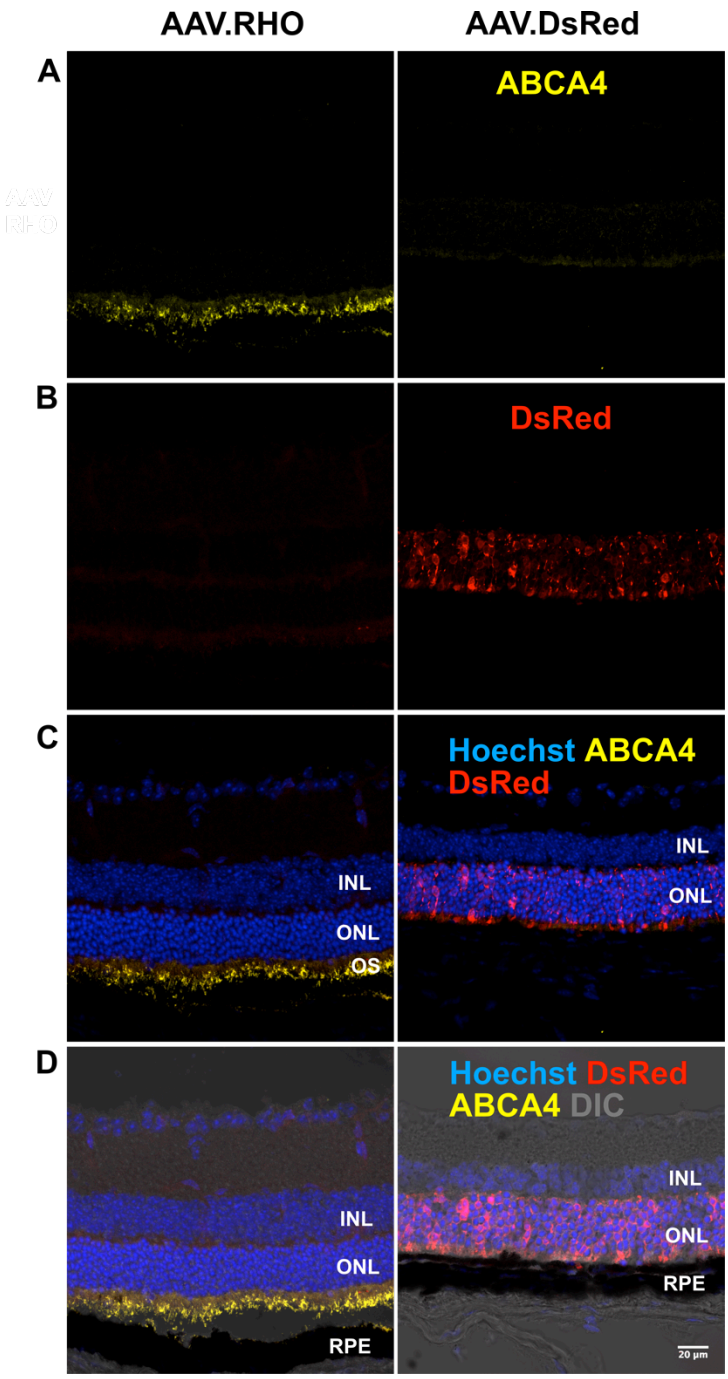


Figure 4.3 ABCA4 expression in outer segments upon the AAV delivery of the rhodopsin gene one month after injection

Rho-/- mice were injected at age 3 weeks with *scAAV2/8^{Y733F}hRHOp-RHO* in one eye and *scAAV2/8^{Y733F}hRHOp-DsRed* in the fellow eye, histology one month post injection.

Panels on the left show the eye treated with *scAAV2/8^{Y733F}hRHOp-RHO* (AAV RHO) with ABCA4 expressed in rod outer segments .

Panels on the right show the absence of ABCA4 expression and DsRed expression in the ONL in the contralateral eye treated with *scAAV2/8^{Y733F}hRHOp-DsRed*. INL: inner nuclear layer, ONL: outer nuclear layer, OS: outer segments, RPE: retinal pigment epithelium, panel A: ABCA4 staining (yellow); panel B: DsRed fluorescence (red); panel C: ABCA4 staining (yellow), DsRed fluorescence (red), Hoechst nuclear staining (blue); panel D: ABCA4 staining (yellow), DsRed fluorescence (red), Hoechst nuclear staining (blue), DIC: differential interference contrast (grey). Scale bar 20 µm.

4.2.3 Rod specificity

The immunolabelling with cone arrestin antibody demonstrated the marked absence of co-localisation of DsRed and cone arrestin staining signifying the specific targeting of rod photoreceptors by the human rhodopsin promoter in the vector and the lack of off-target expression in cone photoreceptors in rhodopsin knockout mice injected with *scAAV2/8^{Y733F}hRHOp-DsRed* **(Figure 4.4**).

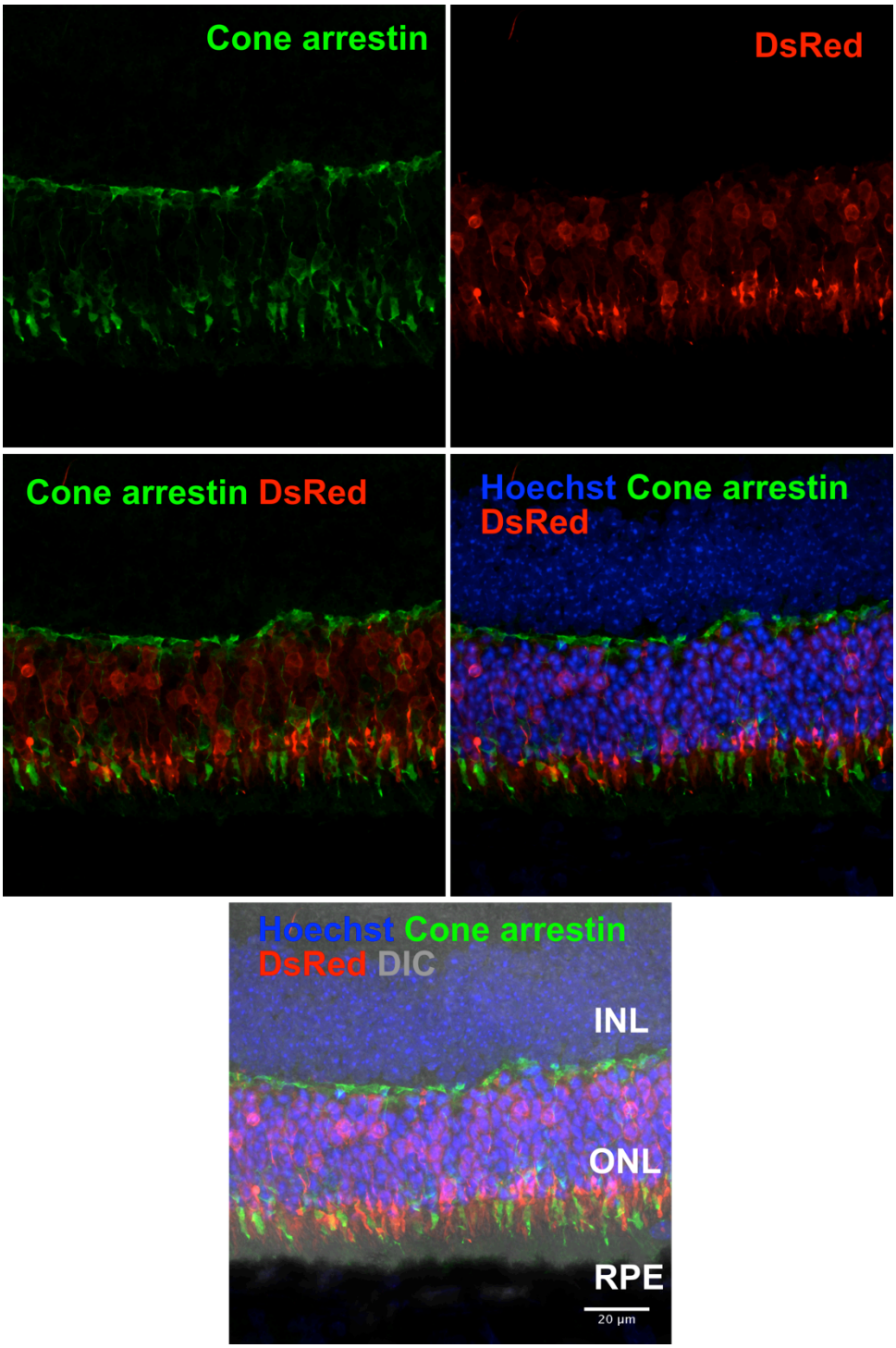


Figure 4.4 The human rhodopsin promoter drives the rod-specific expression of DsRed in rhodopsin knockout mice

Immunohistochemical analysis of the cone arrestin and DsRed co-localisation in the rhodopsin knockout mice, which received *scAAV2/8*^{Y733F}*hRHOp-DsRed* injection at PW3. The eyes were fixed and cones were immunolabelled with cone arrestin antibody. Note the absence of co-localisation between DsRed (from the AAV vector driven by the human rhodopsin promoter) and cone arrestin staining (which stains cone bodies). Cone arrestin (green), DsRed fluorescence (red), Hoechst nuclear staining (blue), DIC: differential interference contrast (grey). Scale bar 20 µm.

4.2.4 DsRed expression of in the primate retina *ex vivo*

The macaque retinal explants obtained from the peripheral retina of freshly sacrificed macaques were transduced with the higher and lower dose of *scAAV2/8^{Y733F}hRHOp-DsRed*; eight days later, the tissue was fixed and immunolabelled for rhodopsin. The histology analysis showed DsRed expression in the outer segments of photoreceptors co-localising with rhodopsin staining at the higher dose (10^{10} gc) of the vector. However, no visible expression of DsRed was apparent in the explants transduced with the lower dose (10^{9} gc) of the vector (**Figure 4.5**). The DsRed expression in the higher dose transduction was specifically targeting the outer segments of photoreceptors and no expression of DsRed was noted in the outer nuclear layer, which represents the bodies of photoreceptors, suggesting correct targeting of DsRed protein from the *scAAV2/8^{Y733F}hRHOp-DsRed.*

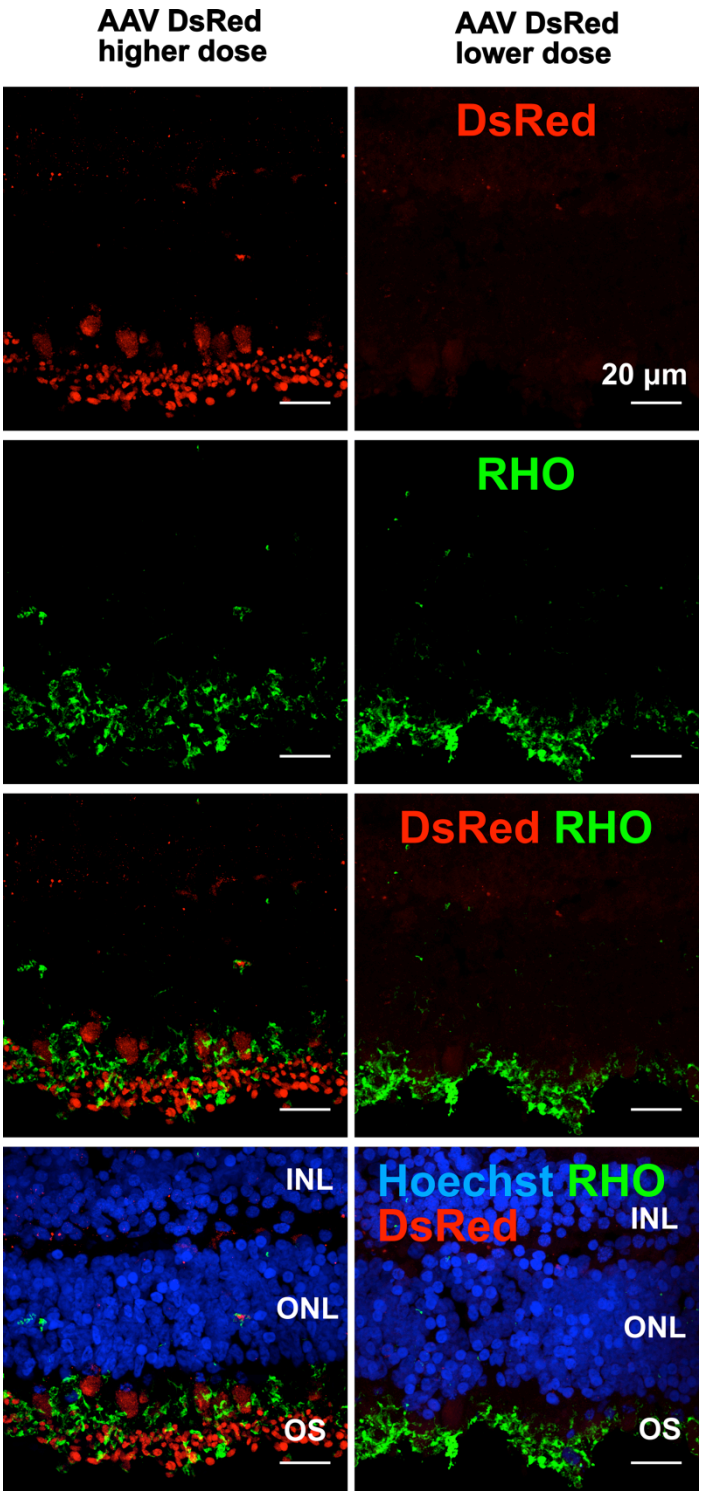


Figure 4.5 *scAAV2/8^{Y733F}hRHOp-DsRed* transduces primate retinal explants
Confocal fluorescence micrographs of the macaque retina explants transduced with the higher (the panels on the left, 10^{10}gc).) and lower dose (the panels on the right, 10^{9} gc) of *scAAV2/8^{Y733F}hRHOp-DsRed* shows the expression of DsRed in the outer segments of photoreceptors transduced with the higher dose of the vector and co-localising with rhodopsin staining (RHO, green), whereas the lower dose of the vector showed no DsRed transduction. Scale bar 20 µm.

4.2.5 Widespread retinal transduction from the vector assessed by SLO

To assess the extent of the transduction by subretinal injection of the vector into the superior retina, rhodopsin knockout mice (n=4) were injected with *scAAV2/8^{Y733F}hRHOp-DsRed* in one eye, the fellow eye was left uninjected. After one month, cSLO imaging showed clear optical media and the imaging in autofluorescence mode demonstrated strong and panretinal fluorescence in treated eyes, whereas no autofluorescence was detected in untreated eyes (**Figure 4.6**). Interestingly, at the lower gain of autofluorescence sensitivity (**Figure 4.6**, AF70), transduced eyes showed levels of autofluorescence higher in the areas proximal to the injection site and lower in areas of the retina to the periphery of injection.

After imaging, the mice were sacrificed, eyes enucleated, and histology analysis also showed widespread expression of DsRed in the ONL in the eyes treated with *scAAV2/8^{Y733F}hRHOp-DsRed* and the absence of DsRed in fellow untreated eyes (n=4) (**Figure 4.7**).

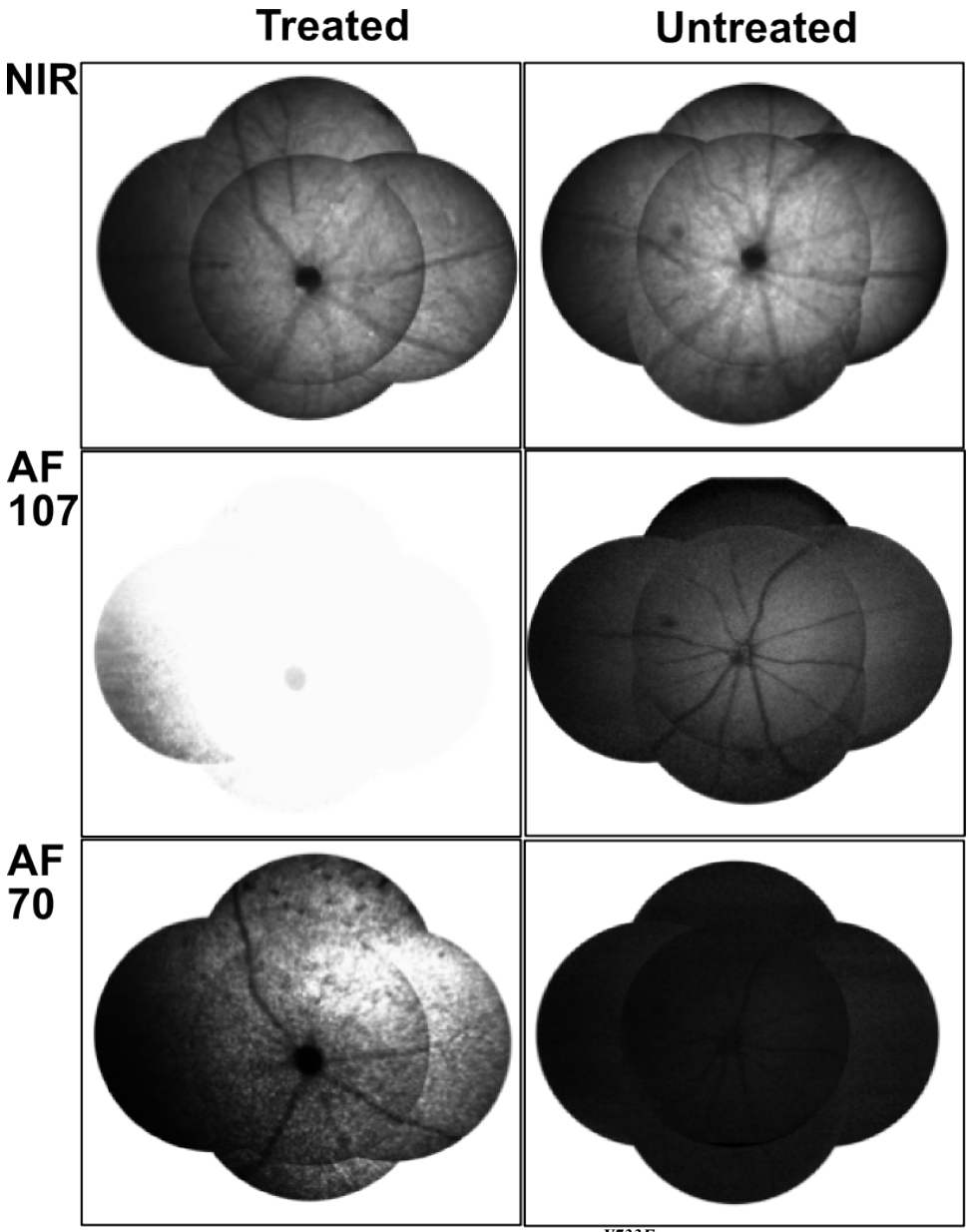


Figure 4.6 Subretinal delivery of *scAAV2/8^{Y733F}hRHOp-DsRed* leads to widespread retinal fluorescence

Confocal scanning laser ophthalmoscopy one month post-injection, in the rhodopsin knockout mouse injected with *scAAV2/8^{Y733F}hRHOp-DsRed* in one eye at PW3, while the fellow eye was left uninjected. The top row shows near-infrared reflectance (NIR). The middle row (AF107) shows cSLO images taken in autofluorescence mode with the highest sensitivity gain: the injected eye shows a high level of fluorescence spanning almost all central and middle retina; the non-injected eye shows no signs of fluorescence. The bottom row shows cSLO images taken with lower gain of sensitivity (AF70): the treated eye shows a higher level of fluorescence near the site of injection and lower level of fluorescence distal to the site of injection; the untreated eye shows no sign of fluorescence.

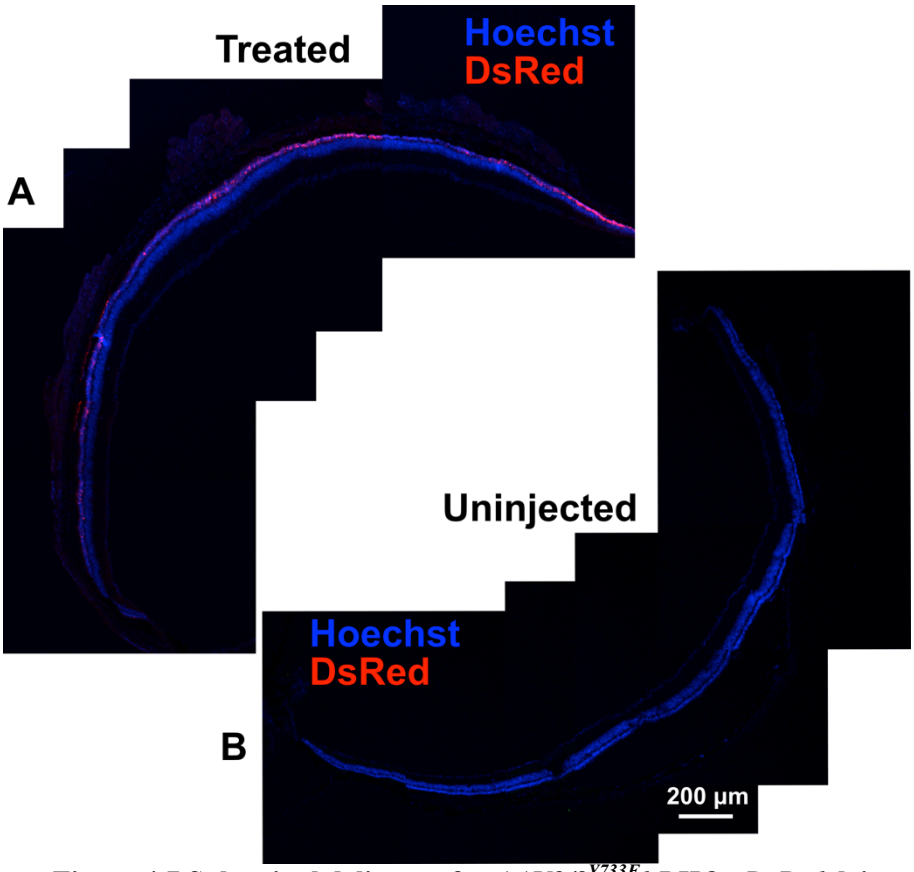


Figure 4.7 Subretinal delivery of *scAAV2/8^{Y733F}hRHOp-DsRed* drives widespread retinal expression of DsRed

Representative images from a rhodopsin knockout mouse, injected with *scAAV2/8^{Y733F}hRHOp-DsRed* in one eye at PW3, while the fellow eye was left uninjected. One month postinjection, histology section of the retina of the injected eye (top panel) and the fellow eye left uninjected (bottom panel). The cryosections were stained with the Hoechst nuclear stain; the injected eye shows the widespread expression of DsRed in the ONL, while the uninjected eye shows no DsRed expression. Scale bar 200 µm. For the detailed images of the DsRed expression in the ONL, refer to Fig 4.2.

4.2.6 Quantification of rhodopsin by Western blot

To quantify rhodopsin expression levels, six *Opn1.EGFP Rho-/-* mice were injected at 3 weeks of age, one eye was injected with *scAAV2/8^{Y733F}hRHOp-RHO* and another left untreated. The mice were sacrificed and the eyes were collected for Western blot two months after injection.

In order to confirm the expression of rhodopsin, the eyes, which received *scAAV2/8^{Y733F}hRHOp-RHO* were compared to the fellow untreated eyes. The injected eyes showed the rhodopsin band of the expected size of 36 kDa while the fellow uninjected eyes showed no rhodopsin expression (**Figure 4.8**).

In order to compare the production of rhodopsin provided with the AAV vector with wild-type rhodopsin expression, six age-matched *Opn1.EGFP Rho+/+* were sacrificed, and the eyes collected for Western blot.

The densitometric analysis of the Western blot revealed that the level of rhodopsin expression in the rhodopsin knockout mice two months after receiving *scAAV2/8^{Y733F}hRHOp-RHO* compared to wild type was approximately 8.2% **(Figure 4.8**).

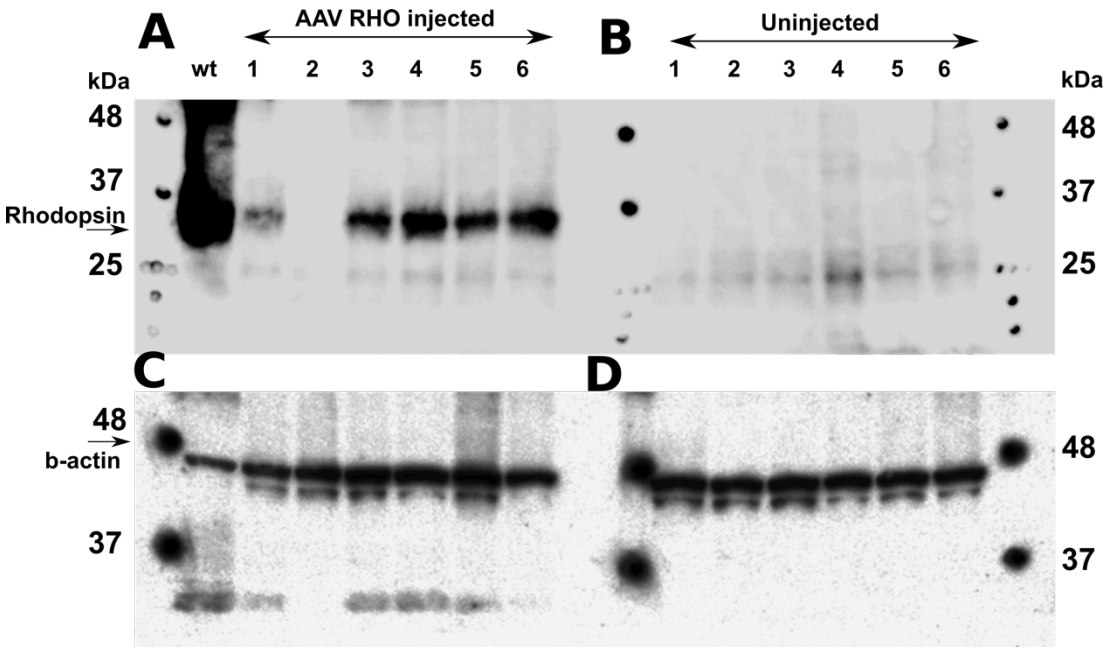


Figure 4.8 Rhodopsin protein expression in treated eyes versus fellow untreated eyes

Opn1.EGFP Rho-/- mice were injected with *scAAV2/8^{Y733F}hRHOp-RHO* at 3 weeks in one eye, the fellow eye was left untreated. Eyes were collected two months after injection for Western blotting.

Panel A shows the rhodopsin protein band size of 36 kDa: the first lane on the left (wt - wild-type mouse eye was used as a positive control) and six eyes of the rhodopsin knockout mice which received the injection (AAV RHO injected). Panel B: the uninjected fellow eyes showed the absence of rhodopsin. Panel C and D show the β-actin levels in the same samples (served as loading control).

The Western blotting confirmed the presence of rhodopsin protein in the eyes of rhodopsin knockout mice injected with *scAAV2/8^{Y733F}hRHOp-RHO,* whereas there was no rhodopsin detected in the uninjected fellow eyes.

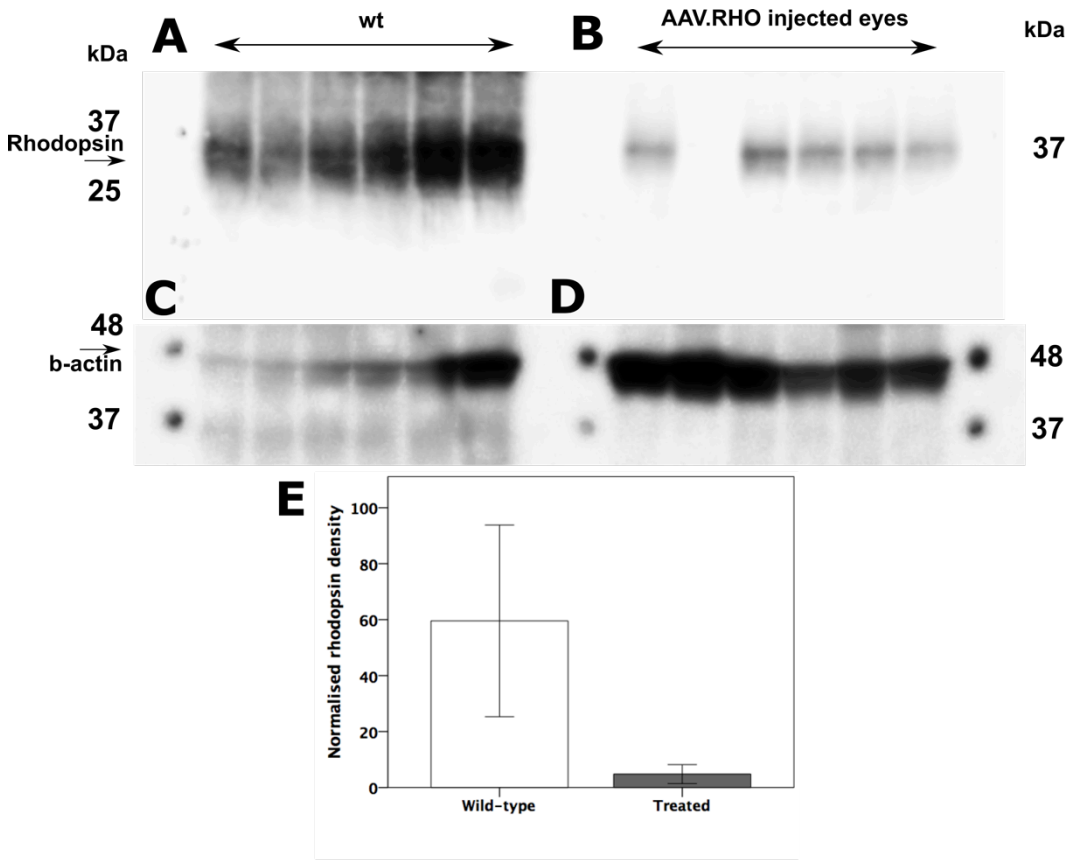


Figure 4.9 Comparison of rhodopsin protein expression in wild-type mice versus treated rhodopsin knockout mice

Six rhodopsin knockout mice were injected with *scAAV2/8^{Y733F}hRHOp-RHO* at 3 weeks in one eye, the fellow eye was left untreated. The eyes were collected two months after injection for Western blotting. The eyes of six age-matched *Opn1.EGFP Rho+/+* mice served as wild-type.

Panel A shows the rhodopsin protein in the wild-type mice, panel B: the rhodopsin knockout mice which received the injection with *scAAV2/8^{Y733F}hRHOp-RHO*.

Panel C: β-actin expression (served as control) in wild-type, panel D: β-actin expression in injected eyes. Panel E: the rhodopsin protein bands density was normalised to β-actin and compared in the injected eyes to wild-type level. The mean rhodopsin density in the treated eyes constituted 8.2% of the wild-type level.

4.3 Discussion

4.3.1 Transgene expression in cell cultures

Transfection of the HEK293T cells with the plasmid pl.*hRHOp-DsRed* showed a minimal expression of the DsRed protein which was significantly lower than in the HEK293T cells transfected with the control plasmid pl.*CAG.Opn4.IRES.DsRed*. Further optimisation of the cell density, amount of plasmid and transfection reagent did not improve expression.

Our findings confirmed, what May and coworkers reported in evaluating the efficiency of the *CMV* and rhodopsin promoters of various mammalian species (human, bovine, murine) to drive the expression of GFP by transfecting different human cell lines with plasmids. They observed minimal GFP expression from all rhodopsin promoters in HEK293 cells (May et al., 2003).

It has been shown that the rhodopsin promoter needs the addition of the specific transcription factors: NRL (neural retinal zipper), CRX (cone-rod homeobox) and NR2E3 (photoreceptor-specific nuclear receptor gene) to drive the expression in HEK293 cells (Cheng et al., 2004).

As the production of three plasmids with the aforementioned transcription factors was not intended within this project, the expression from the produced viral vectors was instead further assessed *in vivo* in rhodopsin knockout mice by delivering the vector via subretinal injection.

4.3.2 Transgene expression in rhodopsin knockout mice

Rhodopsin staining of the eye sections of rhodopsin knockout mice injected at PW3 with *scAAV2/8^{Y733F}hRHOp-RHO* showed newly outgrown rod outer segments. Palfi et co-workers demonstrated previously the expression of rhodopsin by delivering it with AAV2/5 vector and driven by the murine rhodopsin promoter in new-born rhodopsin knockout mice. However in their experiments the expression of rhodopsin was spread through the whole outer nuclear layer, suggesting that the cellular trafficking of rhodopsin protein was affected, impairing proper targeting of rhodopsin to the rod outer segments (Palfi et al., 2010). In our study, rhodopsin was clearly expressed in the outer segments of rod photoreceptors suggesting proper intracellular trafficking. The eye sections of the rhodopsin knockout mice injected with *scAAV2/8^{Y733F}hRHOp-DsRed* showed the expression of the DsRed protein in the outer nuclear layer, suggesting that it is the properties of the rhodopsin protein that allow its targeting to ROS.

4.3.3 Rod-specificity of the rhodopsin human promoter

Given the important role of cones for central high acuity vision, limiting transgene expression to rod photoreceptors is a prerequisite for developing a safe and efficient AAV gene therapy targeting rods. Immunolabelling of cones with the cone arrestin antibody in the eyes of rhodopsin knockout mice treated with *scAAV2/8^{Y733F}hRHOp-DsRed* demonstrated that the expression of DsRed driven by the human rhodopsin promoter was limited to rods.

Previously, Flannery showed that the murine rhodopsin promoter which covered the upstream region of the rhodopsin gene (-385 to +86) allowed it to drive high levels of expression in photoreceptors (Flannery et al., 1997). Allocca demonstrated that the AAV8 gene therapy with the 800 bp fragment of the human rhodopsin promoter (-800 to +6) resulted in a higher level of photoreceptor transduction than using traditional ubiquitous promoters such as *CBA* or *CMV*, however, the transduction was targeting both rods and cones, attaining the rate of 44.6% of cone transduction (Allocca et al., 2007). This targeting of both photoreceptors was confirmed by Glushakova, who showed that the mouse rhodopsin promoter transduced both types of photoreceptors in male Sprague-Dawley rats and rhodopsin knockout mice upon delivery of the *AAV5.GFP* vector (Glushakova et al., 2006). Contrary to the previous reports that the rhodopsin promoter drove expression in both rods and cones in rodents, Beltran showed that in dogs the delivery of *AAV2/5-GFP* gene therapy under the mouse rhodopsin promoter resulted in rod-specific expression of GFP, explaining the disparity between the previous reports and his own findings by differences in cell tropism across species (Beltran et al., 2010). Our experiments confirmed Beltran's findings that the human rhodopsin promoter limited expression to rods. The disparity between the results of Alocca and Glushakova could be explained by a number of factors, among them, the use of confocal microscopy (which offers a higher level of accuracy in analysis) in our study compared to the standard microscopy used in the Alocca et al. and Glushakova et al. studies performed in 2007 (Allocca et al., 2007) and 2005 (Glushakova et al., 2006). Additionally, Glushakova and colleagues used the peanut agglutinin (PNA)

staining which labels cone outer segments that could have complicated the analysis between rod and cone outer segments as the outer segments of both types of photoreceptors are located in a spatially tight space. In our study, cone arrestin antibody was used, which stains whole cone bodies, thus facilitating the analysis. Moreover, the different serotype and the use of human versus murine promoters could have contributed to the observed disparity.

Therefore, based on the evidence in this study, it could be suggested that the use of *scAAV2/8^{Y733F}* under the human rhodopsin promoter targets specifically rod photoreceptors in rhodopsin knockout mice. The question of limiting unspecific expression is of paramount importance for clinical studies as the unspecific targeting of cones could lead to potentially harmful effects on cones expressing an off-target protein.

4.3.4 Primate retinal explants

Given that primates share the majority of genes with humans and have similar retinal anatomy and very similar physiology, they provide a much more accurate model than mice. As this project's eventual aim is to develop a potential treatment for rhodopsin-linked RP in humans, the evaluation of the performance of the produced AAV vectors on primate tissue could therefore provide valuable insights. The *ex vivo* experiments carried out allowed verification of the specificity of targeting by the human rhodopsin promoter in AAV vector on macaque retinal explants, showing that the administration of *scAAV2/8^{Y733F}hRHOp-DsRed* resulted in the expression of the DsRed protein

in the outer segments of photoreceptors of the macaque retina. Surprisingly, the pattern of expression was different from the DsRed expression in the injected rhodopsin knockout mice *in vivo.* In rhodopsin knockout mice, which received *scAAV2/8^{Y733F}hRHOp-DsRed,* the DsRed was expressed throughout the outer nuclear layer (**Figure 4.2**), whereas in the macaque retinal explants DsRed was directed to the outer segments of the photoreceptors (**Figure 4.5**). The disparity of DsRed expression could be explained by the species tropism and the different status of transduced tissue: *in vivo* experiments in otherwise healthy mice versus *ex vivo* experiments on compromised retina. However, both studies in mice and primates confirmed the specific targeting by the human rhodopsin promoter in the vector to transduce retinal photoreceptors.

4.3.5 Extent of transduction

CSLO imaging in the mice treated with *scAAV2/8^{Y733F}hHRO.DsRed* demonstrated robust and widespread autofluorescence covering almost the entire retina, corresponding to the area of the DsRed expression (**Figure 4.6**). The widespread transduction validated the adopted design of the AAV vector: the single capsid mutant AAV8 capsid, self-complementary AAV genome and the surgical method of applying the vector only to the superior half of the retina.

The appearance of the gradient of transduction, where higher levels of transduction were achieved in the areas proximal to the vector injection, suggests that different areas of the retina were exposed to different doses of

the vector. This could result in disparate levels of exposure to the vector and therefore lead to different levels of transduction and potential toxicity from the vector.

This disparity of the applied virus could be overcome by using another delivery route. Potentially, intravitreal delivery could lead to more homogenous exposure to a virus, since a vector could spread initially in the vitreous cavity and only then in the retina achieving more homogenous transduction. However, the intravitreal approach still has hurdles in efficiently targeting photoreceptors, making the subretinal approach an optimal route to target photoreceptors.

4.3.6 Rhodopsin expression level

Western blot analysis confirmed the presence of bands with the size of 36 kDa corresponding to rhodopsin in the eyes, which received *scAAV2/8^{Y733F}hRHOp-RHO* and its absence in untreated eyes (**Figure 4.8**). The level of rhodopsin derived from the AAV vector in treated eyes constituted 8% compared to wild-type level (**Figure 4.9**). Although the achieved level can be perceived as low, however, the prodigiously high levels of rhodopsin production in wild-type mice must be taken into the account, as rhodopsin constitutes 30% of the proteome of rod photoreceptor and 90% of the ROS. The similar results for Western blot levels were described in other studies: in a recent study using a different rhodopsin knockout model, Lem's rhodopsin knockout mice (Lem et al., 1999), the level of rhodopsin expression after the administration of nanoparticles containing the genomic

rhodopsin (a sequence containing the rhodopsin exons and introns) was also 8% of wild-type level one month after injection, in contrast, quantitative RT-PCR measuring the mRNA level of rhodopsin showed 30% of wild-type levels, suggesting that not all rhodopsin mRNA are translated into protein (Han et al., 2015).

In another study, quantitative assessment of the PDEβ protein delivered by *AAV5-PDEβ* driven by the ubiquitous CBA promoter which provided functional rescue, showed protein levels of 10-15% of wild-type mice (Pang et al., 2008). Given that the PDEβ protein is expressed at much lower levels than rhodopsin (about 100 fold less) in wild-type mice, this suggests that even with use of a powerful ubiquitous promoter the levels of AAV delivered low expressed protein would not exceed 20% of wild-type level.

Alternatively, the obtained levels of 8% of rhodopsin expression compared to wild-type in our study highlight the challenges facing rhodopsin AAV gene therapy given that rhodopsin is an extremely highly expressed protein and considerable effort is needed to achieve high level of expression.

Taken together, the data shown in this chapter confirmed the efficacy of the produced rhodopsin vector in driving rhodopsin expression in rhodopsin knockout mice and the ability of the human rhodopsin promoter to specifically target rod photoreceptors.

Chapter 5 AAV vector effects on rods

5.1 Introduction

In the previous chapter, it was shown the administration of the *scAAV2/8^{Y733F}hRHOp-RHO* vector delivering the rhodopsin gene results in rhodopsin expression in rod outer segments, efficiently and specifically targeting rod cells and achieving widespread retinal transduction.

This chapter presents long-term data on the effects of the vector application on rod cells in rhodopsin knockout mice. Functional effects of the rhodopsin gene delivery on rod system were studied by dark-adapted ERG, which allows isolation of rod-derived responses, and anatomical effects of the vector administration were studied on post-mortem eye sections.

5.1.1 ERG

The electroretinogram (ERG) is widely used to evaluate retinal function after experimental treatment in a non-invasive and longitudinal way. Since the ERG summarizes the global electric retinal response to light stimulation and reflects numerous responses from many cell populations as a consequence of serial processing within the retina, understanding of disparate responses within the ERG allows better interpretation of obtained results.

Granit was first to describe the major components of the ERG waveform studying the effects of anaesthesia on ERG responses in the cat (Granit, 1933).

The a-wave is a corneal negative potential, originating from photoreceptors and representing 'light' current, which reflects reduction of 'dark' current due to light absorption in photoreceptor outer segments and closure of cGMP-gated cationic channels. Classically, the a-wave of the dark-adapted ERG is associated with rod photoreceptor activity (Penn and Hagins, 1969).

The b-wave is a corneal positive potential, following the a-wave and reflecting the activity of post-synaptic neurons and is mainly generated in ON-centre bipolar cells with minor contributions from OFF-centre bipolar cells and the 3rd order neurons, providing valuable information on functional integrity of the inner retina.

The basic method of recording the ERG involves the use of an active extracellular electrode usually positioned on the cornea.

5.1.2 ERG amplitude measurements and variability

The size of the a-wave is measured from the baseline, prior to light stimulus, to the trough of the negative wave, the b-wave magnitude is measured from the trough of a-wave to the peak of b-wave (**Figure 5.1**).

The ERG amplitude depends on light intensity. In dim light, the mouse ERG may consist only of the b-wave. With an increase in stimulus intensity, b-waves increase in amplitude and a-waves become evident.

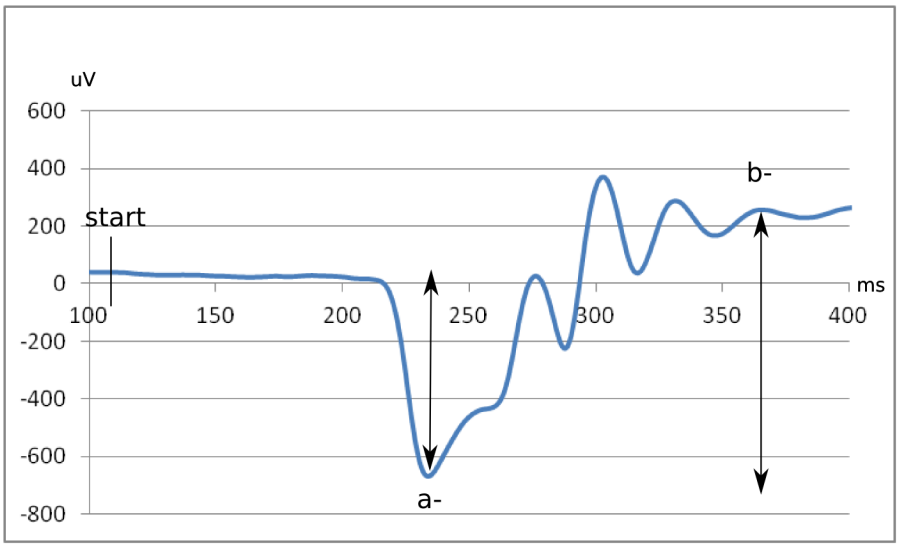


Figure 5.1 Measurements of a- and b-wave amplitudes
Major ERG characteristics include amplitudes of a- and b-wave. The a-wave is measured from the baseline to the trough of the negative wave, b-wave from the trough of the negative wave to the peak of the positive wave.

5.1.3 Isolating rod ERG responses

Given that retinal gene therapy might be applied to one type of photoreceptor, it is practical to assess the separate contribution of rods and cones to the ERG responses. However, this is confounded by the fact that the ERG represents the global and overlapping response of the retina to a light stimulus, where both cone and rod pathways contribute simultaneously. In order to isolate rod responses, various manipulations of the light stimulus and prior preparation were developed based on rods higher sensitivity to light compared to cones (Weymouth and Vingrys, 2008). This rod response isolation was achieved by dark-adapting animals for at least 12 hours before the ERG recording and use of low flash intensities (termed scotopic) to evoke only rod-derived responses.

5.1.4 ERG in rhodopsin knockout mice

Since rhodopsin knockout mice do not produce rhodopsin, they lack rod outer segments and rod-derived ERG responses (Toda et al., 1999). Rod photoreceptors start to degenerate from birth and within six months rod degeneration is complete (Punzo et al., 2009). However, due to the presence of intact cone photoreceptors in young rhodopsin knockout mice, bright flashes in the dark-adapted ERG can illicit cone responses in the form of b-waves, which differ from wild-type responses by having significantly lower amplitude. Due to secondary cone degeneration, these cone-mediated responses are lost by postnatal month three (Toda et al., 1999). Alternatively, a-waves are considered more rod-specific in the mouse and are therefore more specific for rod activity. The following data are presented with b-waves at dim flashes to exclude cone-mediated ERG responses, b-waves at a range of light stimulus intensity and with a-waves at the highest flash intensity and at a range of flash intensity.

It has been shown that AAV-mediated rhodopsin delivery might restore rod-mediated ERG responses, and slow down rod degeneration in the rhodopsin knockout model (Han et al., 2015; Palfi et al., 2010). However, these studies delivered rhodopsin at a very early developmental stage, P0-P3, which on the developmental scale would correspond to prenatal gene therapy in RP patients (notwithstanding the fact that recessive mutations in RHO are rare). Given that this translational research project has the eventual aim to develop

potential therapeutic avenues for patients with rhodopsin-linked RP, administration of a rhodopsin vector at later developmental stages (three weeks) in ongoing rod degeneration in rhodopsin knockout mice might provide additional insight into the potential benefits of this therapy. This is particularly relevant to over-expressing RHO as a means to slow down dominantly inherited disease midway through the retinal degeneration (Mao et al., 2011).

5.2 Aims

To assess the effects of the AAV-mediated rhodopsin delivery on rod photoreceptors in rhodopsin knockout mice by assessing dark-adapted ERG responses and histology analysis post-mortem five months after the vector injection.

5.3 Methods

To assess the effects of rhodopsin gene delivery via an AAV vector, the *Opn1-EGFP Rho-/-* mice were treated *with scAAV2/8^{Y733F}hRHOp-RHO*. Due to the high variability of ERG responses between individual mice, intraindividual testing was chosen within two groups. In the 1st group, one eye was injected with the rhodopsin vector and the fellow eye left uninjected; the second group included mice where one eye was injected with the rhodopsin vector, another eye with *AAV-control* (sham) vector which does not drive protein expression but contained AAV particles with the stuffer

sequence. All animals were injected at P21 ± 3 (postnatal day 21). Treatment consisted of a single subretinal injection of 1.5 µl of *scAAV2/8^{Y733F}hRHOp-RHO* containing 2.5 x 10^9 gc/ml into the superior retina. *AAV-control* was injected at the same dose and volume. ERG was measured at the subsequent points: postnatal month 2 (PM2), PM3, PM4, PM5. Dark-adapted ERG, which primarily measures rod function, were elicited with single 0.5 Hz flashes of white light at 0.0001 cd.s/m^2; 0.001 cd.s/m^2; 0.01 cd.s/m^2; 0.1 cd.s/m^2; 1.0 cd.s/m^2; 10 cd.s/m^2 with appropriate delay between flashes. 3 to 15 scans were averaged at each light intensity. The mice were sacrificed for histology analysis at PM6. The results of dark-adapted ERG are presented at stimulus intensity 0.01 cd.s/m^2 at which no cone responses are detected in young rhodopsin knockout mice which still possess responsive cones and at increasing flash intensities (for full description of ERG technique, please see section 2.4.4)

To quantify ONL thickness, four non-overlapping high-power images from the opposite sides of the retina were taken with a 63X objective on the confocal microscope Zeiss LSM710. The number of Hoechst-positive nuclei in the ONL were counted in each image and then averaged per eye (see section 2.5.3.1 for full details).

Statistical significance between ERG responses at increasing flash intensities was measured by factorial ANOVA for repeated measures (with flash intensity and treatment as factors) and posthoc Bonferroni corrected paired t-test for multiple comparisons.

5.4 Results

5.4.1 Dark-adapted flash ERG in unilaterally injected eyes

Rhodopsin knockout mice do not produce rod-derived ERG responses as they lack rod outer segments. At one month after injection with *scAAV2/8^{Y733F}hRHOp-RHO*, dark-adapted ERG recordings provided evidence of substantial rod function compared with fellow uninjected eyes, in which no significant rod-isolated responses were recorded (**Figure 5.2**). One month after injection the mean value of b-wave at flash intensity 0.01 cd.s/m^2 in treated eyes was 166.03±23.24 μV, whereas in uninjected eyes it was 17.05±4.22 μV, $p<0.0001$ (Bonferroni corrected paired t-test), n=10. The response in treated eyes achieved 24% of the wild-type response, with the mean value of b-wave amplitude in the wild-type mice being 678.34±60.89 μV.

With time there was a gradual decrease in dark-adapted ERG responses, with b-wave amplitudes at PM3 achieving 95.12±26.72 μV in treated eyes, which constituted 57.3% of the initial response; at PM4 b-wave amplitudes in treated eyes were 55.71±17.54 μV (33.56% of the initial response); PM5 35.11±10.01 μV (21% of the initial response) (**Figure 5.3,** panel A).

In assessing globally dark-adapted ERG responses at increasing flash intensities, the delivery of *scAAV2/8^{Y733F}hRHOp-RHO* resulted in therapeutic effect sustained until four postnatal months. B-wave amplitudes were significantly greater in treated compared to untreated eyes at one month after

injection ($F=40.55$; $p<0.001$; $n=10$), two months ($F = 16.67$; $p<0.01$; $n=10$) and three months ($F=7.27$; $p<0.05$; $n=10$), with the loss of statistical significance at four months after injection ($F=5.28$; $p>0.05$; $n=10$) (Factorial ANOVA for repeated measures) (**Figure 5.4**).

The a-waves, which are considered to be rod-specific, also demonstrated the vector efficiency one month after injection with their amplitudes at the highest flash intensity (10 cd.s/m^{-2}) achieving 78.21±10.33 μV in treated eyes compared to 11.71±3.02 in untreated eyes, $p< 0.0001$ (Bonferroni-adjusted paired t-test), $n=10$. The mean of the a-wave amplitude at the same flash intensity in the wild-type mice was 641.14±57.13 μV, thus a-wave amplitudes in the treated group comprised 12% of the wild-type response.

Similar to the b-wave, a-wave amplitudes in treated eyes showed gradual decline with time, with a-wave amplitudes at PM3 achieving 41.46±2.88 μV in treated eyes, which constituted 53.01% of the initial response; at PM4 b-wave amplitudes in treated eyes 30.17±7.08 μV (38.5% of the initial response); at PM5 13.98±5.14 μV (17.87% of the initial response) (**Figure 5.3**, panel B).

Evaluation of a-waves in dark-adapted ERG at a range of flash intensities showed significant therapeutic effect of the rhodopsin gene delivery on a-wave amplitude which was preserved up to three months after injection with a-waves at different flash intensities showing statistical significance between treated eyes compared to untreated for PM2 ($F=43.057$; $p<0.001$; $n=10$), PM3 ($F=9.82$; $p<0.01$) and PM4 ($F=6.84$; $p<0.05$), and loss of significance at

PM5 (F=3.08; p>0.05; n=10) (Factorial ANOVA for repeated measures) (**Figure 5.5**).

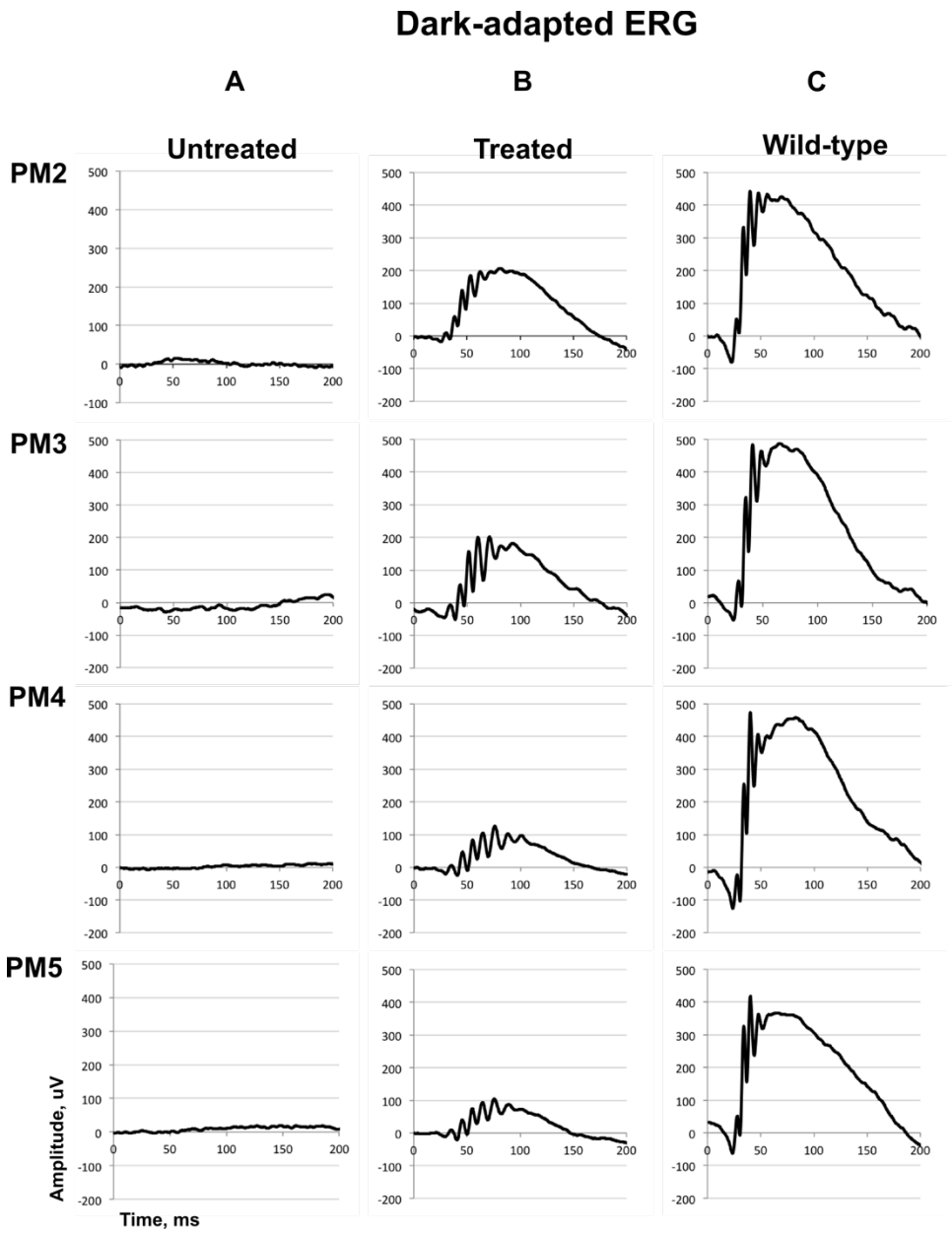


Figure 5.2 Restoration of rod-isolated ERG responses in unilaterally treated eyes at dim light flash intensity

Panels A and B are representative traces from an *Opn1.EGFP Rho-/-* mouse with one eye treated with *scAAV2/8^{Y733F}hRHOp-RHO* (Panel B) at PW3, demonstrating robust dark-adapted b-wave; the fellow eye was left untreated (Panel A), showing flat ERG. On the right, panel C, wild-type mouse ERG traces. ERG recordings taken at PM2, PM3, PM4, and PM5, with flash intensity: 0.01 cd.s/m2.

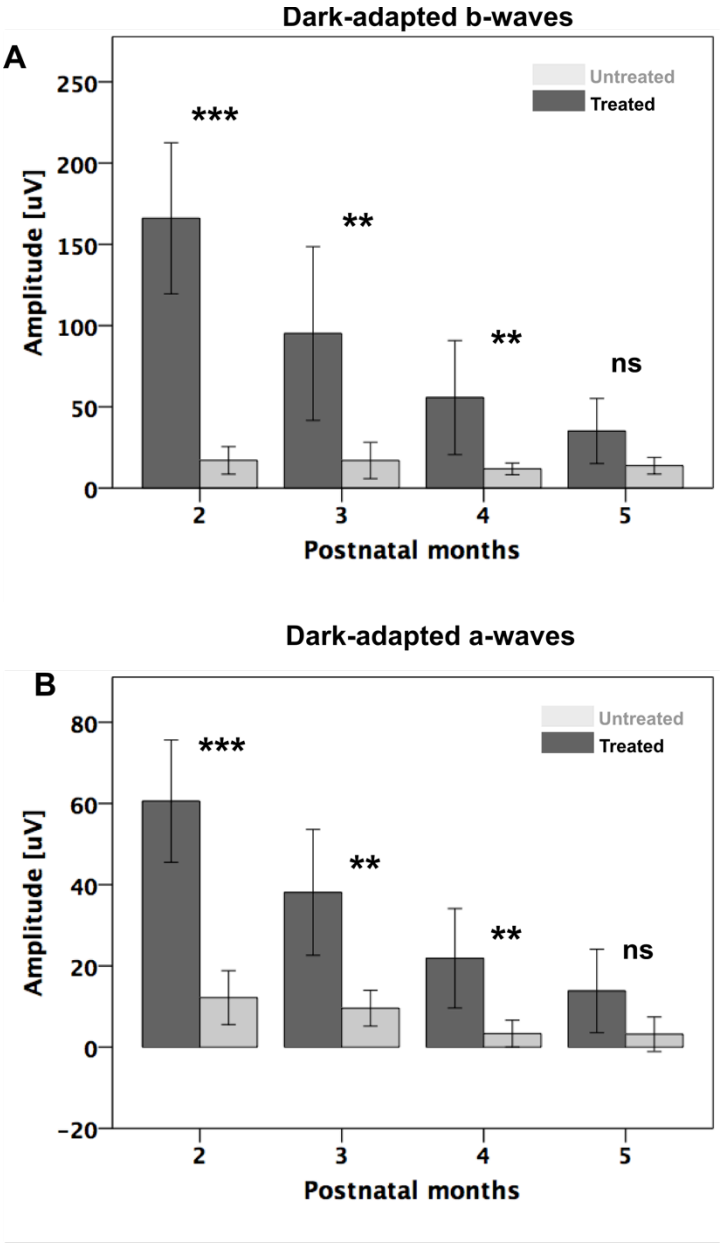


Figure 5.3 Dark-adapted ERG responses in unilaterally treated rhodopsin knock-out mice

Opn1.EGFP Rho-/- injected in one eye with *scAAV2/8^{Y733F}hRHOp-RHO* at P21, the fellow eye left untreated. ERG was taken at 2, 3, 4 and 5 months. **A.** B-waves amplitudes at dim flash intensity (0.01 cd.s/m^{-2}) allowing isolation of rod responses. **B.** A-waves at maximal flash intensity (10 cd.s/m^{-2}) represent rod-specific responses.

Bonferroni-adjusted post hoc paired t-test demonstrated significant increase of rod-specific ERG responses evidencing wide and functional transduction of rod photoreceptors at all time points except PM5. Note the gradual decline of rod-specific responses in time. Error bars represent +/- standard error of the mean, ** - $p < 0.008$; *** - $p < 0.001$; n=10.

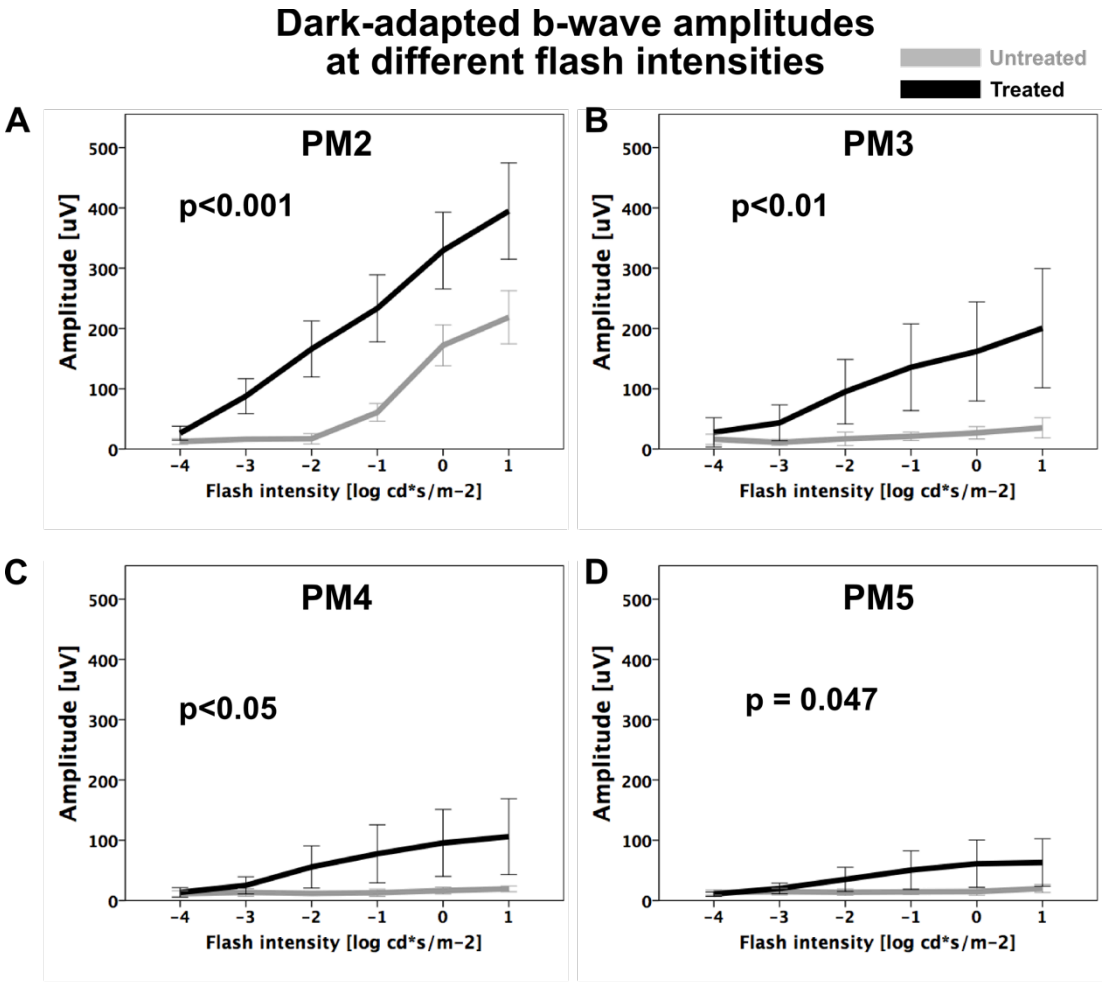


Figure 5.4 Dark-adapted b-wave amplitudes at different flash intensities and time points in unilaterally treated rhodopsin knockout mice
Opn1.EGFP Rho-/- mice injected at one eye with *scAAV2/8^{Y733F}hRHOp-RHO* at PW3, the fellow eye left untreated. ERG measurements were taken at increasing flash intensities (log cd*s/m^2: -4; -3;-2; -1; 0; 1) at postnatal age 2, 3, 4 and 5 months. The therapeutic effect on b-wave amplitudes was sustained up to three months after delivery.
Postnatal Months: **A)** PM2; **B)** PM3; **C)** PM4; **D)** PM5.
Error bars represent +/- standard error of the mean, n = 10, factorial ANOVA for repeated measures.

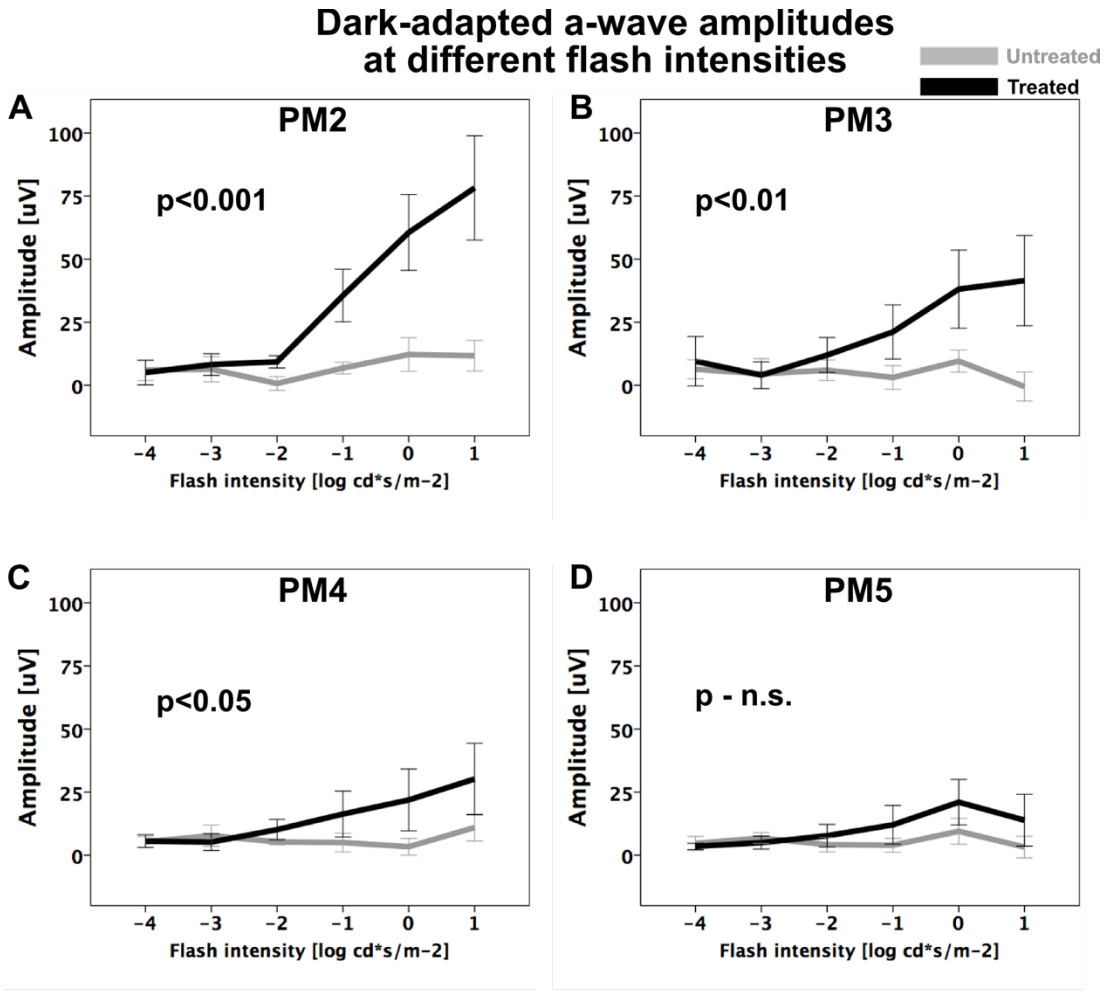


Figure 5.5 Dark-adapted a-wave amplitudes at increasing flash intensities in unilaterally treated rhodopsin knockout mice

Opn1.EGFP Rho-/- mice injected at one eye with *scAAV2/8^{Y733F}hRHOp-RHO* at PW3, the fellow eye left untreated. ERG measurements were taken at increasing flash intensities (log cd*s/m^2: -4; -3; -2; -1; 0; 1) at postnatal age 2, 3, 4 and 5 months. The delivery of the rhodopsin vector resulted in statistically significant improvement of ERG a-waves with the effect sustained to PM4.

Postnatal Months: **A)** PM2; **B)** PM3; **C)** PM4; **D)** PM5.

Error bars represent +/- standard error of the mean, n = 10, factorial ANOVA for repeated measures.

5.4.2 Dark-adapted ERG in bilaterally injected eyes

To control for the effects of injection, rhodopsin knockout mice received bilateral injections: one eye received *scAAV2/8^{Y733F}hRHOp-RHO*, whereas the fellow eye received a sham injection with the AAV-control vector. Taken together, the data from this group followed the same pattern as the unilaterally injected group.

At 1 month after injection, dark-adapted ERG recordings at dim flash intensity provided evidence of substantial rod function in treated eyes compared with fellow sham-injected eyes, in which significant rod isolated responses were not detected (**Figure 5.6,** panel A). The mean value of b-wave at the flash intensity 0.01 cd.s/m^2 in treated eyes was 102.4±20.92 μV, whereas in uninjected eyes 16.84±4.39 μV, $p<0.001$ (Bonferroni-adjusted post hoc paired t-test); n=7. The response in treated eyes achieved 15% of the wild-type response, with the mean value of b-wave amplitude in the wild-type mice being 678.34±60.89 μV.

With time there was a gradual decrease in dark-adapted ERG responses in treated eyes, with b-wave amplitudes at PM3 achieving 65.32±19.26 μV in treated eyes, which constituted 63.7% of the initial response; at PM4 b-wave amplitudes in treated eyes 68.82±19.81 μV (67.2% of the initial response); PM5 30.81±2.03 μV (30% of the initial response) (**Figure 5.6,** panel A).

Globally, the positive effect of the rhodopsin gene delivery was sustained up to three months after injection, with b-wave amplitudes at increasing flash intensities in treated eyes being greater compared to sham-injected eyes for

PM2 ($p<0.001$), PM3 ($p<0.01$) and PM4 ($p<0.05$), with the loss of the effect at PM5 ($p>0.05$) (factorial ANOVA for repeated measures, n=7) (**Figure 5.7**).

The a-waves, which are considered to be rod-specific, also demonstrated the vector efficiency with their amplitudes at the highest flash intensity (10 cd.s/m^{-2}) achieving at PM2 58.7±12.05 μV in treated eyes compared to 13.63±4.66 in untreated eyes, $p< 0.001$ (Bonferroni-adjusted post hoc paired t-test for multiple comparisons); n=7. The mean of a-wave amplitude at 10 cd.s/m^{-2} of flash intensity in the wild-type mice was 641.14±57.13 μV, thus a-wave amplitude in treated group compared to wild-type achieved 9%. As with the b-waves, a-wave amplitudes showed decline with time, with a-wave amplitudes at PM3 achieving 27.9±8.99 μV in treated eyes, which constituted 47.5% of the initial response; at PM4 b-wave amplitudes in treated eyes 28.38±7.9 μV (48.34% of the initial response); PM5 13.5±4.37 μV (22.9% of the initial response) (**Figure 5.6,** panel B).

The analysis of the a-wave amplitudes at increasing flash intensities also revealed significantly greater amplitudes for treated eyes compared to untreated for PM2 ($p<0.001$), PM3 ($p<0.01$) and PM4 ($p<0.05$), with loss of significance at PM5 ($p>0.05$), measured by factorial ANOVA for repeated measures, n=7 (**Figure 5.8**).

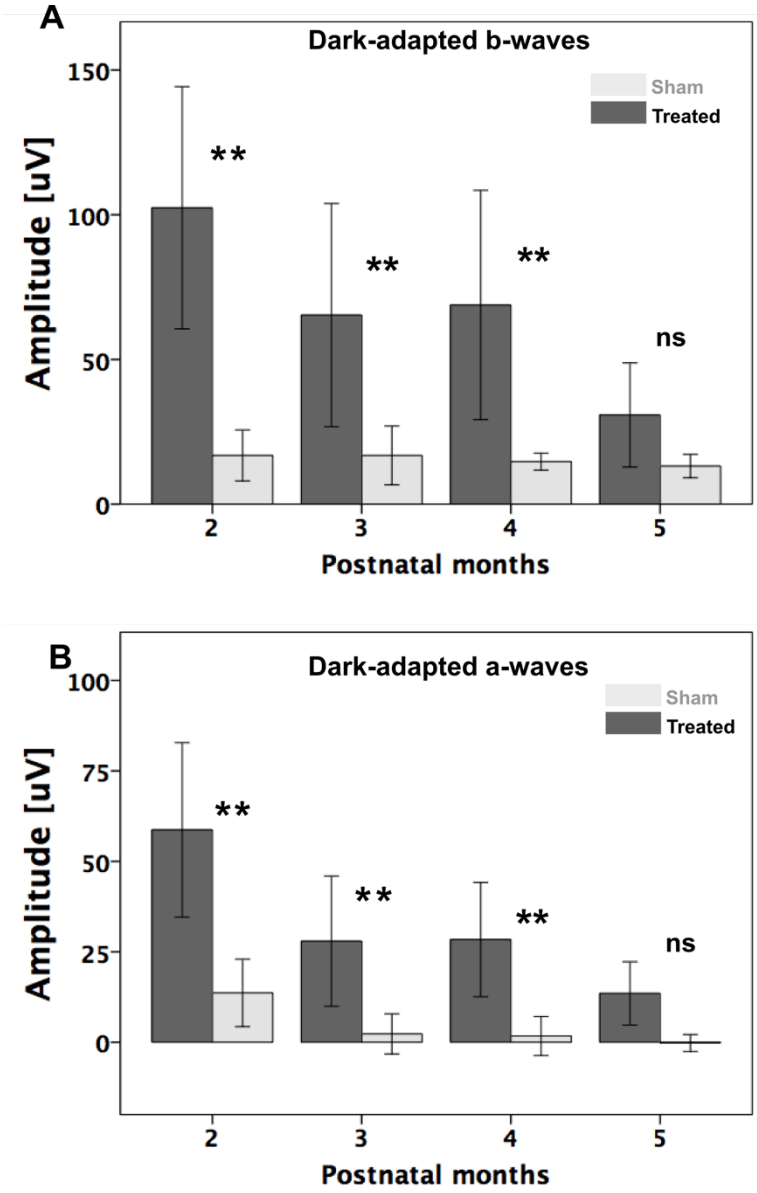


Figure 5.6 Dark-adapted ERG responses in the bilaterally injected rhodopsin knockout mice

Opn1.EGFP Rho-/- mice at PW3 received *scAAV2/8*^{Y733F}*hRHOp-RHO* in one eye, with the fellow eye receiving the *AAV-control*. ERG responses were measured at postnatal months: 2, 3, 4 and 5. **A.** B-wave amplitudes at dim flash intensity (0.01 cd.s/m^{-2}) allowing isolation of rod responses. **B.** A-waves at maximal flash intensity (10 cd.s/m^{-2}) represent rod-specific responses.

Bonferroni-adjusted post hoc paired t-test demonstrated significantly greater rod-specific ERG responses evidencing wide and functional transduction of rod photoreceptors in all time points except PM5 in treated eyes compared to sham-injected. Note the gradual decline of rod-specific responses in time. Error bars represent +/- standard error of the mean, ** - $p < 0.008$; n=7.

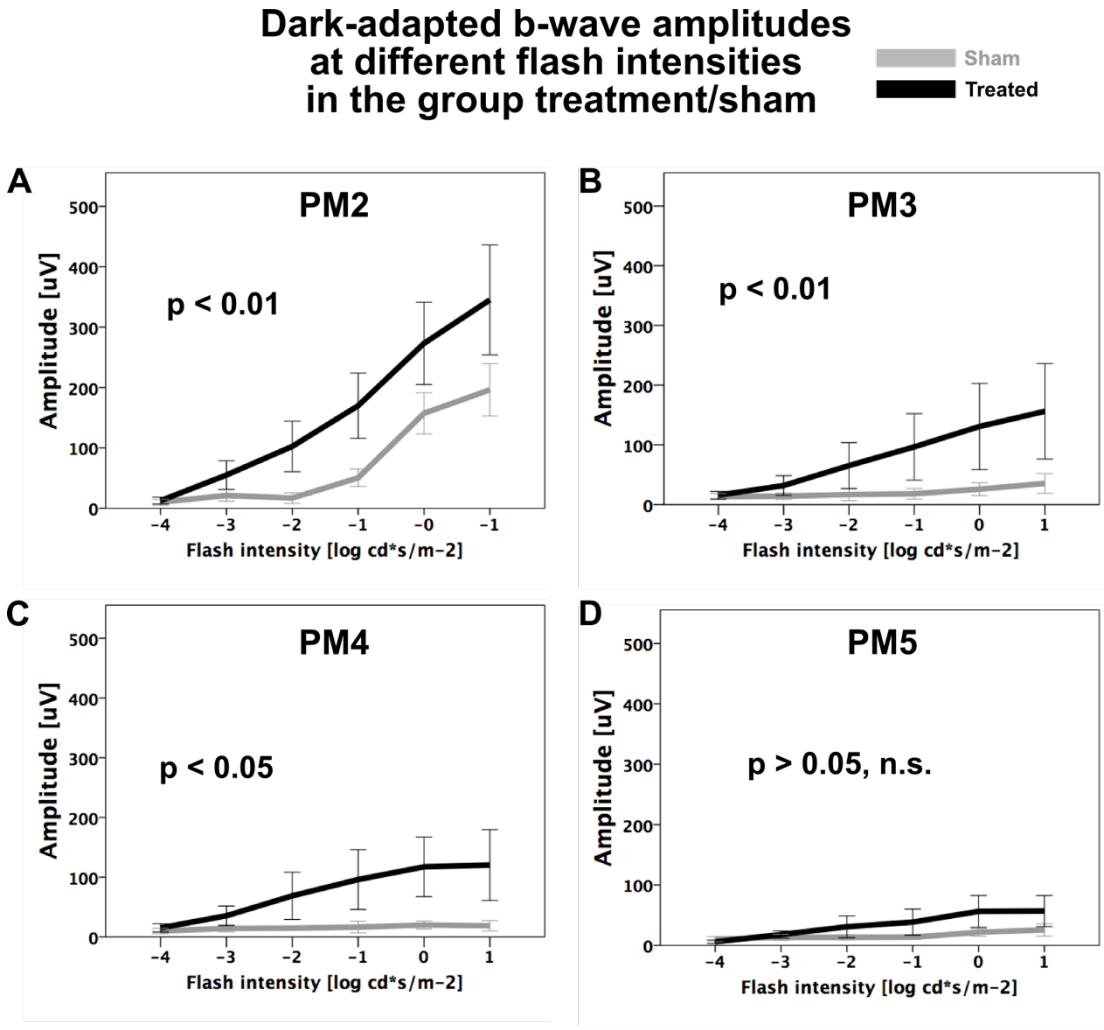


Figure 5.7 Dark-adapted b-wave amplitudes at increasing flash intensities in rhodopsin knockout mice injected bilaterally
Opn1.EGFP Rho-/- mice received *scAAV2/8^{Y733F}hRHOp-RHO* at one eye, with the fellow eye injected with the AAV-control (sham) at PW3. ERG measurements were taken at increasing flash intensities at postnatal age 2, 3, 4 and 5 months. In treated eyes, b-wave amplitudes were significantly greater than in sham-injected eyes, except PM5.
Factorial ANOVA for repeated measures (with flash intensity and treatment as factors) was significant in all time measurements, error bars represent +/- standard error of the mean, n = 7. Postnatal Months: **A)** PM2; **B)** PM3; **C)** PM4; **D)** PM5.

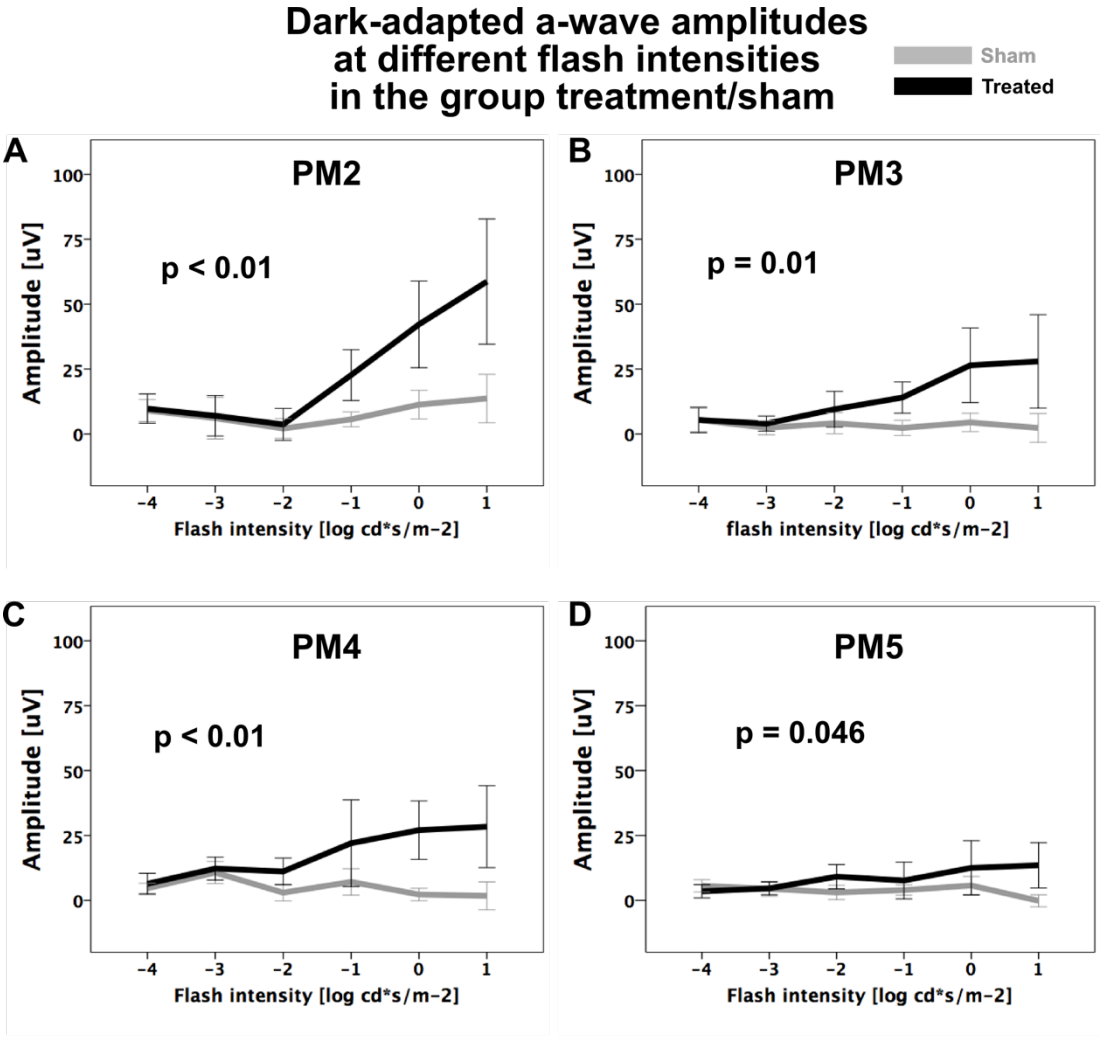


Figure 5.8 Dark-adapted a-wave amplitudes at different flash intensities and time points in bilaterally treated rhodopsin knockout mice
Opn1.EGFP Rho-/- mice at PW3 received *scAAV2/8^{Y733F}hRHOp-RHO* in one eye and the *AAV-control* in the fellow eye (sham). ERG measurements were taken at increasing flash intensities at postnatal age 2, 3, 4 and 5 months. A-wave amplitudes were significantly greater in treated eyes compared to sham-injected eyes, except at PM5.
Factorial ANOVA for repeated measures (with flash intensity and treatment as factors); error bars represent +/- standard error of the mean, n = 7.
Postnatal Months: **A)** PM2; **B)** PM3; **C)** PM4; **D)** PM5.

5.4.3 Preservation of the ONL thickness in the unilaterally treated group

The mice were sacrificed at PM6, and eye sections were labelled with the anti-rhodopsin antibody and Hoechst nuclear stain. Eyes injected with *scAAV2/8^{Y733F}hRHOp-RHO* showed expression of rhodopsin in rod outer segments and 2-4 layers of the preserved ONL, whereas untreated eyes showed no rhodopsin expression and absence of the ONL (**Figure 5.9**).

The Image J software was used to quantify the number of Hoechst-labelled photoreceptors in the ONL. The mean number of Hoechst-labelled photoreceptors in treated eyes was significantly greater (42.07±17.53), than in untreated eyes (2.63±0.83), $p<0.0001$ (paired t-test), n= 10 (**Figure 5.10**, panel A). In the wild-type mice, the number Hoechst-labelled photoreceptors was 744.23±30.1.

5.4.4 Preservation of the ONL thickness in the bilaterally injected group

The same procedure was performed for bilaterally injected eyes. Similarly, eyes treated with *scAAV2/8^{Y733F}hRHOp-RHO* demonstrated expression of rhodopsin and 2-4 layers of the ONL, whereas sham-treated eyes showed no rhodopsin expression and absence of the ONL five months postinjection (**Figure 5.9**).

On histology analysis, treated eyes demonstrated preservation of Hoechst-labelled photoreceptors with the mean number of cells in the ONL in treated

eyes 47.66±4.88, whereas the ONL was practically lost in sham-treated (2.38±0.35), $p<0.001$ (paired t-test), n= 7 (**Figure 5.10**, panel B).

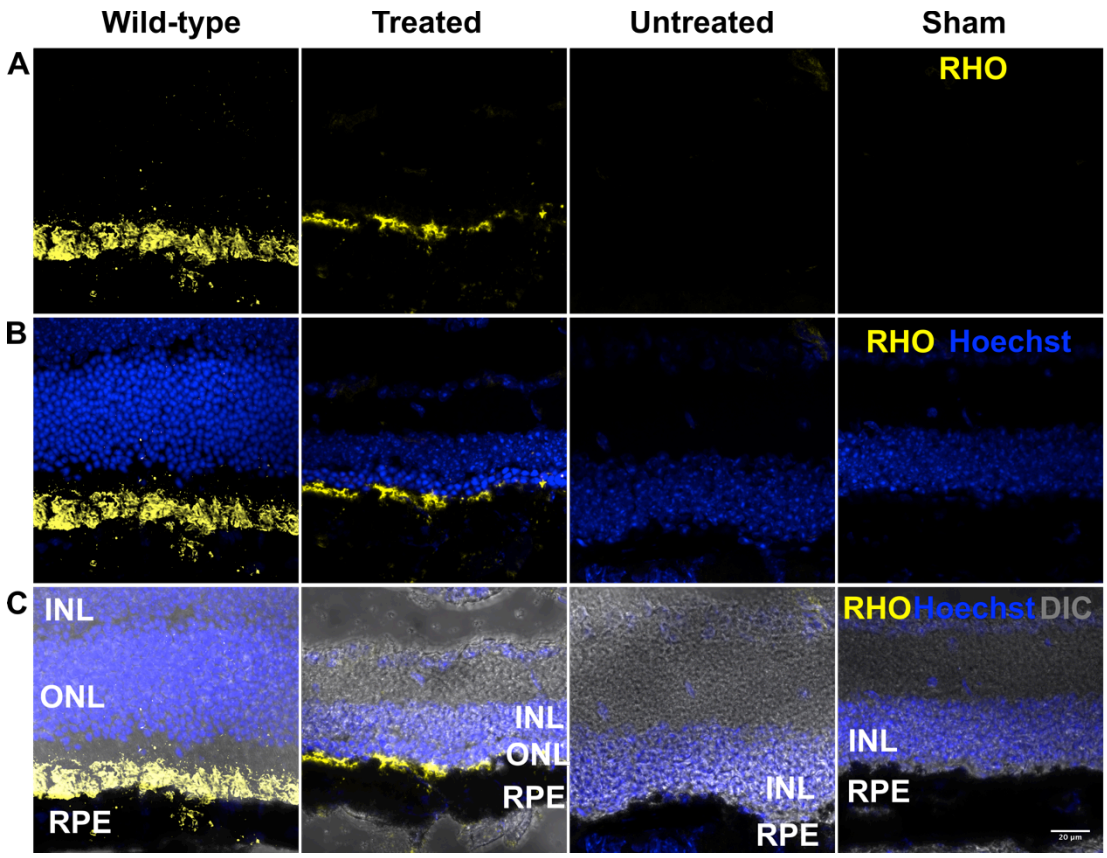


Figure 5.9 Preservation of the ONL and expression of rhodopsin six months after the AAV-mediated rhodopsin delivery in rhodopsin knockout mice
Histological retinal sections of wild-type, treated, untreated and sham-injected *Opn1-EGFP* rhodopsin knockout mice sacrificed six months after injection with *scAAV2/8^{Y733F}hRHOp-RHO*. Treated eyes, which received *scAAV2/8^{Y733F}hRHOp-RHO,* showed expression of rhodopsin in rod outer segments and preservation of 2-3 layers of the ONL, whereas untreated and sham-injected (which received the AAV-control) mice showed no rhodopsin expression and loss of the ONL. Scale bar 20 µm. Panel A: rhodopsin staining (yellow); panel B: rhodopsin (yellow) and Hoechst staining (blue); panel C: rhodopsin (yellow), Hoechst staining (blue) and DIC imagery superimposed.

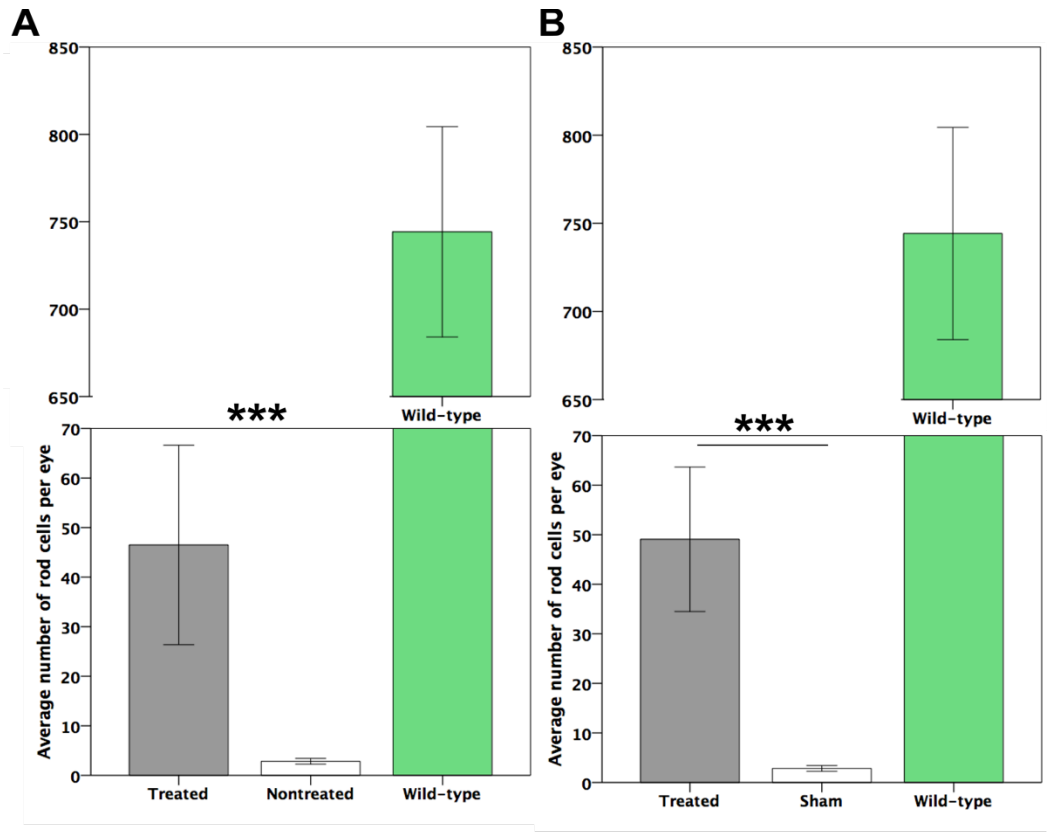


Figure 5.10 Preservation of Hoechst-labelled photoreceptors in the ONL five months after the delivery of *scAAV2/8^{Y733F}hRHOp-RHO*

Opn1.EGFP Rho-/- mice were injected with *scAAV2/8^{Y733F}hRHOp-RHO* at PW3, the fellow eye was left untreated or injected with the *AAV-control* (sham). Mice were sacrificed five months after injection and the number of photoreceptors was quantified by counting Hoechst-labelled photoreceptors in the ONL in four non-overlapping sections of the retina and averaged per eye. The number of Hoechst-labelled photoreceptors in the eyes, which received *scAAV2/8^{Y733F}hRHOp-RHO* was significantly greater than in nontreated (panel A, n=10) or sham-injected (panel B, n=7) eyes (*** - $p<0.001$, paired t-test). The number of Hoechst-labelled photoreceptors in the wild-type mice is provided as a reference, note the change in the y-axis scale after 70. Error bars represent +/- standard error of the mean.

5.5 Discussion

The provided data demonstrated a single subretinal application of *scAAV2/8^{Y733F}hRHOp-RHO* delivered at the age of three weeks in *Opn1-EGFP* rhodopsin knockout mice is safe and can slow down the progression of rod degeneration. Considering that ERG represents the summation of all electric signals of the retina and a large number of transduced cells is needed to provide such responses, these robust dark-adapted ERG responses one month post-injection achieving approximately 20% of wild-type amplitudes suggested high transduction rate for the scAAV vector.

Rhodopsin knockout mice lack dark-adapted ERG responses, however at first two months they preserve cones and corresponding ERG (Toda et al., 1999). In this study the use of dim light flashes allowed isolation of rod-generated responses and given that the responses in fellow untreated eyes remained flat at a young age, it confirmed the absence of cone stimulation. These dark-adapted responses confirmed functional improvement in treated eyes. This functional benefit was also confirmed by histological analysis showing the significantly thicker ONL in the treated eyes and expression of rhodopsin in rod outer segments five months after injection, whereas untreated or sham-injected eyes demonstrated the loss of the ONL and absence of rhodopsin expression.

The results of this study compare well with the published data on the rhodopsin delivery in the rhodopsin knockout mice. Palfi and co-workers injected the higher dose of *AAV2/5.mRhoP.RHO* vector in newly born

rhodopsin knockout mice pups; six weeks after injection, the b-wave amplitudes in the treated eyes constituted 19% of the b-wave amplitudes in RHO-M, the mice which expressed rhodopsin at 70% of wild-type (Palfi et al., 2010). Han and colleagues subretinally injected nanoparticles containing the murine rhodopsin gene driven by the murine rhodopsin promoter in newly born rhodopsin knockout mice, the obtained b-wave amplitudes also constituted approximately 20% of wild-type amplitudes (Han et al., 2015). Both these studies delivered gene therapy to newborn pups, in our study the vector administration was performed much later, at PW3. Given that the rhodopsin knockout mice undergo ongoing rod degeneration from birth, the robustness of dark-adapted responses in our project compared to other studies can potentially suggest the high efficiency of scAAV.

However, longitudinal follow-up revealed a continuous decline of dark-adapted ERG responses, with most of the responses achieving non-significance compared to untreated/sham-injected eyes four months after the treatment. In unilaterally injected eyes, in the time between the first and second months after injection the ERG b-wave amplitudes lost 43% (166.03±23.24 μV versus 95.12±26.72 μV). This general trend of the decrease in ERG responses is also described by Palfi and colleagues in the previously described study, where they injected newly born rhodopsin knockout pups and measured ERG at 6 and 12 weeks; in one month ERG measurements lost approximately 66% of the initial amplitude (61.9±35.6 μV versus 20.6 ±19.3 μV) (Palfi et al., 2010). This decline of ERG responses and non complete rescue of photoreceptors in our project could be explained by

continuous degeneration of photoreceptors despite the delivery of the causative gene of RP degeneration.

The data on continuous photoreceptor degeneration are corroborated by the study on *Rpe65 -/-* mice treated with AAV replacement injection at age of 3 weeks: despite the expression of RPE65 and transient improvement of ERG b-waves, photoreceptor degeneration and apoptotic cell death continued unabated and degeneration was the same at 12 months post-injection in treated and untreated animals (Lai et al., 2004). Similarly, in clinical trials on RPE65 patients, in spite of remarkable improvements in visual function, serial measurements of the outer nuclear layer thickness three years after treatment showed the progression of photoreceptor loss (Cideciyan et al., 2013), albeit considerably better than if no treatment had been administered.

Furthermore, in our study, the gene therapy was delivered later than in other studies on rhodopsin knockout mice. Given the ongoing photoreceptor degeneration, the time of AAV administration can affect the preservation of therapeutic effect. Some clinical trials found an age-dependent therapeutic effect with younger patients showing better results (Maguire et al., 2009; Weleber et al., 2016).

The preservation of the ONL shown in our study is limited to 2-4 layers of the ONL, this limited preservation contrasts with the greater preservation of the ONL shown by Han and colleagues in their study where they injected nanoparticles containing the genomic rhodopsin gene into newborn rhodopsin knockout mice and demonstrated preservation of 10-12 layers of

the ONL in the treated eyes 8 months after injection (Han et al., 2015). However, in their published data the uninjected eye also showed preservation of the ONL up to 5-6 layers (data are shown for a single mouse). This preservation of the ONL in the uninjected eyes in Han's study contradicts with what is described in the model of rhodopsin knockout with the complete loss of the ONL by 3 months (Lem et al., 1999). In our study, we show complete loss of the ONL in the nontreated and sham-injected eyes confirming the correctness of the chosen model.

Taken together, the data from this chapter show that the AAV-mediated delivery of the rhodopsin gene showed positive functional results attested by dark-adapted ERG responses and anatomical benefit demonstrated by the preservation of the ONL layer and rhodopsin expression in treated eyes, to our knowledge this is the first study showing efficient treatment of rhodopsin knockout mice delivering gene therapy at such late stage as three weeks after birth.

Chapter 6 Cone survival

6.1 Introduction

In humans, rod photoreceptors provide night, motion and peripheral vision, whereas cones supply high acuity and colour vision. The 120 million rods outnumber the 6 million cones, however in the fovea cones are exclusively concentrated to provide high acuity vision. In RP, affecting primarily rod photoreceptors, rod death is followed by secondary cone degeneration resulting in vision loss and blindness. In this project, we provided an effective treatment in the form of the AAV-packaged rhodopsin gene to rod photoreceptors lacking rhodopsin and showed that its delivery results in regrowing of rod outer segments and restoration of dark-adapted ERG. In this chapter, we explore the effects of rhodopsin delivery on cone photoreceptor survival in *Opn1.EGFP Rho-/-* mice.

6.1.1 Cone degeneration in rhodopsin knockout mice

Rhodopsin knockout mouse generated by a homologous targeted recombination of the rhodopsin gene has no rhodopsin and no rod outer segments and therefore lack rod signalling on the ERG (Humphries et al., 1997). Light-adapted ERG responses recorded in young rhodopsin knockout mice, reflecting the presence of functioning cones remain normal up to age P47 with a continuous decline after that age. After 80 days of age (P80) the ERG amplitudes decline to a minimal response due to the loss of cones (Toda et al., 1999). In this research project, *Opn1.EGFP Rho-/-* mice were injected at 3 weeks of age (PW3) with *scAAV2/8^{Y733F}hRHOp-RHO*. Therefore

the therapeutic effect of the vector on the ERG would be expected to become apparent around the third month (PM3), when cone responses in nontreated animals decline.

6.1.2 Isolating cone-derived ERG responses

As ERG measurements elicit responses from both rod and cone photoreceptors, different methods of isolating cone ERG responses have been developed. The adaptation method of isolating cone-driven ERG responses relies on the high sensitivity of rod photoreceptors and their saturation at constant background light (Weymouth and Vingrys, 2008). When a bright flash is given after this steady rod-saturating background light, only cone photoreceptors are able to respond. In our experiments, light adaptation was given for 10 minutes before recording photopic ERG responses.

Another method of isolating the cone response is based on higher temporal resolution of cones compared to rods. When a flickering stimulus higher than 3 Hz is presented, only cones are able to perceive it as an alternating signal, and thus cone-mediated responses can be isolated (Weymouth and Vingrys, 2008). To show cone-mediated ERG responses, this work also presents measurements taken at 20 Hz flicker stimulus.

6.2 Aims

In the previous chapters, it was shown that the administration of the *scAAV2/8^{Y733F}hRHOp-RHO* vector into rhodopsin knockout mice resulted in efficient transduction of rod photoreceptors, restoration of rod-isolated ERG responses and preservation of the ONL in treated eyes.

This chapter assesses the effects of the *scAAV2/8^{Y733F}hRHOp-RHO* vector on cone photoreceptors using evaluating light-adapted ERG, cSLO, and histology analysis of post-mortem eye sections.

6.3 Methods

To assess the effects of rhodopsin gene delivery via AAV vector on cone photoreceptors the mice from the previous chapter which received treatment with *scAAV2/8^{Y733F}hRHOp-RHO* were evaluated using light-adapted ERG and two weeks later by cSLO at the subsequent points: postnatal month 2 (PM2), PM3, PM4, PM5.

6.3.1 Isolating cone ERG responses

Light-adapted ERG responses were recorded after dark-adapted ERG; to isolate cone responses, mice were light-adapted for 10 min at 30 cd.s/m^2 background light, and then exposed to white flashes with increasing intensity: 1 cd.s/m^2, 3 cd.s/m^2, 10 cd.s/m^2 and 25 cd.s/m^2 against a steady adapting

light (see details in section 2.4.4). Flicker ERG responses were recorded after light-adapted flash ERG, using 20 Hz flicker light.

6.3.2 SLO imaging

The injected mice were followed longitudinally by cSLO, which allows a non-invasive evaluation of retinal fundus. In autofluorescence mode, cSLO uses a wavelength exciting EGFP-expressing cones which allow their real-time visualisation (Charbel Issa et al., 2012). Normalised images obtained from cSLO in autofluorescence mode were transferred to Image J software, where a region of interest was identified between the lines drawn along the vascular. With the investigator blinded to treatment received by mice, manual counting of cones was performed using the ImageJ plug-in Cell Counter. The initial number of cones obtained at the first counting at postnatal month two was normalized to 100%, subsequent counts were transformed into a percentage of the initial count to accurately reflect a drop in cone numbers in the identified region of interest. The data were copied into Excel and SPSS for analysis**.** Figure 6.1 presents the longitudinal results of such counting.

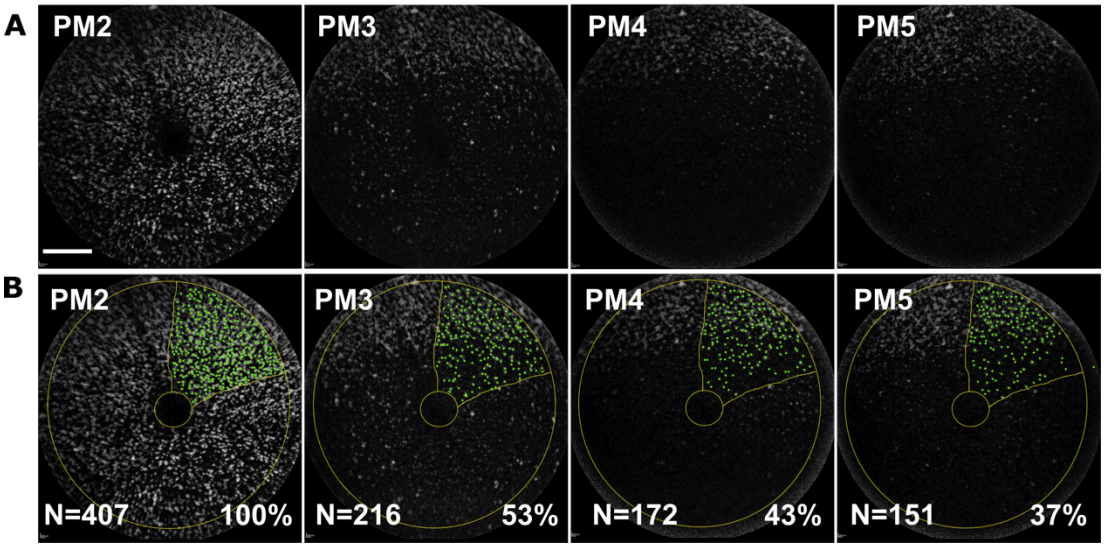


Figure 6.1 Longitudinal quantification of ERGP-cones by SLO
Panel A: autofluorescence imaging of *Opn1.EGFP Rho-/-* mouse injected with *scAAV2/8^{Y733F}hRHOp-RHO* at PW3. Panel B: the constant region of interest (ROI) was identified between vascular arcades and EGFP-expressing cones (white dots) were counted in ImageJ plug-in (green dot overlay). Survival was normalized to 100% at PM2 (baseline) and expressed as a function (%) of cone photoreceptors from the baseline, from PM3 to PM5. Scale bar 2 mm; PM - post-natal month.

6.3.3 Histology analysis of cones

To measure the number of EGFP-expressing cones, three non-overlapping high-power images from the middle superior retina were taken with a 63X objective on the confocal microscope (Zeiss LSM710). The number of EGFP cones per image was counted manually using the ImageJ plug-in Cell counter, then averaged per animal (section 2.5.3.2 for more details).

6.4 Results

6.4.1 Light-adapted ERG in unilaterally treated eyes

Given that at postnatal month two, rhodopsin knockout mice still have cones and preserved light-adapted ERG responses, at the earliest time point the ERG responses at the highest flash intensity 25 cd.s/m^2 in treated eyes did not differ from untreated eyes, however starting at PM3 and PM4 the preservation of light-adapted ERG responses became evident, with the effect declining in time and flattening at PM5 (**Figure 6.2**).

Detailed analysis of b-wave amplitudes at the highest flash intensity (25 cd.s/m^2) showed the absence of significant difference in treated eyes (161.19± 15.58 μV) from untreated eyes (177.89±16.77 μV) at PM2, $p>0.05$, Bonferroni-adjusted paired t-test , n=10 (**Fig. 6.2,** panel A).

Later, as rhodopsin knockout mice lose cones due to secondary cone degeneration, at postnatal month three, the therapeutic effect of the rhodopsin gene delivery was evident as the amplitudes of b-waves in treated eyes (65.37±15.22 μV) were significantly greater from untreated, (22.66±5.36 μV), $p<0.01$. This therapeutic effect was conserved at PM4, with b-waves amplitudes in treated eyes greater (29.32±7.82 μV) than untreated (9.11±2.17 μV), $p<0.01$, Bonferroni-adjusted paired t-test, n=10 (**Fig. 6.2,** panel A).

At postnatal month five, the therapeutic effect declined; and the difference between the treated and untreated eyes was statistically insignificant: with the mean b-wave amplitude in treated eyes (18.22±8.17 μV) compared to the untreated (11±8.17 μV), $p>0.05$, Bonferroni-adjusted paired t-test, n=10 (**Figure 6.3,** panel A).

Assessed globally at increasing flash intensities, light-adapted ERG responses showed that the therapeutic effect was sustained up to three months after injection: the difference between light-adapted b-wave amplitudes in treated compared to untreated eyes was statistically insignificant at PM2 ($p>0.05$). At PM3 and PM4 b-wave amplitudes were significantly greater in treated eyes, $p<0.01$. The decline of the preservation effect was evident at PM5, with the difference between two groups being insignificant, $p>0.05$. The significance was assessed by factorial ANOVA for repeated measures (treatment and flash intensity as factors), n=10 (**Figure 6.4**).

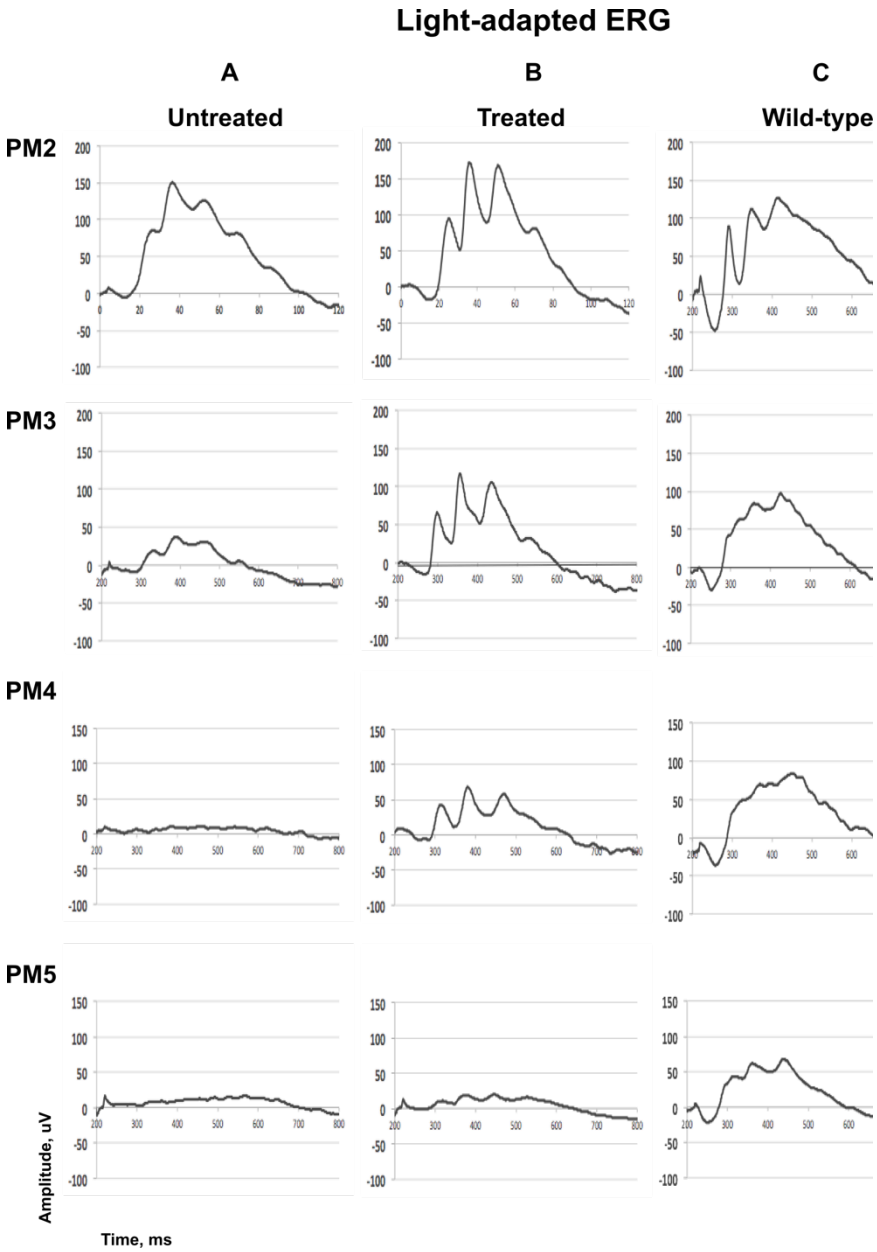


Figure 6.2 Representative light-adapted ERG traces at different time points

Panels A and B show representative light-adapted ERG traces at flash intensity 25 cd.s/m^2. from an *Opn1.EGFP Rho-/-* mouse with one eye treated with *scAAV2/8^{Y733F}hRHOp-RHO* at PW3 (B), and the fellow eye left untreated (A). The C panel shows wild-type mouse ERG responses. ERG was measured at postnatal month 2, 3, 4 and 5.

Given that rhodopsin knockout mice at age PM2 still have preserved cones, at the high flash intensity both eyes have light-adapted ERG traces, similar to wild-type. However, due to secondary cone loss at PM3, light-adapted ERG flattens out in the untreated eye, whereas there is a clear preservation of light-adapted ERG in the treated eye, this preservation effect is maintained at PM4, however, it flattens out at PM5. PM – postnatal month.

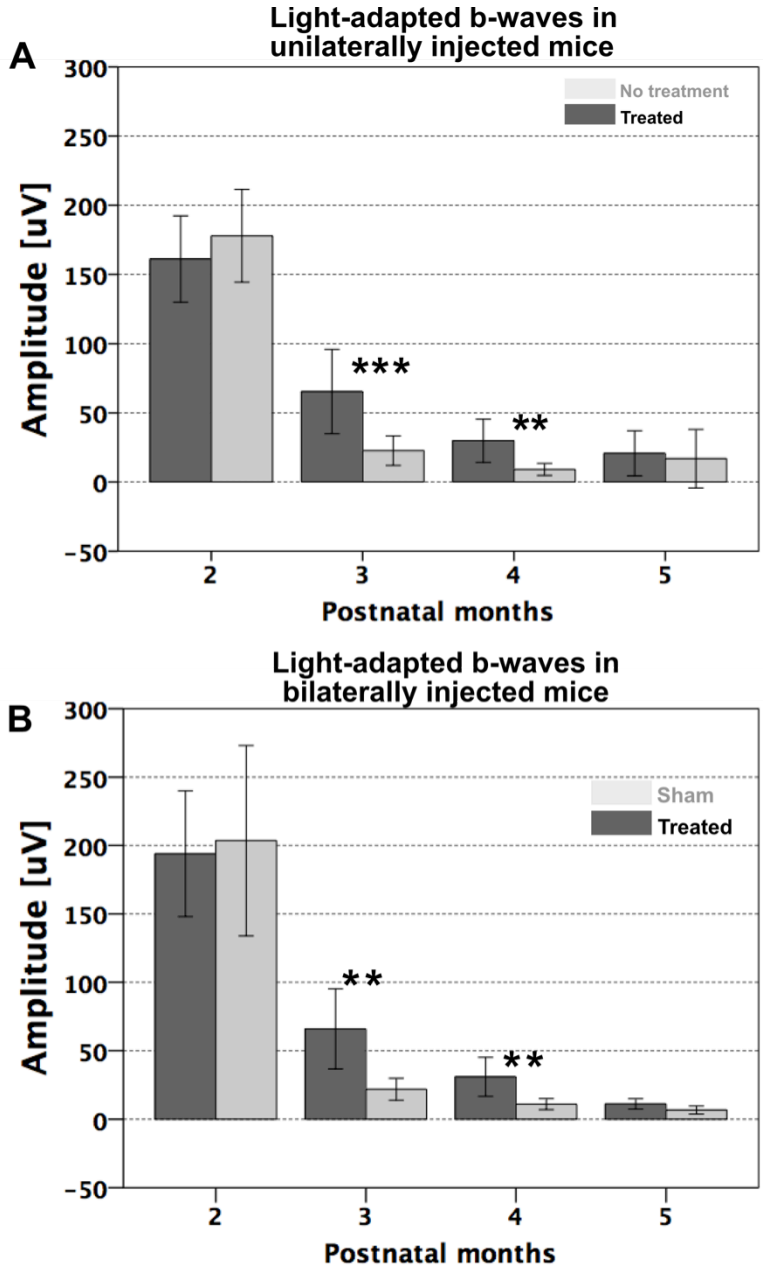


Figure 6.3 B-wave amplitudes in light-adapted ERG in unilaterally and bilaterally treated rhodopsin knockout mice

Opn1.EGFP Rho-/- mice injected in one eye with *scAAV2/8^{Y733F}hRHOp-RHO* at P21; (A) the fellow eye left untreated (n=10); (B) the fellow eye was received the sham injection (n=7). ERG was measured at 2, 3, 4 and 5 postnatal months. The b-waves amplitudes at 25 cd.s/m^{-2} flash intensity, allowing isolation of cone responses, are presented. The light-adapted b-wave amplitudes at PM2 showed no significant difference between two groups since rhodopsin knockout mice at that age still preserve cone photoreceptors. The treatment with *scAAV2/8^{Y733F}hRHOp-RHO* showed statistically significant preservation of cone ERG responses at PM3 and PM4 compared to untreated and sham-injected eyes. At PM5 the difference between the groups is unsignificant. Error bars represent +/- standard error of the mean, *** - $p < 0.001$; ** - $p < 0.01$; Bonferroni-adjusted posthoc paired t-test.

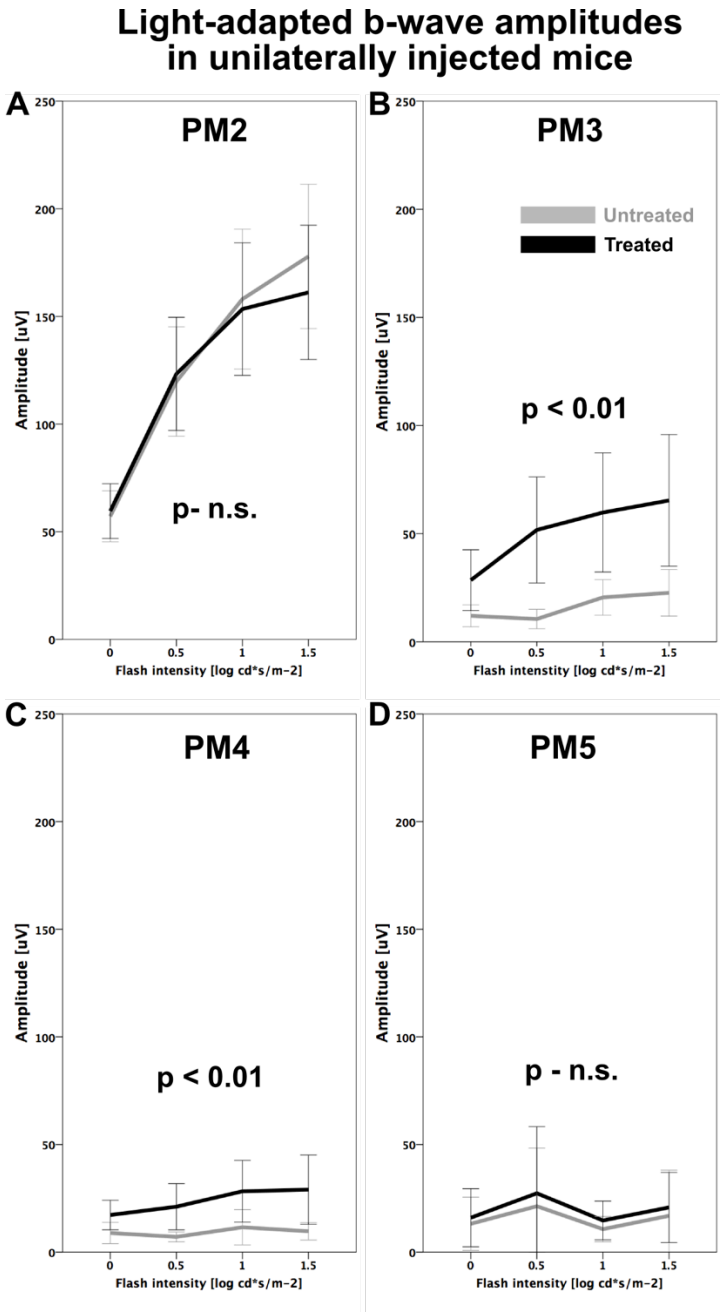


Figure 6.4 Light-adapted b-wave amplitudes at increasing flash intensities in unilaterally treated rhodopsin knockout mice
Opn1.EGFP Rho-/- mice were injected with *scAAV2/8^{Y733F}hRHOp-RHO* in one eye at P21, with the fellow eye, left untreated. After exposing mice to light of 30 cd.s/m^{-2} for 10 min, light-adapted responses were elicited at flash intensities 1; 3; 10 and 25 cd.s/m^{-2} at postnatal age 2, 3, 4 and 5 months A) PM2; B) PM3; C) PM4; D) PM5). The delivery of the rhodopsin vector resulted in the statistically significant preservation of b-waves at postnatal months 3 and 4, with the loss of the effect at postnatal month 5. Error bars represent +/- standard error of the mean, n = 10, factorial ANOVA for repeated measures.

6.4.2 Light-adapted ERG in bilaterally injected eyes

In the bilaterally injected group *Opn1.EGFP Rho-/-* mice were injected at PW3 at one eye with *scAAV2/8^{Y733F}hRHOp-RHO* and the *AAV-control* vector in the contralateral eye.

At the earliest time point, postnatal month two (PM2), the mean b-wave amplitudes at the highest flash intensity 25 cd.s/m^2 in treated eyes (203.49± 34.80 μV) did not differ significantly from sham-injected eyes (193.91±22.96 μV); $p>0.05$; Bonferroni-adjusted paired t-test, n=7 (**Figure 6.3,** panel B).

In later measurements, the preservation effect of the rhodopsin gene delivery was evident at postnatal month three: the mean amplitudes of b-waves in the treated eyes (65.98±14.63 μV) were significantly greater than for sham-injected, (21.88±4.02 μV), $p<0.01$; n=7. This therapeutic effect was conserved at postnatal month 4, with the mean b-wave amplitudes significantly greater in treated eyes (30.96±7.11 μV) compared with sham-injected (11.02±2.02 μV), $p<0.01$, Bonferroni-adjusted paired t-test, n=7.

At the last time point, PM5, mean b-wave amplitudes in treated eyes (11.18±1.91 μV) declined and did not differ statistically from sham-injected (6.72±1.47 μV); $p>0.05$; n=7 (**Figure 6.3,** panel B).

Assessed globally with increasing flash intensities, light-adapted ERG responses showed the therapeutic effect sustained up to three months after injection: the difference between light-adapted b-wave amplitudes in treated compared to sham-injected was statistically insignificant at the earliest time-

point, postnatal month two ($p>0.05$; $n=7$). Later measurements revealed the preservation effect of rhodopsin gene delivery on light-adapted ERG, with b-wave amplitudes significantly greater in treated eyes compared to sham-injected at postnatal months 3 and 4 ($p<0.01$; $n=7$). At PM5, b-wave amplitudes in light-adapted ERG in treated eyes declined and were not statistically different from sham-injected eyes ($p>0.05$; $n=7$) (**Figure 6.5**). The statistical significance was assessed with factorial ANOVA for repeated measures (with treatment and flash intensity as factors).

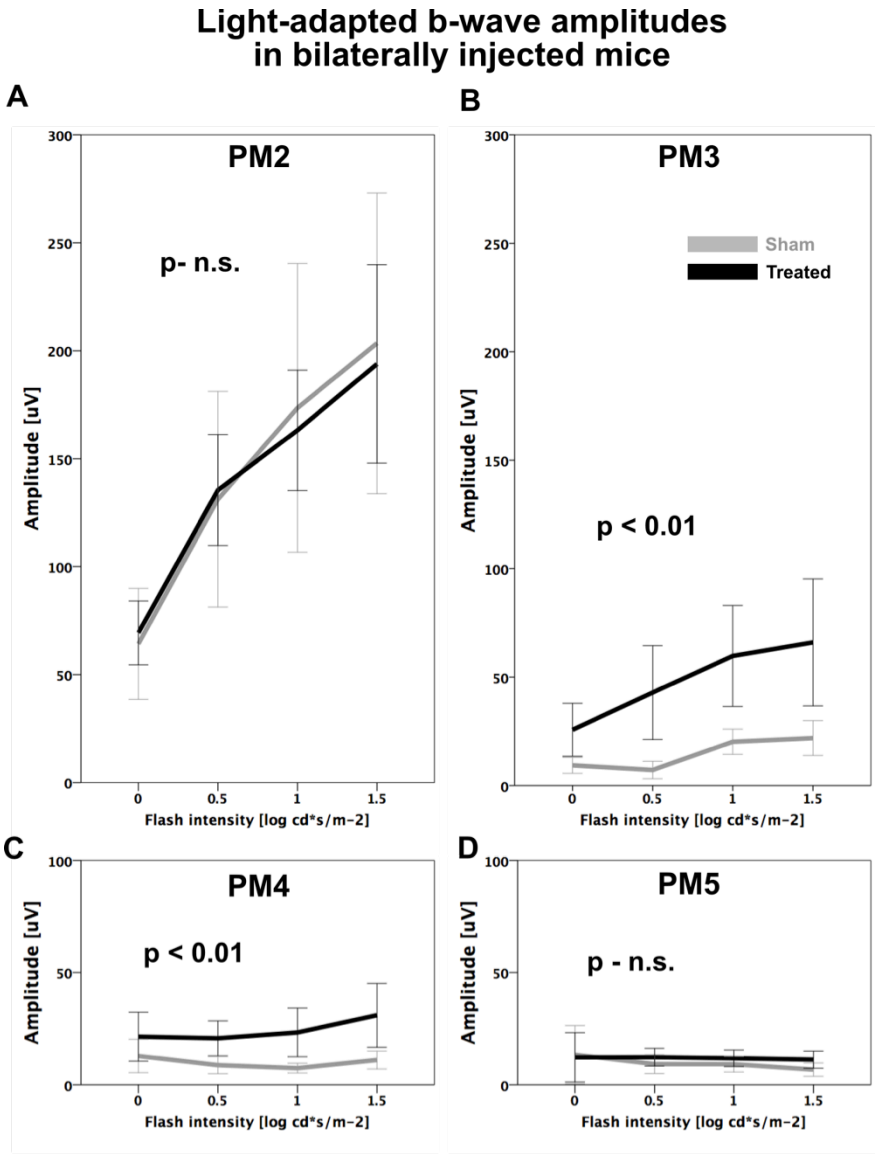


Figure 6.5 Light-adapted b-wave amplitudes at different flash intensities and time points in bilaterally treated rhodopsin knockout mice
Opn1.EGFP Rho-/- mice injected at one eye with *scAAV2/8^{Y733F}hRHOp-RHO* at PW3, the fellow eye received the control AAV. After exposing mice to light of 30 cd.s/m^{-2} for 10 min, light-adapted responses were elicited at flash intensities 1; 3; 10 and 25 cd.s/m^{-2} at postnatal age 2, 3, 4 and 5 months **A)** PM2; **B)** PM3; **C)** PM4; **D)** PM5). The delivery of the rhodopsin vector resulted in the statistically significant preservation of b-waves at postnatal months 3 and 4, with the loss of the effect at postnatal month 5. Error bars represent +/- standard error of the mean, n = 7, factorial ANOVA for repeated measures.

6.4.3 Flicker ERG in unilaterally treated mice

In unilaterally treated *Opn1.EGFP Rho-/-* mice one eye was injected with *scAAV2/8^{Y733F}hRHOp-RHO* at PW3 and the fellow eye left untreated. Light-adapted flicker ERG mean b-wave amplitudes measured at PM2 were not significantly different in treated (73.25±7.08 μV) compared to untreated eyes (84 ±9.21 μV), p=0.58. At PM3, the therapeutic effect of the rhodopsin gene delivery was significant in treated (32±6.8 μV) compared to untreated (11.61±1.59 μV), p=0.009, Bonferroni-adjusted paired t-test, n=10. At PM4 flicker b-amplitudes were preserved in treated eyes (18.54±4.68 μV) versus untreated (3.82±1.45 μV), p=0.003, Bonferroni-adjusted paired t-test, n=10. At PM5, b-amplitudes in treated eyes (12.13±2.61 μV) flattened out and were not significantly different from untreated (7.87±1.46 μV), p=0.12, paired t-test, n=10 (**Figure 6.6,** panel A).

6.4.4 Flicker ERG in bilaterally injected mice

In the bilaterally injected group, *Opn1.EGFP Rho-/-* mice were injected at PW3 in one eye with *scAAV2/8^{Y733F}hRHOp-RHO* and *AAV-control* vector in the contralateral eye. Light-adapted flicker ERG b-wave amplitudes measured at PM2 were not significantly different in treated (98.15±15.39 μV) compared to sham-injected (97.56±15.53 μV), p=0.9, paired t-test, n=7. At PM3, preservation of the cone ERG was significant in treated (36.03±6.3 μV) compared to sham-injected eyes (13.18±1.75 μV), p=0.006, Bonferroni-adjusted paired t-test, n=7. At PM4 flicker b-amplitudes were preserved in treated eyes (19.52±3.37 μV) versus sham-injected (6.81±3.35 μV), p=0.002,

Bonferroni-adjusted paired t-test, n=7. By PM5, however, the mean b-amplitude had declined in treated eyes (11.27±2.59 μV) and was no longer significantly different from the contralateral sham-injected eyes (8.11±3.11 μV), p=0.286, paired t-test, n=7 (**Figure 6.6**, panel B).

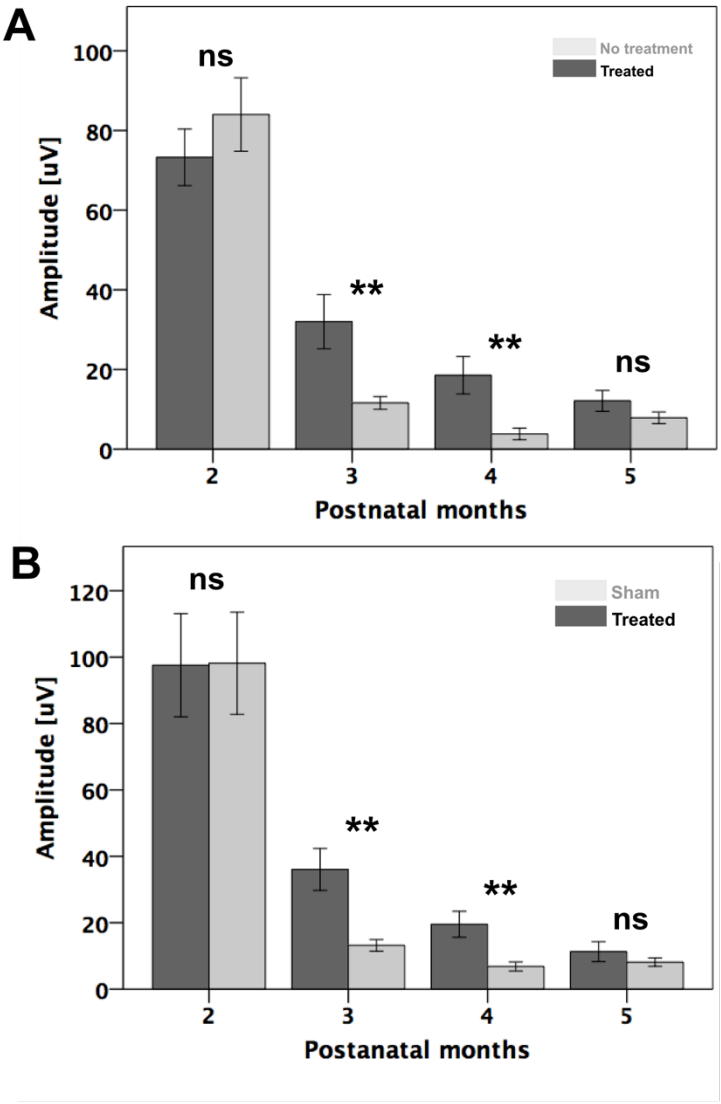


Figure 6.6 Light-adapted b-wave amplitudes flicker ERG after the *scAAV2/8Y733FhRHOp-RHO* delivery
Opn1.EGFP Rho-/- mice injected in one eye with *scAAV2/8*^{Y733F}*hRHOp-RHO* at PW3, with the other left untreated (A, n=10) or injected with the AAV-control (B, sham, n=7). After exposing mice to the light of 30 cd.s/m^{-2} for 10 min, light-adapted ERG responses were recorded using 30 Hz flicker at PM2, PM3, PM4, and PM5. At PM2 b-wave amplitudes were not significantly different. At PM3 and PM4 the delivery of the rhodopsin vector resulted in the statistically significant preservation of b-wave amplitudes (** - $p<0.01$); with the loss of significance at PM5 (ns - $p>0.05$). Error bars represent +/- standard error of the mean, Bonferroni adjusted paired t-test.

6.4.5 Rhodopsin vector delays cone degeneration in unilaterally treated group

Autofluorescence cSLO imaging taken at PM2 showed a similar distribution pattern of EGFP-expressing cones in treated and nontreated eyes (**Figure 6.7**). At PM3 the difference between two groups was insignificant, whereas at PM4 it demonstrated greater survival of cones in treated eyes (54.28±8.18%) versus untreated (30.58±12.73%), t=4.459, p=0.002; n=10 and at the final measurement at PM5: 28.29±6.4% in treated and 15.07±6.67% in untreated; t=3.71; p=0.008; Bonferroni-adjusted paired t-test, n=10 (**Figure 6.8**).

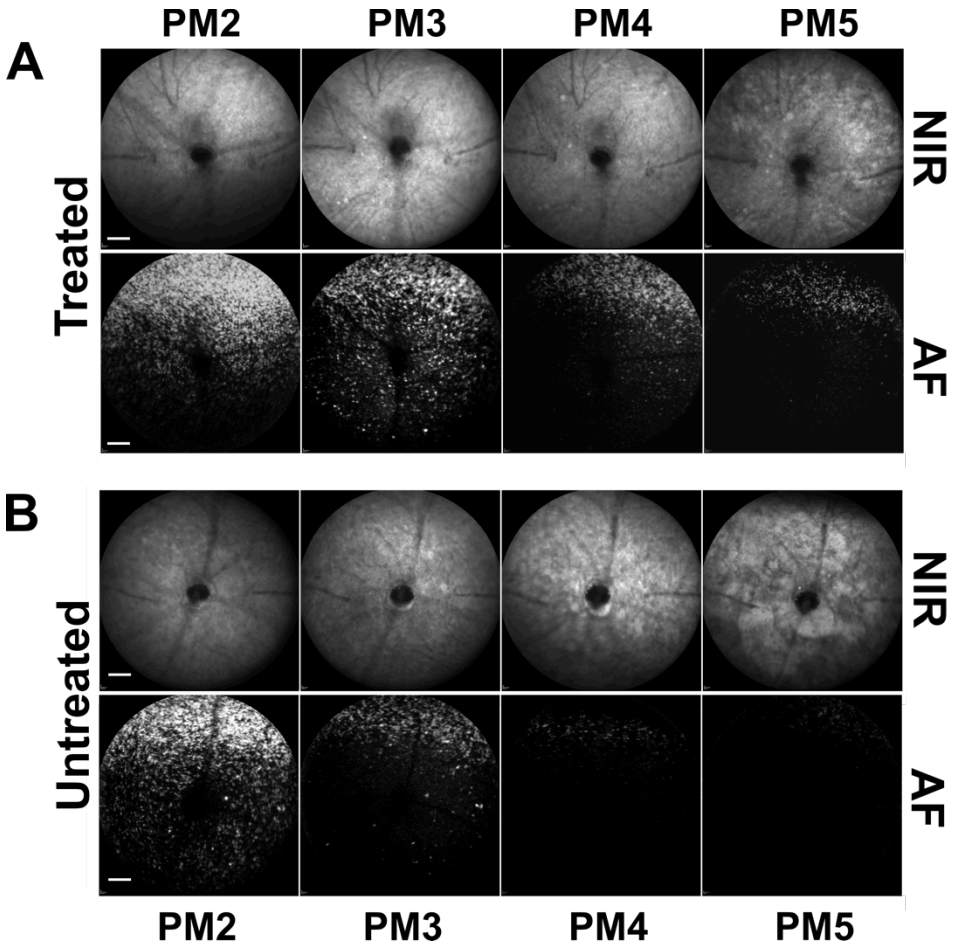


Figure 6.7 Autofluorescence imaging in *Opn1.Rho-/-* mice treated unilaterally with *scAAV2/8^{Y733F}hRHOp-RHO*

Long-term follow-up on *Opn1.EGFP Rho-/-* mice injected at PW3 by cSLO in Near-Infrared reflectance (NIR) and autofluorescence modes (AF). White dots in AF imaging correspond EGFP-expressing cones. Both eyes show a decline in the number of EGFP-expressing cones, however, the loss of cones is slower in treated eyes. Scale bar 1mm.

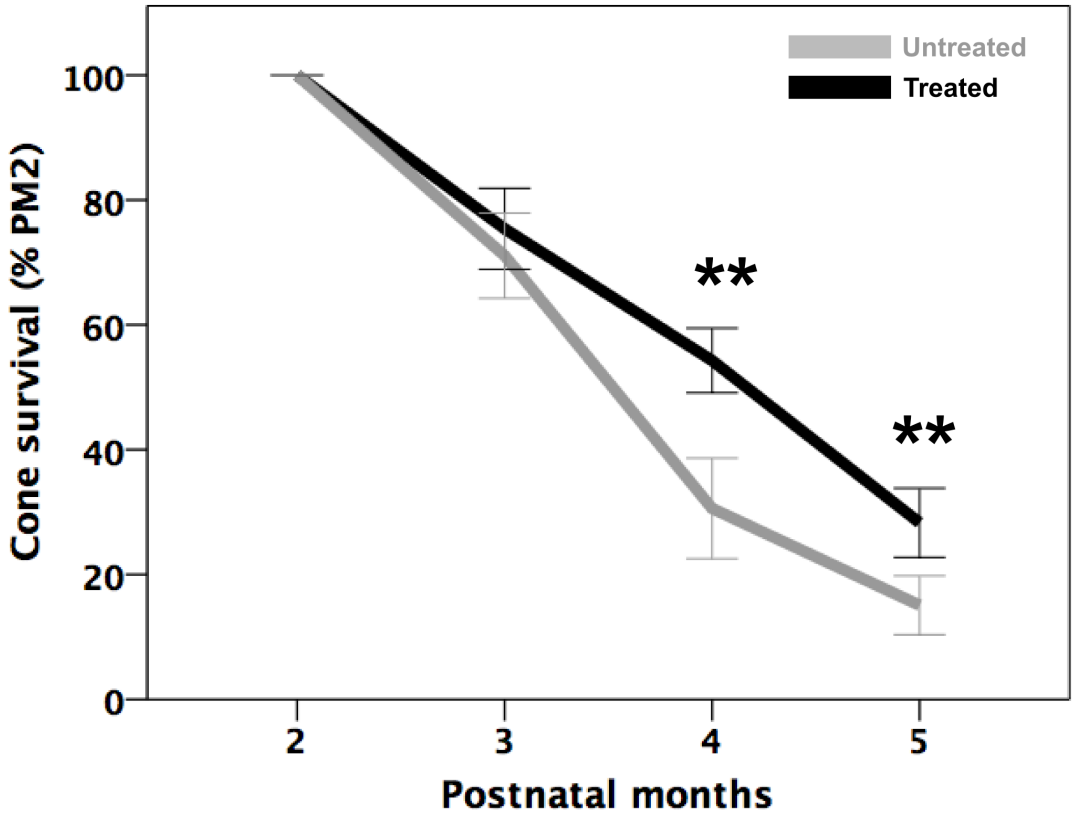


Figure 6.8 SLO quantification of EGFP-fluorescent cones in mice unilaterally treated with *scAAV2/8^{Y733F}hRHOp-RHO* shows preservation of cones in treated eyes
Opn1.EGFP Rho-/- mice at the age of PW3 were injected with *scAAV2/8^{Y733F}hRHOp-RHO* in one eye, with the fellow eye left untreated. SLO imaging was performed at PM 2, 3, 4 and 5. Longitudinal measurements of cone numbers on SLO shows preservation of cones in treated eyes at PM4 and PM5 compared to non-injected eyes.
Longitudinal measurements of cone numbers on SLO shows preservation of cones in treated group at PM4 and PM5.
Survival of EGFP-cones expressed as a function (%) of cones measured at the baseline (PM2). Error bars represent +/- standard error of the mean, n = 10, ** - $p < 0.01$, Bonferroni adjusted paired t-test. PM –postnatal month.

6.4.6 Rhodopsin vector delays cone degeneration in bilaterally injected group

In *Opn1.EGFP Rho-/-* mice with one eye injected with *scAAV2/8^{Y733F}hRHOp-RHO* and the fellow eye with the *AAV-control* at PW3, autofluorescence imaging taken at PM2 showed a similar distribution pattern of EGFP-expressing cones in treated and sham-injected eyes (Figure 6.9) (the measurement technique described in section 6.3.2). Similar to the unilaterally treated group, at PM3 the difference between the two groups was insignificant. At PM4 the therapeutic effect was demonstrated in treated eyes (51.51±7.99%) with greater survival of EGFP-expressing cones compared to sham-injected eyes (32.98±12.2%), t=3.63, p=0.011, n=7. At PM5 the difference between treated (18.11±3.54%) and untreated (14.44±2.98%) was no longer significant, t=1.06; p=0.16, Bonferroni-adjusted paired t-test, n=7 (**Figure 6.10**).

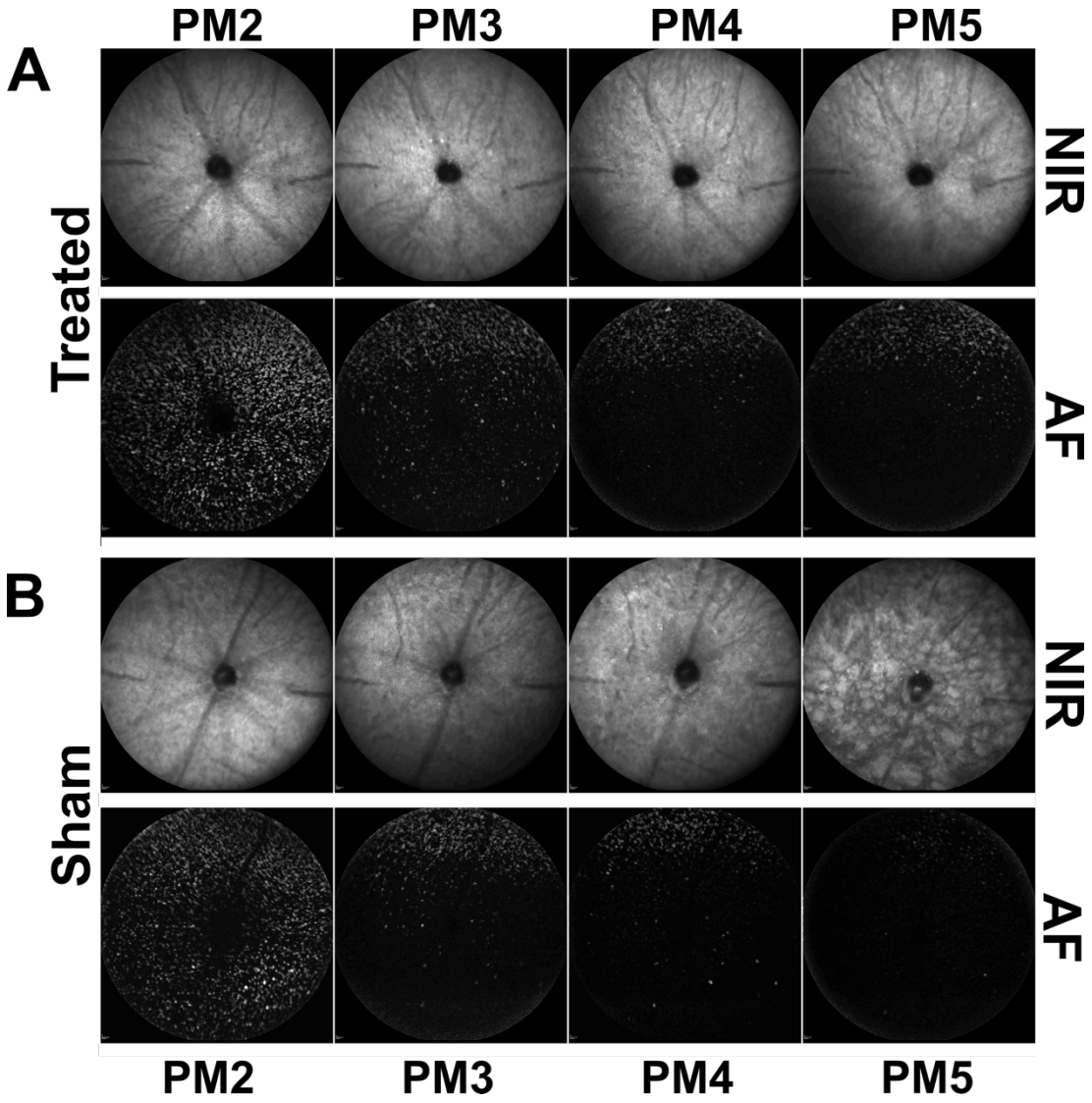


Figure 6.9 Fundus imaging in bilaterally injected mouse shows cone preservation in treated eyes
The *Opn1.EGFP Rho-/-* mouse was injected in one eye with *scAAV2/8^{Y733F}hRHOp-RHO* and the *AAV-control* in the fellow eye (sham). Near-reflectance (NIR) and Autofluorescence (AF) imaging at PM2, PM3, PM4, and PM5. The upper panel shows the treated eye, the bottom panel shows the sham-injected eye. EGFP-expressing cones correspond to white dots in AF imaging. Both eyes demonstrate the loss of EGFP-expressing cones in AF, however, the loss is delayed in treated eyes. Scale bar 1 mm.

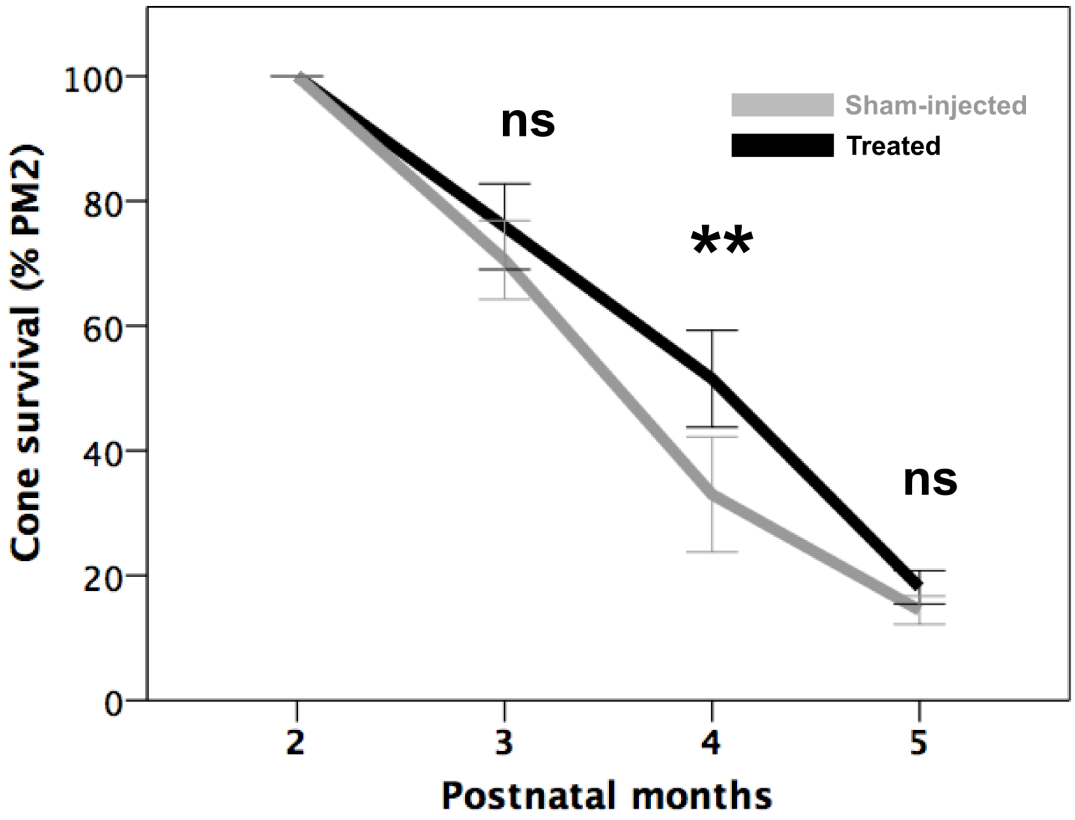


Figure 6.10 SLO quantification of EGFP-fluorescent cones in bilaterally injected mice shows preservation of cones at PM4 in treated eyes
Opn1.EGFP Rho-/- mice at the age of PW3 were injected with *scAAV2/8^{Y733F}hRHOp-RHO* in one eye and *AAV-control* in another. SLO imaging was made at PM 2, 3, 4 and 5.
EGFP-expressing cones were counted as fluorescent dotes in the constant region of interest (ROI) and survival was normalized to 100% at PM2 (baseline) and expressed as a function (%) of cone photoreceptors from the baseline, from PM3 to PM5.
Longitudinal measurements of cone numbers on SLO shows preservation of cones in the treated eyes at PM4 compared to sham-injected eyes.
Error bars represent +/- standard error of the mean, n = 7, ** - $p < 0.01$, Bonferroni adjusted paired t-test, n=7. PM – postnatal month.

6.4.7 Optomotor response

At PM6 *Opn1.EGFP Rho-/-* mice injected at PW3 with *scAAV2/8^{Y733F}hRHOp-RHO* in one eye and either untreated or sham-injected in the fellow eye were assessed for functional effects by optomotor response (see section 2.4.5). *Opn1.EGFP Rho+/+* at PM6 serving as wild-type control scored 3.41±0.4 head turns per minute. In the unilaterally injected group, two individual mice demonstrated head turns on treated side, in each testing, however, the difference between treated (0.2±0.04 turns/min) and untreated eyes (0.06±0.04 turns/min) was insignificant, p=0.39, n=10, paired t-test. Similarly, in the bilaterally treated group, the difference between treated (0.33±0.05 turns/min) and sham-injected (0.11±0.17 turns/min) eyes was not significant p=0.23, n=7, paired t-test (**Figure 6.11**).

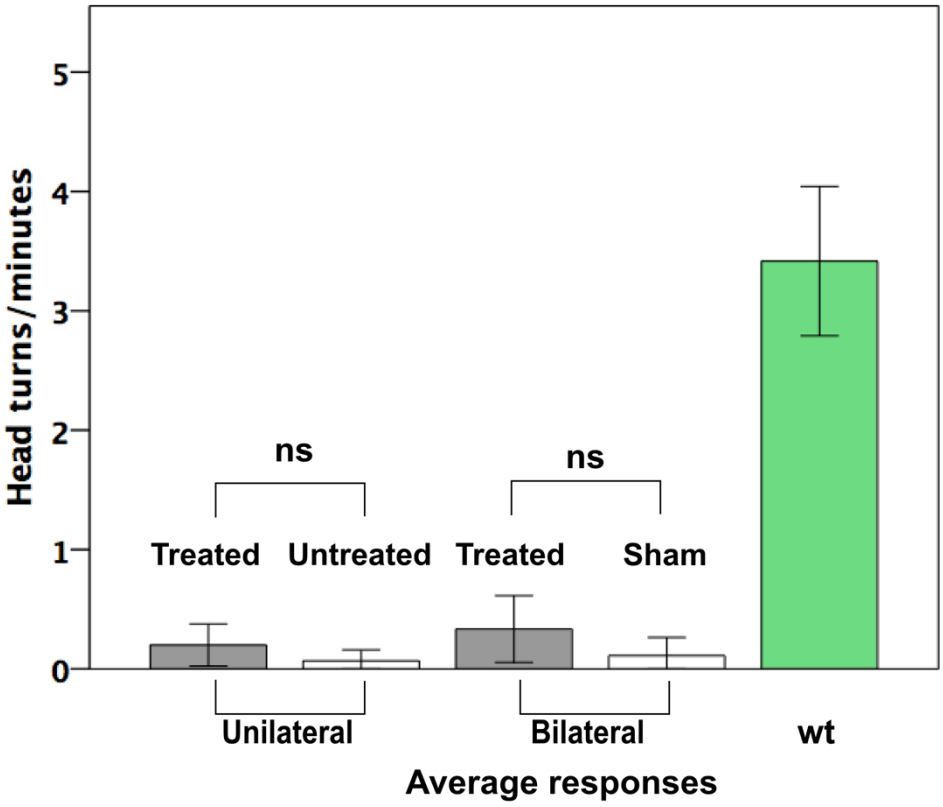


Figure 6.11 Optomotor response of Opn1.EGFP Rho-/- mice injected with scAAV2/8^{Y733F}hRHOp-RHO

Opn1.EGFP Rho-/- mice were injected at PW3 unilaterally with *scAAV2/8^{Y733F}hRHOp-RHO* or bilaterally with *scAAV2/8^{Y733F}hRHOp-RHO* in one eye and *AAV-control* in the fellow eye. 5 months after injection, mice were assessed for an optomotor response. The difference between mean group responses of treated compared to untreated and treated compared to sham-injected was insignificant, $p>0.05$, n=10 unilateral, n=7 bilateral. In *Opn1.EGFP rho+/+* mice (wt), the mean number of head turns constituted 3.41 turn/minute.

6.4.8 Preservation of EGFP-cones six month postinjection on histology

Histology analysis at six months post-injection of *Opn1.EGFP Rho-/-* mice found that the average number of EGFP-cones per eye (measurement technique described in section 6.3.3) was greater in the eyes treated with *scAAV2/8^{Y733F}hRHOp-RHO* than in untreated or sham-injected contralateral eyes (**Figure 6.12**). In the unilaterally injected group, the average number of EGFP-cones in treated eyes was 3.5±1.16; whereas in nontreated eyes 0.03±0.15, $p<0.01$ (paired t-test), n=10. In the bilaterally injected group, the average number of cones in treated eyes was 4±1.07; whereas in sham-injected eyes 0.05±0.13; $p<0.001$ (paired t-test), n=7 (**Figure 6.13**).

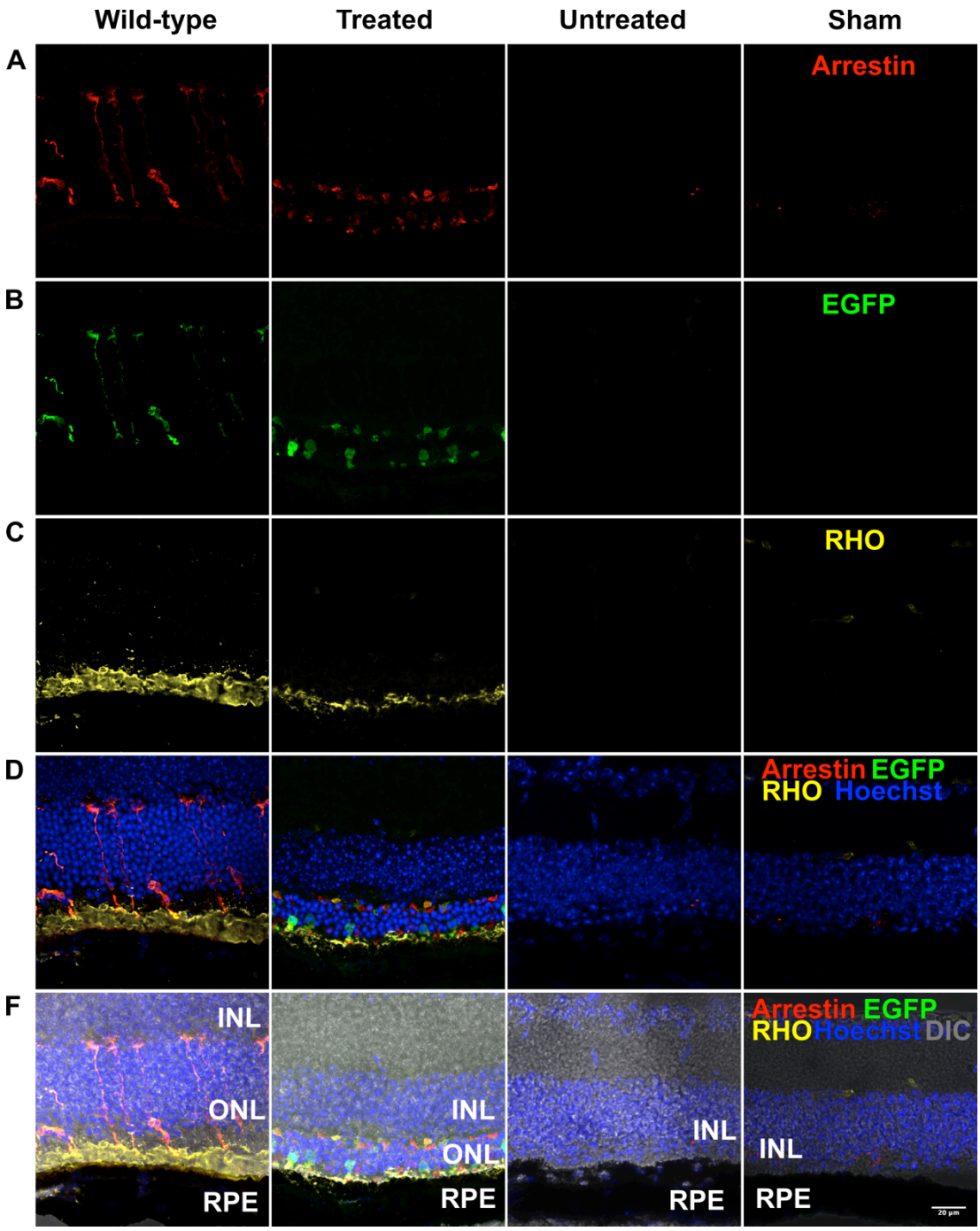


Figure 6.12 Histology analysis showed preservation of EGFP-cones in treated eyes
Opn1.EGFP Rho-/- mice injected at one eye with *scAAV2/8^{Y733F}hRHOp-RHO* at P21, another eye left untreated or injected with the control AAV. At postnatal month 6, eyes were collected for histology analysis and showed preservation of the ONL and cone photoreceptors in treated eyes, whereas in untreated or sham-injected eyes no cones are preserved. Scale bar 20 μm.
Panel A: cone arrestin staining (red); panel B: GFP fluorescence (green); panel C: rhodopsin staining (yellow); panel D: cone arrestin (red), GFP fluorescence (green), rhodopsin staining (yellow), Hoechst staining (blue); panel E: cone arrestin (red), GFP fluorescence (green), rhodopsin staining (yellow), Hoechst staining (blue), DIC (grey).

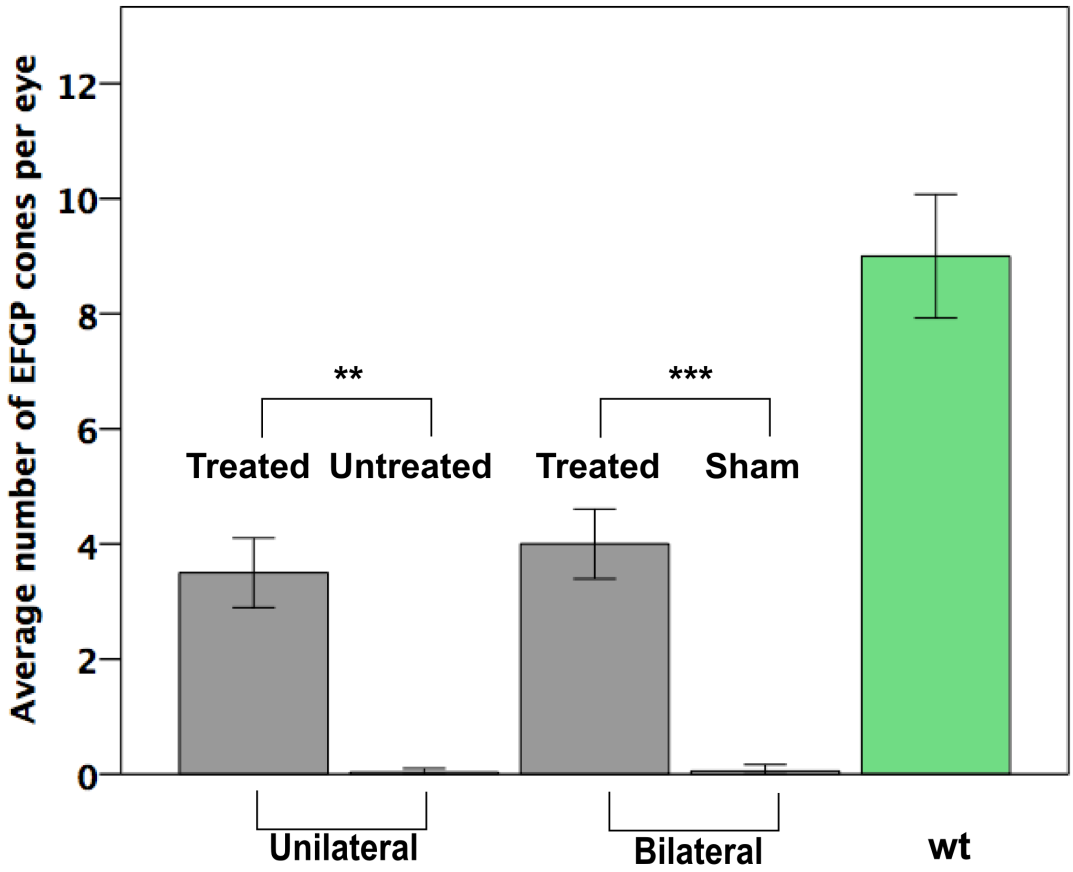


Figure 6.13 Histology quantification of EGFP-cones in *Opn1.EGFP Rho-/-* mice treated at PW3 with *scAAV2/8^{Y733F}hRHOp-RHO*, six months after injection shows preservation of cones in treated eyes

Opn1.EGFP Rho-/- unilaterally injected inone eye with *scAAV2/8^{Y733F}hRHOp-RHO*, with the fellow eye left untreated (n=10); and bilaterally injected with *scAAV2/8^{Y733F}hRHOp-RHO* into one eye, with the fellow eye injected with the *AAV-control* at PW3 (n=7). Six months post-injection. Quantification of preserved EGFP-cones per eye showed preservation EGFP-cone photoreceptors in treated eyes, whereas in untreated or sham-injected eyes practically no cones were preserved. Wild-type (wt, *Opn1.EGFP rho+/+ mice*) quantification provided as reference. Error bars represent +/- standard error of the mean, ** $p<0.01$; *** $p<0.001$, paired t-test.

6.5 Discussion

Mutations in the rhodopsin gene represent the most common cause of autosomal dominant RP, however, due to the dominant character of the mutation, the development of an effective treatment remains elusive. Although the primary defect in rhodopsin-linked RP is in rod photoreceptors, loss of vision and blindness result not from rod loss but from secondary cone degeneration. It is, therefore, important to assess the effects of a therapy targeting rods in stabilising secondary cone loss. Given the increasing evidence that both functional copies of the rhodopsin gene are necessary for a healthy retina and the dominant negative nature of rhodopsin mutations, the current project aimed to explore the possibility of developing an AAV vector delivering wild-type rhodopsin with high level of transduction and expression. Here, in this project, we tested the hypothesis that the supplementation of the rhodopsin gene can effectively slow down the progression of rod degeneration and subsequently secondary cone degeneration.

One of the challenges of rhodopsin supplementation is the task of developing a highly efficient vector capable of recapitulating the prodigious amount of rhodopsin produced in wild-type rods on a daily basis. To enhance treatment efficiency the design of the produced AAV vector included recent advances in the field of AAV vectorology: self-complementary design, the single mutant AAV8 capsid both allowing for high transduction rates and faster onset of transduction; to facilitate further regulatory approval for clinical trials the

vector contained human gene sequences both human rhodopsin promoter and human rhodopsin gene.

The data shown in the previous chapters demonstrated the efficiency and specificity of the produced vector in transducing rod photoreceptors and bringing functional and anatomical benefit to rod photoreceptors in terms of dark-adapted ERG restoration and the ONL preservation 5 months after single subretinal application of *scAAV2/8^{Y733F}hRHOp-RHO*. The current chapter presented the data on the effects of the vector application on cone survival by assessing light-adapted ERG responses, evaluating counts of intrinsically fluorescent cones on cSLO imaging and final histology analysis.

Full field light-adapted ERG is a powerful tool to evaluate cone function in mouse models of ADRP. Although the retinas of mice are rod-predominant, isolation of light-adapted ERG responses allows assessing the therapeutic effect of gene therapy on cones. Given that full field recordings represent the summation of electric responses of the whole retina, light-adapted ERG responses reflect large-scale transduction effects (Rossmiller et al., 2012). The therapeutic effect of *scAAV2/8^{Y733F}hRHOp-RHO* was clearly demonstrated by the preservation of photopic ERG responses: at postnatal age of three months in both untreated and sham-injected eyes, b-wave amplitudes flattened out reflecting secondary cone loss characteristic for rhodopsin knockout mice, whereas treated eyes showed preserved light-adapted b-waves (**Figures 6.3; 6.4; 6.5**). This therapeutic effect was also confirmed at the next measurement, at postnatal age four months, however, light-adapted ERG responses have flattened at PM5. This loss of the effect

on light-adapted ERG corresponded with the loss of the effect on dark-adapted ERG. The combined loss of ERG responses in dark and light-adapted settings four months after injection, may reflect the fact that the rod degeneration still occurred, albeit delayed and resulted in the secondary cone degeneration.

Neuroprotective effects of ciliary neurotrophic factor (CNTF) on cone survival were assessed in the same mouse model by Lipinski and co-workers (Lipinski et al., 2015). *Opn1.EGFP Rho-/-* mice at PW4 were given an intravitreal injection of *AAV2/2-CAG-hCNTF-IRES-DsRed* and the mice were followed by cSLO for up to seven months postnatally. CNTF injection resulted in the long-term preservation of EGFP- expressing cones in a dose-dependent manner in treated eyes, with the higher dose of the vector providing higher rescue effects. However, light-adapted ERG showed significant suppression after injection of the vector in a dose-dependent manner with the higher dose of the vector leading to the more significant extinction of cone-derived ERG responses, which is explained by physiological suppression of function induced by CNTF. Although the positive functional effects of the treatment were demonstrated additionally by laser speckle imaging of the visual cortex and OMR, however, the decline of the cone-derived ERG necessitates further studies into the functionality of preserved cones before proceeding into human trials.

Taken together, the results of this work suggest that the rod treatment with *scAAV2/8^{Y733F}hRHOp-RHO* can slow down both rod and cone degeneration. The use of *Opn1.EGFP Rho-/-* mice with intrinsically fluorescent cones allowed noninvasive longitudinal assessment of cone health by cSLO autofluorescence imaging and demonstrated longer survival of cones in treated eyes compared to nontreated and sham-injected eyes (**Figures 6.8 and 6.10**). This therapeutic effect on cone survival was evident three and four months after injection, however, mirroring ERG responses, the effect was declining with time. The preservation of cones was confirmed by post-mortem histology analysis revealing higher number of EGFP-cones in treated eyes, compared to nontreated and sham-injected. Optomotor response recorded five months after injection showed higher number of head turns in treated eyes, however, it did not reach statistical significance (**Figure 6.11**). This loss of behavioural responses five months after injection can reflect the loss of cones, which can provide behavioural responses at this late stage of degeneration.

The findings of this study can be applicable to humans as secondary cone degeneration in rhodopsin knockout mice model mirrors human RP disease progression and taken together our data suggest that the vector we developed allows delaying rod and cone degeneration delivered at a late stage of the disease.

Chapter 7 General discussion

The major aim of this research project was to develop an efficient AAV vector delivering the human rhodopsin gene into rhodopsin knockout mice and assess its effects on rod and cone survival.

The main findings can be summarised in four parts:

1. The human rhodopsin promoter used in the project allows efficient and specific targeting of rod photoreceptors in rhodopsin knockout mice leading to widespread transduction of the retina.

2. The produced vector *scAAV2/8^{Y733F}hRHOp-RHO*, efficiently transduced rod photoreceptors in rhodopsin knockout mice enabling them to produce functional rod outer segments and rod-derived ERG responses.

3. The therapeutic effect of the *scAAV2/8^{Y733F}hRHOp-RHO* vector administered to *Opn1.EGFP Rho-/-* at age of three weeks resulted in rod preservation evidenced by sustained dark-adapted ERG responses three months after injection and the preservation of the ONL on post-mortem sections five months after injection compared to untreated and sham-injected eyes.

4. The rod rescue following the administration of *scAAV2/8^{Y733F}hRHOp-RHO* resulted in the delay of secondary cone degeneration in *Opn1.EGFP Rho-/-* mice confirmed by the preservation of light-adapted ERG responses up to three months after administration, a greater number of EGFP-expressing cones revealed by cSLO imaging up to three months after the

vector application and larger counts of EGFP- cones found by post-mortem histology five months postinjection.

This project validated the hypothesis that by targeting a primary genetic defect in rod photoreceptors, secondary cone loss can be delayed. To our knowledge, the only study confirming this hypothesis appeared recently, in 2015: Han and co-workers used nanoparticles to deliver genomic rhodopsin into newly born pups of a similar model of rhodopsin knockout mice (produced by Lem (Lem et al., 1999), whereas the mice used in our study were produced by Humphries (Humphries et al., 1997)) and showed sustained dark and light-adapted ERG responses up to eight months after administration. Lem's rhodopsin knockout model undergoes rod degeneration at the same speed as Humphries' rhodopsin knockout model: at the postnatal age of three months all rod photoreceptors should degenerate. Surprisingly, the figures provided in Han's publication suggest that non-injected eyes conserved the ONL layer comprising 5-6 nuclei eight months after injection, which suggests a slow rate of degeneration in the used mice. Additionally, the longer sustained results in Han's study can be explained by the early timing of gene therapy administration, which is addressed later (section 7.1.4). Nevertheless, our findings are confirmed by Han's recent study that by providing the wild-type allele of the causative gene of rod degeneration, secondary cone degeneration can be slowed down (Han et al., 2015).

The key difference is that the timing of intervention in our study was in early adult life, when the rod degeneration was already well underway. This is therefore far closer to the clinical scenario of when patients with RP would be

diagnosed and treated. The fact that cone degeneration can still be slowed, even at these later stages, is therefore highly significant in terms of potential clinical application.

7.1 Key features of the proposed gene therapy

7.1.1 Choice of AAV serotype

AAV8 was shown to be the most effective among other AAV serotypes in transducing photoreceptors in murine, canine and primate models (Allocca et al., 2007; Vandenberghe et al., 2011). Moreover, the substitution one or more of tyrosine residues to phenylalanine led to improvement in transduction due to a decrease in virus degradation (Petrs-Silva et al., 2009). These advances, in the form of the single mutant AAV8^{Y733F} serotype, were used in the design of the produced vector to achieve high transduction efficiency. The data in this research project demonstrated that the produced vectors provided panretinal transduction and achieved high efficiency in rhodopsin knockout mice (**Figure 4.2** and **4.6**).

7.1.2 Self-complementary AAV

Another technical advancement introduced into the design of the produced vector was the use of self-complementary vector. Although the packaging capacity of scAAV is diminished by half, scAAV by bypassing the double DNA conversion step were found to have far superior transduction efficiency

and faster onset of transduction confirmed in numerous studies (McCarty, 2008). An important milestone in scAAV development was achieved with a clinical trial on hemophilia B led by Nathwani, which involved a single intravenous injection of a scAAV vector encoding for the codon-optimised factor IX (*scAAV2/8-LP1-hFIXco*) and targeting liver cells (Nathwani et al., 2014). Long-term results showed a dose-dependent increase in circulating factor IX to a level of 1-6% of the normal value over a median period of 3.2 years, with the high-dose group achieving 5.1±1.7% of the Factor IX level in all six patients, resulting in a dramatic reduction (>90%) in both bleeding episodes and the use of prophylactic factor IX concentrate. This trial highlights the possibility of use of self-complementary AAV and their long-lasting beneficial effects on the health of patients, validating our use of self-complementary design of AAV. We designed our vector small enough to accommodate the human rhodopsin promoter (806 bp), rhodopsin gene (1,047 bp) and posttranscriptional element (polyadenylation site, 269 bp) to allow efficient packaging of the self-complementary genome (2,153 bp in total).

7.1.3 The human rhodopsin promoter

Initial clinical trials used robust ubiquitous promoters, such as the *CMV* and *CAG* promoters, which provided maximal expression across multiple cell types, however, the use of tissue-specific promoters allows accurate targeting of expression and thus enhances the safety of treatment. The experiments in this thesis made use of the photoreceptor-specific human rhodopsin promoter and showed that this promoter specifically targeted rod

photoreceptors with the notable absence of expression in cones in rhodopsin knockout mice (section 4.2.3). The use of the human sequence facilitates further regulatory approval for a future clinical trial and tissue specificity suggests high safety of the vector.

7.1.4 Timing of AAV administration

Given that hereditary retinal degenerations are usually caused by mutations in genes encoding proteins in photoreceptors or the RPE, it has been hypothesized that corrective gene therapy in recessive diseases would restore biochemical deficiency and delay photoreceptor loss. However, it was shown in a clinical trial on AAV delivery of *RPE65* gene, that gene therapy, despite bringing substantial visual improvement, slowed, but did not stop the progression of photoreceptor degeneration (Jacobson et al., 2015). One possible reason for this may be simply because surgery in humans is complex and needs refinement so that an adequate dose of vector is applied. It is notable that several patients in this particular trial had surgical complications such as macular hole and retinal tears, which would have reduced the amount of vector in contact with the RPE (Hauswirth et al., 2008). Moreover, observations in animal models suggested that the therapeutic effects of AAV gene therapy were dependent on the timing of intervention – the earlier the treatment is administered, the longer its benefits would last (Cideciyan et al., 2013) (**Figure 7.1**).

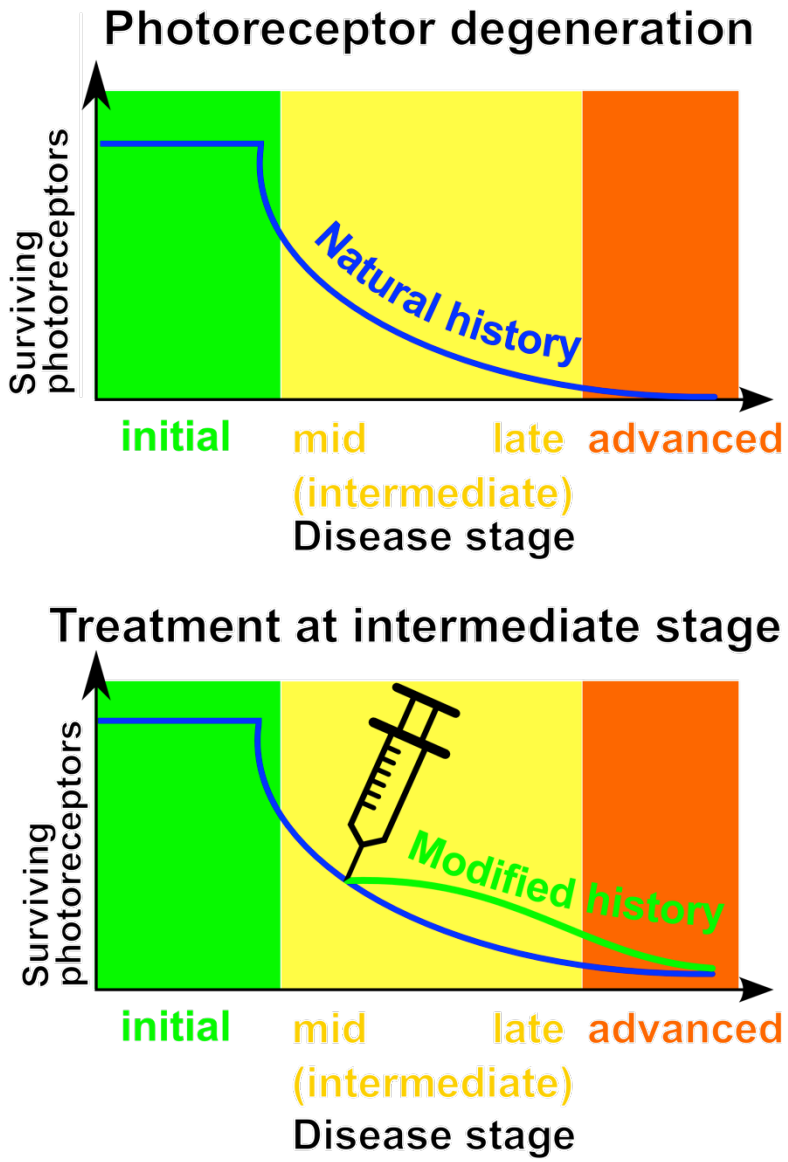


Figure 7.1 Effects of treatment on degeneration rate

Schematic of photoreceptor degeneration and temporal interaction of potential treatment, seeking to alter the natural history of RP.

A) Natural history of photoreceptor degeneration with three stages of RP: initial (where the number of photoreceptors remains the same), intermediate (where there is a progressive decline in number of photoreceptors), advanced (where the number of surviving photoreceptors is minimal).

B) Gene therapy, administered at an intermediate stage of photoreceptor degeneration, aiming at delaying the natural progression of photoreceptor loss. Note that even corrective treatment does not necessarily rescue all photoreceptors but it allows slowing down the natural rate of degeneration (Adapted from William A Beltran et al. 2015).

The pioneering clinical trials in the field of retinal hereditary degenerations involved patients with Leber's Congenital Amaurosis (LCA), which is characterised by a mutation in the gene *RPE65* encoding a protein abundantly expressed in the RPE cells and playing a role in the recycling of the chromophore 11-*cis*-retinal (Bainbridge et al., 2008; Hauswirth et al., 2008; Maguire et al., 2009). The lack of RPE65 induces apoptosis of adjoining photoreceptors. The *Rpe65* knockout mouse is a model of slow rod-cone degeneration, where residual rod function can be demonstrated up to 24 months (Caruso et al., 2010). In a study on *Rpe65 -/-* mice treated with an AAV replacement injection driven by the CMV promoter at age of 3 weeks, despite the expression of RPE65 and transient improvement of ERG b-waves, the photoreceptor degeneration and apoptotic cell death continued unabated and the rate of degeneration was the same at 12 months post-injection in treated and untreated animals (Lai et al., 2004). Similarly, in the clinical trial on RPE65 patients, in spite of remarkable initial improvements in visual function, serial measurements of the outer nuclear layer thickness 3 years after treatment showed the progression of photoreceptor loss (Cideciyan et al., 2013; Jacobson et al., 2015) These data may suggest that photoreceptors destined for degeneration may be irreversibly lost if the dose of corrective gene therapy is insufficient.

However, this could just be a dose effect of the viral vector, for instance, if only 20% of RPE cells were transduced efficiently, then one might expect the remaining 80% to continue degenerating over time. There would be an initial gain in function from the 20% now able to isomerise 11-*cis*-retinal, but the

photoreceptors overlying the remaining 80% would degenerate. Furthermore, the situation in human RPE65 is quite different to the mouse and dog models in which intervention is applied earlier, because lipid inclusion granules of retinyl esters are highly toxic to the RPE and accumulate in the absence of RPE65 over time (Maeda et al., 2008, 2009; Sparrow et al., 2000). Hence the RPE cells in the human disease are already compromised by the disease process and may be beyond the point of rescue, even with the correct dose of gene therapy.

Certainly, the timing of AAV administration appears to be of importance, as it has been shown that the recovery of retinal function does not appear life-long unless treatment was started before retinal apoptosis (Rakoczy and Narfström, 2014). Comparing age-dependent effects of *RPE65* gene for LCA delivered via AAV gene therapy in a phase 1 dose-escalation trial, Maguire et al. found the greatest improvements were noted in children, all of whom gained ambulatory vision (Maguire et al., 2009). This age-dependent effect was confirmed by another RPE65 – LCA clinical trial by Weleber *et al.* including four children and eight adults, that showed that younger patients attained better functional gains in visual acuity and kinetic visual field than older patients suggesting that treatment at an early age is more effective at slowing down photoreceptor loss (Weleber et al., 2016). However, this could simply reflect the fact that the childhood retina is thicker and may still have adherent posterior vitreous. In children, therefore, there is likely to be much less reflux of vector through the retinotomy into the vitreal cavity - a higher

therapeutic dose of AAV would reach the RPE with reduced risk of inflammation from intravitreal spread.

Currently, only a few studies have addressed the issue of gene therapy in older animals after onset of retinal degeneration. The gene replacement therapy with AAV2/2 delivering *Prph2* administered at different age to a mouse model of retinal degeneration slow (*rds*), which lacks *rds/peripherin-2* gene demonstrated that the potential for ultrastructural improvement was dependent upon the age at which animals are treated, with treatment applied at younger age giving greater initial restoration of structure (Sarra et al., 2001). In a study addressing the time-dependent rescue of cones in *Rpe65*-deficient mice showed that cone function was preserved when lentiviral *RPE65* gene transfer was applied at an early stage of the disease - postnatal day 5, whereas the same type of vector, administered at 1 month of age, failed to rescue cones: the immunofluorescence determined by PNA labelling and GNAT2, was in the same range for treated and untreated animals (Bemelmans et al., 2006). Li et al. showed that late delivery of *AAV-RPE65* vector in *rd12* mice (a naturally occurring model of RPE65-LCA) resulted in only limited cone rescue: two months after treatment cone b-wave amplitudes in the mice injected at P90 achieved only a third of the amplitudes in the mice injected at P14 and cone counts were five times lower correspondingly (Li et al., 2011), suggesting that earlier timing of injection results in better rescue effects. Koch and co-authors studied therapeutic window for *Pde6b* mouse model, which allowed restoration of the mutant gene in all diseased photoreceptors using Cre-lox system(Koch et al., 2015). By activating Pde6b

expression at the age of two, four and eight weeks, they demonstrated that greater the earlier the protein was activated the greater rescue effect was achieved with only minor rescue effect achieved in mice in which Pde6b expression was restored at eight weeks. These data confirm that earlier treatment is associated with better therapeutic effects in mice. In dogs with RPGR deficiency, however, late intervention with *AAV8.RPGR* has been shown to be effective (Bainbridge et al., 2015). The earlier failings may therefore simply reflect surgical difficulties in effectively transducing the small mouse eye or less than optimal vector preparations using older technologies. In a most recent clinical study, the improvements in visual acuity in 2 of 6 patients treated for choroideremia with AAV2 have lasted for over 4 years and in each case the visual acuity in their untreated eyes has declined significantly over this period (Edwards et al., 2016).

Given that current data suggest the existence of therapeutic window for corrective gene therapy intervention and difficulty to delay retinal degeneration at later stages of degeneration, our research project aimed to show the possibility of therapeutic effects of gene therapy at intermediate stage of degeneration. Below, we will address the timing issue in studies performed on rhodopsin knockout mice.

7.1.5 AAV rhodopsin delivery and timing of intervention

The possibility of delivery of the rhodopsin gene into rhodopsin knockout mice was first demonstrated by Palfi and coauthors, who subretinally injected newly born rhodopsin knockout mice with the AAV2/5 vector containing the

coding sequence of the human rhodopsin gene driven by the optimized murine rhodopsin promoter (Palfi et al., 2010). The functional benefit on rods was evidenced by the restoration of rod-isolated ERG responses sustained up to three months post-injection, however, the amplitudes of b-wave diminished three-fold at 12 weeks compared to 6-week measurements, suggesting ongoing rod degeneration despite the delivery of rhodopsin – the primary causative gene of rod degeneration in rhodopsin knockout mice. In contrast to the rod response, the cone ERG in injected eyes was significantly lower than in uninjected eyes suggesting potential toxic effects of the vector on cones in newly born pups. Cone function was less impaired when the vector was delivered later at P10, however, to ensure maximum rod rescue all following experiments in the study were performed on newly born pups. In a recent study appeared in 2015, the same group compared viral vectors with different capsid: AAV2/8 and AAV2/rh10 to deliver the rhodopsin gene driven by the same optimised murine rhodopsin promoter on freshly born rhodopsin knockout mice. All treated eyes showed the preservation of the outer nuclear layer and rod-derived ERG responses up to 11 months post-injection, however a two-fold decline of ERG amplitudes over nine months was observed highlighting the limitations of the gene therapy performed even at this early stage of the disease (Palfi et al., 2015). Another recent study, using compacted nanoparticles, compared the delivery of genomic (the full sequence of the rhodopsin gene including introns) and the cDNA rhodopsin sequence, both constructs driven by the mouse rhodopsin promoter in the newly born rhodopsin knockout mice (Han et al., 2015). The eyes treated with the nanoparticles containing the genomic rhodopsin showed

preservation of rod-derived ERG responses up to 8 months post-injection, furthermore, cone ERG responses were sustained as well.

In these both studies the rhodopsin gene was delivered at early age – to newborn pups at early stages of retinal degeneration, whereas in our study the gene therapy was administered at PW3. The produced therapeutic effects from the treatment applied to newly born pups can be long lasting due to larger number of surviving photoreceptors in newly born pups. In contrast, successful and long-lasting rescue of photoreceptors is difficult to achieve when applied late in the natural history of disease, with the challenge to treat ongoing rod degeneration effectively and potentially already switched-on apoptotic pathways (Beltran et al., 2015). Moreover, this rationale is difficult to replicate in clinical practice as this early administration in mice corresponds to *in utero* treatment in humans, an approach that at present seems hardly feasible. Treating at later stages of degeneration in mice is more reflective of the clinical setting where patients would present themselves at an advanced stage of disease with significant loss of rod photoreceptors and certain secondary cone loss. Thus, by proving evidence of the vector efficiency on older rhodopsin knockout mice rather than newborn pups, which have very little loss of photoreceptors, this project more accurately models the situation, when treating patients with rhodopsin-linked RP.

7.2 Variables affecting treatment efficiency

7.2.1 Vector dosing

One of the important factors affecting the outcome of AAV gene therapy is the concentration of the injected vector. Using the much weaker cell-specific human *RPE65* promoter, Bainbridge and co-workers showed dose-dependent effect on the canine model of LCA: lower doses of *AAV2-RPE65* provided limited functional rescue, whereas only higher doses corresponded to ERG responses (Bainbridge et al., 2015). In this regard, the potential way to improve transduction and therapeutic effect is the use of higher doses of AAV vector, however, this risks increasing the capsid load to the target cells and enhancing viral toxicity. Higher doses of *AAV2-CAG-hRPE65* showed cone cell loss indicating cellular toxicity of high viral vectors on canine model of LCA (Jacobson et al., 2006). Additionally, dose-dependent toxicity effect was also demonstrated on non-human primates with AAV2 and AAV8 vectors expressing GFP: at higher doses of both vectors animals showed histopathological evidence of inflammatory foci and retinal degeneration (Vandenberghe et al., 2011). This could however be caused by additional toxic effects of GFP.

7.2.2 AAV quantification

qPCR has established itself as a reliable and reproducible standard method of AAV quantification adopted worldwide and therefore was used in the experiments of this study. However, in a study on developing a common reference for AAV quantification, when a reference standard for AAV8 was sent to 16 different laboratories, the quantification by standardised assays revealed little variation within a laboratory, but substantial disparity among different laboratories, varying up to 100-fold by a standardised qPCR method amongst the 16 institutions (Ayuso et al., 2014). This amount of variability suggests a need to develop more comparable quantification methods between different laboratories, which would allow more accurate comparability between the results of different groups.

7.2.3 AAV contamination

The success of clinical trials with AAV vectors highlights the importance of thorough quality control for AAV preparations. Despite exhaustive downstream purification, final AAV preparation can contain a variety of impurities, including: empty viral capsids, subgenomic viral particles, chemicals, lipids, proteins and encapsidated procaryotic DNA sequences. The insufficient characterization of DNA contaminants was one of the six main concerns raised by the European Medicines Agency in 2012 during the marketing authorization for Glybera (*AAV2/1-CMV-LPL*^{S447X}) (Bryant et al., 2013; Lecomte et al., 2015). Furthermore, the US Food and Drug Administration recently issued a statement encouraging scientists to develop

"robust, accurate and consistent testing methodologies" to characterize AAV vectors (Gavin, 2015). The presence of prokaryotic sequences in viral preparations was addressed in this research project, finding that in the *scAAV2/8^{Y733F}hRHOp-RHO* vector preparation the fraction of particles containing the ampicillin resistance sequence from the plasmid backbone was approximately 5% which compared well to what had been published (up to 6%) (Chadeuf et al., 2005). The presence of prokaryotic sequences is potentially safe at the stage of animal studies, however, it can present problems during regulatory approval for clinical trials. More extensive methods could be required in future to fully characterise present contamination of AAV preparations, such as newly described Next-generation sequencing which can provide unprecedented resolution and exhaustiveness of DNA impurities (Lecomte et al., 2015).

7.2.4 Empty capsids

Upon AAV production a virus preparation can comprise not only functional AAV particles but inadvertent product - "empty" capsids, which lack the vector genome and therefore do not bring any therapeutic benefit (Gao et al., 2014). The amount of these defective particles in an AAV preparation is dependent on the size and sequence of the transgene cassette and AAV production and purification methods; the assessment of the clinical grade self-complementary AAV2/8 estimated that "empty" capsids exceeded "full" vector particles by 10-fold (Allay et al., 2011; Lock et al., 2010). Although the methods of quantification used in this research project assess only the number of genome copies and would not count empty capsids, however, the

presence of empty capsids can increase the total viral load and lead to greater toxicity of an AAV vector and even suppression of AAV transduction by competing with full particles for cell uptake (Gao et al., 2014). A canonical method of to assess the full to empty capsid ratio is the electron microscopy (EM) assay, a technique, which involves negative staining of viral particles and visualising them at high magnification and is highly dependent on contaminating protein and can produce spurious results (Grieger et al., 2006). Novel methods of quantifying empty capsids, such as chromatographic separation of empty and full capsids by charge, are currently being developed to address this issue (Lock et al., 2012).

7.2.5 Immunogenicity

AAV became a preferred vehicle for gene therapy due to its low immunogenicity, however, a growing body of evidence indicated that one of the major problem facing AAV gene transfer are immune responses which can hinder transgene expression and reduce therapeutic effect. (Fields et al., 2000; Mingozzi and High, 2013) The administration of AAV induces the innate and adaptive immune responses, with the innate immune system being the first line of defense to encounter pathogens. Martino and coworkers demonstrated that self-complementary AAV2 and AAV8 induced higher innate immune responses compared to single-stranded AAV2 and AAV8 in the liver gene transfer in mice at two hours after vector injection (Martino et al., 2011). It was suggested that the toll-like receptors 9 (TLR9) signaling pathway detecting viral DNA could be responsible for the enhanced release of inflammatory cytokines. TLR9 signalling recruits *MyD88* (myeloid

differentiation primary response gene 88) which in turn activates the classic NF-κB (nuclear factor kappa-light-chain-enhancer of activated B cells) pathway resulting in an increased production of pro-inflammatory cytokines such as TNF-α, monocyte chemotactic protein-1, IFN-ϒ inducible protein-10, IFN-α/β and circulating IL-6. Furthermore, the number of neutrophil, macrophage and natural killer cell liver infiltrates were substantially higher upon the injection of scAAV. To confirm the role of the TLR9 signaling pathway sensing viral DNA, scAAV was administered to TLR9 -/- mice or the TLR9 inhibitory oligodeoxynucleotide (ODN) 2088 (TLR-9i) was used; in both groups the innate immune responses were blunted compared to wild-type mice, suggesting that previous immune responses were mediated by TLR9.

Another study, led by Wu and coworkers showed that after administering AAV vectors, expressing a highly immunogenic viral transgene gag of HIV-1, peak CD8+ T and B cell responses against the transgene on a mouse model were earlier in time and markedly enhanced in scAAV7 and scAAV8 compared to the corresponding ssAAV even at late time points (Wu et al., 2012). As a potential explanation of enhanced immune responses to scAAV, Wu suggested that dsDNA genome of scAAV could be recognized by an innate sensor of viral intracellular dsDNA - DAI (DNA-dependent activator of IFN- regulatory factors), though the mechanism was not addressed in the study.

Confirming the similar trend, Rogers and colleagues (Rogers et al., 2014), showed that the injection of scAAV1 encoding for Factor IX in the mice with a null mutation of the *Factor IX* gene and consequently lacking the tolerance to

Factor IX antigen, produced more robust and destructive CD8+ T cell response compared to ssAAV1, with the titers of anti-Factor IX antibodies being nearly identical for both vector types. The authors concluded that the underlying mutation is an important determinant of the B and T cell responses, and on the null mutation background scAAV are more prone to cause potent cellular immune responses, while the mutations preserving some level of endogenous though non-functional expression reduce the risk of CD8+ T cell responses, indicating potential tolerance towards gene transfer.

Taken together, the findings of these studies suggest that in contrast to ssAAV, scAAV can induce heightened immune responses, and the immune responses are enhanced when AAV gene therapy is delivered on a null background, at least, in mice. With regard to our project, the application of scAAV to more mature rhodopsin knockout mice rather than to newly born pups as in other studies could have induced more pronounced immune responses and led to extinction of therapeutic effect. In the clinical trial using scAAV8 to deliver factor IX in haemophilia B led by Nathwani (2014) a transient mild elevation of transaminase levels associated with the drop of factor IX levels was observed between week 7 and week 10 in 4 of 6 patients in the high-dose group, which resolved after a short course of prednisolone (Nathwani et al., 2014). This transaminitis can suggest potential immune reactions against AAV8 capsid in the gene therapy delivered intravenously in humans. In contrast, clinical trials involving AAV gene therapy in retinal degenerations predominantly use subretinal approach. The subretinal

compartment is an immune-privileged and enclosed space protected by the selective blood-retinal barrier which limits classical antigen presentation and immune response; and thus AAV gene therapy for retinal degeneration delivered subretinally is considered more safe (MacLaren, 2016). In three seminal clinical trials on LCA and choroideremia, no major adverse events have been reported (Bainbridge et al., 2008; Hauswirth et al., 2008; MacLaren et al., 2014; Maguire et al., 2009). Biodistribution studies using polymerase chain reaction of AAV sequences in tears, serum, saliva, and semen have been generally negative. Adaptive humoral responses to the AAV2 capsid measured with functional neutralising antibodies (NAb) assays were generally negative, except one patient in the study by Maguire who had an increase in Nab titer, which returned to a level slightly above baseline. Adaptive cellular immunity to the AAV2 capsid was measured by ELISPOT and was negative in all studies. This benign nature of immune responses to ssAAV delivered subretinally in clinical trials suggest that the subretinal space provides certain immune protection, however further studies are needed to establish the safety and immunogenicity of subretinal delivery of scAAV assessing whether higher transduction efficiency of scAAV is matched with heightened immune responses.

7.3 Future work

7.3.1 Challenges for clinical trials on rhodopsin-linked RP

Rhodopsin-linked RP is an attractive choice for AAV gene therapy as rhodopsin mutations are most common in autosomal dominant RP (representing 15% of all ADRP). Another positive feature is the small size of the coding sequence of the rhodopsin gene (1,047 bp), which fits easily not only into a conventional AAV, but even into a smaller-sized scAAV vector. Clinical course of rhodopsin-linked RP is dependent on many factors, including biochemical properties of mutant protein; in many cases rhodopsin-linked RP represents a moderate course of disease with a potential therapeutic window for intervention. Moreover, numerous studies revealed dominant-negative nature of rhodopsin mutations, which suggests that by increasing the ratio of wild-type to mutant protein rod degeneration could be slowed down. Given that patients affected with rhodopsin-linked RP lose their vision not due to rod loss, but to secondary cone degeneration and that this research project provided evidence that the supplementation of a defective rod gene at later stages of rod degeneration can slow down secondary cone degeneration, the data of this project provide the basis for future clinical trial on rhodopsin-linked RP patients. Future work in our lab (which already started in our lab by a new DPhil student funded by an MRC grant) will concentrate on evaluating the therapeutic effects of the produced scAAV vector on dominant mice models of rhodopsin-linked RP with a robust

potential of translating the project into a clinical trial and can result in a paradigm shift towards gene therapy in dominant mutations.

7.3.2 CRISPR-Cas9 approach

With all impressive successes of AAV-based gene therapy, demonstrated in a prodigious number of clinical trials around the world, one should remember, however, the limitations of current corrective AAV gene therapy. The principle of current AAV-mediated gene transfer does not allow the full correction of the genetic defect, as the delivered viral DNA is preserved episomally in the nucleus and is not integrated into the genome. Thus the expression of a delivered gene is regulated not by intrinsic mechanisms having complex positive and negative feedback loops, but by the extrinsically delivered regulating sequences (such as the promoter and expression enhancing sequences) delivered on the same AAV vector. As the AAV vector size is constrained to 4.4 kb in conventional AAV, and 2.4 kb in scAAV, this limits the size of regulating sequences that could be delivered into cells. These hurdles can be potentially overcome by a novel revolutionary approach of genome editing called CRISPR-Cas9 (which was discovered when this research project just started), based on the endonuclease protein - Cas9 and a short guiding RNA – CRISPR (clustered regularly interspaced short palindromic repeats), which allows editing genes directly on the chromosomes (Cong et al., 2013; Jinek et al., 2012; Mali et al., 2013). The further exciting advancement in the field was the use of a shorter version of Cas9 (from Staphylococcus aureus), which allows packaging CRISPR-Cas9 into an AAV vector (Ran et al., 2015). Potential treatment for rhodopsin-

linked RP could involve direct editing of the mutation in the human genome by CRISPR-Cas9 excision and providing a DNA template for correction of the gene, however the use of CRISPR-Cas9 for future clinical trials is currently limited by off-target effects of CRISPR and still unpredictable mutation repairing mechanism (Tu et al., 2015).

Taken together, this research project resulted in the production of highly efficient AAV vector delivering the rhodopsin gene and provided evidence that AAV-mediated gene therapy targeting rods in rod degeneration can delay secondary cone degeneration at later stages in the disease. It thus builds a base for the use of the produced vector for further work towards a clinical trial in patients with rhodopsin-linked RP.

Appendix

The full sequence of the transgene cassette
ITR.hRHOp-RHO.bGHpolyA.mutantITR.

GGCCACTCCCTCTCTGCGCGCTCGCTCGCTCACTGAGGCCGGGCGACCAAAGGTCGCCCGACGCCCGG
GCTTTGCCCGGGCGGCCTCAGTGAGCGAGCGAGCGCGCAGAGAGGGAGTGGCCAACTCCATCACTAGG
GGTTCCTGGAGGGGTGGAGTCGTGACCTAGGTACCCAGATCTTCCCCACCTAGCCACCTGGCAAACTG
CTCCTTCTCTCAAAGGCCCAAACATGGCCTCCCAGACTGCAACCCCCAGGCAGTCAGGCCCTGTCTCC
ACAACCTCACAGCCACCCTGGACGGAATCTGCTTCTTCCCACATTTGAGTCCTCCTCAGCCCCTGAGC
TCCTCTGGGCAGGGCTGTTTCTTTCCATCTTTGTATTCCCAGGGGCCTGCAAATAAATGTTTAATGAA
CGAACAAGAGAGTGAATTCCAATTCCATGCAACAAGGATTGGGCTCCTGGGCCCTAGGCTATGTGTCT
GGCACCAGAAACGGAAGCTGCAGGTTGCAGCCCCTGCCCTCATGGAGCTCCTCCTGTCAGAGGAGTGT
GGGGACTGGATGACTCCAGAGGTAACTTGTGGGGGAACGAACAGGTAAGGGGCTGTGTGACGAGATGA
GAGACTGGGAGAATAAACCAGAAAGTCTCTAGCTGTCCAGAGGACATAGCACAGAGGCCCATGGTCCC
TATTTCAAACCCAGGCCACCAGACTGAGCTGGGACCTTGGGACAGACAAGTCATGCAGAAGTTAGGGG
ACCTTCTCCTCCCTTTTCCTGGATCCTGAGTACCTCTCCTCCCTGACCTCAGGCTTCCTCCTAGTGTC
ACCTTGGCCCCTCTTAGAAGCCAATTAGGCCCTCAGTTTCTGCAGCGGGGATTAATATGATTATGAAC
ACCCCCAATCTCCCAGATGCTGATTCAGCCAGGAGCTTAGGAGGGGGAGGTCACTTTATAAGGGTCTG
GGGGGGTCAGAACCCAGAGTCATCCGCCACCATGAATGGCACAGAAGGCCCTAACTTCTACGTGCCCT
TCTCCAATGCGACGGGTGTGGTACGCAGCCCCTTCGAGTACCCACAGTACTACCTGGCTGAGCCATGG
CAGTTCTCCATGCTGGCCGCCTACATGTTTCTGCTGATCGTGCTGGGCTTCCCCATCAACTTCCTCAC
GCTCTACGTCACCGTCCAGCACAAGAAGCTGCGCACGCCTCTCAACTACATCCTGCTCAACCTAGCCG
TGGCTGACCTCTTCATGGTCCTAGGTGGCTTCACCAGCACCCTCTACACCTCTCTGCATGGATACTTC
GTCTTCGGGCCCACAGGATGCAATTTGGAGGGCTTCTTTGCCACCCTGGGCGGTGAAATTGCCCTGTG
GTCCTTGGTGGTCCTGGCCATCGAGCGGTACGTGGTGGTGTGTAAGCCCATGAGCAACTTCCGCTTCG
GGGAGAACCATGCCATCATGGGCGTTGCCTTCACCTGGGTCATGGCGCTGGCCTGCGCCGCACCCCCA
CTCGCCGGCTGGTCCAGGTACATCCCCGAGGGCCTGCAGTGCTCGTGTGGAATCGACTACTACACGCT
CAAGCCGGAGGTCAACAACGAGTCTTTTGTCATCTACATGTTCGTGGTCCACTTCACCATCCCCATGA
TTATCATCTTTTTCTGCTATGGGCAGCTCGTCTTCACCGTCAAGGAGGCCGCTGCCCAGCAGCAGGAG
TCAGCCACCACACAGAAGGCAGAGAAGGAGGTCACCCGCATGGTCATCATCATGGTCATCGCTTTCCT
GATCTGCTGGGTGCCCTACGCCAGCGTGGCATTCTACATCTTCACCCACCAGGGCTCCAACTTCGGTC
CCATCTTCATGACCATCCCAGCGTTCTTTGCCAAGAGCGCCGCCATCTACAACCCTGTCATCTATATC
ATGATGAACAAGCAGTTCCGGAACTGCATGCTCACCACCATCTGCTGCGGCAAGAACCCACTGGGTGA
CGATGAGGCCTCTGCTACCGTGTCCAAGACGGAGACGAGCCAGGTGGCCCCGGCCTAAGGACTCCGCT
GATCAGCCTCGACTGTGCCTTCTAGTTGCCAGCCATCTGTTGTTTGCCCCTCCCCCGTGCCTTCCTTG
ACCCTGGAAGGTGCCACTCCCACTGTCCTTTCCTAATAAAATGAGGAAATTGCATCGCATTGTCTGAG
TAGGTGTCATTCTATTCTGGGGGGTGGGGTGGGGCAGGACAGCAAGGGGGAGGATTGGGAAGACAATA
GCAGGCATGCTGGGGATGCGGTGGGCTCTATGGCTTCTGAGGCGGAAAGAACCAGCTGGGGACTAGTC
CACTCCCTCTCTGCGCGCTCGCTCGCTCACTGAGGCCGGGCGACCAAAGGTCGCCCGACGCCCGGGCT
TTGCCCGGGCGGCCTCAGTGAGCGAGCGAGCGCGCAGAGAGGGA

The individual components of the transgene cassette (shown separately)

The normal ITR

GGCCACTCCCTCTCTGCGCGCTCGCTCGCTCACTGAGGCCGGGCGACCAAAGGTCGCCCGACGCCCGG
GCTTTGCCCGGGCGGCCTCAGTGAGCGAGCGAGCGCGCAGAGAGGGAGTGGCCAACTCCATCACTAGG
GGTTCCTGGAGGGGTGGAGTCGTGA

The *Kpn1* restriction site GGTACC

The human rhodopsin promoter

CAGATCTTCCCCACCTAGCCACCTGGCAAACTGCTCCTTCTCTCAAAGGCCCAAACATGGCCTCCCAG
ACTGCAACCCCCAGGCAGTCAGGCCCTGTCTCCACAACCTCACAGCCACCCTGGACGGAATCTGCTTC
TTCCCACATTTGAGTCCTCCTCAGCCCCTGAGCTCCTCTGGGCAGGGCTGTTTCTTTCCATCTTTGTA
TTCCCAGGGGCCTGCAAATAAATGTTTAATGAACGAACAAGAGAGTGAATTCCAATTCCATGCAACAA
GGATTGGGCTCCTGGGCCCTAGGCTATGTGTCTGGCACCAGAAACGGAAGCTGCAGGTTGCAGCCCCT
GCCCTCATGGAGCTCCTCCTGTCAGAGGAGTGTGGGGACTGGATGACTCCAGAGGTAACTTGTGGGGG
AACGAACAGGTAAGGGGCTGTGTGACGAGATGAGAGACTGGGAGAATAAACCAGAAAGTCTCTAGCTG
TCCAGAGGACATAGCACAGAGGCCCATGGTCCCTATTTCAAACCCAGGCCACCAGACTGAGCTGGGAC
CTTGGGACAGACAAGTCATGCAGAAGTTAGGGGACCTTCTCCTCCCTTTTCCTGGATCCTGAGTACCT
CTCCTCCCTGACCTCAGGCTTCCTCCTAGTGTCACCTTGGCCCCTCTTAGAAGCCAATTAGGCCCTCA
GTTTCTGCAGCGGGGATTAATATGATTATGAACACCCCCAATCTCCCAGATGCTGATTCAGCCAGGAG
CTTAGGAGGGGGAGGTCACTTTATAAGGGTCTGGGGGGGTCAGAACCCAGAGTCATCC

The Kozak sequence GCCACC

The human Rhodopsin gene (cDNA)

ATGAATGGCACAGAAGGCCCTAACTTCTACGTGCCCTTCTCCAATGCGACGGGTGTGGTACGCAGCCC
CTTCGAGTACCCACAGTACTACCTGGCTGAGCCATGGCAGTTCTCCATGCTGGCCGCCTACATGTTTC
TGCTGATCGTGCTGGGCTTCCCCATCAACTTCCTCACGCTCTACGTCACCGTCCAGCACAAGAAGCTG
CGCACGCCTCTCAACTACATCCTGCTCAACCTAGCCGTGGCTGACCTCTTCATGGTCCTAGGTGGCTT
CACCAGCACCCTCTACACCTCTCTGCATGGATACTTCGTCTTCGGGCCCACAGGATGCAATTTGGAGG
GCTTCTTTGCCACCCTGGGCGGTGAAATTGCCCTGTGGTCCTTGGTGGTCCTGGCCATCGAGCGGTAC
GTGGTGGTGTGTAAGCCCATGAGCAACTTCCGCTTCGGGGAGAACCATGCCATCATGGGCGTTGCCTT
CACCTGGGTCATGGCGCTGGCCTGCGCCGCACCCCCACTCGCCGGCTGGTCCAGGTACATCCCCGAGG
GCCTGCAGTGCTCGTGTGGAATCGACTACTACACGCTCAAGCCGGAGGTCAACAACGAGTCTTTTGTC
ATCTACATGTTCGTGGTCCACTTCACCATCCCCATGATTATCATCTTTTTCTGCTATGGGCAGCTCGT
CTTCACCGTCAAGGAGGCCGCTGCCCAGCAGCAGGAGTCAGCCACCACACAGAAGGCAGAGAAGGAGG
TCACCCGCATGGTCATCATCATGGTCATCGCTTTCCTGATCTGCTGGGTGCCCTACGCCAGCGTGGCA
TTCTACATCTTCACCCACCAGGGCTCCAACTTCGGTCCCATCTTCATGACCATCCCAGCGTTCTTTGC
CAAGAGCGCCGCCATCTACAACCCTGTCATCTATATCATGATGAACAAGCAGTTCCGGAACTGCATGC
TCACCACCATCTGCTGCGGCAAGAACCCACTGGGTGACGATGAGGCCTCTGCTACCGTGTCCAAGACG
GAGACGAGCCAGGTGGCCCCGGCCTAA

The bovine growth hormone poly A

CGCTGATCAGCCTCGACTGTGCCTTCTAGTTGCCAGCCATCTGTTGTTTGCCCCTCCCCCGTGCCTTC
CTTGACCCTGGAAGGTGCCACTCCCACTGTCCTTTCCTAATAAAATGAGGAAATTGCATCGCATTGTC
TGAGTAGGTGTCATTCTATTCTGGGGGGTGGGGTGGGGCAGGACAGCAAGGGGGAGGATTGGGAAGAC
AATAGCAGGCATGCTGGGGATGCGGTGGGCTCTATGGCTTCTGAGGCGGAAAGAACCAGCTGGGG

The *SpeI* restriction site ACTAGT

The mutant ITR

CCACTCCCTCTCTGCGCGCTCGCTCGCTCACTGAGGCCGGGCGACCAAAGGTCGCCCGACGCCCGGGC
TTTGCCCGGGCGGCCTCAGTGAGCGAGCGAGCGCGCAGAGAGGGA

Acknowledgements

First and foremost, I would like to express my deepest gratitude to my supervisor, Professor Robert Maclaren for showing me trust and getting me aboard to the exciting journey of intellectual betterment, for his insightful guidance and support throughout all these years at the Nuffield Laboratory of Ophthalmology.

I would like to thank as well the post-docs of the lab for their wise advice, immense help and time generously spent on me: Alun Barnard, Michelle McClements.

I'm also thankful to all team members who accompanied me closely and helped me through this long journey: Dominik Fischer, Doron Hickey, Alona Cramer, Maria Patricio.

My thanks go as well to Mandeep Singh, Sher Aslam, Haidong Shan, Samantha de Silva, Jasmin Balmer, Shaun Wood, Mark Hassall, Harry Orlans, Jasleen Jolly.

I would like to thank Marco Bellini for his administrative and human support.

I'm deeply grateful to my funding bodies: the Islamic Development Bank and the Centre for International Programs of the Ministry of Education of Kazakhstan - without their financial support this work would not have been possible.

I'm also thankful to my family, my wife Gulzhan, my daughters: Zhaniya and Aya.

Bibliography

Abdeljalil, J., Hamid, M., Abdel-mouttalib, O., Stéphane, R., Raymond, R., Johan, A., José, S., Pierre, C., and Serge, P. (2005). The optomotor response: A robust first-line visual screening method for mice. Vision Res. *45*, 1439–1446.

Acharya, S., and Karnik, S.S. (1996). Modulation of GDP release from transducin by the conserved Glu134-Arg135 sequence in rhodopsin. J. Biol. Chem. *271*, 25406–25411.

Aït-Ali, N., Fridlich, R., Millet-Puel, G., Clérin, E., Delalande, F., Jaillard, C., Blond, F., Perrocheau, L., Reichman, S., Byrne, L.C., Olivier-Bandini, A., Bellalou, J., Moyse, E., Bouillaud, F., Nicol, X., Dalkara, D., van Dorsselaer, A., Sahel, J.-A., and Léveillard, T. (2015). Rod-derived cone viability factor promotes cone survival by stimulating aerobic glycolysis. Cell *161*, 817–832.

al-Jandal, N., Farrar, G.J., Kiang, A.S., Humphries, M.M., Bannon, N., Findlay, J.B., Humphries, P., and Kenna, P.F. (1999). A novel mutation within the rhodopsin gene (Thr-94-Ile) causing autosomal dominant congenital stationary night blindness. Hum. Mutat. *13*, 75–81.

Allay, J.A., Sleep, S., Long, S., Tillman, D.M., Clark, R., Carney, G., Fagone, P., McIntosh, J.H., Nienhuis, A.W., Davidoff, A.M., Nathwani, A.C., and Gray, J.T. (2011). Good manufacturing practice production of self-complementary serotype 8 adeno-associated viral vector for a hemophilia B clinical trial. Hum. Gene Ther. *22*, 595–604.

Allocca, M., Mussolino, C., Garcia-Hoyos, M., Sanges, D., Iodice, C., Petrillo, M., Vandenberghe, L.H., Wilson, J.M., Marigo, V., Surace, E.M., and Auricchio, A. (2007). Novel adeno-associated virus serotypes efficiently transduce murine photoreceptors. J. Virol. *81*, 11372–11380.

Atchinson, R.W., Casto, B.C., and Hammon, W.M. (1965). Adenovirus-

associated defective virus particles. Science *149*, 754–756.

Auricchio, A., Hildinger, M., O'Connor, E., Gao, G.P., and Wilson, J.M. (2001). Isolation of highly infectious and pure adeno-associated virus type 2 vectors with a single-step gravity-flow column. Hum. Gene Ther. *12*, 71–76.

Ayuso, E., Blouin, V., Lock, M., McGorray, S., Leon, X., Alvira, M.R., Auricchio, A., Bucher, S., Chtarto, A., Clark, K.R., Darmon, C., Doria, M., Fountain, W., Gao, G., Gao, K., Giacca, M., Kleinschmidt, J., Leuchs, B., Melas, C., et al. (2014). Manufacturing and Characterization of a Recombinant Adeno-Associated Virus Type 8 Reference Standard Material. Hum. Gene Ther. *25*, 977–987.

Bainbridge, J.W.B., Smith, A.J., Barker, S.S., Robbie, S., Henderson, R., Balaggan, K., Viswanathan, A., Holder, G.E., Stockman, A., Tyler, N., Petersen-Jones, S., Bhattacharya, S.S., Thrasher, A.J., Fitzke, F.W., Carter, B.J., Rubin, G.S., Moore, A.T., and Ali, R.R. (2008). Effect of gene therapy on visual function in Leber's congenital amaurosis. N. Engl. J. Med. *358*, 2231–2239.

Bainbridge, J.W.B., Mehat, M.S., Sundaram, V., Robbie, S.J., Barker, S.E., Ripamonti, C., Georgiadis, A., Mowat, F.M., Beattie, S.G., Gardner, P.J., Feathers, K.L., Luong, V. a., Yzer, S., Balaggan, K., Viswanathan, A., de Ravel, T.J.L., Casteels, I., Holder, G.E., Tyler, N., et al. (2015). Long-Term Effect of Gene Therapy on Leber's Congenital Amaurosis. N. Engl. J. Med. *372*, 1887–1897.

Beer, S., Bellovin, D.I., Lee, J.S., Komatsubara, K., Wang, L.S., Koh, H., Börner, K., Storm, T.A., Davis, C.R., Kay, M.A., Felsher, D.W., and Grimm, D. (2010). Low-level shRNA cytotoxicity can contribute to MYC-induced hepatocellular carcinoma in adult mice. Mol. Ther. *18*, 161–170.

Beltran, W.A., Boye, S.L., Boye, S.E., Chiodo, V.A., Lewin, A.S., Hauswirth, W.W., and Aguirre, G.D. (2010). rAAV2/5 gene-targeting to rods:dose-dependent efficiency and complications associated with different promoters.

Gene Ther. *17*, 1162–1174.

Beltran, W.A., Cideciyan, A. V, Iwabe, S., Swider, M., Kosyk, M.S., McDaid, K., Martynyuk, I., Ying, G.-S., Shaffer, J., Deng, W.-T., Boye, S.L., Lewin, A.S., Hauswirth, W.W., Jacobson, S.G., and Aguirre, G.D. (2015). Successful arrest of photoreceptor and vision loss expands the therapeutic window of retinal gene therapy to later stages of disease. Proc Natl Acad Sci USA *112*, E5844–E5853.

Bemelmans, A.-P., Kostic, C., Crippa, S. V, Hauswirth, W.W., Lem, J., Munier, F.L., Seeliger, M.W., Wenzel, A., and Arsenijevic, Y. (2006). Lentiviral gene transfer of RPE65 rescues survival and function of cones in a mouse model of Leber congenital amaurosis. PLoS Med. *3*, e347.

Bennett, J., Ashtari, M., Wellman, J., Marshall, K. a., Cyckowski, L.L., Chung, D.C., McCague, S., Pierce, E. a., Chen, Y., Bennicelli, J.L., Zhu, X., Ying, G. -s., Sun, J., Wright, J.F., Auricchio, a., Simonelli, F., Shindler, K.S., Mingozzi, F., High, K. a., et al. (2012). AAV2 Gene Therapy Readministration in Three Adults with Congenital Blindness. Sci. Transl. Med. *4*, 120ra15-120ra15.

Bernales, S., Papa, F.R., and Walter, P. (2006). Intracellular signaling by the unfolded protein response. Annu. Rev. Cell Dev. Biol. *22*, 487–508.

Berns, K.I., and Adler, S. (1972). Separation of two types of adeno-associated virus particles containing complementary polynucleotide chains. J. Virol. *9*, 394–396.

Bhootada, Y., Choudhury, S., Gully, C., and Gorbatyuk, M. (2015). Targeting Caspase-12 to Preserve Vision in Mice With Inherited Retinal Degeneration. Invest. Ophthalmol. Vis. Sci. *56*, 4725–4733.

Boudreau, R.L., Monteys, A.M., and Davidson, B.L. (2008). Minimizing variables among hairpin-based RNAi vectors reveals the potency of shRNAs. RNA *14*, 1834–1844.

Boye, S.E., Alexander, J.J., Boye, S.L., Witherspoon, C.D., Sandefer, K.J.,

Conlon, T.J., Erger, K., Sun, J., Ryals, R., Chiodo, V.A., Clark, M.E., Girkin, C.A., Hauswirth, W.W., and Gamlin, P.D. (2012). The human rhodopsin kinase promoter in an AAV5 vector confers rod- and cone-specific expression in the primate retina. Hum. Gene Ther. *23*, 1101–1115.

Brill, E., Malanson, K.M., Radu, R.A., Boukharov, N. V, Wang, Z., Chung, H.-Y., Lloyd, M.B., Bok, D., Travis, G.H., Obin, M., and Lem, J. (2007). A novel form of transducin-dependent retinal degeneration: accelerated retinal degeneration in the absence of rod transducin. Invest. Ophthalmol. Vis. Sci. *48*, 5445–5453.

Brown, T. (2001). Dot and slot blotting of DNA. Curr. Protoc. Mol. Biol. *Chapter 2*, Unit2.9B.

Bryant, L.M., Christopher, D.M., Giles, A.R., Hinderer, C., Rodriguez, J.L., Smith, J.B., Traxler, E.A., Tycko, J., Wojno, A.P., and Wilson, J.M. (2013). Lessons learned from the clinical development and market authorization of Glybera. Hum. Gene Ther. Clin. Dev. *24*, 55–64.

Buie, L.K., Rasmussen, C.A., Porterfield, E.C., Ramgolam, V.S., Choi, V.W., Markovic-Plese, S., Samulski, R.J., Kaufman, P.L., and Borrás, T. (2010). Self-complementary AAV virus (scAAV) safe and long-term gene transfer in the trabecular meshwork of living rats and monkeys. Invest. Ophthalmol. Vis. Sci. *51*, 236–248.

Bush, R.A., Hawks, K.W., and Sieving, P.A. (1995). Preservation of inner retinal responses in the aged Royal College of Surgeons rat. Evidence against glutamate excitotoxicity in photoreceptor degeneration. Invest. Ophthalmol. Vis. Sci. *36*, 2054–2062.

Byrne, L.C., Dalkara, D., Luna, G., Fisher, S.K., Clérin, E., Sahel, J.-A., Léveillard, T., and Flannery, J.G. (2015). Viral-mediated RdCVF and RdCVFL expression protects cone and rod photoreceptors in retinal degeneration. J. Clin. Invest. *125*, 105–116.

Carter-Dawson, L.D., LaVail, M.M., and Sidman, R.L. (1978). Differential effect of the rd mutation on rods and cones in the mouse retina. Invest. Ophthalmol. Vis. Sci. *17*, 489–498.

Caruso, R.C., Aleman, T.S., Cideciyan, A. V, Roman, A.J., Sumaroka, A., Mullins, C.L., Boye, S.L., Hauswirth, W.W., and Jacobson, S.G. (2010). Retinal disease in Rpe65-deficient mice: comparison to human leber congenital amaurosis due to RPE65 mutations. Invest. Ophthalmol. Vis. Sci. *51*, 5304–5313.

Chadeuf, G., Ciron, C., Moullier, P., and Salvetti, A. (2005). Evidence for encapsidation of prokaryotic sequences during recombinant adeno-associated virus production and their in vivo persistence after vector delivery. Mol. Ther. *12*, 744–753.

Chapman, M.S., and Rossmann, M.G. (1993). Structure, Sequence, and Function Correlations among Parvoviruses. Virology *194*, 491–508.

Charbel Issa, P., Singh, M.S., Lipinski, D.M., Chong, N. V., Delori, F.C., Barnard, A.R., and MacLaren, R.E. (2012). Optimization of In Vivo Confocal Autofluorescence Imaging of the Ocular Fundus in Mice and Its Application to Models of Human Retinal Degeneration. Investig. Opthalmology Vis. Sci. *53*, 1066.

Cheng, H., Khanna, H., Oh, E.C.T., Hicks, D., Mitton, K.P., and Swaroop, A. (2004). Photoreceptor-specific nuclear receptor NR2E3 functions as a transcriptional activator in rod photoreceptors. Hum. Mol. Genet. *13*, 1563–1575.

Chuang, J.-Z., Vega, C., Jun, W., and Sung, C.-H. (2004). Structural and functional impairment of endocytic pathways by retinitis pigmentosa mutant rhodopsin-arrestin complexes. J. Clin. Invest. *114*, 131–140.

Cideciyan, A. V, Hood, D.C., Huang, Y., Banin, E., Li, Z.Y., Stone, E.M., Milam, A.H., and Jacobson, S.G. (1998). Disease sequence from mutant

rhodopsin allele to rod and cone photoreceptor degeneration in man. Proc. Natl. Acad. Sci. U. S. A. *95*, 7103–7108.

Cideciyan, A. V, Jacobson, S.G., Aleman, T.S., Gu, D., Pearce-Kelling, S.E., Sumaroka, A., Acland, G.M., and Aguirre, G.D. (2005). In vivo dynamics of retinal injury and repair in the rhodopsin mutant dog model of human retinitis pigmentosa. Proc. Natl. Acad. Sci. U. S. A. *102*, 5233–5238.

Cideciyan, A. V, Jacobson, S.G., Beltran, W.A., Sumaroka, A., Swider, M., Iwabe, S., Roman, A.J., Olivares, M.B., Schwartz, S.B., Komáromy, A.M., Hauswirth, W.W., and Aguirre, G.D. (2013). Human retinal gene therapy for Leber congenital amaurosis shows advancing retinal degeneration despite enduring visual improvement. Proc. Natl. Acad. Sci. U. S. A. *110*, E517-25.

Cideciyan, A. V, Aguirre, G.K., Jacobson, S.G., Butt, O.H., Schwartz, S.B., Swider, M., Roman, A.J., Sadigh, S., and Hauswirth, W.W. (2015). Pseudo-fovea formation after gene therapy for RPE65-LCA. Invest. Ophthalmol. Vis. Sci. *56*, 526–537.

Clark, K.R., Liu, X., McGrath, J.P., and Johnson, P.R. (1999). Highly purified recombinant adeno-associated virus vectors are biologically active and free of detectable helper and wild-type viruses. Hum. Gene Ther. *10*, 1031–1039.

Clément, N., and Grieger, J.C. (2016). Manufacturing of recombinant adeno-associated viral vectors for clinical trials. Mol. Ther. Methods Clin. Dev. *3*, 16002.

Colella, P., and Auricchio, A. (2012). Gene Therapy of Inherited Retinopathies: A Long and Successful Road from Viral Vectors to Patients. Hum. Gene Ther. *23*, 796–807.

Cong, L., Ran, F.A., Cox, D., Lin, S., Barretto, R., Habib, N., Hsu, P.D., Wu, X., Jiang, W., Marraffini, L.A., and Zhang, F. (2013). Multiplex genome engineering using CRISPR/Cas systems. Science *339*, 819–823.

D'Costa, S., Blouin, V., Broucque, F., Penaud-Budloo, M., François, A.,

Perez, I.C., Le Bec, C., Moullier, P., Snyder, R.O., and Ayuso, E. (2016). Practical utilization of recombinant AAV vector reference standards: focus on vector genomes titration by free ITR qPCR. Mol. Ther. Methods Clin. Dev. *5*, 16019.

Daiger, S.P., Bowne, S.J., and Sullivan, L.S. (2007). Perspective on genes and mutations causing retinitis pigmentosa. Arch. Ophthalmol. (Chicago, Ill. 1960) *125*, 151–158.

Daiger, S.P., Bowne, S.J., and Sullivan, L.S. (2014). Genes and Mutations Causing Autosomal Dominant Retinitis Pigmentosa. Cold Spring Harb. Perspect. Med. *5*.

Dalkara, D., Byrne, L.C., Klimczak, R.R., Visel, M., Yin, L., Merigan, W.H., Flannery, J.G., and Schaffer, D. V (2013). In vivo-directed evolution of a new adeno-associated virus for therapeutic outer retinal gene delivery from the vitreous. Sci. Transl. Med. *5*, 189ra76.

Dalkara, D., Goureau, O., Marazova, K., and Sahel, J.-A. (2016). Let There Be Light: Gene and Cell Therapy for Blindness. Hum. Gene Ther. *27*, 134–147.

Dalke, C., and Graw, J. (2005). Mouse mutants as models for congenital retinal disorders. Exp. Eye Res. *81*, 503–512.

Davies, W.L., Carvalho, L.S., and Hunt, D.M. (2007). SPLICE: a technique for generating in vitro spliced coding sequences from genomic DNA. Biotechniques *43*, 785–789.

Douglas, R.M., Alam, N.M., Silver, B.D., McGill, T.J., Tschetter, W.W., and Prusky, G.T. (2005). Independent visual threshold measurements in the two eyes of freely moving rats and mice using a virtual-reality optokinetic system. Vis. Neurosci. *22*, 677–684.

Dryja, T.P., Berson, E.L., Rao, V.R., and Oprian, D.D. (1993). Heterozygous missense mutation in the rhodopsin gene as a cause of congenital stationary

night blindness. Nat. Genet. *4*, 280–283.

Dryja, T.P., Hahn, L.B., Kajiwara, K., and Berson, E.L. (1997). Dominant and digenic mutations in the peripherin/RDS and ROM1 genes in retinitis pigmentosa. Invest. Ophthalmol. Vis. Sci. *38*, 1972–1982.

Du, B., Wu, P., Boldt-Houle, D.M., and Terwilliger, E.F. (1996). Efficient transduction of human neurons with an adeno-associated virus vector. Gene Ther. *3*, 254–261.

Edwards, T.L., Jolly, J.K., Groppe, M., Barnard, A.R., Cottriall, C.L., Tolmachova, T., Black, G.C., Webster, A.R., Lotery, A.J., Holder, G.E., Xue, K., Downes, S.M., Simunovic, M.P., Seabra, M.C., and MacLaren, R.E. (2016). Visual Acuity after Retinal Gene Therapy for Choroideremia. N. Engl. J. Med. *374*, 1996–1998.

Fagone, P., Wright, J.F., Nathwani, A.C., Nienhuis, A.W., Davidoff, A.M., and Gray, J.T. (2012). Systemic errors in quantitative polymerase chain reaction titration of self-complementary adeno-associated viral vectors and improved alternative methods. Hum. Gene Ther. Methods *23*, 1–7.

Ferrari, F.K., Samulski, T., Shenk, T., and Samulski, R.J. (1996). Second-strand synthesis is a rate-limiting step for efficient transduction by recombinant adeno-associated virus vectors. J. Virol. *70*, 3227–3234.

Fields, P.A., Kowalczyk, D.W., Arruda, V.R., Armstrong, E., McCleland, M.L., Hagstrom, J.N., Pasi, K.J., Ertl, H.C., Herzog, R.W., and High, K.A. (2000). Role of vector in activation of T cell subsets in immune responses against the secreted transgene product factor IX. Mol. Ther. *1*, 225–235.

Filipek, S., Stenkamp, R.E., Teller, D.C., and Palczewski, K. (2003). G protein-coupled receptor rhodopsin: a prospectus. Annu. Rev. Physiol. *65*, 851–879.

Fisher, K.J., Gao, G.P., Weitzman, M.D., DeMatteo, R., Burda, J.F., and Wilson, J.M. (1996). Transduction with recombinant adeno-associated virus

for gene therapy is limited by leading-strand synthesis. J. Virol. *70*, 520–532.

Flannery, J.G., Zolotukhin, S., Vaquero, M.I., LaVail, M.M., Muzyczka, N., and Hauswirth, W.W. (1997). Efficient photoreceptor-targeted gene expression in vivo by recombinant adeno-associated virus. Proc. Natl. Acad. Sci. U. S. A. *94*, 6916–6921.

Fotiadis, D., Liang, Y., Filipek, S., Saperstein, D.A., Engel, A., and Palczewski, K. (2003). Atomic-force microscopy: Rhodopsin dimers in native disc membranes. Nature *421*, 127–128.

Frederick, J.M., Krasnoperova, N. V, Hoffmann, K., Church-Kopish, J., Rüther, K., Howes, K., Lem, J., and Baehr, W. (2001). Mutant rhodopsin transgene expression on a null background. Invest. Ophthalmol. Vis. Sci. *42*, 826–833.

Gaj, T., Epstein, B.E., and Schaffer, D. V (2015). Genome Engineering Using Adeno-associated Virus: Basic and Clinical Research Applications. Mol. Ther. 1–7.

Gao, G.-P., Lu, Y., Sun, X., Johnston, J., Calcedo, R., Grant, R., and Wilson, J.M. (2006). High-level transgene expression in nonhuman primate liver with novel adeno-associated virus serotypes containing self-complementary genomes. J. Virol. *80*, 6192–6194.

Gao, K., Li, M., Zhong, L., Su, Q., Li, J., Li, S., He, R., Zhang, Y., Hendricks, G., Wang, J., and Gao, G. (2014). Empty Virions In AAV8 Vector Preparations Reduce Transduction Efficiency And May Cause Total Viral Particle Dose-Limiting Side-Effects. Mol. Ther. Methods Clin. Dev. *1*, 20139.

Gavin, D.K. (2015). FDA statement regarding the use of adeno-associated virus reference standard materials. Hum. Gene Ther. Methods *26*, 3.

Ghosh, F., Engelsberg, K., English, R. V, and Petters, R.M. (2007). Long-term neuroretinal full-thickness transplants in a large animal model of severe retinitis pigmentosa. Graefe's Arch. Clin. Exp. Ophthalmol. = Albr. von

Graefes Arch. Für Klin. Und Exp. Ophthalmol. *245*, 835–846.

Glushakova, L.G., Timmers, A.M., Issa, T.M., Cortez, N.G., Pang, J., Teusner, J.T., and Hauswirth, W.W. (2006). Does recombinant adeno-associated virus-vectored proximal region of mouse rhodopsin promoter support only rod-type specific expression in vivo? Mol. Vis. *12*, 298–309.

Graham, F.L., Smiley, J., Russell, W.C., and Nairn, R. (1977). Characteristics of a Human Cell Line Transformed by DNA from Human Adenovirus Type 5. J. Gen. Virol. *36*, 59–72.

Granit, R. (1933). The components of the retinal action potential in mammals and their relation to the discharge in the optic nerve. J. Physiol. *77*, 207–239.

Gray, J.T., and Zolotukhin, S. (2011). Design and construction of functional AAV vectors. Methods Mol. Biol. *807*, 25–46.

Greenwald, D.L., Cashman, S.M., and Kumar-Singh, R. (2013). Mutation-independent rescue of a novel mouse model of Retinitis Pigmentosa. Gene Ther. *20*, 425–434.

Grieger, J.C., and Samulski, R.J. (2012). Adeno-Associated Virus Vectorology, Manufacturing, and Clinical Applications (Elsevier Inc.).

Grieger, J.C., Choi, V.W., and Samulski, R.J. (2006). Production and characterization of adeno-associated viral vectors. Nat. Protoc. *1*, 1412–1428.

Grimm, D., Streetz, K.L., Jopling, C.L., Storm, T.A., Pandey, K., Davis, C.R., Marion, P., Salazar, F., and Kay, M.A. (2006). Fatality in mice due to oversaturation of cellular microRNA/short hairpin RNA pathways. Nature *441*, 537–541.

Gupta, N., Brown, K.E., and Milam, A.H. (2003). Activated microglia in human retinitis pigmentosa, late-onset retinal degeneration, and age-related macular degeneration. Exp. Eye Res. *76*, 463–471.

Haim, M. (2002). Epidemiology of retinitis pigmentosa in Denmark. Acta Ophthalmol. Scand. Suppl. 1–34.

Han, Z., Banworth, M.J., Makkia, R., Conley, S.M., Al-Ubaidi, M.R., Cooper, M.J., and Naash, M.I. (2015). Genomic DNA nanoparticles rescue rhodopsin-associated retinitis pigmentosa phenotype. FASEB J.

Harvey, R.., De'sperati, C., and Strata, P. (1997). The Early Phase of Horizontal Optokinetic Responses in the Pigmented Rat and the Effects of Lesions of the Visual Cortex. Vision Res. *37*, 1615–1625.

Hauck, S.M., Kinkl, N., Deeg, C.A., Swiatek-de Lange, M., Schöffmann, S., and Ueffing, M. (2006). GDNF family ligands trigger indirect neuroprotective signaling in retinal glial cells. Mol. Cell. Biol. *26*, 2746–2757.

Hauswirth, W.W., and Lewin, A.S. (2000). Ribozyme uses in retinal gene therapy. Prog. Retin. Eye Res. *19*, 689–710.

Hauswirth, W.W., Aleman, T.S., Kaushal, S., Cideciyan, A. V, Schwartz, S.B., Wang, L., Conlon, T.J., Boye, S.L., Flotte, T.R., Byrne, B.J., and Jacobson, S.G. (2008). Treatment of leber congenital amaurosis due to RPE65 mutations by ocular subretinal injection of adeno-associated virus gene vector: short-term results of a phase I trial. Hum. Gene Ther. *19*, 979–990.

Herskowitz, I. (1987). Functional inactivation of genes by dominant negative mutations. Nature *329*, 219–222.

Hirata, R.K., and Russell, D.W. (2000). Design and packaging of adeno-associated virus gene targeting vectors. J. Virol. *74*, 4612–4620.

Hobbelen, J.F., and Collewijn, H. (1971). Effect of cerebro-cortical and collicular ablations upon the optokinetic reactions in the rabbit. Doc. Ophthalmol. *30*, 227–236.

Hofmann, L., and Palczewski, K. (2015). The G protein-coupled receptor rhodopsin: a historical perspective. Methods Mol. Biol. *1271*, 3–18.

Hollingsworth, T.J., and Gross, A.K. (2012). Defective trafficking of rhodopsin and its role in retinal degenerations. Int. Rev. Cell Mol. Biol. *293*, 1–44.

Hou, Y., Zhang, H., Miranda, L., and Lin, S. (2010). Serious Overestimation in Quantitative PCR by Circular (Supercoiled) Plasmid Standard: Microalgal pcna as the Model Gene. PLoS One *5*, e9545.

Huang, N., Lee, I., Marcotte, E.M., and Hurles, M.E. (2010). Characterising and predicting haploinsufficiency in the human genome. PLoS Genet. *6*, e1001154.

Hubard, R., and Wald, G. (1952). Cis-trans isomers of vitamin A and retinene in the rhodopsin system. J. Gen. Physiol. *36*, 269–315.

Humphries, M.M., Rancourt, D., Farrar, G.J., Kenna, P., Hazel, M., Bush, R.A., Sieving, P.A., Sheils, D.M., McNally, N., Creighton, P., Erven, A., Boros, A., Gulya, K., Capecchi, M.R., and Humphries, P. (1997). Retinopathy induced in mice by targeted disruption of the rhodopsin gene. Nat. Genet. *15*, 216–219.

Illing, M.E., Rajan, R.S., Bence, N.F., and Kopito, R.R. (2002). A rhodopsin mutant linked to autosomal dominant retinitis pigmentosa is prone to aggregate and interacts with the ubiquitin proteasome system. J. Biol. Chem. *277*, 34150–34160.

Jacobson, S.G., Acland, G.M., Aguirre, G.D., Aleman, T.S., Schwartz, S.B., Cideciyan, A. V, Zeiss, C.J., Komaromy, A.M., Kaushal, S., Roman, A.J., Windsor, E.A.M., Sumaroka, A., Pearce-Kelling, S.E., Conlon, T.J., Chiodo, V.A., Boye, S.L., Flotte, T.R., Maguire, A.M., Bennett, J., et al. (2006). Safety of recombinant adeno-associated virus type 2-RPE65 vector delivered by ocular subretinal injection. Mol. Ther. *13*, 1074–1084.

Jacobson, S.G., Cideciyan, A. V, Roman, A.J., Sumaroka, A., Schwartz, S.B., Heon, E., and Hauswirth, W.W. (2015). Improvement and decline in vision with gene therapy in childhood blindness. N. Engl. J. Med. *372*, 1920–

1926.

Jellinger, K.A. (2006). Challenges in neuronal apoptosis. Curr. Alzheimer Res. *3*, 377–391.

Jeon, C.J., Strettoi, E., and Masland, R.H. (1998). The major cell populations of the mouse retina. J. Neurosci. *18*, 8936–8946.

Jiménez, A.J., García-Fernández, J.M., González, B., and Foster, R.G. (1996). The spatio-temporal pattern of photoreceptor degeneration in the aged rd/rd mouse retina. Cell Tissue Res. *284*, 193–202.

Jinek, M., Chylinski, K., Fonfara, I., Hauer, M., Doudna, J.A., and Charpentier, E. (2012). A programmable dual-RNA-guided DNA endonuclease in adaptive bacterial immunity. Science *337*, 816–821.

Kaur, J., Mencl, S., Sahaboglu, A., Farinelli, P., van Veen, T., Zrenner, E., Ekström, P., Paquet-Durand, F., and Arango-Gonzalez, B. (2011). Calpain and PARP activation during photoreceptor cell death in P23H and S334ter rhodopsin mutant rats. PLoS One *6*, e22181.

Kaushal, S., Ridge, K.D., and Khorana, H.G. (1994). Structure and function in rhodopsin: the role of asparagine-linked glycosylation. Proc. Natl. Acad. Sci. U. S. A. *91*, 4024–4028.

Kay, C.N., Ryals, R.C., Aslanidi, G. V, Min, S.H., Ruan, Q., Sun, J., Dyka, F.M., Kasuga, D., Ayala, A.E., Van Vliet, K., Agbandje-McKenna, M., Hauswirth, W.W., Boye, S.L., and Boye, S.E. (2013). Targeting photoreceptors via intravitreal delivery using novel, capsid-mutated AAV vectors. PLoS One *8*, e62097.

Kedzierski, W., Bok, D., and Travis, G.H. (1998). Non-cell-autonomous photoreceptor degeneration in rds mutant mice mosaic for expression of a rescue transgene. J. Neurosci. *18*, 4076–4082.

Kleinman, M.E., Kaneko, H., Cho, W.G., Dridi, S., Fowler, B.J., Blandford,

A.D., Albuquerque, R.J.C., Hirano, Y., Terasaki, H., Kondo, M., Fujita, T., Ambati, B.K., Tarallo, V., Gelfand, B.D., Bogdanovich, S., Baffi, J.Z., and Ambati, J. (2012). Short-interfering RNAs induce retinal degeneration via TLR3 and IRF3. Mol. Ther. *20*, 101–108.

Koch, S.F., Tsai, Y.-T., Duong, J.K., Wu, W.-H., Hsu, C.-W., Wu, W.-P., Bonet-Ponce, L., Lin, C.-S., and Tsang, S.H. (2015). Halting progressive neurodegeneration in advanced retinitis pigmentosa. J. Clin. Invest. *125*, 3704–3713.

Koenekoop, R.K. (2009). Why do cone photoreceptors die in rod-specific forms of retinal degenerations? Ophthalmic Genet. *30*, 152–154.

Komáromy, A.M., Acland, G.M., and Aguirre, G.D. (2008). Operating in the dark: a night-vision system for surgery in retinas susceptible to light damage. Arch. Ophthalmol. (Chicago, Ill. 1960) *126*, 714–717.

Kotterman, M.A., and Schaffer, D. V. (2014). Engineering adeno-associated viruses for clinical gene therapy. Nat. Rev. Genet. *15*, 445–451.

Kozak, M. (1999). Initiation of translation in prokaryotes and eukaryotes. Gene *234*, 187–208.

Kühne, W. (1877). Chemical processes in the retina. Vision Res. *17*, 1269–1316.

Lai, C.-M., Yu, M.J., Brankov, M., Barnett, N.L., Zhou, X., Redmond, T.M., Narfstrom, K., and Rakoczy, P.E. (2004). Recombinant adeno-associated virus type 2-mediated gene delivery into the Rpe65-/- knockout mouse eye results in limited rescue. Genet. Vaccines Ther. *2*, 3.

LaVail, M.M., Yasumura, D., Matthes, M.T., Drenser, K.A., Flannery, J.G., Lewin, A.S., and Hauswirth, W.W. (2000). Ribozyme rescue of photoreceptor cells in P23H transgenic rats: long-term survival and late-stage therapy. Proc. Natl. Acad. Sci. U. S. A. *97*, 11488–11493.

Lecomte, E., Tournaire, B., Cogné, B., Dupont, J.-B., Lindenbaum, P., Martin-Fontaine, M., Broucque, F., Robin, C., Hebben, M., Merten, O.-W., Blouin, V., François, A., Redon, R., Moullier, P., and Léger, A. (2015). Advanced Characterization of DNA Molecules in rAAV Vector Preparations by Single-stranded Virus Next-generation Sequencing. Mol. Ther. Nucleic Acids *4*, e260.

Lem, J., and Fain, G.L. (2004). Constitutive opsin signaling: night blindness or retinal degeneration? Trends Mol. Med. *10*, 150–157.

Lem, J., Krasnoperova, N. V, Calvert, P.D., Kosaras, B., Cameron, D.A., Nicolò, M., Makino, C.L., and Sidman, R.L. (1999). Morphological, physiological, and biochemical changes in rhodopsin knockout mice. Proc. Natl. Acad. Sci. U. S. A. *96*, 736–741.

Léveillard, T., Mohand-Saïd, S., Lorentz, O., Hicks, D., Fintz, A.-C., Clérin, E., Simonutti, M., Forster, V., Cavusoglu, N., Chalmel, F., Dollé, P., Poch, O., Lambrou, G., and Sahel, J.-A. (2004). Identification and characterization of rod-derived cone viability factor. Nat. Genet. *36*, 755–759.

Lewin, A.S., Rossmiller, B., and Mao, H. (2014). Gene augmentation for adRP mutations in RHO. Cold Spring Harb. Perspect. Med. *4*, a017400.

Li, J., Samulski, R.J., and Xiao, X. (1997). Role for highly regulated rep gene expression in adeno-associated virus vector production. J. Virol. *71*, 5236–5243.

Li, X., Li, W., Dai, X., Kong, F., Zheng, Q., Zhou, X., Lü, F., Chang, B., Rohrer, B., Hauswirth, W.W., Qu, J., and Pang, J. (2011). Gene therapy rescues cone structure and function in the 3-month-old rd12 mouse: a model for midcourse RPE65 leber congenital amaurosis. Invest. Ophthalmol. Vis. Sci. *52*, 7–15.

Liang, F.Q., Anand, V., Maguire, A.M., and Bennett, J. (2001). Intraocular delivery of recombinant virus. Methods Mol. Med. *47*, 125–139.

Liang, Y., Fotiadis, D., Maeda, T., Maeda, A., Modzelewska, A., Filipek, S., Saperstein, D.A., Engel, A., and Palczewski, K. (2004). Rhodopsin signaling and organization in heterozygote rhodopsin knockout mice. J. Biol. Chem. *279*, 48189–48196.

Lipinski, D.M., Barnard, A.R., Singh, M.S., Martin, C., Lee, E.J., Davies, W.I.L., and MacLaren, R.E. (2015). CNTF Gene Therapy Confers Lifelong Neuroprotection in a Mouse Model of Human Retinitis Pigmentosa. Mol. Ther. *23*, 1308–1319.

Liu, C., Li, Y., Peng, M., Laties, A.M., and Wen, R. (1999). Activation of caspase-3 in the retina of transgenic rats with the rhodopsin mutation s334ter during photoreceptor degeneration. J. Neurosci. *19*, 4778–4785.

Lock, M., McGorray, S., Auricchio, A., Ayuso, E., Beecham, E.J., Blouin-Tavel, V., Bosch, F., Bose, M., Byrne, B.J., Caton, T., Chiorini, J.A., Chtarto, A., Clark, K.R., Conlon, T., Darmon, C., Doria, M., Douar, A., Flotte, T.R., Francis, J.D., et al. (2010). Characterization of a recombinant adeno-associated virus type 2 Reference Standard Material. Hum. Gene Ther. *21*, 1273–1285.

Lock, M., Alvira, M.R., and Wilson, J.M. (2012). Analysis of particle content of recombinant adeno-associated virus serotype 8 vectors by ion-exchange chromatography. Hum. Gene Ther. Methods *23*, 56–64.

Loewen, C.J., Moritz, O.L., and Molday, R.S. (2001). Molecular characterization of peripherin-2 and rom-1 mutants responsible for digenic retinitis pigmentosa. J. Biol. Chem. *276*, 22388–22396.

Ma, S., Venkatesh, A., Langellotto, F., Le, Y.Z., Hall, M.N., Rüegg, M.A., and Punzo, C. (2015). Loss of mTOR signaling affects cone function, cone structure and expression of cone specific proteins without affecting cone survival. Exp. Eye Res. *135*, 1–13.

MacLaren, R.E. (2016). Benefits of gene therapy for both eyes. Lancet

(London, England) *388*, 635–636.

MacLaren, R.E., Groppe, M., Barnard, A.R., Cottriall, C.L., Tolmachova, T., Seymour, L., Clark, K.R., During, M.J., Cremers, F.P.M., Black, G.C.M., Lotery, A.J., Downes, S.M., Webster, A.R., and Seabra, M.C. (2014). Retinal gene therapy in patients with choroideremia: initial findings from a phase 1/2 clinical trial. Lancet *383*, 1129–1137.

Maeda, A., Maeda, T., Golczak, M., and Palczewski, K. (2008). Retinopathy in mice induced by disrupted all-trans-retinal clearance. J. Biol. Chem. *283*, 26684–26693.

Maeda, A., Maeda, T., Golczak, M., Chou, S., Desai, A., Hoppel, C.L., Matsuyama, S., and Palczewski, K. (2009). Involvement of all-trans-retinal in acute light-induced retinopathy of mice. J. Biol. Chem. *284*, 15173–15183.

Maguire, A.M., Simonelli, F., Pierce, E.A., Pugh, E.N., Mingozzi, F., Bennicelli, J., Banfi, S., Marshall, K.A., Testa, F., Surace, E.M., Rossi, S., Lyubarsky, A., Arruda, V.R., Konkle, B., Stone, E., Sun, J., Jacobs, J., Dell'Osso, L., Hertle, R., et al. (2008). Safety and efficacy of gene transfer for Leber's congenital amaurosis. N. Engl. J. Med. *358*, 2240–2248.

Maguire, A.M., High, K.A., Auricchio, A., Wright, J.F., Pierce, E.A., Testa, F., Mingozzi, F., Bennicelli, J.L., Ying, G., Rossi, S., Fulton, A., Marshall, K.A., Banfi, S., Chung, D.C., Morgan, J.I.W., Hauck, B., Zelenaia, O., Zhu, X., Raffini, L., et al. (2009). Age-dependent effects of RPE65 gene therapy for Leber's congenital amaurosis: a phase 1 dose-escalation trial. Lancet (London, England) *374*, 1597–1605.

Makino, C.L., Wen, X.-H., Michaud, N.A., Covington, H.I., DiBenedetto, E., Hamm, H.E., Lem, J., and Caruso, G. (2012). Rhodopsin expression level affects rod outer segment morphology and photoresponse kinetics. PLoS One *7*, e37832.

Malanson, K.M., and Lem, J. (2009). Rhodopsin-mediated retinitis

pigmentosa. Prog. Mol. Biol. Transl. Sci. *88*, 1–31.

Mali, P., Yang, L., Esvelt, K.M., Aach, J., Guell, M., DiCarlo, J.E., Norville, J.E., and Church, G.M. (2013). RNA-guided human genome engineering via Cas9. Science *339*, 823–826.

Mangini, N.J., Vanable, J.W., Williams, M.A., and Pinto, L.H. (1985). The optokinetic nystagmus and ocular pigmentation of hypopigmented mouse mutants. J. Comp. Neurol. *241*, 191–209.

Mansergh, F.C., Millington-Ward, S., Kennan, A., Kiang, A.S., Humphries, M., Farrar, G.J., Humphries, P., and Kenna, P.F. (1999). Retinitis pigmentosa and progressive sensorineural hearing loss caused by a C12258A mutation in the mitochondrial MTTS2 gene. Am. J. Hum. Genet. *64*, 971–985.

Mao, H., James, T., Schwein, A., Shabashvili, A.E., Hauswirth, W.W., Gorbatyuk, M.S., and Lewin, A.S. (2011). AAV delivery of wild-type rhodopsin preserves retinal function in a mouse model of autosomal dominant retinitis pigmentosa. Hum. Gene Ther. *22*, 567–575.

Mao, H., Gorbatyuk, M.S., Rossmiller, B., Hauswirth, W.W., and Lewin, A.S. (2012). Long-term rescue of retinal structure and function by rhodopsin RNA replacement with a single adeno-associated viral vector in P23H RHO transgenic mice. Hum. Gene Ther. *23*, 356–366.

Marigo, V. (2007). Programmed cell death in retinal degeneration: targeting apoptosis in photoreceptors as potential therapy for retinal degeneration. Cell Cycle *6*, 652–655.

Martin, J.N., Wolken, N., Brown, T., Dauer, W.T., Ehrlich, M.E., and Gonzalez-Alegre, P. (2011). Lethal toxicity caused by expression of shRNA in the mouse striatum: implications for therapeutic design. Gene Ther. *18*, 666–673.

Martino, A.T., Suzuki, M., Markusic, D.M., Zolotukhin, I., Ryals, R.C., Ertl, H.C.J., Muruve, D. a, Lee, B., Herzog, R.W., Dc, W., Moghimi, B., Ertl,

H.C.J., Muruve, D. a, Lee, B., and Herzog, R.W. (2011). The genome of self-complementary adeno-associated viral vectors increases Toll-like receptor 9–dependent innate immune responses in the liver. Blood *117*, 6459–6468.

Masland, R.H. (2001). The fundamental plan of the retina. Nat. Neurosci. *4*, 877–886.

Matsushita, T., Elliger, S., Elliger, C., Podsakoff, G., Villarreal, L., Kurtzman, G.J., Iwaki, Y., and Colosi, P. (1998). Adeno-associated virus vectors can be efficiently produced without helper virus. Gene Ther. *5*, 938–945.

May, L.A., Lai, C.-M., and Rakoczy, P.E. (2003). In vitro comparison studies of truncated rhodopsin promoter fragments from various species in human cell lines. Clin. Experiment. Ophthalmol. *31*, 445–450.

McAlear, S.D., Kraft, T.W., and Gross, A.K. (2010). 1 Rhodopsin Mutations in Congenital Night Blindness. In Advances in Experimental Medicine and Biology, pp. 263–272.

McBride, J.L., Boudreau, R.L., Harper, S.Q., Staber, P.D., Monteys, A.M., Martins, I., Gilmore, B.L., Burstein, H., Peluso, R.W., Polisky, B., Carter, B.J., and Davidson, B.L. (2008). Artificial miRNAs mitigate shRNA-mediated toxicity in the brain: implications for the therapeutic development of RNAi. Proc. Natl. Acad. Sci. U. S. A. *105*, 5868–5873.

McCarty, D.M. (2008). Self-complementary AAV vectors; advances and applications. Mol. Ther. *16*, 1648–1656.

McCarty, D.M., Monahan, P.E., and Samulski, R.J. (2001). Self-complementary recombinant adeno-associated virus (scAAV) vectors promote efficient transduction independently of DNA synthesis. Gene Ther. *8*, 1248–1254.

McCarty, D.M., Fu, H., Monahan, P.E., Toulson, C.E., Naik, P., and Samulski, R.J. (2003). Adeno-associated virus terminal repeat (TR) mutant generates self-complementary vectors to overcome the rate-limiting step to

transduction in vivo. Gene Ther. *10*, 2112–2118.

Mendes, H.F., van der Spuy, J., Chapple, J.P., and Cheetham, M.E. (2005). Mechanisms of cell death in rhodopsin retinitis pigmentosa: implications for therapy. Trends Mol. Med. *11*, 177–185.

Miao, C.H., Nakai, H., Thompson, A.R., Storm, T.A., Chiu, W., Snyder, R.O., and Kay, M.A. (2000). Nonrandom transduction of recombinant adeno-associated virus vectors in mouse hepatocytes in vivo: cell cycling does not influence hepatocyte transduction. J. Virol. *74*, 3793–3803.

Millington-Ward, S., Chadderton, N., O'Reilly, M., Palfi, A., Goldmann, T., Kilty, C., Humphries, M., Wolfrum, U., Bennett, J., Humphries, P., Kenna, P.F., and Farrar, G.J. (2011). Suppression and replacement gene therapy for autosomal dominant disease in a murine model of dominant retinitis pigmentosa. Mol. Ther. *19*, 642–649.

Mingozzi, F., and High, K. a. (2013). Immune responses to AAV vectors: overcoming barriers to successful gene therapy. Blood *122*, 23–36.

Mitchiner, J.C., Pinto, L.H., and Vanable, J.W. (1976). Visually evoked eye movements in the mouse (Mus musculus). Vision Res. *16*, 1169–1171.

Mohand-Said, S., Deudon-Combe, A., Hicks, D., Simonutti, M., Forster, V., Fintz, A.C., Léveillard, T., Dreyfus, H., and Sahel, J.A. (1998). Normal retina releases a diffusible factor stimulating cone survival in the retinal degeneration mouse. Proc. Natl. Acad. Sci. U. S. A. *95*, 8357–8362.

Mussolino, C., Sanges, D., Marrocco, E., Bonetti, C., Di Vicino, U., Marigo, V., Auricchio, A., Meroni, G., and Surace, E.M. (2011). Zinc-finger-based transcriptional repression of rhodopsin in a model of dominant retinitis pigmentosa. EMBO Mol. Med. *3*, 118–128.

Nakai, H., Storm, T.A., and Kay, M.A. (2000). Recruitment of single-stranded recombinant adeno-associated virus vector genomes and intermolecular recombination are responsible for stable transduction of liver in vivo. J. Virol.

74, 9451–9463.

Nakai, H., Wu, X., Fuess, S., Storm, T. a, Munroe, D., Montini, E., Burgess, S.M., Grompe, M., and Kay, M. a (2005). Large-scale molecular characterization of adeno-associated virus vector integration in mouse liver. J. Virol. *79*, 3606–3614.

Nathwani, A.C., Gray, J.T., Ng, C.Y.C., Zhou, J., Spence, Y., Waddington, S.N., Tuddenham, E.G.D., Kemball-Cook, G., McIntosh, J., Boon-Spijker, M., Mertens, K., and Davidoff, A.M. (2006). Self-complementary adeno-associated virus vectors containing a novel liver-specific human factor IX expression cassette enable highly efficient transduction of murine and nonhuman primate liver. Blood *107*, 2653–2661.

Nathwani, A.C., Tuddenham, E.G.D., Rangarajan, S., Rosales, C., McIntosh, J., Linch, D.C., Chowdary, P., Riddell, A., Pie, A.J., Harrington, C., O'Beirne, J., Smith, K., Pasi, J., Glader, B., Rustagi, P., Ng, C.Y.C., Kay, M.A., Zhou, J., Spence, Y., et al. (2011). Adenovirus-Associated Virus Vector–Mediated Gene Transfer in Hemophilia B. N. Engl. J. Med. *365*, 2255–2265.

Nathwani, A.C., Reiss, U.M., Tuddenham, E.G.D., Rosales, C., Chowdary, P., McIntosh, J., Della Peruta, M., Lheriteau, E., Patel, N., Raj, D., Riddell, A., Pie, J., Rangarajan, S., Bevan, D., Recht, M., Shen, Y.-M., Halka, K.G., Basner-Tschakarjan, E., Mingozzi, F., et al. (2014). Long-Term Safety and Efficacy of Factor IX Gene Therapy in Hemophilia B. N. Engl. J. Med. *371*, 1994–2004.

Natkunarajah, M., Trittibach, P., McIntosh, J., Duran, Y., Barker, S.E., Smith, A.J., Nathwani, A.C., and Ali, R.R. (2008). Assessment of ocular transduction using single-stranded and self-complementary recombinant adeno-associated virus serotype 2/8. Gene Ther. *15*, 463–467.

Nemet, I., Ropelewski, P., and Imanishi, Y. (2015). Rhodopsin Trafficking and Mistrafficking: Signals, Molecular Components, and Mechanisms. Prog Mol Biol Transl Sci. *132:39-71*, 39–71.

Nickell, S., Park, P.S.-H., Baumeister, W., and Palczewski, K. (2007). Three-dimensional architecture of murine rod outer segments determined by cryoelectron tomography. J. Cell Biol. *177*, 917–925.

Nonnenmacher, M., and Weber, T. (2012). Intracellular transport of recombinant adeno-associated virus vectors. Gene Ther. *19*, 649–658.

O'Reilly, M., Palfi, A., Chadderton, N., Millington-Ward, S., Ader, M., Cronin, T., Tuohy, T., Auricchio, A., Hildinger, M., Tivnan, A., McNally, N., Humphries, M.M., Kiang, A.-S., Humphries, P., Kenna, P.F., and Farrar, G.J. (2007). RNA Interference–Mediated Suppression and Replacement of Human Rhodopsin In Vivo. Am. J. Hum. Genet. *81*, 127–135.

Ogilvie, J.M., Tenkova, T., Lett, J.M., Speck, J., Landgraf, M., and Silverman, M.S. (1997). Age-related distribution of cones and ON-bipolar cells in the rd mouse retina. Curr. Eye Res. *16*, 244–251.

Palczewski K (2006). G Protein-Coupled Receptor Rhodopsin. Annu. Rev. Biochem. *75*, 743–767.

Palfi, A., Millington-Ward, S., Chadderton, N., O'Reilly, M., Goldmann, T., Humphries, M.M., Li, T., Wolfrum, U., Humphries, P., Kenna, P.F., and Farrar, G.J. (2010). Adeno-associated virus-mediated rhodopsin replacement provides therapeutic benefit in mice with a targeted disruption of the rhodopsin gene. Hum. Gene Ther. *21*, 311–323.

Palfi, A., Chadderton, N., O'Reilly, M., Nagel-Wolfrum, K., Wolfrum, U., Bennett, J., Humphries, P., Kenna, P., Millington-Ward, S., and Farrar, J. (2015). Efficient gene delivery to photoreceptors using AAV2/rh10 and rescue of the Rho–/– mouse. Mol. Ther. — Methods Clin. Dev. *2*, 15016.

Pang, J., Boye, S.L., Kumar, A., Dinculescu, A., Deng, W., Li, J., Li, Q., Rani, A., Foster, T.C., Chang, B., Hawes, N.L., Boatright, J.H., and Hauswirth, W.W. (2008). AAV-Mediated Gene Therapy for Retinal Degeneration in the rd10 Mouse Containing a Recessive PDEβ Mutation. Investig. Opthalmology

Vis. Sci. *49*, 4278.

Park, P.S.-H. (2014). Constitutively active rhodopsin and retinal disease. Adv. Pharmacol. *70*, 1–36.

Park, P.S.-H., Filipek, S., Wells, J.W., and Palczewski, K. (2004). Oligomerization of G protein-coupled receptors: past, present, and future. Biochemistry *43*, 15643–15656.

Patel, A.K., and Tikoo, S.K. (2006). 293T cells expressing simian virus 40 T antigen are semi-permissive to bovine adenovirus type 3 infection. J. Gen. Virol. *87*, 817–821.

Penn, R.D., and Hagins, W.A. (1969). Signal transmission along retinal rods and the origin of the electroretinographic a-wave. Nature *223*, 201–204.

Petrs-Silva, H., Dinculescu, A., Li, Q., Min, S.-H., Chiodo, V., Pang, J.-J., Zhong, L., Zolotukhin, S., Srivastava, A., Lewin, A.S., and Hauswirth, W.W. (2009). High-efficiency transduction of the mouse retina by tyrosine-mutant AAV serotype vectors. Mol. Ther. *17*, 463–471.

Da Pozzo, P., Cardaioli, E., Malfatti, E., Gallus, G.N., Malandrini, A., Gaudiano, C., Berti, G., Invernizzi, F., Zeviani, M., and Federico, A. (2009). A novel mutation in the mitochondrial tRNA(Pro) gene associated with late-onset ataxia, retinitis pigmentosa, deafness, leukoencephalopathy and complex I deficiency. Eur. J. Hum. Genet. *17*, 1092–1096.

Price, B.A., Sandoval, I.M., Chan, F., Nichols, R., Roman-Sanchez, R., Wensel, T.G., and Wilson, J.H. (2012). Rhodopsin Gene Expression Determines Rod Outer Segment Size and Rod Cell Resistance to a Dominant-Negative Neurodegeneration Mutant. PLoS One *7*, e49889.

Punzo, C., Kornacker, K., and Cepko, C.L. (2009). Stimulation of the insulin/mTOR pathway delays cone death in a mouse model of retinitis pigmentosa. Nat. Neurosci. *12*, 44–52.

Rajan, R.S., and Kopito, R.R. (2005). Suppression of wild-type rhodopsin maturation by mutants linked to autosomal dominant retinitis pigmentosa. J. Biol. Chem. *280*, 1284–1291.

Rakoczy, E.P., and Narfström, K. (2014). Gene therapy for eye as regenerative medicine? Lessons from RPE65 gene therapy for Leber's Congenital Amaurosis. Int. J. Biochem. Cell Biol. *56*, 153–157.

Rakshit, T., and Park, P.S.-H. (2015). Impact of Reduced Rhodopsin Expression on the Structure of Rod Outer Segment Disc Membranes. Biochemistry *54*, 2885–2894.

Ran, F.A., Cong, L., Yan, W.X., Scott, D.A., Gootenberg, J.S., Kriz, A.J., Zetsche, B., Shalem, O., Wu, X., Makarova, K.S., Koonin, E. V., Sharp, P.A., and Zhang, F. (2015). In vivo genome editing using Staphylococcus aureus Cas9. Nature *520*, 186–191.

Reiling, J.H., and Sabatini, D.M. (2006). Stress and mTORture signaling. Oncogene *25*, 6373–6383.

Ripps, H. (2002). Cell death in retinitis pigmentosa: gap junctions and the "bystander" effect. Exp. Eye Res. *74*, 327–336.

Rogers, G.L., Martino, A.T., Zolotukhin, I., Ertl, H.C.J., and Herzog, R.W. (2014). Role of the vector genome and underlying factor IX mutation in immune responses to AAV gene therapy for hemophilia B. J. Transl. Med. *12*, 25.

Rosenfeld, P.J., Cowley, G.S., McGee, T.L., Sandberg, M.A., Berson, E.L., and Dryja, T.P. (1992). A null mutation in the rhodopsin gene causes rod photoreceptor dysfunction and autosomal recessive retinitis pigmentosa. Nat. Genet. *1*, 209–213.

Rossmiller, B., Mao, H., and Lewin, A.S. (2012). Gene therapy in animal models of autosomal dominant retinitis pigmentosa. Mol. Vis. *18*, 2479–2496.

Sagdullaev, B.T., DeMarco, P.J., and McCall, M.A. (2004). Improved contact lens electrode for corneal ERG recordings in mice. Doc. Ophthalmol. *108*, 181–184.

Saliba, R.S., Munro, P.M.G., Luthert, P.J., and Cheetham, M.E. (2002). The cellular fate of mutant rhodopsin: quality control, degradation and aggresome formation. J. Cell Sci. *115*, 2907–2918.

Sampath, A.P., and Rieke, F. (2004). Selective transmission of single photon responses by saturation at the rod-to-rod bipolar synapse. Neuron *41*, 431–443.

Samulski, R.J., Chang, L.S., and Shenk, T. (1989). Helper-free stocks of recombinant adeno-associated viruses: normal integration does not require viral gene expression. J. Virol. *63*, 3822–3828.

Sarantis, M., and Attwell, D. (1990). Glutamate uptake in mammalian retinal glia is voltage- and potassium-dependent. Brain Res. *516*, 322–325.

Sarra, G.M., Stephens, C., de Alwis, M., Bainbridge, J.W., Smith, A.J., Thrasher, A.J., and Ali, R.R. (2001). Gene replacement therapy in the retinal degeneration slow (rds) mouse: the effect on retinal degeneration following partial transduction of the retina. Hum. Mol. Genet. *10*, 2353–2361.

Sawicki, J.A., Morris, R.J., Monks, B., Sakai, K., and Miyazaki, J. (1998). A composite CMV-IE enhancer/beta-actin promoter is ubiquitously expressed in mouse cutaneous epithelium. Exp. Cell Res. *244*, 367–369.

Schröder, M., and Kaufman, R.J. (2005). The mammalian unfolded protein response. Annu. Rev. Biochem. *74*, 739–789.

Shen, J., Yang, X., Dong, A., Petters, R.M., Peng, Y.-W.W., Wong, F., and Campochiaro, P. a. (2005). Oxidative damage is a potential cause of cone cell death in retinitis pigmentosa. J. Cell. Physiol. *203*, 457–464.

Sieving, P.A., Richards, J.E., Naarendorp, F., Bingham, E.L., Scott, K., and

Alpern, M. (1995). Dark-light: model for nightblindness from the human rhodopsin Gly-90-->Asp mutation. Proc. Natl. Acad. Sci. U. S. A. *92*, 880–884.

Sioud, M. (2007). RNA interference and innate immunity. Adv. Drug Deliv. Rev. *59*, 153–163.

Snyder, R., Moullier, P., Weitzman, M.D., and Linden, R.M. (2011). Adeno-Associated Virus Biology. Adeno-Associated Virus Methods Protoc. *807*, 219–237.

Sonntag, F., Schmidt, K., and Kleinschmidt, J.A. (2010). A viral assembly factor promotes AAV2 capsid formation in the nucleolus. Proc. Natl. Acad. Sci. U. S. A. *107*, 10220–10225.

Sparrow, J.R., Nakanishi, K., and Parish, C.A. (2000). The lipofuscin fluorophore A2E mediates blue light-induced damage to retinal pigmented epithelial cells. Invest. Ophthalmol. Vis. Sci. *41*, 1981–1989.

Srivastava, A., Lusby, E.W., and Berns, K.I. (1983). Nucleotide sequence and organization of the adeno-associated virus 2 genome. J. Virol. *45*, 555–564.

Stroes, E.S., Nierman, M.C., Meulenberg, J.J., Franssen, R., Twisk, J., Henny, C.P., Maas, M.M., Zwinderman, A.H., Ross, C., Aronica, E., High, K.A., Levi, M.M., Hayden, M.R., Kastelein, J.J., and Kuivenhoven, J.A. (2008). Intramuscular administration of AAV1-lipoprotein lipase S447X lowers triglycerides in lipoprotein lipase-deficient patients. Arterioscler. Thromb. Vasc. Biol. *28*, 2303–2304.

Sung, C.H., Schneider, B.G., Agarwal, N., Papermaster, D.S., and Nathans, J. (1991). Functional heterogeneity of mutant rhodopsins responsible for autosomal dominant retinitis pigmentosa. Proc. Natl. Acad. Sci. U. S. A. *88*, 8840–8844.

Szegezdi, E., Logue, S.E., Gorman, A.M., and Samali, A. (2006). Mediators

of endoplasmic reticulum stress-induced apoptosis. EMBO Rep. *7*, 880–885.

Tam, B.M., and Moritz, O.L. (2009). The role of rhodopsin glycosylation in protein folding, trafficking, and light-sensitive retinal degeneration. J. Neurosci. *29*, 15145–15154.

Thomas, C.E., Storm, T.A., Huang, Z., and Kay, M.A. (2004). Rapid uncoating of vector genomes is the key to efficient liver transduction with pseudotyped adeno-associated virus vectors. J. Virol. *78*, 3110–3122.

Toda, K., Bush, R.A., Humphries, P., and Sieving, P.A. (1999). The electroretinogram of the rhodopsin knockout mouse. Vis. Neurosci. *16*, 391–398.

Tu, Z., Yang, W., Yan, S., Guo, X., and Li, X.-J. (2015). CRISPR/Cas9: a powerful genetic engineering tool for establishing large animal models of neurodegenerative diseases. Mol. Neurodegener. *10*, 35.

Tzekov, R., Stein, L., and Kaushal, S. (2011). Protein misfolding and retinal degeneration. Cold Spring Harb. Perspect. Biol. *3*, a007492.

Ulshafer, R.J., Sherry, D.M., Dawson, R., and Wallace, D.R. (1990). Excitatory amino acid involvement in retinal degeneration. Brain Res. *531*, 350–354.

Usui, S., Komeima, K., Lee, S.Y., Jo, Y.-J., Ueno, S., Rogers, B.S., Wu, Z., Shen, J., Lu, L., Oveson, B.C., Rabinovitch, P.S., and Campochiaro, P.A. (2009). Increased expression of catalase and superoxide dismutase 2 reduces cone cell death in retinitis pigmentosa. Mol. Ther. *17*, 778–786.

Vandenberghe, L.H., Wang, L., Somanathan, S., Zhi, Y., Figueredo, J., Calcedo, R., Sanmiguel, J., Desai, R.A., Chen, C.S., Johnston, J., Grant, R.L., Gao, G., and Wilson, J.M. (2006). Heparin binding directs activation of T cells against adeno-associated virus serotype 2 capsid. Nat. Med. *12*, 967–971.

Vandenberghe, L.H., Bell, P., Maguire, A.M.A.C., Cearley, C.N., Xiao, R., Calcedo, R., Wang, L., Castle, M.J., Maguire, A.M.A.C., Grant, R., Wolfe, J.H., Wilson, J.M., and Bennett, J. (2011). Dosage thresholds for AAV2 and AAV8 photoreceptor gene therapy in monkey. Sci. Transl. Med. *3*, 88ra54.

Venkatesh, A., Ma, S., Le, Y.Z., Hall, M.N., Rüegg, M.A., and Punzo, C. (2015). Activated mTORC1 promotes long-term cone survival in retinitis pigmentosa mice. J. Clin. Invest. *125*, 1446–1458.

Van Vliet, K.M., Blouin, V., Brument, N., Agbandje-McKenna, M., and Snyder, R.O. (2008). The role of the adeno-associated virus capsid in gene transfer. Methods Mol. Biol. *437*, 51–91.

Wagner, A., Röhrs, V., Kedzierski, R., Fechner, H., and Kurreck, J. (2013). A novel method for the quantification of adeno-associated virus vectors for RNA interference applications using quantitative polymerase chain reaction and purified genomic adeno-associated virus DNA as a standard. Hum. Gene Ther. Methods *24*, 355–363.

Wald, G. (1935). CAROTENOIDS AND THE VISUAL CYCLE. J. Gen. Physiol. *19*, 351–371.

Wald, G., and Brown, P.K. (1953). The molar extinction of rhodopsin. J. Gen. Physiol. *37*, 189–200.

Wang, F., Cui, X., Wang, M., Xiao, W., and Xu, R. (2013). A reliable and feasible qPCR strategy for titrating AAV vectors. Med. Sci. Monit. Basic Res. *19*, 187–193.

Wang, J., Xie, J., Lu, H., Chen, L., Hauck, B., Samulski, R.J., and Xiao, W. (2007). Existence of transient functional double-stranded DNA intermediates during recombinant AAV transduction. Proc. Natl. Acad. Sci. U. S. A. *104*, 13104–13109.

Wang, Y., Ling, C.C., Song, L., Wang, L., Aslanidi, G. V, Tan, M., Ling, C.C., and Srivastava, A. (2012). Limitations of encapsidation of recombinant self-

complementary adeno-associated viral genomes in different serotype capsids and their quantitation. Hum. Gene Ther. Methods *23*, 225–233.

Wang, Z., Ma, H.-I., Li, J., Sun, L., Zhang, J., and Xiao, X. (2003). Rapid and highly efficient transduction by double-stranded adeno-associated virus vectors in vitro and in vivo. Gene Ther. *10*, 2105–2111.

Weleber, R.G., Pennesi, M.E., Wilson, D.J., Kaushal, S., Erker, L.R., Jensen, L., McBride, M.T., Flotte, T.R., Humphries, M., Calcedo, R., Hauswirth, W.W., Chulay, J.D., and Stout, J.T. (2016). Results at 2 Years after Gene Therapy for RPE65-Deficient Leber Congenital Amaurosis and Severe Early-Childhood-Onset Retinal Dystrophy. Ophthalmology *123*, 1606–1620.

Werling, N.J., Satkunanathan, S., Thorpe, R., and Zhao, Y. (2015). Systematic Comparison and Validation of Quantitative Real-Time PCR Methods for the Quantitation of Adeno-Associated Viral Products. Hum. Gene Ther. Methods *26*, 82–92.

Weymouth, A.E., and Vingrys, A.J. (2008). Rodent electroretinography: methods for extraction and interpretation of rod and cone responses. Prog. Retin. Eye Res. *27*, 1–44.

Wheatley, M., and Hawtin, S.R. Glycosylation of G-protein-coupled receptors for hormones central to normal reproductive functioning: its occurrence and role. Hum. Reprod. Update *5*, 356–364.

Wheatley, M., Wootten, D., Conner, M.T., Simms, J., Kendrick, R., Logan, R.T., Poyner, D.R., and Barwell, J. (2012). Lifting the lid on GPCRs: the role of extracellular loops. Br. J. Pharmacol. *165*, 1688–1703.

Wilson, J.H., and Wensel, T.G. (2003). The nature of dominant mutations of rhodopsin and implications for gene therapy. Mol. Neurobiol. *28*, 149–158.

Wu, J., Zhao, W., Zhong, L., Han, Z., Li, B., Ma, W., Weigel-Kelley, K.A., Warrington, K.H., and Srivastava, A. (2007). Self-Complementary Recombinant Adeno-Associated Viral Vectors: Packaging Capacity And The

Role of Rep Proteins in Vector Purity. Hum. Gene Ther. *18*, 171–182.

Wu, T., Töpfer, K., Lin, S.-W., Li, H., Bian, A., Zhou, X.Y., High, K. a, and Ertl, H.C. (2012). Self-complementary AAVs Induce More Potent Transgene Product-specific Immune Responses Compared to a Single-stranded Genome. Mol. Ther. *20*, 572–579.

Xiao, X., Li, J., and Samulski, R.J. (1998). Production of high-titer recombinant adeno-associated virus vectors in the absence of helper adenovirus. J. Virol. *72*, 2224–2232.

Xiong, W., MacColl Garfinkel, A.E., Li, Y., Benowitz, L.I., and Cepko, C.L. (2015). NRF2 promotes neuronal survival in neurodegeneration and acute nerve damage. J. Clin. Invest. *125*, 1433–1445.

Yang, Y., Nunes, F.A., Berencsi, K., Furth, E.E., Gönczöl, E., and Wilson, J.M. (1994). Cellular immunity to viral antigens limits E1-deleted adenoviruses for gene therapy. Proc. Natl. Acad. Sci. U. S. A. *91*, 4407–4411.

Yang, Y., Li, Q., Ertl, H.C., and Wilson, J.M. (1995). Cellular and humoral immune responses to viral antigens create barriers to lung-directed gene therapy with recombinant adenoviruses. J. Virol. *69*, 2004–2015.

Yokoi, K., Kachi, S., Zhang, H.S., Gregory, P.D., Spratt, S.K., Samulski, R.J., and Campochiaro, P.A. (2007). Ocular gene transfer with self-complementary AAV vectors. Invest. Ophthalmol. Vis. Sci. *48*, 3324–3328.

Yu, D.Y., Cringle, S.J., Su, E.N., and Yu, P.K. (2000). Intraretinal oxygen levels before and after photoreceptor loss in the RCS rat. Invest. Ophthalmol. Vis. Sci. *41*, 3999–4006.

Zeiss, C.J., Allore, H.G., Towle, V., and Tao, W. (2006). CNTF induces dose-dependent alterations in retinal morphology in normal and rcd-1 canine retina. Exp. Eye Res. *82*, 395–404.

Zeitz, C., Gross, A.K., Leifert, D., Kloeckener-Gruissem, B., McAlear, S.D., Lemke, J., Neidhardt, J., and Berger, W. (2008). Identification and functional characterization of a novel rhodopsin mutation associated with autosomal dominant CSNB. Invest. Ophthalmol. Vis. Sci. *49*, 4105–4114.

Zhong, L., Li, B., Jayandharan, G., Mah, C.S., Govindasamy, L., Agbandje-McKenna, M., Herzog, R.W., Weigel-Van Aken, K.A., Hobbs, J.A., Zolotukhin, S., Muzyczka, N., and Srivastava, A. (2008a). Tyrosine-phosphorylation of AAV2 vectors and its consequences on viral intracellular trafficking and transgene expression. Virology *381*, 194–202.

Zhong, L., Li, B., Mah, C.S., Govindasamy, L., Agbandje-McKenna, M., Cooper, M., Herzog, R.W., Zolotukhin, I., Warrington, K.H., Weigel-Van Aken, K.A., Hobbs, J.A., Zolotukhin, S., Muzyczka, N., and Srivastava, A. (2008b). Next generation of adeno-associated virus 2 vectors: point mutations in tyrosines lead to high-efficiency transduction at lower doses. Proc. Natl. Acad. Sci. U. S. A. *105*, 7827–7832.

Zhong, L., Zhou, X., Li, Y., Qing, K., Xiao, X., Samulski, R.J., and Srivastava, A. (2008c). Single-polarity recombinant adeno-associated virus 2 vector-mediated transgene expression in vitro and in vivo: mechanism of transduction. Mol. Ther. *16*, 290–295.

Zhou, X., Zeng, X., Fan, Z., Li, C., McCown, T., Samulski, R.J., and Xiao, X. (2008). Adeno-associated virus of a single-polarity DNA genome is capable of transduction in vivo. Mol. Ther. *16*, 494–499.

Zhu, L., Jang, G.-F., Jastrzebska, B., Filipek, S., Pearce-Kelling, S.E., Aguirre, G.D., Stenkamp, R.E., Acland, G.M., and Palczewski, K. (2004). A naturally occurring mutation of the opsin gene (T4R) in dogs affects glycosylation and stability of the G protein-coupled receptor. J. Biol. Chem. *279*, 53828–53839.

Zolotukhin, S., Byrne, B.J., Mason, E., Zolotukhin, I., Potter, M., Chesnut, K., Summerford, C., Samulski, R.J., and Muzyczka, N. (1999). Recombinant

adeno-associated virus purification using novel methods improves infectious titer and yield. Gene Ther. *6*, 973–985.